# Hydrodeoxygenation of Levulinic Acid over Supported Catalysts

*Hydrodeoxygenatie van Levulinezuur over Gedragen Katalysatoren*

*(met een samenvatting in het Nederlands)*

**Proefschrift**

ter verkrijging van de graad van doctor aan de Universiteit Utrecht op gezag van de rector magnificus, prof. dr. G. J. van der Zwaan, ingevolge het besluit van het college voor promoties in het openbaar te verdedigen om woensdag 10 december 2014 des middags te 4.15 uur

door

**Wenhao Luo**

geboren op 18 maart 1984 te Jilin, China

Promotor: Prof. dr. ir. B. M. Weckhuysen

Copromotor: Dr. P. C. A. Bruijnincx

This research was funded by the Smart Mix Program of the Netherlands Ministry of Economic Affairs and the Netherlands Ministry of Education, Culture and Science within the framework of the CatchBio Program.

There is no royal road to science, only those who do not dread the fatiguing climb of its steep paths have the chance of gaining its luminous summits.

**Karl Marx**
Capital, Volume 1: A Critical Analysis of Capitalist Production

Print: Gildeprint, Enschede, The Netherlands

# Contents

# Chapter 1

# Introduction

## 1.1 Biomass as a Renewable Resource

Fossil resources (coal, petroleum and natural gas), the dominant feedstock for the production of fuels and chemicals in our current society, are non-renewable. Various factors, such as the growing global energy demand, atmospheric $CO_2$ accumulation, price fluctuations and dwindling supplies of the fossil fuels, difficulties with exploitation of the limited reserves, as well as legislation and mandates, have all stimulated the search for alternative feedstocks and by doing so drive the ongoing transition to a more sustainable, renewables-based society.[1-3]

Biomass is one particularly promising, alternative feedstock for fuels and chemicals production, given its general abundance and the potential of such processes to be more sustainable. Indeed, biomass is the main renewable alternative that can serve as feedstock for the fixed carbon on which our society relies.[1, 3-6] Biomass comprised 76% of the renewable contribution to the energy mix in 2012, and holds the potential to deliver at least one-quarter of the world's projected energy needs by 2035.[7] The U.S. Department of Energy (DOE) has estimated that more than 1 billion tons of dry biomass, enough to displace 30% of U.S. annual petroleum consumption, could be harvested annually from fields and forests without major agricultural changes and while still meeting the food, feed and export demands of the U.S.[8] Practical and logistical challenges aside, it is clear that the implementation of a substantial volume of biomass-derived fuels and chemicals would have a positive impact on the environment. Indeed, the current global consumption of fossil fuel accounts for ca. 56% of greenhouse gas emissions,[9] while biomass can, in principle, reduce these greenhouse gas emissions significantly given the consumption of $CO_2$ during biomass growth. In addition, establishing a renewables-based energy supply and deployment of routes for bio-based products could also strengthen and propel the (local) economy, with job creation and a reduced dependence on the fluctuations in oil price as a result.[8]

Given the ethical issues surrounding the utilization of first-generation, edible biomass for the large-scale production of fuels and chemicals, attention has shifted to the exploration of nonfood-based biomass sources, i.e. second generation biomass, such as dedicated crops, or agricultural and municipal waste. While the specific chemical

composition of lignocellulosic biomass is highly dependent on the resource, lignocellulosic biomass always consists of three main components: cellulose (30-50 wt%), hemicellulose (15-30 wt%) and lignin (15-30 wt%).[10] The lower cost, faster growth and high abundance of lignocellulosic biomass from agricultural resources, forestry, and industrial waste streams (e.g., paper manufacturing) make this resource an attractive raw material for substitution of petroleum. From a chemical and process engineering point of view, the efficient and selective conversion lignocellulosic biomass at economical costs poses considerable challenges, though. In order to address these challenges in an economically viable fashion, biorefining operations need to be developed, aimed at efficient and full valorization of the renewable feedstock, in analogy to current petrochemical refining. Such a biorefinery facility would consist of highly integrated biomass pretreatment and conversion processes to produce power, fuels, and chemicals from biomass.[11] Indeed, biorefineries should aim for complete valorization of all components of the biomass source into a range of profitable products with a minimum loss of energy and mass with the aim of maximizing the overall value of the production chain.

Different approaches can be taken to the conversion of biomass in a biorefinery. One option is to convert the whole biomass in one single-step to give a bio-oil that needs to be further processed and upgraded to give fuels and chemicals as end products. While such single-step approaches, with high temperature (catalytic) pyrolysis being a prime example, can lead to lower costs as drying, pretreatment and separation steps are prevented, the downstream upgrading of the resulting bio-oil (a mixture of hundreds of compounds) will, however, require additional costs.[10]

Another option is to first subject the whole biomass to a pretreatment process that is aimed at the separation of the different components, after which these components can be individually upgraded further (Fig. 1.1). First, separation of the biomass into main components in a primary fractionation/de-polymerization unit is required. A number of different pretreatment technologies are being studied and applied, typically involving traditional separation processes, such as filtration, solvent extraction and distillation. Second, the individual fractions are converted into valuable chemical intermediates, so-called platform chemicals, in a secondary refinery process. Two of the main constituents

of lignocellulose, cellulose and hemicellulose, are carbohydrate-based polymers that can be depolymerized to C6 and C5 sugars by hydrolysis.[12-14] Further conversion of these sugars can yield a large variety of platform molecules. Two prominent examples include 5-hydroxymethylfurfural (HMF),[15, 16] and levulinic acid (LA), but many other compounds have been proposed as potential, renewable platform molecules.[14, 17-20] Indeed, which particular compounds will serve as the renewable equivalents of the building blocks of the petrochemical industry (mainly mixtures of benzene, toluene and xylene isomers (BTX), small olefins, and $CO/H_2$) remains to be seen. In any case, typical technologies applied in these secondary refining processes can be distinguished into thermo-chemical processes (e.g., gasification, liquefaction), biochemical processes (e.g., fermentation) and chemocatalytic processes (e.g. catalytic depolymerization). Finally, (off-site) further catalytic processing of the renewable platform molecules to high value-added end-products can then produce a broad range of chemicals of increasing complexity and functionality, similar (or in cases even identical) to the current output of the petrochemical industry. The research described in this PhD thesis is focused on the role that LA might assume as a renewable, platform molecule in second-generation biorefinery operations, exploring the chemocatalytic aspects of upgrading LA to various value-added end products by hydrodeoxygenation.

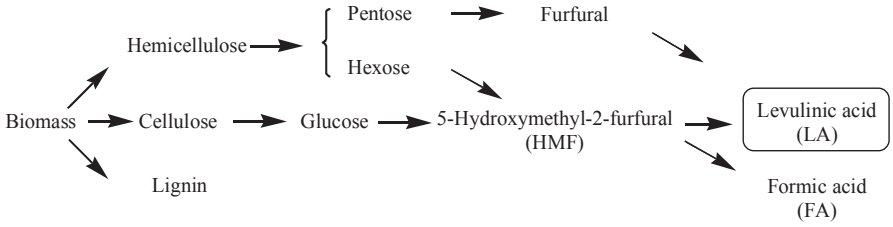


Figure 1.1. Generalized reaction scheme for the production of levulinic acid from lignocellulosic biomass, adapted from ref. [20].

## 1.2 Production of Levulinic Acid

Levulinic acid (LA), also known as 4-oxopentanoic acid or 4-ketopentanoic acid, is a crystalline solid containing two reactive functional groups (–C=O and –COOH), with a melting point at around room temperature (311 K) and a boiling point as high as 520 K. LA was first synthesized in 1840 from sucrose in the presence of mineral acids[21] and

since then its properties and chemical reactivity have been studied extensively. In the 1940s, quite some research on the potential of large-scale LA production was done, but these and later efforts did not result in the commercial production of LA in any significant volume, mainly as a result of the expensive raw materials, low yields, and lack of suitable equipment for separation and purification.[22, 23]

Recent developments in science and technology have enabled a re-evaluation of the industrial potential of LA. Indeed, it has been shown that it can be produced on an exploratory scale from the C6-sugar fraction of various lignocellulosic biomass feedstocks through a simple and high yielding acid hydrolysis process.[19, 24] Feedstocks tested include cane sugar,[25] corn starch,[22, 26] rice straw,[27] pulp slurry,[28] woods,[29, 30] newspaper,[31] cellulose,[32] and sugars.[23, 33, 34] The theoretical yield of LA by dehydration from C6-sugars is 64.5 wt%, owing to the coproduction of equimolar amounts of formic acid.[34] Only ~2/3 (or less) of this theoretical yield are typically reached, however, due to the formation of an unwanted black, insoluble solid residue called humins; these humins are formed by degradation reactions involving HMF and a large number of intermediates.[35] The various recent developments thus show that the commercial production of LA can potentially become feasible from a variety of feedstocks, but challenges still remain with respect to achieving good selectivities and high yield at economical costs.

In addition to these more exploratory studies, over the years several strategies for the large-scale production of LA have also been pursued. In 1957, an approach for the industrial LA production from corncob furfural residue was patented by the Quaker Oats Corporation. The process made use of a 3 wt% of sulfuric acid solution at 442 K to achieve a yield of 20 wt% LA.[36] In this approach, the insoluble humins that are formed during the process are separated from the product mixture in a filter unit. LA is extracted with the water-immiscible solvent methyl isobutyl ketone, which is later recovered by evaporation and recycled for extraction of LA. The aqueous mixture containing the acid catalyst after extraction is also recycled. Ghorpade and Hanna later proposed a concept based on reactive extrusion for the continuous production of LA at variable temperatures. Corn starch and sulfuric acid are mixed with water in a pre-conditioner unit, and the slurry is then fed into a twin-screw extruder at a variable

temperature (353 to 423 K).[37] The LA yield obtained was significantly increased to about 48 wt%, owing to the use of easily hydrolysable feedstock and a more concentrated 5 wt% sulfuric acid solution.

At the moment, the Biofine process is probably the most promising and furthest developed approach to commercial LA production. The process consists of a double-reactor approach to continuous LA production, which minimizes the formation of by-products and associated separation problems.[38, 39] Acid-catalyzed degradation of the carbohydrate source to hydroxymethylfurfural (HMF) is first conducted at high temperature (483-503 K) and short time residence times (13- 25 s) in the presence of 1-5 wt% mineral acid, after which the HMF solution is fed to a second reactor and further converted to LA at a lower temperature (468-488 K) and longer residence time (15-30 min). With this technology yields of approximately 40 wt% of LA based on the hexose content of the carbohydrate-containing feedstock have been claimed. In addition, the application of this approach has also been extended to diverse, inexpensive waste cellulosic materials, such as agriculture residues, urban waste paper, paper mill sludge and cellulose fines from papermaking, all with the aim of lowering the cost of LA production. As a result, LA could be produced at 8-20 $/kg, based on an annual production level of 450 tons, from agriculture residues, and cellulose fines from papermaking.[8, 40] The first, commercial-scale plant operating on the Biofine process for the conversion of lignocellulosic biomass to LA was constructed and operated in Caserta, Italy.[41] This unit reportedly operated at a capacity of 50 ton/day of dry feedstock, originating from local tobacco bagasse and paper mill sludge, with major products being LA and ethyl levulinate. Severe clogging of the reactors by salts and humins posed a major challenge to the operation, though. Biofine technology is now operating a smaller scale demonstration facility in the U.S. at Gorham, Maine, producing 0.27 ton/day of levulinic acid from 1 ton/day dry biomass (i.e. paper mill sludge).[42] Segetis also recently announced that it has successfully started a U.S.-based pilot plant facility in Golden Valley, Minnesota, demonstrating the viability of its proprietary process to convert biomass to levulinic acid. The pilot plant holds a capacity of 0.22 tons/year with corn sugar as the feedstock, with the intention of testing other feedstocks as well.[42] In addition, a larger plant is planned in New England (U.S.),

which will hold a capacity of 125 dry ton/day waste cardboard producing over 8 million gallons per year of levulinate ester and formic acid.[43]

### 1.3 Levulinic Acid Derivatives

A wide variety of value-added products can be obtained from LA by various different catalytic conversion processes. The LA-derived products can in turn find application in numerous ways, for instance as building blocks for polymers, additives, resin, herbicides, pharmaceuticals, or can be applied directly as antifreeze agents, solvents, plasticizers, oxygenated fuel additives or liquid biofuels.[8, 40, 44-51] Given the scope of this PhD thesis, of the myriad of products that can be produced from LA, the primary focus here will be on that subset of LA derivatives that can be obtained through hydrodeoxygenation (HDO) reactions, i.e., through consecutive hydrogentation/dehydration steps. Fig.1.2 gives an overview of the main products that can be obtained via LA HDO reactions. The LA derivatives, γ-valerolactone (GVL), 2-methyltetrahydrofuran (MTHF) and pentanoic acid (PA), will be discussed in more detail.

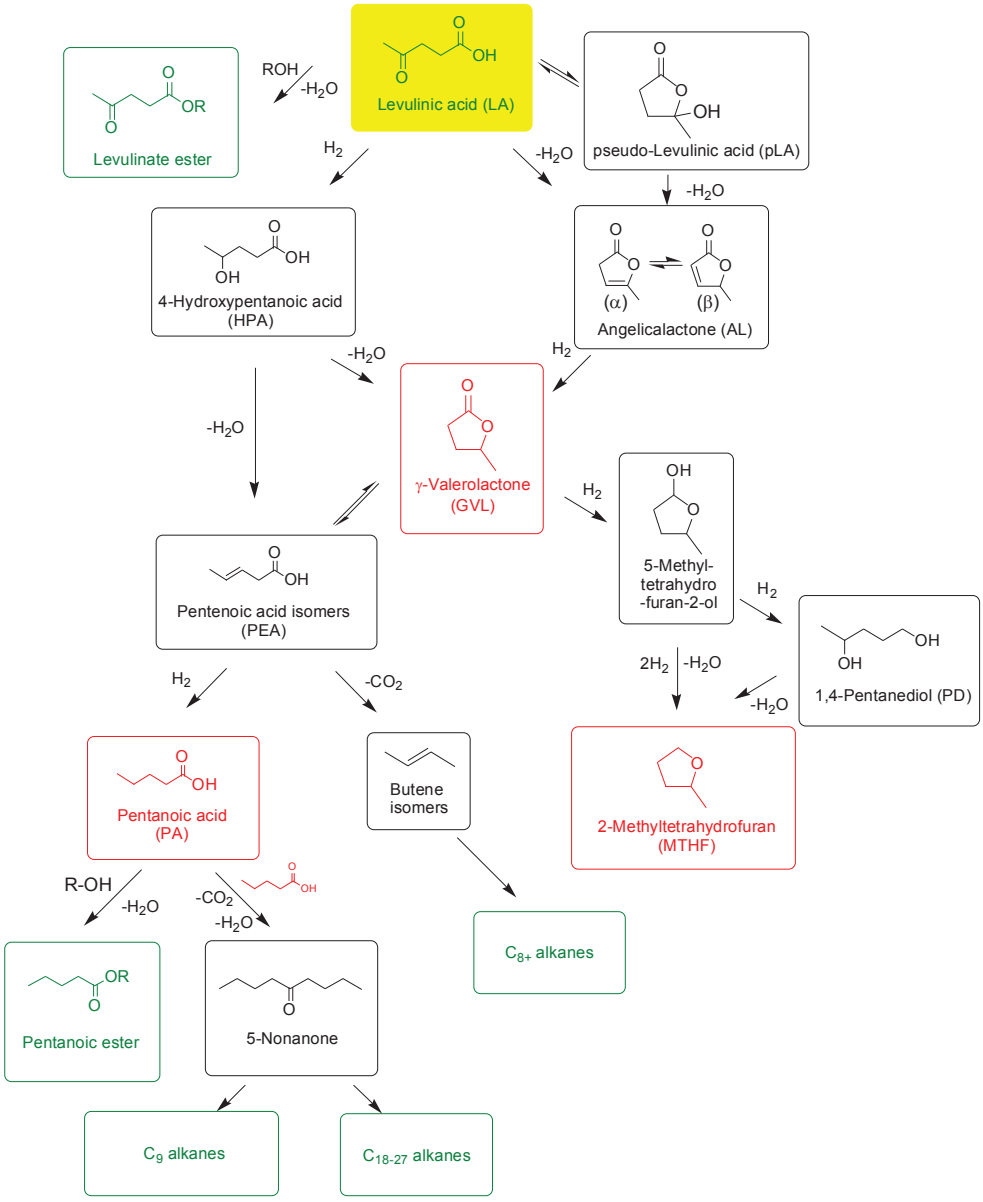


Figure 1.2. Selected pathways to value-added fuels and chemicals that can be obtained from LA by hydrodeoxygenation reactions.

Of the compounds shown in Fig. 1.2 that can be obtained from LA, γ-valerolactone (GVL) is a particularly interesting one and can be considered as a platform molecule in its own

right. GVL is a stable, colorless liquid at room temperature. It can be used as a green solvent, due to its good miscibility with a variety of compounds derived from biomass, its stability at moderate temperatures even in the presence of water or oxygen, and low toxicity;[10] GVL is also used for the production of perfumes and food additives, owing to its sweet, herbaceous odor and stability under normal conditions;[52] GVL has furthermore been proposed to be a promising fuel additive. Horvath et al.,[52] for instance, compared mixing 90 vol% conventional gasoline with 10 vol% GVL or ethanol, and found that the mixture with GVL had a lower vapor pressure and proved to be superior in combustion properties. The combustion energy of GVL is similar to ethanol (29.7 MJ/kg), but GVL has a higher energy density.

The cyclic ether 2-methyltetrahydrofuran (MTHF) has a promising environmental footprint, being bio-based and abiotically degradable by sunlight and air, presumably via oxidation and ring-opening.[44] MTHF is advocated as a renewable solvent with broad application in organic chemistry.[44] Another use of 2-methyltetrahydrofuran (MTHF) as automobile fuel extenders has recently been suggested to have potential,[6, 53-55] given its good miscibility with gasoline and favorable oxygenate and vapor pressure properties.[53] It can be blended in gasoline in up to 60% by volume without adverse engine performance, as a component of 'P-series' fuels. The volume of this potential market could be as high as $2.6 \times 10^5$ $m^3$ per year.[40] In addition, MTHF can be further converted into $C_{4-9}$ alkanes for fuels in the presence of a metal and acid catalyst at high pressure and moderate temperatures.[56, 57] 1,4-Pentanediol, an intermediate in the production of MTHF, can be used for the production of new polyesters,[51] or applied as a fine chemical intermediate.[58, 59]

The straight-chain carboxylic acid pentanoic acid (PA) is also known as valeric acid. PA finds its primary use in the synthesis of its pentanoate esters, which have pleasant odors and are used in perfumes and, cosmetics and as food additives because of their fruity flavors.[60] Recently, Lange et al. reported the great potential of pentanoate esters as building blocks for novel oxygenated fuels, so-called 'valeric biofuels', which can be blended into both gasoline and diesel.[49] Dumesic and co-workers proposed a different strategy for upgrading PA into energy-dense, drop-in fuels.[8, 46, 48] A series of hydrogenation, dehydration, decarboxylation, decarbonylation, ketonization, and

oligomerization reactions of PA produced hydrocarbon fuels with a carbon range from C6 to C27. It should be noted in this respect that levulinate esters themselves can also be readily used as fuel additives.[61]

### 1.4 Levulinic Acid Hydrodeoxygenation

An overview of the various reaction pathways that have been reported for the conversion of LA into value-added chemicals and fuel components from LA by sequential hydrodeoxygenation (HDO) reactions is given in Fig. 1.2. The first, key conversion involves the formation of GVL from LA. This can occur via two pathways, i.e. either by dehydration to angelicalactone (AL) followed by hydrogenation or via hydrogenation to 4-hydroxypentanoic acid (4-HPA) and subsequent dehydration.[10, 62] In the first pathway, AL can either be formed directly from the enol tautomer, but the involvement of pseudo-LA (pLA) as intermediate has also been proposed.[34, 63, 64]

Two major pathways are now accessible from GVL. Further hydrogenation of the lactone GVL can initially yield the yield 5-methyltetrahydrofuran-2-ol and after ring-opening of the hemiacetal and subsequent hydrogenation, 1,4-pentanediol (PD).[52] Alternatively, 5-methyltetrahydrofuran-2-ol can also undergo consecutive dehydration and hydrogenation steps to give MTHF. The latter compound can also be obtained from PD by dehydration.[65, 66] The alternative pathway that is open to GVL involves lactone ring-opening to give pentenoic acid (PEA),[48, 67] a compound that is also directly accessible from HPA by dehydration. PEA offers various opportunities for the production of (ultimately) cellulosic biofuels production. Hydrogenation of PEA, for instance, yields pentanoic acid (PA), which can be esterified to give valeric esters that can be used as biofuels. Alternatively, the increase in carbon-chain length that is required for fuel application can be achieved by PA ketonization. The 5-nonanone obtained can be further converted to nonane, which can be used as an additive of diesel fuel or gasoline through via further isomerization to branched $C_9$ alkanes;[50] 5-nonanone can also be converted to $C_9$ olefins via hydrogenation and dehydration, which can be oligomerized to yield a mixture of $C_{18-27}$ olefins as diesel fuel.[68] Another route available from PEA is its decarboxylation, which gives butene isomers. These butenes

can be oligomerized and hydrogenated to C8+ alkanes that can then be used as jet fuel.[48]

The fact that the various end products shown in Fig. 1.2 can thus be obtained by closely related, consecutive hydrogenation, dehydration, and isomerisation steps in reactions that are run under often rather similar conditions, immediately points at the challenges involved in selectively converting LA into only one of these end products. It is therefore of prime importance and one of the goals of the work described in this PhD thesis, to get insight into what is required of a catalyst for each step in the HDO valorization platform of LA.

Both homogeneous and heterogeneous catalysts have been used for these HDO reactions, with the LA-to-GVL step having received most of the attention. The homogeneous catalysts are typically Ru-based ones and have been studied for the hydrogenation of LA to GVL, PD or MTHF.[57, 59, 69] Such homogeneous catalysts might, however, not be too well suited for large-scale conversion of LA, given the high cost of the noble metal catalysts and the difficulties regarding catalyst/product separation and recycling that are associated with the high boiling points of GVL (480-481 K) and PA (459-460 K).[57] Indeed, Heeres et al. reported that upon recycling of a Ru-based homogeneous catalyst in the aqueous phase, a significant decrease in LA conversion from 81% to 55% was observed. Heterogeneous catalysts seem certainly better suited and more economical for the large-scale production of derivatives of LA, as they can be more easily and economically separated. Here, we focus therefore on heterogeneous catalyst systems for the hydrodeoxygenation of LA. In particular, three reaction routes will be discussed in detail: (1) LA to GVL; (2) LA to PD and MTHF; and (3) LA to PA.

## 1.5 LA to γ-Valerolactone

LA to γ-valerolactone (GVL) reactions are typically run with hydrogen pressures ranging from 1 to 150 bar and at moderate reaction temperatures in the range of 298 to 538 K. While most of these reactions are performed in the liquid phase, some vapor

phase reactions have also been reported, with different sources of hydrogen resources, including molecular hydrogen and formic acid.

### 1.5.1 Reduction of LA to GVL with Molecular Hydrogen

A continuous process for the commercial-scale manufacturing of GVL via vapor-phase hydrogenation has been explored by the Quaker Oats Company in the 1950s.[70] Quantitative conversion to GVL was achieved by passing a mixture of LA and $H_2$ over $CuO/Cr_2O_3$ at 473 K and atmospheric pressure. The yield of GVL decreased at higher reaction temperatures owing to the consecutive conversion of GVL to pentanoic acid. Similarly, Chang et al. recently screened Ru/C, Pd/C and Pt/C in a vapor-phase continuous setup.[71] Ru/C showed the highest activity for LA to GVL conversion, and no loss of activity was observed after 240 h in a continuous down-flow fixed-bed reactor system (538 K, 1 bar). Vapor phase approaches can be beneficial as they can be run as continuous processes and do not require high $H_2$ pressures, which are costly from an equipment point of view. However, the high energy input required for the vaporization of LA (boiling point 518–519 K) and possible corrosion of the equipment as a result of co-vaporized residues of strong acid (i.e., HCl and $H_2SO_4$) from carbohydrate feedstocks make such methodologies less advantageous.

The liquid-phase hydrogenation of LA to GVL under hydrogen atmosphere with heterogeneous catalysts has been more extensively studied. Already in 1930, Schuette and Thomas conducted the liquid-phase hydrogenation of LA in diethyl ether, ethanol, and acetic acid with $PtO_2$.[72] A maximum GVL yield of 87% was obtained in diethyl ether after 48 h at room temperature under 2.3-3.0 bar hydrogen. A few years later in 1947, the use of Raney Ni under 493 K, 50 bar enabled a GVL yield up to 94% after 3 h of reaction without a solvent.[73] Around the same time, the metallic Re 'black' was also reported to be active for this reaction, giving a 71% yield of GVL at 376 K, 148 bar for 18 h in neat LA.[74] More recently, mostly supported noble and non-noble metal catalysts have been studied for LA hydrogenation. Manzer screened the catalytic capacity (activity/selectivity) of 5 wt% Ir, Rh, Pd, Ru, Pt, Re and Ni supported on activated carbon, prepared by incipient wetness impregnation. The catalysts were evaluated at 423 K, 55 bar in 1,4-dioxane.[75, 76] The 5 wt% Ru/C combined the highest activity

with high selectivity. Further optimization allowed for qualitative LA conversion and a GVL selectivity of >95%. Yan et al. compared 5 wt% Ru/C with Pd/C, Raney Ni and Urushibara Ni at 403 K, 12 bar $H_2$ in methanol, with Ru/C again showing the highest GVL yield (92%) with a GVL selectivity of 99%.[63] Complete LA conversion could be also achieved with 5 wt% Ru/C in neat LA at room temperature, 12 bar $H_2$ after 50 h.[77] The Shell laboratory reported a screening study of 50 catalysts using a flow reactor, choosing Ni, Rh, Pd, Pt, Re, Ru or a combination of two or more of them. Catalytic performance was studied over a temperature range of 423-523 K and hydrogen pressures of 50-80 bar; Pt on $TiO_2$ or $ZrO_2$ provided the best performance with constant GVL yields (95%) over 100 h time on stream at 473 K, 40 bar $H_2$.[49] In addition, a combination of a homogeneous and heterogeneous system for the conversion of C6-sugars directly into GVL without isolation of the intermediate LA was also reported by Heeres and coworkers.[78] A 62% yield of GVL from fructose was obtained using an acid catalyst (TFA) and a 5 wt% Ru/C catalyst for hydrogenation of LA to GVL at 453 K, 94 bar. As a result, a 29% yield of GVL was achieved directly from cellulose. Taken together, these results all show that the choice of the metal greatly affects the catalytic performance of the LA-GVL step, and, expectedly, noble metals such as Ru and Pt typically show superior activity and selectivity.

Not only does the choice of hydrogenation metal influence catalytic performance, so does the choice of support, as shown by a more limited set of examples. Palkovits et al. reported that 5 wt% Ru/C gave a higher GVL yield of 89%, than 5 wt% $Ru/Al_2O_3$ (76%) and $Ru/SiO_2$ (75%) at 403 K, 12 bar $H_2$ in ethanol/water after a reaction time of 160 min.[77] Also, it was observed that the activity of $Ru/TiO_2$ depended on the type of $TiO_2$. $Ru/TiO_2$ from Tronox showed no LA conversion, while $Ru/TiO_2$ from Degussa (P25) gave a high GVL yield of 71% at 81% LA conversion.[77] The difference in performance of the $Ru/TiO_2$ catalyst was attributed to differences in the extent of metal dispersion and metal particle size. Ru catalysts with good dispersion and a smaller average particle size showed superior catalytic activity. Corma et al. also obtained better results with 0.64% $Ru/TiO_2$ (average Ru particle size of 2.0 nm) than with 5.7% $Ru/TiO_2$ (31.4 nm) and 0.5-5% Ru/C (2.2-2.6 nm) catalysts.[79] More research is still required in order to rationalize the influence of the support on the performance; for a fair comparison such

studies in which the support is changed need to assess catalyst performance at a similar metal dispersion and particle size.

The use of an acid co-catalyst for GVL synthesis has also been reported. Such an acid would accelerate the dehydration step,[80] allowing the LA-GVL conversion to occur at milder conditions, thus further reducing the costs of this process. For example, Galletti et al. performed LA hydrogenation reactions with Ru-supported catalysts and acidic co-catalysts (Amberlyst-70, -15, niobium phosphate and niobium oxide).[81] Under mild conditions (323-343 K, 5-30 bar $H_2$), both 5 wt% $Ru/Al_2O_3$ and Ru/C showed limited LA conversion after 3 h (24% and 48% respectively); the addition of the acid co-catalyst improved the catalytic performance. The best co-catalyst was Amberlyst-70, increasing LA conversion to 57 and 100% with 5 wt% $Ru/Al_2O_3$ and Ru/C, respectively, with a GVL selectivity of >98% for both. Notably, with 5 wt% Ru/C in the presence of Amberlyst-70 at 343 K, 5 bar $H_2$ in water, a LA conversion of 90% and GVL selectivity of 100% was achieved within 30 min, and a 99% yield to GVL at 3 h reaction time. 4-Hydroxypentanoic acid was detected as intermediate, indicating that the hydrogenation of LA in water indeed proceeds via the LA-HPA-GVL route (Fig. 1.2). Only very few examples have been reported of the use of bi- or multi-metallic catalysts for the LA-to-GVL conversion. The examples provided by Dumesic's group showed that improved tolerance to sulfuric acid can be gained by using a Ru-Sn[82] and Ru-Re[83] catalysts (see below), while the Shell laboratory noted no improvement of catalytic performance upon alloying Pt-based catalysts with other noble metals.[49]

The production of GVL from LA has also been investigated in supercritical (sc) fluids. A high yield of GVL (>99%) was obtained in a batch reaction with (sc)$CO_2$ with 5 wt% $Ru/Al_2O_3$ at 423 K for 2 h with dioxane as cosolvent under a total pressure of 250 bar ($H_2$ pressure 145 bar). Hydrogenation under $scCO_2$ in a continuous flow reactor over 1 wt% $Ru/Al_2O_3$ gave a GVL yield of >99.5%. Both examples show that LA can be efficiently hydrogenated in $scCO_2$;[84] Inspired by these examples, Poliakoff et al. explored a new process for the hydrogenation of aqueous LA ($LA/H_2O$=75/25) in $scCO_2$. GVL is separated in $scCO_2$ layer after the reaction, and a near quantitative yield of GVL was obtained with 5 wt% $Ru/SiO_2$ at 473 K and total pressure 100 bar.[85]

### 1.5.2 Reduction of LA to GVL with Formic Acid

The conversion of LA to GVL step can also be achieved without using molecular hydrogen. One strategy is to use fomic acid (FA), which is formed as a byproduct in a 1:1 stoichiometry with LA in the conversion of HMF to LA, as hydrogen source, as has been pioneered by Fu and Guo et al.[86, 87] Direct hydrogen transfer from FA to LA would be attractive as this would avoid any costly purification of LA as well as the need for external hydrogen. Both homogeneous and heterogeneous systems have been explored for this transfer hydrogenation reaction. A Ru complex formed in situ from $PPh_3$ and $RuCl_3 \cdot H_2O$ in the presence of a base (i.e., pyridine or $NEt_3$) at 423 K gave a GVL yield of 94% in an aqueous solution with equimolar LA and FA. Interestingly, a two-stage process with sequential addition of heterogeneous catalysts was developed. First, LA and FA mixtures were heated in the presence of a Ru-P/$SiO_2$ catalyst at 443 K for formic acid decomposition, followed by addition of Ru/$TiO_2$ for the actual hydrogenation of LA at 443 K. A 90% LA conversion with 99% selectivity to GVL was achieved and the catalysts showed no decrease in activity and selectivity over eight recycle runs, potentially enabling a two-stage continuous process for GVL synthesis. In this strategy, using Ru/C instead of Ru/$TiO_2$ gave a low yield of GVL, as Ru/C was poisoned by any remaining FA.

With the aim of increasing the decomposition rate of FA to $CO_2$ and $H_2$ and of improving catalyst stability in FA, Dumesic and co-workers introduced a second metal to Ru/C. A RuSn(3.6:1)/C catalyst material was employed for GVL synthesis after phase separation of LA/FA from aqueous solution using alkylphenol solvents.[88] The presence of Sn improves the FA decomposition to $CO_2$ and $H_2$ and the stability of hydrogenation metal (Ru). RuSn(3.6:1)/C was found to be stable even after 230 h time on stream. A 15 wt% RuRe(3:4)/C was also reported by the same group for the conversion of an aqueous solution of equimolar of LA and FA in a continuous fix-bed system.[82, 89] A stable catalyst was attained with a high selectivity to GVL (>95%), albeit with a considerably lower activity than the Ru/C catalyst; interestingly, the RuRe catalyst showed no significant deactivation upon addition of $H_2SO_4$ to the feed, an impurity that is invariably present in the LA/FA streams owing to the $H_2SO_4$ required for the previous sugar degradation process. In contrast, Ru/C rapidly deactivated in the presence of sulfuric

acid. The RuSn and RuRe catalysts thus provide two rare examples of the great advantages that the use of bimetallic catalysts can bring in the hydrogenation of LA.

Further efforts have been made to improve the stability and robustness of the catalyst in such a mixture of acids. Au-based catalyst materials for the conversion of equimolar aqueous solution of LA and FA to GVL have been reported by Cao et al.[90] with Au nanoparticles (1.2-2.5 nm) supported on acid-tolerant $ZrO_2$ affording quantitative conversion to GVL at 423 K. Furthermore, the catalyst showed good recyclability. Moreover, Au particle size was found to influence the catalytic performance. Large Au particles (~3 nm) showed a decrease in activity, and a small Au particle size was preferred for FA decomposition and LA reduction. $Au/ZrO_2$ showed the highest activity for a series of zirconia-supported noble metals, including Pd, Au, Pt and Ru. Furthermore, the $Au/ZrO_2$ catalyst could be used with aqueous LA and FA solutions obtained by hydrolysis/dehydration of fructose, glucose, starch and cellulose (albeit with an intermediate filtration and neutralization step) to give quantitative conversion of LA to GVL. The use of this $Au/ZrO_2$ catalyst was later combined with a separation strategy that entailed LA and FA removal as hydrophobic butyl esters.[91] This approach allowed for 98 and 95% of LA and FA to be extracted from the aqueous phase as butyl LA and FA esters, effectively enabling separation from $H_2SO_4$. Butyl formate was subsequently decomposed over $Au/ZrO_2$ to $H_2$, $CO_2$ and butanol, and the hydrogen produced was used for the hydrogenation of the butyl LA ester into GVL. A quantitative yield of GVL was attained at 443 K and 6 h and it was found that the reaction rates could be enhanced by the addition of water. Characterization of the spent catalyst by X-ray photoelectron spectroscopy (XPS) and transmission electron microscopy (TEM) showed no changes in the $Au/ZrO_2$ material. A similar approach for the separation of LA and FA from the aqueous phase, but with butene instead of butanol, was proposed by Dumesic et al.[92] A dual bed reactor containing Pd/C for the conversion of FA and formate ester into hydrogen, and Ru/C for efficient hydrogenation of LA to GVL, achieved a quantitative yield of the butyl ester to GVL. This dual bed had shown no loss of activity after 400 h on stream. This approach again suggests that the efficient separation LA from the aqueous, $H_2SO_4$-containing phase into an organic solvent is beneficial for sustained catalyst stability.

### 1.5.3 Development of Non-Noble Metal Catalysts for LA-to-GVL

Although noble metal-based catalysts typically perform best in the conversion of LA to GVL, the high price of these metals could be a disadvantage of these systems and non-noble alternatives are being sought as a result. Indeed, Dumesic et al. evaluated the costs of a large-scale cellulose conversion process to liquid alkenes which included the conversion of LA to GVL over a RuRe(3:4)/C catalyst.[82] The estimated costs of the metals for the catalyst was $33 million for a large-scale plant.[89] In addition, price fluctuations resulting from limited and geographically uneven reserves of noble metals, further emphasize the need to develop non-expensive transition metal-based catalysts to reduce the cost of LA hydrogenation. With this in mind, $Cu/SiO_2$ was investigated by Hwang and Chang for LA hydrogenation.[93] A range of 5-80 wt% of Cu could be loaded onto the silica via a precipitation-deposition methodology. The 5 wt% Cu catalyst attained a quantitative conversion to GVL under vapor-phase conditions at 538 K, while higher Cu loadings (30-80 wt%) gave a lower GVL selectivity owing to further hydrogenation of the GVL product to MTHF, 1-pentanol and PD. Relatedly, 5-20 wt% $Cu/ZrO_2$ catalysts, prepared by co-precipitation, were reported by Rode et al.[94] to give 90% and >99.9% yields to GVL at 473 K in methanol and water, respectively, under a liquid phase conditions. However, the catalytic activity of the first row transition metals is typically lower than with the active noble metals, requiring a higher loading of the metal. In addition, the more limited stability of those metals (leaching and sintering) poses an additional an issue for LA HDO reactions.

Dumesic et al. have also shown that inexpensive bulk metal oxides, such as zirconia, can reduce levulinic acid and its esters to GVL. This innovative approach is based on a transfer hydrogenation step in which a secondary alcohol is used as the hydrogen source. This is more economical compared to using FA as the hydrogen donor, owing to the requirement of noble metal catalysts for the FA decomposition step. In addition, separation of the excess alcohol hydrogen donor from the ketone co-product and subsequent recycling is possible. An initial catalyst screening showed $ZrO_2$ to be most active at 373 K with 2-butanol. A higher GVL yield could be obtained by raising the temperature or changing the sacrificial alcohol. LA esters were found to be more easily transfer-hydrogenated into GVL than LA. A GVL yield of 92% could be attained over

$ZrO_2$ with LA and butanol at 423 K. However, rapid deactivation of the catalyst was found upon testing the catalyst for 100 h on stream, which was attributed to the blocking of the active basic sites of the amphoteric $ZrO_2$ by LA coordination. The catalyst could be regenerated via a simple calcination step in air.

In summary, a large number of heterogeneous catalysts and several hydrogen donors have been investigated for the LA to GVL process. Good activities and selectivities can be achieved with active hydrogenation metals, such as Ru and Pt, in different solvents, such as water, alcohols, dioxane and $scCO_2$. While many metal/support/solvent/hydrogen donor combinations have been tested under varying experimental conditions, often using commercial catalysts, less emphasis has been devoted to understanding the structure-activity relationships for these catalysts, and to the study of catalyst stability, in particular in the presence of various impurities that can be expected in biorefinery-derived LA feeds. There is therefore still ample room to improve the performance and the rational design of the LA hydrogenation catalysts for a more economical process for the sustainable production of GVL.

### 1.6 LA to 2-Methyltetrahydrofuran and 1,4-Pentanediol

The production of 1,4-pentanediol (PD) from LA requires further hydrogenation of the GVL intermediate, whereas the consecutive product, MTHF, requires both hydrogenation of GVL to PD followed by subsequent dehydration. The latter step is easily accomplished by thermal heating or by acid-catalysis. Alternatively, MTHF can also be obtained by dehydration and hydrogenation of the hemi-acetal that is obtained after hydrogenation of the lactone in GVL.

The reduction of GVL to PD was already reported in 1931. Hydrogenation of GVL over a copper–barium-chromium oxide catalyst gave 79% PD at 523 K 200-300 bar after a little over 3 h of reaction time.[95] In a later study,[73] PD yields up to 83% were achieved over the same catalyst at temperatures in the range of 513-533 K. The yields of PD dropped upon increasing the reaction temperature to 543-563 K, as a result of PD dehydration to MTHF. 11% of GVL and 44% of PD were obtained over copper chromium-oxide at 573 K and 200 bar after 80 min of reaction time. The strong odor of

the product that was detected provided the first example of the formation of MTHF as a by-product in the LA-to-PD reaction. Du et al. reported that GVL was converted in ethanol with 98% conversion and 93% selectivity to MTHF over copper–zirconia catalysts at 473 K, 60 bar $H_2$ pressure; when the same catalyst was used in ethanol at the same temperature after calcination in the presence of $H_2$ instead of air, GVL was hydrogenated to PD rather than to MTHF with 97% conversion and >98% selectivity.[96] Pinel et al. attained a 82% yield to PD from GVL over a 1.9% Ru-3.6% Re/C catalyst at 413 K under 150 bar after 28 h.[97] The choice and ratio of the two metals showed an influence on the selectivity to PD or MTHF. Palkovits et al. reported an efficient method for the solvent-free hydrogenation reaction of LA to MTHF,[98] using a Ru/C catalyst at 463 K to obtain a 90% conversion of LA with a yield of MTHF of 61% by removing water from the system in a two-step approach. In general, higher $H_2$ pressures and reaction temperatures[57] are required to further hydrogenate GVL to PD or MTHF. Homogeneous systems have also been recently investigated for PD and MTHF production. Horváth et al. reported on the total conversion of levulinic acid and the formation of GVL (37%) and 1,4-pentanediol (63%) with a $Ru(acac)_3/PBu_3$ catalyst.[57] Leitner et al. also studied use of homogeneous Ru catalysts for the conversion of LA hydrogenation to PD and MTHF via GVL.[59] A PD yield of 95% was obtained with $Ru(acac)_3$/triphos , while the same catalyst system in the presence of acidic ionic liquids gave MTHF in a 92% yield at 433 K and 100 bar $H_2$ .

### 1.7 LA to Pentenoic and Pentanoic acid

Pentanoic acid (PA) can be obtained by ring-opening of GVL to give pentenoic acid (PEA) followed by hydrogenation. PEA are also interesting platform molecules, for which other routes to cellulosic biofuels have been reported as well, e.g. via decarboxylation to butenes followed by oligomerization to C8+ alkenes (Scheme 1.1).[48, 49] While both approaches mentioned above report promising value chains, the hydrodeoxygenation of LA to PA (or PEA) and further conversion of these platform molecules to, for example, biofuels has only been limitedly explored.

PA has been prepared via a two-step strategy involving the hydrogenation of LA to GVL, followed by a separate second conversion step of GVL to PA. The second step was

achieved over a bifunctional metal-acid Pt/ZSM5 catalyst at elevated temperature of 523 K and 10 bar by Lange et al.[49] A PA selectivity of 83% was obtained at 62% GVL conversion. Notably, the Pt/ZSM5 catalyst could be run for more than 1500 h time on stream, requiring only intermittent regenerations by hot $H_2$ and/or an airflow at 673 K.[49] Dumesic et al. reported on a similar strategy using a bifunctional $Pd/Nb_2O_5$ catalyst for the GVL to PA step. A high PA yield of 92% was reported at 598 K, 35 bar in 50 wt% water.[18] Zaccheria et al. showed that the direct conversion of GVL into pentyl pentanoate is possible over $Cu/SiO_2$-$ZrO_2$ using pentanol as solvent, giving 83% selectivity at 90% conversion.[99] While the two-step conversion has been (limitedly) explored, the direct conversion of LA to PA and the required interplay between the acid and metal functionality had at the start of the work reported here not yet been reported; direct conversion would be desirable from a process intensification point of view, however.

The increase in carbon chain length and reduction in oxygen content that is required for upgrading PA and its derivatives for fuel application also be achieved by ketonization, as shown by Dumesic and co-workers.[18] Drop-in fuels could thus be produced via a few additional steps. First, PA can be nearly quantitative converted to 5-nonanone via ketonization. A dual-bed reactor was used for conversion of 50 wt% GVL in water to 5-nonanone via PA, and an overall 5-nonanone yield of 84% was achieved.[18] Other options for upgrading of 5-nonanone to fuels include its conversion to nonane, which can be used as a fuel additive for diesel, with metal and acid catalysts.[50] Nonane can be isomerized over zeolites to a gasoline mixture of branched C9 alkanes;[50] Finally, 5-nonanone can be hydrogenated to 5-nonanol, which can be dehydrated to a mixture of C9 olefins. Oligomerization of these olefins over acid catalysts, such as Amberlyst-70, gave C18-C27 olefins that can be used as diesel fuel.[68]

PEA can be converted to fuels by an acid-catalyzed decarboxylation to give butene and $CO_2$.[48, 100, 101] Over silica-alumina as solid acid, a butene yield of 99% was achieved from an aqueous solution of GVL at 648 K and 35 bar. After separation of any butane from the product mixture, butenes formed could be further oligomerized to C8+ olefins over solid acids, such as Amberlyst-70 or ZSM-5. More than 90% yield was achieved with Amberlyst-70 at 423-443 K and high pressures, which favor butene

oligomerization. Guo et al. [102] reported on the production of aromatic hydrocarbons from GVL over the porous materials MCM-41 and H-ZSM5 through a related pathway. Over 55% aromatics, for example, benzene, toluene and xylene, were attained at 773 K. The GVL to aromatics route is thought to involve PEA formation, followed by butene production via decarbonylation and decarboxylation; the aromatics are finally formed by isomerization and aromatization at high reaction temperature.

### 1.8 LA Hydrodeoxygenation and Catalyst Deactivation

LA hydrodeoxygenation reactions, be it to GVL or to deeper HDO products, such as MTHF or PA, pose considerable challenges to catalyst stability. Indeed, the use of an acidic substrate (the $pK_a$ of LA is 4.59)[103] at elevated temperatures provides a harsh environment for (supported) catalyst materials. The severity of the reaction furthermore depends on the concentration of LA and the choice of solvent, with reactions run in neat LA presenting the extreme end of the spectrum. In addition, formic acid is co-produced with LA in sugar dehydration/rehydration processes that make use of strong acids, such as $H_2SO_4$, which are in turn also invariably present in the resulting product stream. Such reaction media at high temperature can therefore cause corrosion of reaction equipment as well as result in the disintegration of the support material and in leaching of the supported metals from the catalyst material. Catalyst stability is therefore a major concern and should be studied with the same emphasis as is given to activity and selectivity. Indeed, leaching of the support under reaction solution has been noted. Alumina and silica-alumina suffered from leaching or even dissolved into the pure LA.[49] Dumesic et al. also reported on the severity of the conditions, pointing at extensive corrosion of the stainless steel reactors resulting in relatively high concentrations of metal ions, such Fe, Ni, Cr, Co, and Mo, in solution. The leached metals were, however, not able to catalyze LA conversion, nor did they influence the stability or performance of a RuRe catalyst much.[82] Schlaf et al. actually aimed to make use of active metal species on the reactor walls of 316 stainless steel reactions vessels and use them as catalysts for LA hydrogenation.[104] Exposing the reactor to aqueous solutions of triflic acid under reducing conditions is proposed to generate an active metal surface on the reactor wall by etching away the passivating chromium oxide layer. Although quantitative yields of GVL were obtained in heated

aqueous solution of LA with 55 bar $H_2$ after 24 h, such on purpose corrosion could lead to a high cost for reactors.

Reversible or irreversible inhibition of the catalysts by impurities present in the LA feed can also be a major cause of catalyst deactivation. Ru/C, which has been widely investigated in the hydrogenation of pure LA, was shown, for instance, to be rapidly deactivated in the presence of $H_2SO_4$.[82] Sulfur species originating from the sulfuric acid, expected to be present as an impurity as a result of the acid-catalyzed carbohydrate hydrolysis process to produce LA, are thought to poison the metal catalyst.[90] Additionally, formic acid poisoning of Ru/C was evidenced in the FA/LA transfer hydrogenation to GVL.[87] The details of such deactivation processes have only been (too) limitedly studied, however, and only a few solutions have been presented. For example, as efficient separation of $H_2SO_4$ and LA prior to hydrogenation is required, approaches for phase extraction of LA from the aqueous phase containing $H_2SO_4$ have been proposed.[91, 92, 105] Alternatively, the stabilization of a Ru/C catalyst under these acidic conditions by introducing a second metal (Sn or Re) has been proposed by Dumesic and co-workers.[82, 88, 89]

The structural changes to the support, either by a phase change of even dissolution, have also been reported to cause catalyst instability and deactivation. In the $Pd/Nb_2O_5$-catalyzed upgrading of GVL to PA,[18] it was noted for instance that the niobia support deactivated with time on steam owing to poor hydrothermal stability. The niobia was found to lose surface area as a result of a transformation from an amorphous to a crystalline structure at high reaction temperature.[18] Catalyst deactivation can also originate from blocking of active sites by coke deposition, which leads to lower catalyst activity over time. If this is the major cause of deactivation, the catalyst material's activity can typically be restored by a simple coke burn-off, if the thermal stability of the catalyst support allows such a decoking procedure. Shell researchers,[106] for instance, showed that the deactivation of 0.8% $Pt/SiO_2$, exemplified by a drop in GVL effluent composition from 86% to 26% over 460 h on stream, could be attributed to gradual coke build-up, as regeneration of the catalyst by calcination in air was sufficient to regain the initial activity. Under the applied conditions, AL was proposed to be mainly responsible for the observed coke formation.[18, 64, 103] It should be noted in

this respect that the carbon supports that are often used (with Ru/C being the most studied LA to GVL catalyst) are actually not suited for such a decoking procedure. Indeed, Lange et al. noted that carbon supports were not suited for long-term continuous operation, as the support would not survive multiple regeneration steps.[49] Instead, preference was given to $SiO_2$, $TiO_2$ and $ZrO_2$ as supports given their resistance to frequent regeneration processes and acidic media at high temperature. More research is needed, however, to get more insight into the structural stability of supported metal catalysts under the rather severe conditions required for LA HDO as well as into the various modes of catalyst deactivation.

## 1.9 Aim and Outline of the PhD Thesis

The work presented and discussed in this PhD thesis focuses on the synthesis, characterization and use of supported (bifunctional) metal catalysts for the hydrodeoxygenation (HDO) of levulinic acid (LA) in the presence of $H_2$. The aim of this work is to elucidate the various factors controlling the catalyst activity, selectivity and deactivation, leading to structure-activity relationships for the various pathways available in the LA HDO platform, as depicted in Fig. 1.2. This entails an improved understanding of how the choice of metal and support and the influence of process parameters, determines the outcome of the LA HDO process. Based on these insights, new heterogeneous catalysts have been developed for the efficient conversion of LA to GVL and for the one-pot conversion of LA to PA. Extensive characterization studies provided insight into the main causes of deactivation and provide guidelines for improvements in catalyst stability.

In **Chapter 2**, the LA HDO performance of different Ru-based catalysts with supports of varying acidity, prepared by a wet impregnation method, is compared. The catalysts are tested in different solvents to assess stability under increasingly harsh conditions. The first example of the one-pot conversion of LA to PA is presented over a bifunctional zeolite-supported Ru catalysts. Catalyst deactivation is shown to be mainly caused by dealumination of the zeolite material. As such, the influence of support and solvent on LA HDO reactions is identified.

The cause of the gradual deactivation of the zeolite-supported Ru catalysts that is observed in Chapter 2 and was linked to loss of acidity of the support, is studied in more detail in **Chapter 3**. In this chapter, a detailed description is given of the changes in aluminum speciation and related deactivation, as investigated by a combined Fourier transform infrared (FT-IR) and $^{27}Al$ magic angle spinning (MAS) nuclear magnetic resonance (NMR) study.

**Chapter 4** presents a study of the influence of the cation form of ZSM5, ruthenium precursor and Si/Al ratio of ZSM5 on the metal dispersion and acidity, which further affects the catalysts' performance in the one-pot conversion of LA to PA. The metal dispersion and location as well as acidity of the support material are optimized. A highly active, bifunctional 1wt% Ru/H-ZSM5 catalyst was developed, showing a substantially improved yield of PA.

**Chapter 5** focuses on the development of new catalysts for the conversion of LA to GVL. Variation of the catalyst preparation methodology as well as the exploration of bimetallic nano-alloys resulted in the development and use of highly active, selective and stable catalysts for this conversion. Extensive characterization using scanning transmission electron microscopy (STEM), X-ray absorption spectroscopy (XAS), X-ray photoelectron spectroscopy (XPS), and FT-IR of CO adsorption provided insight into the structure-activity relationships for these systems.

Finally, **Chapter 6** gives a summary of the most important results described in this PhD thesis, together with some concluding remarks and a future perspective.

**References**


[1] A. Corma, S. Iborra, and A. Velty, Chem. Rev. 107 (2007) 2411-2502.

[2] M. Poliakoff, and P. Licence, Nature 450 (2007) 810-812.

[3] G.W. Huber, S. Iborra, and A. Corma, Chem. Rev. 106 (2006) 4044-4098.

[4] L. Petrus, and M.A. Noordermeer, Green Chem. 8 (2006) 861-867.

[5] R.A. Sheldon, Catal. Today 167 (2011) 3-13.

[6] J.N. Chheda, G.W. Huber, and J.A. Dumesic, Angew. Chem. Int. Ed. 46 (2007) 7164-7183.

[7] H. Kopetz, Nature 494 (2013) 29-31.

[8] J.C. Serrano-Ruiz, R.M. West, and J.A. Dumesic, Annu. Rev. Chem. Biomol. Eng. 1 (2010) 79-100.

[9] O. Edenhofer, R. Pichs-Madruga, Y. Sokona, K. Seyboth, S. Kadner, T. Zwickel, P. Eickemeier, G. Hansen, S. Schlömer, C.v. Stechow, and P. Matschoss, IPCC Special Report on Renewable Energy Sources and Climate Change Mitigation, Cambridge University Press, Cambridge, UK and NY, USA (2011).

[10] D.M. Alonso, S.G. Wettstein, and J.A. Dumesic, Green Chem. 15 (2013) 584-595.

[11] http://www.nrel.gov/biomass/biorefinery.html.

[12] N. Mosier, C. Wyman, B. Dale, R. Elander, Y.Y. Lee, M. Holtzapple, and M. Ladisch, Bioresour. Technol. 96 (2005) 673-686.

[13] R. Rinaldi, and F. Schüth, ChemSusChem 2 (2009) 1096-1107.

[14] P. Gallezot, Chem. Soc. Rev. 41 (2012) 1538-1558.

[15] J.J. Bozell, and G.R. Petersen, Green Chem. 12 (2010) 539-554.

[16] R.-J. van Putten, J.C. van der Waal, E. de Jong, C.B. Rasrendra, H.J. Heeres, and J.G. de Vries, Chem. Rev. 113 (2013) 1499-1597.

[17] J.C. Serrano-Ruiz, R. Luque, and A. Sepulveda-Escribano, Chem. Soc. Rev. 40 (2011) 5266-5281.

[18] J.C. Serrano-Ruiz, D. Wang, and J.A. Dumesic, Green Chem. 12 (2010) 574-577.

[19] B. Girisuta, L.P.B.M. Janssen, and H.J. Heeres, Ind. Eng. Chem. Res. 46 (2007) 1696-1708.

[20] B. Girisuta, L.P.B.M. Janssen, and H.J. Heeres, Chem. Eng. Res. Des. 84 (2006) 339-349.

[21] G.J. Mulder, J. Prakt. Chem. 21 (1840) 203-240.

[22] W.W. Moyer, U.S. Patent No. 2270328 (1942).
[23] L.F. Wiggins, in: W.W. Pigm, and M.L. Wolfro, (Eds.), Advances in Carbohydrate Chemistry, Academic Press. 293-336.
[24] D.W. Rackemann, and W.O.S. Doherty, Biofuels, Bioprod. Biorefin. 5 (2011) 198-214.
[25] B.F. McKenzie, Organic Synthesis(IX). Wiley, New York, 1929.
[26] R.W. Thomas, and H.A. Schuette, J. Am. Chem. Soc. 53 (1931) 2324-2328.
[27] Y. Sumiki, Japanese Patent No. 176438 (1948).
[28] L.J. Carlson, U.S. Patent No. 3065263 (1962).
[29] C.P. Sassenrath, and W.L. Shilling, U.S. Patent No. 3258481 (1966).
[30] A.A. Efremov, G.G. Pervyshina, and B.N. Kuznetsov, Chem. Nat. Compd. 34 (1998) 182-185.
[31] W.A. Farone, and J.E. Cuzens, U.S. Patent No. 6054611 (2000).
[32] A.A. Efremov, G.G. Pervyshina, and B.N. Kuznetsov, Chem. Nat. Compd. 33 (1997) 84-88.
[33] B.C. Redmon, U.S. Patent No. 2738367 (1956).
[34] R.H. Leonard, Ind. Eng. Chem. 48 (1956) 1330-1341.
[35] J. Horvat, B. Klaić, B. Metelko, and V. Šunjić, Tetrahedron Lett. 26 (1985) 2111-2114.
[36] A.P. Dunlop, and P.A. Wells, U.S. Patent No. 2813900 (1957).
[37] V.M. Ghorpade, and M.A. Hanna, U.S. Patent No. 5859263 (1999).
[38] S.W. Fitzpatrick, WO1989010362 (1989).
[39] S.W. Fitzpatrick, U.S. Patent No. 5608105 (1997).
[40] J.J. Bozell, L. Moens, D.C. Elliott, Y. Wang, G.G. Neuenschwander, S.W. Fitzpatrick, R.J. Bilski, and J.L. Jarnefeld, Resour. Conserv. Recycl. 28 (2000) 227-239.
[41] M.H.B. Hayes, Nature 443 (2006) 144-144.
[42] http://greenchemicalsblog.com/2013/10/10/segetis-starts-levulinic-acid-pilot-production/.
[43] http://www.biofuelsdigest.com/biobased/2013/02/27/biofine-technology-the-digests-5-minute-guide/.
[44] V. Pace, P. Hoyos, L. Castoldi, P. Domínguez de María, and A.R. Alcántara, ChemSusChem 5 (2012) 1369-1379.
[45] R.E. Holmen, U.S. Patent No. 3471554 (1969).

[46] D.M. Alonso, J.Q. Bond, and J.A. Dumesic, Green Chem. 12 (2010) 1493-1513.

[47] R. Mao, Q. Zhao, G. Dima, and D. Petraccone, Catal. Lett. 141 (2011) 271-276.

[48] J.Q. Bond, D.M. Alonso, D. Wang, R.M. West, and J.A. Dumesic, Science 327 (2010) 1110-1114.

[49] J.-P. Lange, R. Price, P.M. Ayoub, J. Louis, L. Petrus, L. Clarke, and H. Gosselink, Angew. Chem. Int. Ed. 49 (2010) 4479-4483.

[50] J.C. Serrano-Ruiz, D.J. Braden, R.M. West, and J.A. Dumesic, Appl. Catal. B: Environ. 100 (2010) 184-189.

[51] http://www1.eere.energy.gov/bioenergy/pdfs/35523.pdf.

[52] I.T. Horvath, H. Mehdi, V. Fabos, L. Boda, and L.T. Mika, Green Chem. 10 (2008) 238-242.

[53] J.J. Thomas, and R.G. Barile, Energy Biomass Wastes, 8 (1984), 1461–1494.

[54] T.W. Rudolph, and J.J. Thomas, Biomass 16 (1988) 33-49.

[55] http://www.afdc.energy.gov/afdc/fuels/emerging_pseries.html

[56] S.W. Fitzpatrick, in *Feedstocks for the Future: Renewables for the Production of Chemicals and Materials*, ed. J.J. Bozell, and M.K. Patel, Am. Chem. Soc., Washington, DC, 921 (2006) 271-287.

[57] H. Mehdi, V. Fábos, R. Tuba, A. Bodor, L. Mika, and I. Horváth, Top. Catal. 48 (2008) 49-54.

[58] D.C. Elliott, and J.G. Frye, U.S. Patent No. 5883266 (1999).

[59] F.M.A. Geilen, B. Engendahl, A. Harwardt, W. Marquardt, J. Klankermayer, and W. Leitner, Angew. Chem. Int. Ed. 122 (2010) 5642-5646.

[60] http://en.wikipedia.org/wiki/Pentanoic_acid.

[61] D.J. Hayes, Catal. Today 145 (2009) 138-151.

[62] W.R.H. Wright, and R. Palkovits, ChemSusChem 5 (2012) 1657-1667.

[63] Z.-p. Yan, L. Lin, and S. Liu, Energy Fuels 23 (2009) 3853-3858.

[64] M. Kitano, F. Tanimoto, and M. Okabashi, Chem. Econ. Eng. Rev. 7 (1975) 25-29.

[65] M. Balat, Energ. Source 27 (2005) 569-577.

[66] Y. Kar, and H. Deveci, Energ. Source, Part A 28 (2006) 909-921.

[67] J.-P. Lange, and P.M. Ayoub, WO2008142127 (2008).

[68] D.M. Alonso, J.Q. Bond, J.C. Serrano-Ruiz, and J.A. Dumesic, Green Chem. 12 (2010) 992-999.

[69] F.M.A. Geilen, B. Engendahl, M. Hölscher, J. Klankermayer, and W. Leitner, J. Am. Chem. Soc. 133 (2011) 14349-14358.

[70] A.P. Dunlop, and J.W. Madden, U.S. Patent No. 2786852 (1957).

[71] P.P. Upare, J.-M. Lee, D.W. Hwang, S.B. Halligudi, Y.K. Hwang, and J.-S. Chang, J. Ind. Eng. Chem. 17 (2011) 287-292.

[72] H.A. Schuette, and R.W. Thomas, J. Am. Chem. Soc. 52 (1930) 3010-3012.

[73] R.V. Christian, H.D. Brown, and R.M. Hixon, J. Am. Chem. Soc. 69 (1947) 1961-1963.

[74] H.S. Broadbent, G.C. Campbell, W.J. Bartley, and J.H. Johnson, J. Org. Chem. 24 (1959) 1847-1854.

[75] L.E. Manzer, Appl. Catal. A: Gen. 272 (2004) 249-256.

[76] L.E. Manzer, WO2002074760A1 (2002).

[77] M.G. Al-Shaal, W.R.H. Wright, and R. Palkovits, Green Chem. 14 (2012) 1260-1263.

[78] H. Heeres, R. Handana, D. Chunai, C. Borromeus Rasrendra, B. Girisuta, and H. Jan Heeres, Green Chem. 11 (2009) 1247-1255.

[79] A. Primo, P. Concepcion, and A. Corma, Chem. Commun. 47 (2011) 3613-3615.

[80] O.A. Abdelrahman, A. Heyden, and J.Q. Bond, ACS Catal. 4 (2014) 1171-1181.

[81] A.M.R. Galletti, C. Antonetti, V. De Luise, and M. Martinelli, Green Chem. 14 (2012) 688-694.

[82] D.J. Braden, C.A. Henao, J. Heltzel, C.C. Maravelias, and J.A. Dumesic, Green Chem. 13 (2011) 1755-1765.

[83] S.G. Wettstein, J.Q. Bond, D.M. Alonso, H.N. Pham, A.K. Datye, and J.A. Dumesic, Appl. Catal. B: Environ. 117–118 (2012) 321-329.

[84] L.E. Manzer, and K.W. Hutchenson, U.S. Patent No. 20040254384A1 (2004).

[85] R.A. Bourne, J.G. Stevens, J. Ke, and M. Poliakoff, Chem. Commun. (2007) 4632-4634.

[86] L. Deng, J. Li, D.-M. Lai, Y. Fu, and Q.-X. Guo, Angew. Chem. Int. Ed. 121 (2009) 6651-6654.

[87] L. Deng, Y. Zhao, J. Li, Y. Fu, B. Liao, and Q.-X. Guo, ChemSusChem 3 (2010) 1172-1175.

[88] D.M. Alonso, S.G. Wettstein, J.Q. Bond, T.W. Root, and J.A. Dumesic, ChemSusChem 4 (2011) 1078-1081.

[89] S. Murat Sen, C.A. Henao, D.J. Braden, J.A. Dumesic, and C.T. Maravelias, Chem. Eng. Sci. 67 (2012) 57-67.

[90] X.-L. Du, L. He, S. Zhao, Y.-M. Liu, Y. Cao, H.-Y. He, and K.-N. Fan, Angew. Chem. Int. Ed. 50 (2011) 7815-7819.

[91] X.-L. Du, Q.-Y. Bi, Y.-M. Liu, Y. Cao, and K.-N. Fan, ChemSusChem 4 (2011) 1838-1843.

[92] E.I. Gürbüz, D.M. Alonso, J.Q. Bond, and J.A. Dumesic, ChemSusChem 4 (2011) 357-361.

[93] P.P. Upare , J.-M. Lee, Y.K. Hwang , D.W. Hwang, J.-H. Lee, S.B. Halligudi, J.-S. Hwang, and J.-S. Chang, ChemSusChem 4 (2011) 1749-1752.

[94] A.M. Hengne, and C.V. Rode, Green Chem. 14 (2012) 1064-1072.

[95] K. Folkers, and H. Adkins, J. Am. Chem. Soc. 54 (1932) 1145-1154.

[96] X.-L. Du, Q.-Y. Bi, Y.-M. Liu, Y. Cao, H.-Y. He, and K.-N. Fan, Green Chem. 14 (2012) 935-939.

[97] L. Corbel-Demailly, B.-K. Ly, D.-P. Minh, B. Tapin, C. Especel, F. Epron, A. Cabiac, E. Guillon, M. Besson, and C. Pinel, ChemSusChem 6 (2013) 2388-2395.

[98] M.G. Al-Shaal, A. Dzierbinski, and R. Palkovits, Green Chem. 16 (2014) 1358-1364.

[99] C.E. Chan-Thaw, M. Marelli, R. Psaro, N. Ravasio, and F. Zaccheria, RSC Adv. 3 (2013) 1302-1306.

[100] J.Q. Bond, D.M. Alonso, R.M. West, and J.A. Dumesic, Langmuir 26 (2010) 16291-16298.

[101] J.Q. Bond, D. Wang, D.M. Alonso, and J.A. Dumesic, J. Catal. 281 (2011) 290-299.

[102] Y. Zhao, Y. Fu, and Q.-X. Guo, Bioresour. Technol. 114 (2012) 740-744.

[103] B. V. Timokhin, V. A. Baransky, and G. D. Eliseeva, Russ. Chem. Rev. 68 (1999) 73-84.

[104] D. Di Mondo, D. Ashok, F. Waldie, N. Schrier, M. Morrison, and M. Schlaf, ACS Catal. 1 (2011) 355-364.

[105] P.M. Ayoub, WO2005070867 (2005).

[106] P.M. Ayoub, and J.-P. Lange, WO2008142127 (2008).

# Chapter 2

# Ruthenium-Catalyzed Hydrogenation of Levulinic Acid: Influence of the Support and Solvent on Selectivity and Stability

**Abstract**

The catalytic performance of 1 wt% Ru-based catalysts in the hydrogenation of levulinic acid (LA) has been studied at 40 bar $H_2$ and 473 K. This was done by assessing the influence of the support acidity (i.e., $Nb_2O_5$, $TiO_2$, H-β and H-ZSM5) and solvent (i.e., dioxane, 2-ethylhexanoic acid (EHA) and neat LA). The $Ru/TiO_2$ gave excellent selectivity to GVL (97.5%) at 100% conversion and was remarkably stable even under severe reaction conditions. Ru/H-ZSM5 showed a 45.8% yield of pentanoic acid (PA) and its esters in dioxane, which is the first example of this one-pot conversion directly from LA at 473 K. The gradual deactivation of zeolite-supported catalysts in EHA and neat LA was mainly caused by dealumination, as confirmed by $^{27}Al$ magic angle spinning (MAS) nuclear magnetic resonance (NMR). Coke build-up originated from angelicalactone and, remarkably, occured preferentially in the zigzag channels of H-ZSM-5 as shown by systematic shifts in the XRD patterns. The GVL ring-opening step is considered to be the rate-determining step on the pathway to PA, necessitating an acidic support.

Based on: Luo W., Deka U., Beale A.M., van Eck E.R.H., Bruijnincx P.C.A., Weckhuysen B.M., J. Catal. 301 (2013) 175-186.

## 2.1 Introduction

Levulinic acid (LA) has been identified as a promising, sustainable platform molecule as it can be produced easily and economically from lignocellulosic biomass via a simple and robust hydrolysis process.[1-3] LA can be further converted into many valuable derivatives of which the conversion to γ-valerolactone (GVL) has been studied most. GVL can find use as a renewable solvent, fuel additive or can be subsequently converted into a whole slate of valuable chemicals, such as 1,4-pentanediol (PD), methyltetrahydrofuran (MTHF), pentenoic acid (PEA), pentanoic acid (PA) or its esters (PE).[4-6] The various routes to value-added chemicals and fuel components from LA by sequential hydrogenation, (de)hydration and hydrogenolysis reactions is depicted in Scheme 2.1. LA can be converted to GVL via either dehydration to angelicalactone (AL) followed by reduction or via reduction to 4-hydroxypentanoic acid (4-HPA) and subsequent dehydration. These reactions are generally performed at a moderate reaction temperature in the range of 298 to 523 K with hydrogen pressures from 1 to 150 bar. Many examples of commercial heterogeneous ruthenium catalysts on neutral supports, mostly Ru/C, were reported to catalyze the conversion of LA into GVL in different solvents, such as water,[7] alcohols,[8, 9] dioxane,[10] and supercritical $CO_2$.[11] Less attention has been devoted to the second part of Scheme 2.1, in which GVL is further converted to the depicted deeper hydrogenation products. GVL can, for instance, be further reduced to 1,4-pentanediol (PD) and subsequently dehydrated to MTHF [4], a process for which high yields were reported over a PtRe/C catalyst.[12]

Recently, two new directions have been proposed for the valorization of LA via the alternative PEA pathway. Lange et al. [6] reported on the production of so-called valeric (pentanoic) biofuels, via Pt/$TiO_2$-catalyzed LA hydrogenation to GVL, followed by GVL hydrogenation to PA over Pt/H-ZSM-5 and finally esterification to give the desired pentanoic acid esters (PE). Related to this are two patents by the Shell laboratories in which a two-step process of LA to GVL followed by GVL to PA conversion is described. A 70 % yield of PA was in this case achieved with a Pt/H-ZSM-5/$SiO_2$ catalyst.[13] PA and PE could also be obtained in 62 % yield in a direct one-pot reaction from ethyl levulinate over a Ru/H-β/silica catalyst.[14]

The Dumesic group, on the other hand, has shown that GVL can be converted to PA over a bifunctional metal/acid catalyst, e.g. $Pd/Nb_2O_5$, after which PA can be upgraded to 5-nonanone by ketonization.[7] In both approaches, a combination of acid functionality and hydrogenation function is sought to reduce the oxygen content and produce better suited fuel components by ring opening, dehydration or hydrogenation. Alternatively, Dumesic and coworkers also reported an integrated strategy for the production of $C_{8+}$ alkenes via GVL ring opening to PEA, followed by decarboxylation and oligomerization of the obtained butenes.[15] This ring-opening/decarboxylation sequence does not require hydrogen and is catalyzed by an acidic catalyst, $SiO_2/Al_2O_3$, in the absence of a metal hydrogenation function.[16]

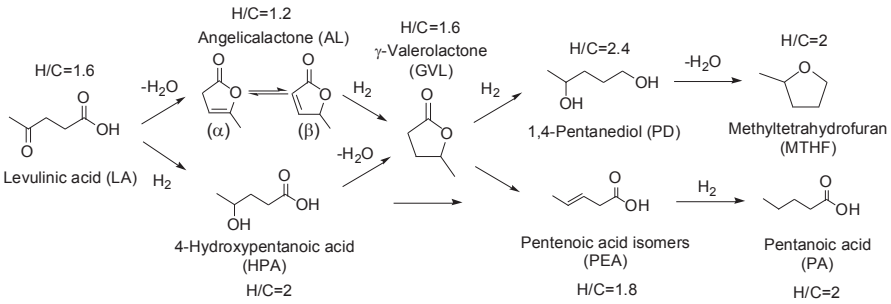


Scheme 2.1. Hydrogenation platform of levulinic acid (H/C: hydrogen-to-carbon ratio of each compound).

Indeed, many examples of heterogeneous catalysts are now available for the selective conversion of LA to GVL, most of which use a hydrogenating metal (preferably ruthenium) on a neutral support, usually under dilute and mild solvent conditions. Furthermore, the Shell and Dumesic examples of using a metal on an acidic support for the ring-opening/hydrogenation of GVL to PA show the potential of the PEA pathway for the valorization of levulinic acid. Building on these promising results, the direct, one-pot reaction of LA to PA, without isolation of the GVL intermediate, would be desired to further simplify the process. To achieve this, more insight is required into the influence of the support, in particular the role of support acidity, on selectivity in LA hydrogenation. In addition, the stability of the catalyst, both of the metal component as well as the support, should be assessed under the harsh conditions that can be expected for a highly polar and corrosive LA conversion process. Here, we present the activity,

selectivity and stability of four 1 wt% ruthenium catalysts on non-acidic ($Nb_2O_5$ and $TiO_2$) and strongly acidic (H-ZSM5 and H-β) supports in the hydrogenation of LA under increasingly harsh conditions, using dioxane, 2-ethylhexanoic acid and neat LA as solvents. It was found that zeolite-supported catalysts are capable of the direct synthesis of PA from LA in a one-pot reaction without isolation of the intermediate GVL. An extensive characterization study of the fresh and spent catalysts provided insight into the stability and related deactivation of the catalyst materials under investigation.

## 2.2 Experimental Section

### 2.2.1 Catalyst Preparation

Four 1 wt% Ru catalysts on supports of different acidity were prepared. The supports were treated as follows before wet impregnation: $TiO_2$ (P25, Evonik) was dried at 393 K for 4 h; $Nb_2O_5$ was obtained by calcination of niobic acid (HY-340, CBMM) at 673 K for 4 h under air flow with a temperature ramp of 10 K/min; H-ZSM5 and H-β (H-ZSM5: CBV2314, Si/Al=11.5; H-β: CP814E, Si/Al=12.5, Zeolyst) were converted into the H-form by heating the samples at 1 K/min to 393 K for 1 h and at 2 K/min to 823 K for 4 h. The 1 wt% supported ruthenium catalysts were prepared by wet impregnation using aqueous solutions of ruthenium nitrosyl nitrate ($RuNO(NO_3)_3$, Alfa Aesar). After evaporation of the water, the catalysts were dried at 333 K over-night, calcined at 723 K for 4 h with a heating ramp 2 K/min under $N_2$ (100 mL/min), followed by reduction at 673 K, for 6 h, under $H_2$ flow (80 mL/min).

### 2.2.2 Catalyst Characterization

#### 2.2.2.1 Temperature-Programmed Desorption of $NH_3$

Catalyst acidity was investigated by temperature-programmed desorption (TPD) of $NH_3$ under He flow (25 mL/min) using a Micromeritics AutoChem II equipped with a TCD detector. 0.15 to 0.2 g of catalyst was loaded and dried at 873 K for 1 h, after which the sample was cooled down to 373 K. Subsequently, pulses of ammonia were introduced up to saturation of the sample. The temperature-programmed desorption was

performed up to 873 K, with a heating ramp of 5 K/min. The total number of acid sites (mmol $NH_3$/gram zeolite) was determined from the total amount of desorbed ammonia.

#### 2.2.2.2 $N_2$ Physisorption

$N_2$ physisorption isotherms were recorded to determine surface areas and pore volumes using a Micromeritics Tristar 3000 set-up operating at 77 K. All samples were outgassed for 12 h at 473 K in a nitrogen flow prior to the physisorption measurements. BET surface areas were determined using 10 points between 0.06 and 0.25. Micropore volumes ($cm^3$/g) were determined by *t*-plot analysis for $t$ between 3.5 and 5.0 Å to ensure inclusion of the minimum required pressure points.

#### 2.2.2.3 Atomic Absorption Spectrophotometry

The liquid phase was tested after reaction by flame atomic absorption spectrophotometry (AAS) for the presence of Ru, and Si. All elements (Ru, Si, Fe and Cr) were analyzed on a ContrAA 700 apparatus using the following conditions: Ru: 349.9 nm (air/acetylene flame); Si: 251.6 nm ($N_2O$/acetylene flame); Fe: 248.3 nm (air/acetylene flame); Cr: 357.9 nm ($N_2O$/acetylene flame).

#### 2.2.2.4 Thermal Gravimetric Analysis

Thermal gravimetric analysis (TGA) has been coupled to mass spectrometry (MS), to evaluate the spent catalysts, was performed with a Perkin–Elmer Pyris 1 apparatus. The sample was initially heated to 423 K for 1 h with a temperature ramp of 10 K/min in a 20 mL/min flow of argon to exclude physisorbed water and acetone, followed by a ramp of 5 K/min to 873 K in a 10 mL/min flow of oxygen to burn off the coke. Analysis was performed with a quadrupole Pfeiffer Omnistar mass spectrometer, which was connected to the outlet of the TGA apparatus. Ion currents were recorded for $m/z$ values of 18 and 44.

#### 2.2.2.5 Transmission Electron Microscopy

Transmission electron microscopy (TEM) measurements in bright field mode were conducted with a Tecnai 20FEG microscope operating at 200 kV. The ruthenium particle diameters counted from more than 200 particles for each sample were measured using iTEM software (soft Imaging System GmbH). For non-symmetrical particle shapes, both the largest and shortest diameter was measured to obtain an average value.

#### 2.2.2.6 X-Ray Diffraction

Powder X-ray diffraction (XRD) patterns were measured with a Bruker D2 and D8 Advance powder X-ray diffractometer equipped with automatic divergence slits, a Vantec detector and a cobalt $K\alpha_{1,2}$ ($\lambda$ = 1.78897/1.79026 Å) source. Diffraction patterns were collected between 5-40 or 5-55 2θ (deg) with an increment of 0.017 (in 2θ) and an acquisition time of 1 second per step. Unit cell parameters on Ru/H-ZSM5 samples were obtained by performing Le Bail extractions between 5-29 2θ (deg) using the Rietica LHPM package. Background corrections on all patterns were performed using a 5th order polynomial. The peak profile parameters were calculated using a pseudo-Voigt function. The initial lattice parameters were taken from the IZA database (www.iza-structure/database) for the MFI framework. Silicon (NBS 640) was used as an internal standard, physically mixed with the powdered samples in each measurement. To account for 2θ shifts caused by instrumental errors, i.e. sample height or displacement, the Si (111) reflection was centered at 33.149 2θ for all patterns before performing any analysis.

#### 2.2.2.7 Infrared Spectroscopy

Fourier transform infrared (FT-IR) spectra were recorded on a Perkin-Elmer 2000 instrument after pyridine desorption at various temperatures. Self-supported catalyst wafers (12-19 mg/16 mm) were pressed at 3 ton bar pressure for 10 s. The wafer was placed inside a synchrotron cell with a $CaF_2$ window. The cell was evacuated to $10^{-6}$ bar followed by drying of the sample at 573 K (3 K/min) for 1 h. The cell was cooled down to 323 K and the sample was brought into contact with pyridine vapors (3.1 mbar) for

10 s, kept for 30 min reaching equilibrium, and followed by vacuum for 30 min in order to remove physisorbed and loosely bound pyridine. FT-IR spectra were recorded under vacuum at different temperature (3 K/min) from 323 to 723 K. For each spectrum, 25 scans were recorded with a resolution of 4 $cm^{-1}$.

#### 2.2.2.8 Nuclear Magnetic Resonance

$^{27}Al$ magic angle spinning (MAS) nuclear magnetic resonance (NMR) measurements were performed on a 600 MHz Varian solid state NMR spectrometer using a 1.6 mm T3 design probe. The probe was tuned to 599.99 MHz for protons and 156.341 MHz for $^{27}Al$. Magic angle spinning at 25 kHz was employed. All samples were weighed to enable quantitative measurements. $T_1$ saturation recovery experiments showed that a repetition time of 0.4 s was more than sufficient for all magnetization to relax back to Boltzmann equilibrium. To ensure that intensities are quantitative regardless of the quadrupole coupling constant,[17] the single pulse measurements were done using an radio frequency (rf)-field strength of 10 kHz and a pulse length of 2 μs, (equaling a tip angle of 7 degrees). Proton decoupling did not improve spectral quality in the one-dimensional (1D) experiments. Care was taken to subtract the small background signal from the MAS rotor, prior to integration of the spectra. Intensities were also corrected for the presence of a small amount of satellite sideband intensity that overlaps with the central transition signal by reducing the intensity by an amount equal to the intensity of the ± 1 sideband, however, this did not change relative intensities significantly.

Relative amounts of aluminum were obtained by integrating the 1D spectra. The limits of integration were determined with triple-quantum (3Q) MAS spectra (see Appendix A, Fig. S9 for an example) and set to a range from -20 to 8 ppm for octahedral aluminum (Al(VI)), 8 to 41 ppm for penta-coordinated aluminum (Al(V)) and 41 to 70 ppm for tetrahedral aluminum (Al(IV)) for Ru/H-β. For both Ru/H-ZSM5 samples only a trace amount of Al(V) was detected in the 3QMAS, while the Al(IV) signal extended down to 20 ppm. Hence, integration limits were set from -20 to 20 ppm for Al(VI) and 20 to 70 ppm for Al(IV) for these samples.

### 2.2.3 Catalyst Testing

In a typical reaction, the batch autoclave reactor was loaded with catalyst, substrate and solvent, purged three times with argon after which the reaction mixture was heated to reaction temperature and charged with $H_2$ to 40 bar. This was taken as the starting point of the reaction. After the reaction was cooled to room temperature, the $H_2$ was released and 2 wt% anisole was added as internal standard. The catalyst was separated by centrifugation, filtration and finally washed with acetone. The reaction products were analyzed using a Shimadzu GC-2010A gas chromatograph equipped with a CP-WAX 57-CB column (25 m × 0.2 mm × 0.2 μm) and flame ionization detector (FID). Products were identified with a GC–MS from Shimadzu with a CP-WAX 57CB column (30 m × 0.2 mm × 0.2 μm). The gas phase reaction products were analyzed by an online dual channel Varian CP4900 micro-GC equipped with a $CO_X$ column and thermal conductivity detector (TCD), for analysis of $H_2$, $CO_2$, CO and $CH_4$.

Dioxane runs were performed with 10 wt% levulinic acid (2.5 g, 21.5 mmol) in dioxane (22.5 g) over a series of 1 wt% Ru catalysts (0.3 g) containing different supports. The reaction were run in a 50 mL Parr batch autoclave at a temperature of 473 K for 4 h using a hydrogen pressure 40 bar and a stirring speed of 1600 rpm. The 2-ethylhexanoic acid runs were performed with 10 wt% levulinic acid (6.0 g, 51.7 mmol) in 2-ethylhexanoic acid (54 g) with 1 wt% Ru catalysts (0.6 g). The reactions were run in 100 mL Parr batch autoclave at a temperature of 473 K for 10 h using a hydrogen pressure 40 bar and a stirring speed of 1600 rpm. 1 mL of solution was sampled at various intervals during the reaction. Reactions with intermediates GVL (2.2 g, 21.5 mmol) or PEA (2.2 g, 21.5 mmol) in EHA (22.8 g) were conducted with catalysts (0.3 g) in the 50 mL Parr batch autoclave.

Finally, neat LA runs were performed with LA (20 g, 172 mmol) over 1 wt% Ru catalysts (0.3 g or 0.5 g). The reactions were run in a 50 mL Parr batch autoclave at a temperature of 473 K for 4 h and 10 h using a hydrogen pressure 40 bar and a stirring speed of 1600 rpm.

## 2.3 Results and Discussion

### 2.3.1 Catalyst Characterization

The 1 wt% ruthenium catalysts were synthesized by wet impregnation of the $TiO_2$, $Nb_2O_5$, H-ZSM5 (Si/Al = 11.5) and H-β (Si/Al = 12.5) supports. The fresh catalysts were characterized by XRD, TEM, $N_2$ physisorption and $NH_3$-TPD, IR after pyridine adsorption and solid state $^{27}Al$ (1D MAS, 2D 3QMAS) NMR. The bright field TEM images of the fresh catalysts (Appendix A, Fig. S2), show that the average particle sizes of the $Ru/TiO_2$, Ru/H-ZSM5 and Ru/H-β were very similar and around 3.5 nm mean particle size. Unfortunately, the ruthenium particle size of the $Ru/Nb_2O_5$ catalyst could not be determined by TEM due to lack of contrast. No Ru phase could be observed in the XRD diffractograms of the fresh catalysts (Appendix A, Fig. S5).

Table 2.1. Acid concentrations calculated from $NH_3$-TPD

| Catalyst | Total acidity ($mmol/g_{cat}$) | Low T region ($mmol/g_{cat}$) | High T region ($mmol/g_{cat}$) |
|---|---|---|---|
| Ru/H-ZSM5 | 1.35 | 0.93 | 0.42 |
| Ru/H-β | 1.07 | 0.71 | 0.36 |
| $Ru/TiO_2$ | 0.26 | 0.26 | 0 |
| $Ru/Nb_2O_5$ | 0.14 | 0.14 | 0 |

The acid properties, namely the quantity and strength of the acid sites, of the fresh catalysts were determined by $NH_3$-TPD. Table 2.1 lists the total amount of acidic sites of the four catalysts under investigation, as well as a distinction between weak and strong acid sites. Woolery et al. attributed the TPD peak at high temperature to Brønsted acid sites (strong acid) connected with framework Al (FAl) sites and the low temperature peak to extraframework Al species (EFAl), which act as Lewis acid sites (weak acid).[18]

Table 2.2. $N_2$ physisorption data of the fresh and spent catalyst materials under investigation.

| | Catalyst | BET ($m^2/g$) | Micropore surface area ($m^2/g$) | External surface area ($m^2/g$) | Micropore volume ($cm^3/g$) [a] | Coke contents (wt%) [b] |
|---|---|---|---|---|---|---|
| Fresh | $Ru/Nb_2O_5$ | 98 | | 98 | | |
| | $Ru/TiO_2$ | 56 | | 56 | | |
| | Ru/H-β | 515 | 329 | 184 | 0.161 | |
| | Ru/H-ZSM5 | 343 | 258 | 85 | 0.126 | |
| Spent, 4 h in dioxane | $Ru/Nb_2O_5$ | 70 | | 70 | | |
| | $Ru/TiO_2$ | 55 | | 55 | | |
| | Ru/H-β | 436 | 264 | 172 | 0.129 | |
| | Ru/H-ZSM5 | 229 | 182 | 47 | 0.090 | |
| Spent, 10 h in EHA | $Ru/Nb_2O_5$ | 55 | | 55 | | 1.3 |
| | $Ru/TiO_2$ | 54 | | 54 | | 0.8 |
| | Ru/H-β | 478 | 292 | 180 | 0.143 | 3.4 |
| | Ru/H-ZSM5 | 152 | 116 | 36 | 0.057 | 5.5 |
| Spent, 10 h in LA | $Ru/TiO_2$ | 52 | | 52 | | 1.8 |
| | Ru/H-β | 373 | 200 | 172 | 0.098 | 10.7 |

[a] Data obtained by the t-plot method.

[b] Data determined by TGA.

Here, the low and high temperature regions are defined as 373-523 K and 523-673 K, respectively (Appendix A, Fig. S1). The differences in acidity between the different catalysts are evident both from the amount and the strength of the acid sites, with acidity decreasing in the order: Ru/H-ZSM5 > Ru/H-β > $Ru/TiO_2$ > $Ru/Nb_2O_5$. $Ru/TiO_2$ and $Ru/Nb_2O_5$ can therefore be considered as non-acidic catalysts with only a very small amount of Lewis acid sites and their activity and selectivity in the LA hydrogenation be compared with the strongly acidic zeolite-supported Ru/H-ZSM5 and Ru/H-β catalysts, which have both Brønsted and Lewis acid sites in the respective MFI and BEA framework types. The surface areas and pore volumes of the catalysts were determined by $N_2$ physisorption and are listed in Table 2.2. Of the non-acidic catalysts, $Ru/Nb_2O_5$ has a larger surface area than $Ru/TiO_2$, while Ru/H-β has a higher micropore surface and external surface area than Ru/H-ZSM5.

### 2.3.2 Catalytic Reactions in Dioxane

#### 2.3.2.1 Catalyst Performance

The influence of the support on catalytic activity and selectivity was initially screened at 473 K and 40 bar $H_2$ in dioxane as the solvent. The system under study is a three-phase gas-liquid-solid system, consisting of hydrogen gas and an organic phase with the heterogeneous catalyst. The conversion of LA after 30 minutes as a function of the stirring speed is shown in Fig. 2.1. The conversion is essentially independent of the stirrer speed when it is above 900 rpm. To exclude any influence of external mass transfer limitations, reactions were run at different stirrer speeds (Fig. 2.1) and to ensure that the hydrogenation reactions take place in the kinetic regime, all experiments were subsequently run at a stirrer speed of 1600 rpm.

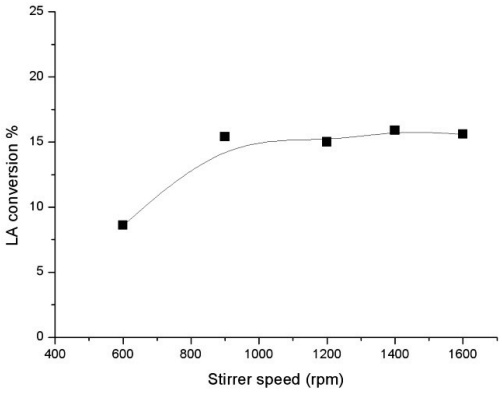


Figure 2.1. Conversion of LA at various agitation rates at 200 °C, 40 bar, with 25 g (20 wt%) LA in dioxane, 0.03 g of 5 wt% Ru/C, 0.5 h.

Fig. 2.2 shows the large differences in selectivity between the four supported catalysts in the hydrogenation of a 10 wt% solution of levulinic acid in dioxane. Full conversion of LA was achieved with all catalysts except for $Ru/Nb_2O_5$. The non-acidic supported catalysts mainly show formation of GVL (yields of 61.8% for $Ru/Nb_2O_5$ and 92.3% for $Ru/TiO_2$) with minor amounts of MTHF (2.6% for $Ru/Nb_2O_5$ and 2.3% for $Ru/TiO_2$) and PD (1.7% for $Ru/TiO_2$), with mass balances of 92.0 and 96.3% for $Ru/Nb_2O_5$ and $Ru/TiO_2$, respectively. Trace amounts (< 0.1%) of AL (α and β), but no 4-HPA were

detected at the beginning of the reaction (i.e. at low LA conversion levels) with all four catalysts. $Ru/TiO_2$ showed the highest GVL yield of 92.3% (selectivity = 95.8%) under these conditions.

These results are comparable to previously reported GVL yields over $Ru/TiO_2$ catalysts in various solvents. Corma et al., for instance, obtained a 93.0% yield of GVL after 5 h reaction over a 0.6 wt% $Ru/TiO_2$ at 423 K, 35 bar hydrogen pressure in water.[19] Palkovits et al. reported a yield of 71.2% after 160 min reaction time over 5 wt% $Ru/TiO_2$ at 403 K, 12 bar hydrogen pressure in ethanol and water.[9] Ruthenium supported on the strongly acidic zeolites showed a quite different product distribution. Full conversion is achieved in both cases, but in addition to GVL, the deep hydrogenation product PA and its ester derivatives (PE) were obtained in considerable amounts with Ru on H-ZSM5 or H-β. PD was not observed with the zeolite catalysts, however.

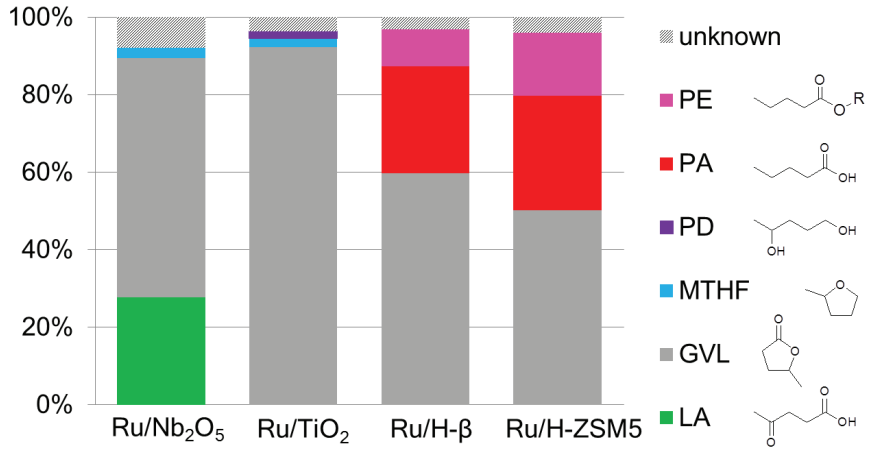


Figure 2.2. Catalytic hydrogenation of 10 wt% levulinic acid in dioxane at 473 K, 40 bar, 4 h reaction time, 1 wt% Ru on different supports, stirrer speed 1600 rpm. LA: levulinic acid; GVL: γ-valerolactone; MTHF: methyltetrahydrofuran; PD: 1,4-pentanediol; PA: pentanoic acid; PE: pentanoic acid esters (butyl pentanoate isomers, 2-ethoxy-ethyl pentanoate and valeric pentanoate); and unknown: missing mass balance.

The more acidic Ru/H-ZSM5 yielded more PA and PE, but at the expense of a slight increase in loss of mass balance (4% for Ru/H-ZSM5 vs. 3.3% for Ru/H-β). The PE derivatives are the result of esterification of PA with dioxane decomposition products, as the solvent was found not to be fully stable in the presence of the acidic catalysts under the applied conditions. Indeed, decomposition of dioxane (2 to 4% in total) to ethanol, butanol isomers and other dioxane-derived small molecules (2-ethoxy-ethanol, ethoxy-ethane) was detected after the runs. The n-butanol included in the n-butyl ester of pentanoic acid is probably the product of a Guerbet-type reaction of the ethanol formed. The total combined yields of PA and PE from LA are 37.5% with Ru/H-β and 45.8% with Ru/H-ZSM5. These results show that the direct conversion to PA is feasible in a one-pot reaction already at the fairly low temperature of 473 K. Interestingly, a metal/zeolite-catalyzed process from GVL to PA was patented by Shell,[14, 20] but not a process from LA directly to PA; furthermore, a 62% yield of PA and PE was claimed over a 1 wt% Ru/H-β/silica catalyst at 523 K and 80 bar $H_2$ with ethyl levulinate rather than LA as the substrate in a batch autoclave reactor.[14] The gas phase composition of the dioxane runs was also checked by online GC analysis, with only minute amounts of CO and $CO_2$ (carbon balance <0.03%) being detected, which suggests that decarboxylation, e.g. by PA conversion to butene does not occur under the applied reaction conditions.

#### 2.3.2.2 Catalyst Stability

Spent catalysts were extensively characterized to assess stability and detect any changes in either the metal phase or the support. The ruthenium particle sizes and support morphologies of different catalysts were examined by TEM (Appendix A, Fig. S2). The average diameters of the ruthenium particles with standard deviations of the fresh and spent catalysts are given in Fig. 2.3. The lack of contrast did not allow the particle size to be determined for the niobia samples.

The average Ru particle diameter of the fresh catalysts was around 3.5 nm for all three catalysts. All catalysts showed a small increase in particle size in the spent catalysts to around 4 nm, now with a slightly broader distribution around the mean. In general, the observed sintering after a 4 h reaction in dioxane was limited, though. The increased

standard deviation of the spent catalysts nonetheless illustrates that more large Ru particles are formed during reaction with $Ru/TiO_2$, H-β, and H-ZSM5. The extent of Ru loss to the liquid phase by leaching was determined by AAS after 4 h reaction and found to be marginal. Ru/H-ZSM5 showed the highest loss, but at only 2.4 % of the original weight of ruthenium (Table 2.3).

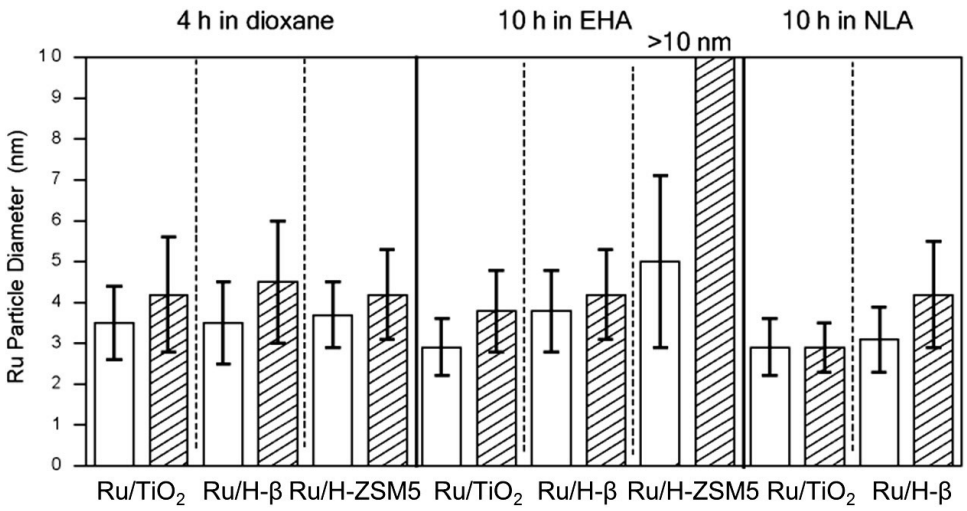


Figure 2.3. Ru particle size (nm) determined by TEM for the fresh and spent catalysts after reaction in dioxane, 2-ethylhexanoic acid (EHA) and neat levulinic acid (NLA) (blank pattern: fresh catalyst; and diagonal pattern: spent catalyst).

Table 2.3. Ruthenium leaching of the liquid phase, after reaction in dioxane, 2-ethylhexanoic acid (EHA) and neat levulinic acid (LA) as determined by AAS.

| Spent catalyst | Ru leaching 4 h in dioxane (%) | Ru leaching 10 h in EHA (%) | Ru leaching 10 h in neat LA (%) |
|---|---|---|---|
| $Ru/TiO_2$ | 2.1 | 2.9 | 0.5 |
| $Ru/Nb_2O_5$ | 1.8 | 0.9 | - |
| Ru/H-β | 1.6 | 0.7 | 0.5 |
| Ru/H-ZSM5 | 2.4 | 0.9 | - |

A comparison of the powder XRD patterns of the fresh and spent catalysts (Appendix A, Fig. S5) showed patterns similar in peak intensity and peak center, indicating that there

was no phase change of the supports under the applied conditions and that the zeolites maintained their structural integrity. $N_2$ physisorption data provided insight into the extent of coke build-up. The formation of carbon residues or coke on the catalyst surface resulted in a decrease in surface area and pore volume (Table 2.2) for the niobia and zeolite-supported catalysts, but not for the titania-supported one. The results obtained in dioxane thus show large selectivity differences for the ruthenium catalysts on supports of different acidity, while the limited leaching and sintering points at good catalyst stability under the applied reaction conditions.

### 2.3.3 Catalytic Reactions in 2-Ethylhexanoic Acid

The reactions run in dioxane were well suited for initial studies into the selectivity, activity and stability of the catalysts, but the use of this particular solvent also showed to have some disadvantages. In particular in the presence of the strongly acidic catalysts, dioxane was found to be unstable, hampering product analysis due to dioxane-derived byproduct formation, i.e. the pentanoic acid esters. The use of an alternative solvent could alleviate this and would also provide an opportunity to subject the catalysts to harsher conditions to further assess their stability under the typically highly polar and acidic conditions encountered in a more commercial levulinic acid conversion process. With this in mind, 2-ethylhexanoic acid (EHA) was selected as solvent. EHA is stable under the typical hydrogenation conditions and, having a similar $pK_a$, is a good mimic of LA. This allowed the study of catalyst activity and selectivity in the conversion of LA, but, importantly, also of intermediates such as GVL. In addition, catalyst stability under conditions that are similar to running the reaction in neat LA could be determined. The latter is important as supported metal catalysts can suffer from leaching of both the metal phase as well as of the support under the corrosive and highly polar liquid phase conditions typically employed in the conversion of renewable platform molecules such as LA and more insight is needed into possible deactivation pathways.

#### 2.3.3.1 Catalyst Performance

Concentration profiles of substrate and products are depicted in Fig. 2.4. As with the runs in dioxane, clear differences in selectivity and activity are observed. Both the

$Ru/Nb_2O_5$ and $Ru/TiO_2$ catalysts are highly selective for GVL in EHA, with only very small amounts of MTHF formed as the only byproduct (< 1 mol%). The reaction over $Ru/TiO_2$ is faster, however, as full conversion is obtained after 4 h, while 2.4 mol% of LA was still left after 5 h reaction with the $Ru/Nb_2O_5$ catalyst. The Ru/H-β catalyst also showed full LA conversion in 4 h, while Ru/H-ZSM5 is the fastest catalyst achieving full LA conversion in only 3 h.

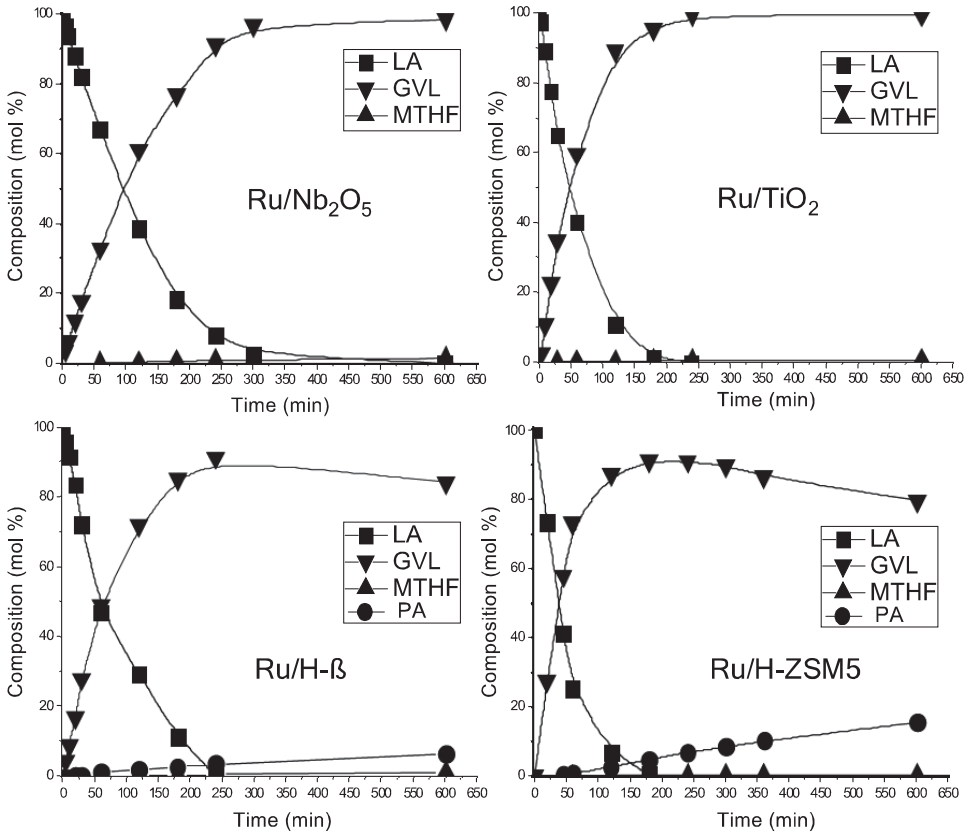


Figure 2.4. Time profiles of the catalytic hydrogenation of 10 wt% levulinic acid in 2-ethylhexanoic acid. Conditions: 473 K, 40 bar, 10 h reaction time, 1wt% Ru loading with different supports, stirrer speed of 1600 rpm LA: levulinic acid; GVL: γ-valerolactone; MTHF: methyltetrahydrofuran; PA: pentanoic acid.

The activity of the catalyst is illustrated by the turnover frequencies (TOF) (at LA conversions of ~ 20%), which follow the sequence: Ru/H-ZSM5 (0.204 $s^{-1}$) > $Ru/TiO_2$ (0.164 $s^{-1}$) > Ru/H-β (0.131 $s^{-1}$) > $Ru/Nb_2O_5$ (0.088 $s^{-1}$). Only GVL is observed as the

product for both the $Ru/Nb_2O_5$ and $Ru/TiO_2$ catalysts as the support is too weakly acidic to open the ring of GVL under the applied conditions. The acid-supported catalysts Ru/H-ZSM5 and Ru/H-β again showed the formation of the deep hydrogenation product PA with PA yields of 15.5% (Ru/H-ZSM5) and 6.3% (Ru/H-β) after 10 hours of reaction.

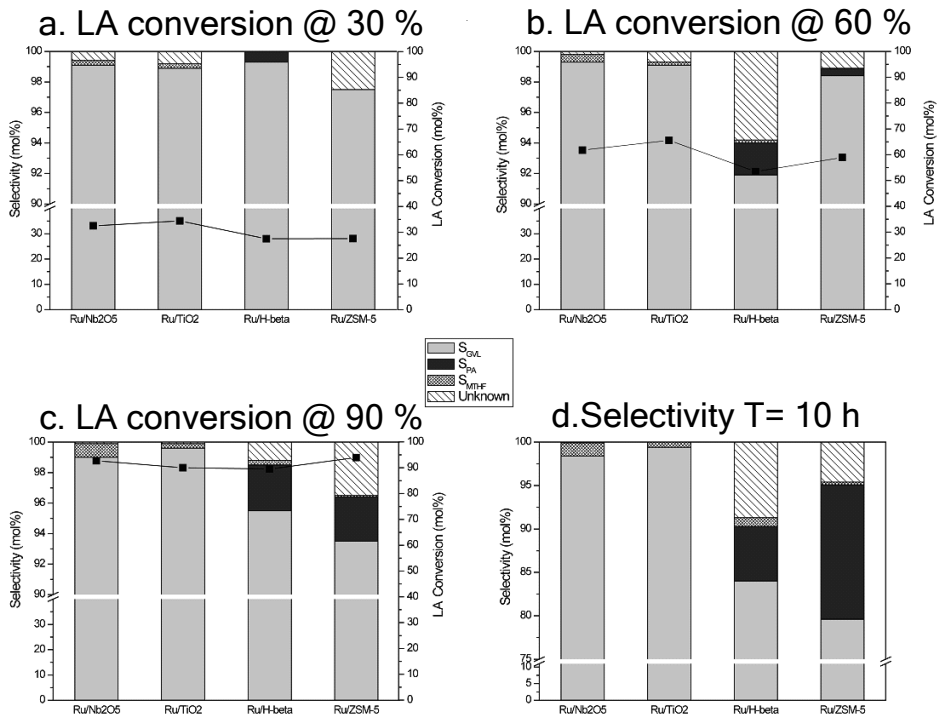


Figure 2.5. Selectivity comparison of different catalysts at different levulinic acid (LA) conversion levels; LA conversion at: a) 30%; b) 60%; c) 90%; d) after 10 h of reaction time with full conversion of LA.

Again, only minute amounts of MTHF (< 1%) were detected and no PD was observed. The PA yields in EHA were lower than those observed in dioxane, illustrating that the substrate LA and the intermediate GVL, which is the precursor to PA, compete with the solvent for adsorption on or interaction with the catalyst. Related to this, the extent and origin of catalyst deactivation is different in this solvent (see below). The data thus illustrates that while the influence of the acid functionality is rather subtle in the first LA-to-GVL step, the strong acid sites on the zeolites are clearly required for the consecutive GVL-to-PA conversion.

The selectivity patterns of the different catalysts are compared at different LA conversion levels in Fig. 2.5. At low LA conversion (~30%), all catalysts show high GVL selectivity ($S_{GVL}$ > 97%), with only Ru/H-β producing already some PA. No PA is observed at this point with Ru/H-ZSM5, which might be attributed to a more limited accessibility of GVL to the acid sites in H-ZSM5. Increasing LA conversion (~ 60% and 90%) leads to increased selectivity for PA over the acidic zeolite supports, with GVL selectivity still over 98% for the less acidic supports $TiO_2$ and $Nb_2O_5$. Full LA conversion was achieved after 10 h of reaction with all catalysts. Although Ru/H-β initially produced more PA, PA selectivity was lower for Ru/H-β than for Ru/H-ZSM5 after 10 h, suggesting that deactivation is more rapid for Ru/H-β than for Ru/H-ZSM5 (see below).

#### 2.3.3.2 Hydrogenation of Intermediates

As is clear from the LA hydrogenation results presented above, the gradual catalyst deactivation limits the yield of PA under these more severe conditions. To get more insight into the inherent ability of the zeolite-supported catalysts to catalyze the steps after GVL formation, i.e. ring opening and hydrogenation to PA, reactions with the implicated intermediates GVL and PEA were also performed in EHA. $Ru/TiO_2$ and Ru/H-β were chosen to compare the non-acid and acid-supported catalysts (Table 2.4).

As expected, PA was not observed with $Ru/TiO_2$ after 4 h or even 10 h of reaction (Table 2.4, entries 1-3). Ru/H-β slowly, but cleanly converts GVL to PA in EHA, with a yield of 7.2% after 15 min, which increases to 34.0% after 10 h. This PA yield is higher than the one obtained in the LA run, pointing at the key role of the acid sites in the GVL-to-PA conversion and partial deactivation by acid-site loss (be it due to blockage or dealumination) in the first LA-to-GVL step (Table 2.4, entries 4-9).

Table 2.4. Results for the catalytic hydrogenation of γ-valerolactone (GVL) or pentenoic acid (PEA) in 2-ethylhexanoic acid (PA, pentanoic acid; and MTHF, methyltetrahydrofuran).

| Entry | Catalyst | Time (h) | C-balance (%) | GVL conv. (%) | PA yield (%) | MTHF yield (%) | PEA yield (%) |
|---|---|---|---|---|---|---|---|
| **GVL** | | | | | | | |
| 1 | $Ru/TiO_2$ | 4 | 97.9 | 2.3 | 0 | 0.2 | 0 |
| 2 | $Ru/TiO_2$ | 10 | 95.8 | 4.9 | 0 | 0.7 | 0 |
| 3 | $TiO_2$ | 4 | 99.9 | 0.2 | 0 | 0.1 | 0 |
| 4 | Ru/H-β | 0.25 | 94.5 | 12.7 | 7.2 | 0 | 0 |
| 5 | Ru/H-β | 1 | 92.5 | 17.3 | 9.8 | 0 | 0 |
| 6 | Ru/H-β | 2 | 93.8 | 23.1 | 16.9 | 0 | 0 |
| 7 | Ru/H-β | 3 | 93.7 | 26.7 | 20.4 | 0 | 0 |
| 8 | Ru/H-β | 4 | 95.1 | 28.7 | 23.7 | 0.1 | 0 |
| 9 | Ru/H-β | 10 | 93.7 | 40.5 | 34.0 | 0.2 | 0 |
| 10 | H-β | 4 | 96.3 | 17.6 | 11.0 | 0 | 2.9 |
| 11 | H-β | 4 | 97.1 | 19.2 | 14.8 | 0 | 1.3 |
| 12 | H-ZSM5 | 4 | 99.3 | 6.0 | 5.3 | 0 | 0 |
| 13 | H-β | 10 | 95.2 | 30.0 | 23.2 | 0 | 2.0 |
| 14 | No Cat | 4 | 102.9 | -2.8 | 0 | 0.1 | 0 |
| 15 | No Cat | 10 | 99.6 | 0.6 | 0 | 0.2 | 0 |
| | | Time (h) | C-balance (%) | PEA conv. (%) | PA yield (%) | GVL yield (%) | |
| **PEA** | | | | | | | |
| 16 | H-β | 4 | 99.3 | 99.6 | 18.0 | 80.9 | |
| 17 | No Cat | 4 | 99.9 | 15.5 | 12.1 | 3.3 | |

Conditions: 473 K, 40 bar, 1 wt% Ru on different supports, stirrer speed of 1600 rpm, 21.6 mmol of GVL or PEA in EHA (equimolar to 10 wt% LA)

Unexpectedly, a standard check of the activity of the support itself in the reaction (Table 2.4, entries 10, 11, 13), showed that PA was also obtained with only H-β present. Trace amounts of residual Ru were held responsible for this hydrogenation activity, but the (limited) activity of just H-β remained even after extensive dismantling and cleaning of the batch autoclave. AAS analysis of the liquid phase after reaction did not detect any Ru or Cr,[21] but trace amounts of iron were found (Appendix A, Table S1). The activity in the blank reactions with just the zeolite support is thus attributed to acid-catalyzed ring opening by the zeolite to form PEA, which is subsequently hydrogenated to PA by any

iron leached from the autoclave walls. Indeed, runs with PEA showed hydrogenation activity to yield some PA in the absence of the zeolite (Table 2.4, entry 16), while in the presence of the zeolite both equilibration with GVL as well as PA formation was observed. Importantly, blank reactions (no support, no catalyst) did not show any conversion (Table 2.4, entries 14, 15). The background hydrogenation reaction therefore does not influence the catalytic results as it is much slower than the Ru-catalyzed hydrogenation reactions. These results show that ring-opening is the rate-limiting step in the GVL-to-PA conversion and that PEA hydrogenation is very straightforward. Furthermore, ring opening from GVL to PEA is reversible (Table 2.4, entry 17) with the equilibrium favoring GVL under the applied conditions. H-β showed higher yield of PA than H-ZSM5 (Table 2.4, entries 10-12), further pointing at the better accessibility of the acid sites in the larger-pore H-β.

The gradual deactivation of the catalyst, in particular with respect to its ability to catalyze the second GVL-to-PA conversion, is illustrated by a longer 24 h run with Ru/H-β in which additional fresh catalyst was added after 4 and 14 h of reaction. Changes in composition of the liquid phase are depicted in Fig. 2.6. The reaction was run with half the amount of catalyst (0.3 g) compared to the results in Fig. 2.5 for Ru/H-β with the second half of catalyst (0.3 g) only being added after 4 h. As a result, conversion dropped from full (0.6 g catalyst) to 68.9% (0.3 g). The yield of PA after 10 h of reaction was higher, however, for the sequential addition experiment (10.1% vs. 6.3%), which shows that the deactivation of the catalyst (by loss of acid sites, see below) happens already in the first stage of the reaction, which is concerned mostly with the conversion of LA to GVL. PA production seems to level off after 10 h, indicating that the acid sites are no longer accessible. Addition of a fresh batch of catalysts restored activity with PA yields increasing almost linearly over the next 14 h.

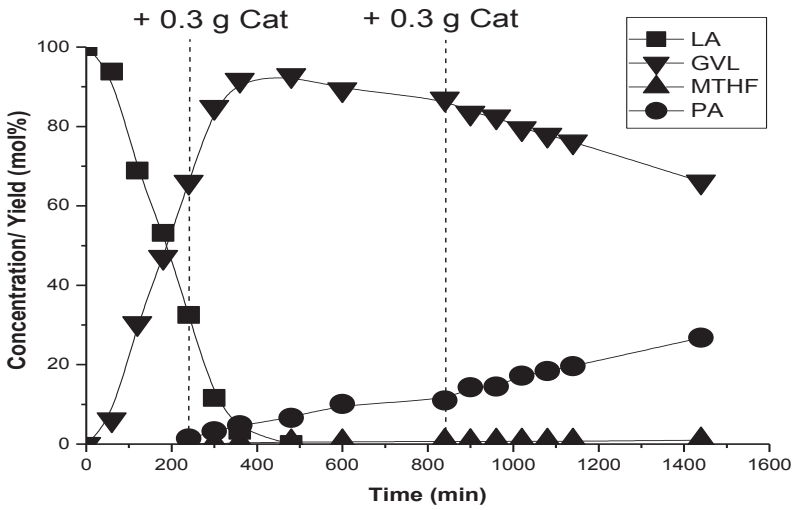


Figure 2.6. Catalytic hydrogenation of levulinic acid (LA) and formation of γ-valerolactone (GVL), pentanoic acid (PA) and methyltetrahydrofuran (MTHF) as a function of time at 473 K, 40 bar with 1 wt% Ru/H-β in 2-ethylhexanoic acid with twice the addition of fresh catalyst.

#### 2.3.3.3 Catalyst Stability

The stability of the catalysts under these more severe conditions was again studied by TEM and AAS to quantify any sintering or leaching of ruthenium (Appendix A, Fig. S3, Fig. 2.3 and Table 2.3). Similar to the results obtained in dioxane, limited sintering of the Ru particles was observed for the spent $Ru/TiO_2$ (particle size increase from 2.9 to 3.8 nm, Table 2.3) and Ru/H-β (3.8 to 4.5 nm) after 10 h reaction in EHA. Some bigger clusters were found on the spent catalysts, however, causing broadening of the distribution. A major difference with the reactions run in dioxane is that severe sintering was observed for the spent Ru/H-ZSM5 catalyst, as TEM showed that some of the H-ZSM5 particles contained no Ru, while others showed big clusters of Ru, as confirmed by EDX (Appendix A, Fig. S3). Loss of ruthenium to the liquid phase was marginal (< 3%), nonetheless, for all four catalysts (Table 2.3).

**Coke formation.** The lower PA yield that is observed in EHA with the Ru/zeolite catalysts points at deactivation of the catalyst material. In addition to any changes to the metal phase, changes to the support, e.g. deactivation by coking, loss of active sites by dealumination or phase changes can also be expected. TGA measurements did show different extents of coke formation on the different supports (Table 2.2). More carbon residue or coke is deposited on the acid-supported catalysts. The weight loss measured by TGA decreases in the order of H-ZSM5 > H-β > $Nb_2O_5$ > $TiO_2$. $N_2$ physisorption measurements of the spent catalysts also show a decrease in surface area and pore volume (Table 2.2). TGA-MS analysis of the spent Ru/H-β catalyst provided some further insight into the probable coke-precursors. Indeed, the H/C ratio, determined from the $CO_2$ and $H_2O$ MS signals, reaches a plateau at H/C 1.4 (Appendix A, Fig. S8). Given the H/C ratios of the various intermediates in the LA hydrogenation platform (see Scheme 2.1), AL is the only intermediate with a H/C ratio lower than 1.4 and must therefore be involved in the coke formation. This is further corroborated by the GC and GC-MS results obtained at low conversion, in which AL, but not 4-HPA, is detected in minor amounts.

The XRD patterns of the spent catalysts showed no evidence for formation of new phases after 10 h of reaction in EHA (Appendix A, Fig. S6). Closer inspection of the X-ray diffraction pattern of the spent Ru/H-ZSM5, however, showed a shift of peaks to lower $2\theta$ values (higher corresponding d-values) suggesting an expansion of the unit cell (Fig. 2.6). Considering the respective bond distances of Al-O and Si-O (~1.75 Å and ~1.61 Å respectively), dealumination of framework aluminum would result in the opposite effect, i.e. a shift of peaks to higher $2\theta$ values (lower d-values) as a result of a 'shrinking' unit cell. As also shown by solid state $^{27}Al$ NMR, there was indeed loss of aluminum (Fig. 2.9) in the Ru/H-ZSM5 sample. Further considering the initial amount of Al in the fresh sample (3.1 wt%), this would not be reflected in lattice parameter changes, as was already previously noted [22, 23].

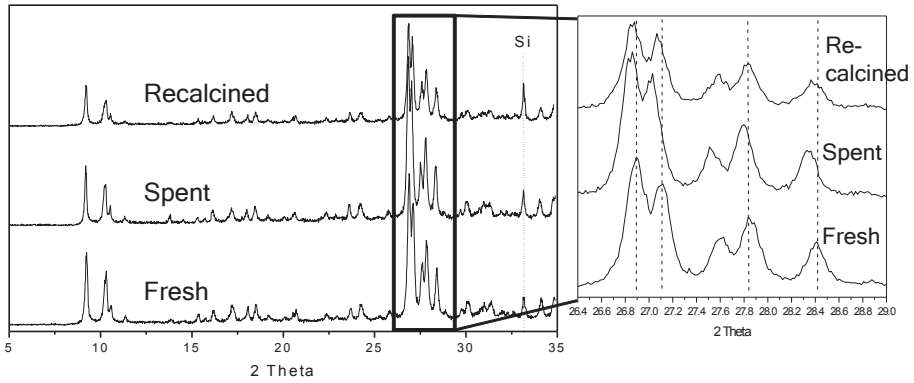


Figure 2.7. Top: XRD powder diffraction patterns of a fresh Ru/H-ZSM5 catalyst, after reaction in 2-ethylhexanoic acid (EHA), and after recalcination. Silicon (NBS 640) was used as internal standard by physical mixing.

Table 2.5. Unit cell lattice parameters of the 1 wt% Ru/H-ZSM5 catalyst before and after reaction and after regeneration.

| **Ru/H-ZSM5 samples** | **Lattice constants (Å)** | | |
|---|---|---|---|
| | a | b | c |
| Fresh | 20.100 | 19.909 | 13.376 |
| Spent | 20.100 | 19.957 | 13.419 |
| Re-calcined | 20.101 | 19.924 | 13.399 |

However, the porosity studies indicated a significant loss in the internal pore volume of the H-ZSM5 zeolite, which could be associated with possible coke buildup within the zeolite channels. This could lead to an expansion of the unit cell, consistent with the observation from the diffraction patterns. To test this hypothesis further, the spent Ru/H-ZSM5 sample was exposed to a stream of pure oxygen at 723 K for 4 h to remove as much coke from the material as possible. The XRD pattern of the recalcined Ru/H-ZSM5 sample is compared to the fresh and spent material in Fig. 2.7. Clearly, the pattern corresponding to the spent catalyst is shifted to the right as compared to the fresh catalyst suggesting an 'expanded' unit cell for the former. After recalcination of the spent catalysts, the pattern is comparable, however, to the fresh pattern suggesting the

unit cells are similar in size. Table 2.5 lists the lattice parameters obtained for each pattern. While lattice parameter *'a'* remains constant for all three patterns, unit cell parameter '*b*' and '*c*' are seen to change (as expected) over the three samples. The spent sample shows the largest unit cell, while treating the sample in an oxygen-rich feed appears to result in a unit cell comparable to the fresh sample.

It is important to recall that H-ZSM5 is made up of a 3-dimensional porous network with large straight channels that are oriented perpendicular to smaller zig-zag channels. From a unit cell perspective, the former are oriented perpendicular to axes *a* and *c,* whilst the latter are (almost) perpendicular to axes *b* and *c*. Since the analysis shows lattice parameter *a* to be constant and parameters *b* and *c* to increase in the spent sample, it can be deduced that coke forms within the zigzag channels of the zeolite (oriented parallel to axis *a*), which attributes to the deactivation of the catalyst. After treatment in an oxygen-rich flow, most of the coke gets burnt off and values for *b* and *c* closer to the values seen for the fresh catalyst are again obtained. The preferential deposition of coke in the zig-zag channels is further substantiated by the larger shifts of the peaks corresponding to *0kl* planes compared to peaks corresponding to *h00* planes.

**Support dealumination.** Although the Ru/H-ZSM5 catalyst showed more coke deposition (Table 2.2), a lower PA selectivity at low LA conversion level (Fig. 2.5) and more sintering of Ru (Appendix A, Fig. S3) during the reaction in EHA, a higher yield of PA than with Ru/H-β was still obtained with this catalyst after 10 h of reaction. As the GVL-to-PA conversion is critically dependent on the acid sites of the zeolite, factors other than active site blockage, e.g. loss of active sites by dealumination should therefore also be taken into account. A first indication for Al loss came from the AAS measurements and was further studied by pyridine adsorption and solid state $^{27}$Al NMR.

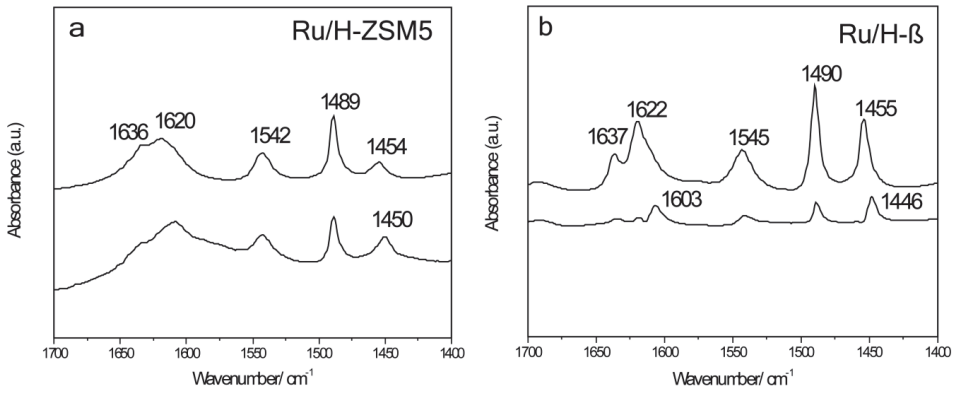


Figure 2.8. FT-IR absorbance spectra of adsorbed pyridine of a) Ru/H-ZSM5 and b) Ru/H-β (top: fresh catalyst; bottom: spent catalyst after reaction in 2-ethylhexanoic acid).

The FT-IR spectra in Fig. 2.8 show pyridine adsorbed on the two types of zeolite catalysts. With fresh Ru/H-ZSM5, pyridine adsorption resulted in the formation of protonated (1636, 1489, and 1542 $cm^{-1}$) and coordinated (1620, 1489, and 1454 $cm^{-1}$) species.[24-26] The former interaction (specifically the 1542 $cm^{-1}$ vibration) can be assigned to pyridine interacting with a Brønsted acid site (BAS), while the 1454 $cm^{-1}$ vibration is indicative of an interaction with Lewis acid sites (LAS). The decrease in BAS after the 10 h reaction is very limited, as only a slight decrease in intensity of the band at 1542 $cm^{-1}$ is observed, while a small increase of the intensity and a shift to 1450 $cm^{-1}$ of the vibration originally at 1454 $cm^{-1}$ (Fig. 2.8a) suggests an increase in LAS, probably by framework dealumination.[27]

On fresh Ru/H-β, vibrations assigned to adsorbed protonated pyridine (1637, 1490, and 1545 $cm^{-1}$) and coordinated pyridine (1622, 1490, and 1455 $cm^{-1}$) are observed as well. After reaction, a decrease in all the bands is seen with spent Ru/H-β, indicating loss of acid sites. The two new bands at 1603 and 1446 $cm^{-1}$ (Fig. 2.8b) most likely correspond to pyridine adsorbed on a new type of LAS in the spent catalyst, as a result again of dealumination.[28] The severe loss of BAS and LAS can also be seen in the FT-IR spectra of the Ru/H-β catalyst without pyridine, as the bands at 3779 (LAS), 3662 (LAS), and

3607 $cm^{-1}$ (BAS) corresponding to the various OH groups that are observed in the fresh catalyst, disappear after reaction in EHA, as observed in Chapter 3.

The 1D $^{27}Al$ MAS NMR spectra of the fresh and spent Ru/zeolite catalysts are depicted in Fig. 2.9. The $^{27}Al$ NMR spectra of fresh and spent Ru/H-ZSM5 show two resonances in both the tetrahedral as well as in the octahedral aluminum region, a broad and a narrow one. The sharp resonance at 54 ppm, is assigned to tetrahedral framework aluminum (FAl) species (Al(IV), FAl, BAS) while the broad tetrahedral resonance with an isotropic shift of 57 ppm represents distorted extraframework aluminum (EFAl) species (Al(IV), EFAl, LAS).[29, 30] There are also two types of octahedral aluminum to be seen: a narrow line originating from octahedral aluminum (Al(VI), EFAl, LAS) in a highly symmetric environment, such as for instance $Al(OH)_3 \cdot 3H_2O$ in addition to a broad octahedral resonance also at 0 ppm that has been assigned to extra framework aluminum by some [31] but others have referred to this as framework Al(VI) (Fig. 2.9a, b).[32, 33]

The distorted tetrahedral aluminum is much more prevalent than the tetrahedral framework Al in the spent Ru/H-ZSM5 which shows that conversion of FAl to EFAl sites takes place during the reaction in the hot acid EHA. Not only is tetrahedral FAl converted to EFAL, there is also an overall decrease in the amount of aluminum as seen by the decrease in intensity of the spectra. The dealumination is more severe for the octahedral species than for the tetrahedral aluminum (Al(IV): 11.5% decrease, Al(VI): 34.6% decrease). The loss of acid sites for Ru/H-ZSM5 after reaction is also indicated by the pyridine adsorption data (Fig. 2.9). Moreover, the reduction in tetrahedral FAL coincides with the reduction in intensity of the 1542 $cm^{-1}$ FT-IR line, both pointing towards a reduction in the number of BAS. At the same time, the increase in tetrahedral EFAL together with growth of the band at 1450 $cm^{-1}$ both support an increase in LAS.

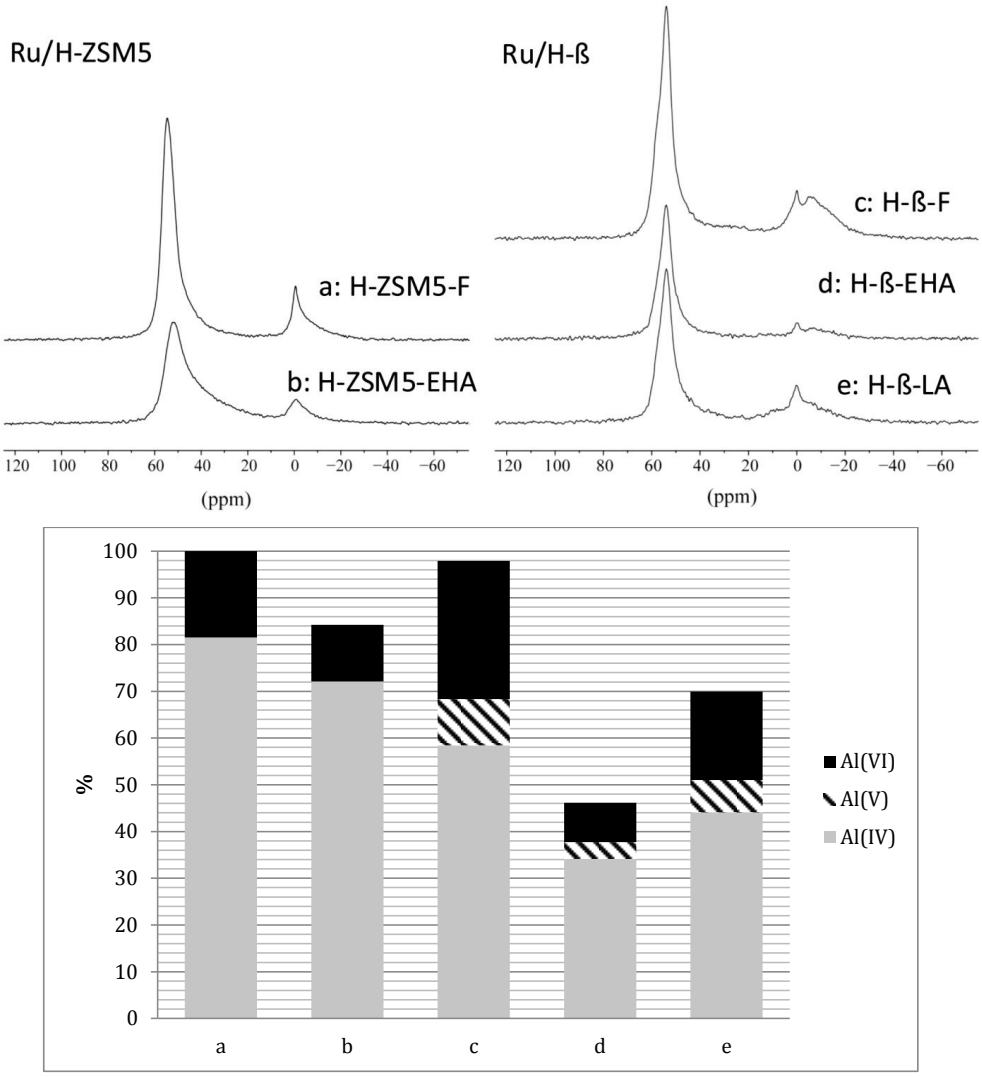


Figure 2.9. Top: $^{27}$Al MAS NMR spectra of fresh and spent Ru catalysts. a) fresh Ru/H-ZSM5; b) spent Ru/H-ZSM5 (reaction in 2-ethylhexanoic acid for 10 h); c) fresh Ru/H-β; d) spent Ru/H-β (reaction in 2-ethylhexanoic acid for 10 h); e) spent Ru/H-β (reaction in neat levulinic acid for 10 h). Bottom: relative amounts of tetrahedral, penta- and octahedral coordinated aluminum normalized to the aluminum content in the fresh Ru/H-ZSM5 catalyst as determined by $^{27}$Al MAS NMR (accuracy ±2%).

The $^{27}$Al MAS NMR spectra of the Ru/H-β samples are shown in Fig. 2.9c-e. In the fresh Ru/H-B sample (Fig. 2.9c) three tetrahedral species can be discerned in the MQMAS (Appendix A, Fig. S9). However, these are severely overlapping in the 1D MAS spectra. The tetrahedral region consists of both FAL and EFAL aluminum. As in ZSM-5, two octahedral species can be detected, both with an isotropic shift around 0 ppm, one type in a highly symmetric environment and one more distorted. Trace amounts of penta-coordinated aluminum species Al(V), with a peak center at 33 ppm, are also detected in the $^{27}$Al 3QMAS NMR (Appendix A, Fig. S11).[34, 35] After 10 h of reaction in EHA, dealumination is illustrated by the decrease in intensity of all peaks (Fig. 2.9d) with a very sharp decrease in six-coordinated suggesting the loss of both FAl and EFAl species. (after 10 h reaction in EHA, Al(IV): 41.1%, Al(V): 63.6%, Al(VI): 71.6% decrease. The $^{27}$Al NMR spectrum of the reaction of Ru/H-β in neat levulinic acid (NLA, see below) shows that the loss of acid sites in NLA is less severe than in EHA (after 10 h in NLA, Al(IV): 24.5%, Al(V): 30.3%, Al(VI): 36.1% decrease). This can be attributed to the larger total amount of acid used (54 g EHA + 6 g LA vs. 20 g LA in the NLA run) and the fact that in the NLA run, the acid reacts away to form GVL. The $^{27}$Al NMR spectra agree with the pyridine data as they both reflect the loss of BAS as well as LAS for Ru/H-β.

H-β is thus more easily dealuminated than H-ZSM-5 in the presence of the hot acid EHA. Müller et al. previously already showed that H-β was more easily dealuminated than H-ZSM-5 by a hydrothermal treatment in the presence of oxalic acid. [36] The severe dealumination of H-β corresponds with the lower yield of PA in the EHA runs with Ru/H-β as compared to Ru/H-ZSM5 (Fig. 2.5). The continuous loss of acid sites of Ru/H-β hampers the GVL to PEA conversion (Scheme 2.1). Although Ru/H-ZSM5 suffers more from sintering and coke formation (Table 2.2), less acid sites are lost, resulting in a higher PA yield in EHA, and more details will be presented in Chapter 3.

### 2.3.4 Catalytic Reactions in Neat Levulinic Acid

#### 2.3.4.1 Catalyst Performance

The acidity of the support was also shown to influence activity and selectivity in the catalytic hydrogenation of neat LA by Ru/$TiO_2$ or Ru/H-β (Table 2.6). Indeed, Ru/H-β

showed higher activity for the hydrogenation of LA. Reaching full conversion with 0.3 g Ru/H-β in 4 h (TOF > 0.403 $s^{-1}$) (Table 2.6, entry 4), compared to 57.8 % LA conversion with 0.3 g $Ru/TiO_2$ (TOF = 0.233 $s^{-1}$) (Table 2.6, entry 1). Conversion could be increased to 98.1% after 4 h when 0.5 g $Ru/TiO_2$ was used (TOF = 0.239 $s^{-1}$) (Table 2.6, entry 2). These results are similar to those reported by Manzer for the conversion of neat LA using a 5 wt% $Ru/Al_2O_3$ catalyst at 473 K and 33.4 bar hydrogen (TOF = 0.405 $s^{-1}$) [37].

Table 2.6. Catalytic performances for the hydrogenation of neat levulinic acid (LA) with GVL, γ-valerolactone; PA, pentanoic acid; MTHF, methyltetrahydrofuran and PD, 1,4-pentanediol.

| Entry | Catalyst | Time (h) | Catalyst amount (g) | Carbon balance | LA conv. (%) | GVL yield (%) | PA yield (%) | MTHF yield (%) | PD yield (%) |
|---|---|---|---|---|---|---|---|---|---|
| 1 | $Ru/TiO_2$ | 4 | 0.3 | 100.4 | 57.8 | 57.8 | 0.3 | 0.1 | 0.0 |
| 2 | $Ru/TiO_2$ | 4 | 0.5 | 99.6 | 98.8 | 97.7 | 0.4 | 0.2 | 0.1 |
| 3 | $Ru/TiO_2$ | 10 | 0.5 | 98.9 | 100.0 | 97.5 | 0.4 | 0.4 | 0.6 |
| 4 | Ru/H-β | 4 | 0.3 | 92.8 | 100.0 | 91.0 | 1.7 | 0.1 | 0.0 |
| 5 | Ru/H-β | 4 | 0.5 | 91.7 | 100.0 | 89.2 | 2.3 | 0.2 | 0.0 |
| 6 | Ru/H-β | 10 | 0.5 | 91.3 | 100.0 | 86.6 | 4.0 | 0.7 | 0.0 |

Conditions: 473 K, 40 bar, 0.3 g 1 wt% Ru catalyst, stirrer speed of 1600 rpm, 20 g LA

Palkovits et al. recently showed that full conversion of neat LA can also be achieved with Ru/C (5 wt%) at very mild conditions (298 K, 12 bar $H_2$), but at the longer reaction time of 50 h.[9] A comparison of TOF numbers shows that the LA–to-GVL conversion is accelerated by the acid sites on Ru/H-β; the TOF numbers obtained in neat LA runs are larger than those of EHA runs ($Ru/TiO_2$: 0.239 vs. 0.164; Ru/H-β: > 0.403 vs. 0.131), illustrating that the substrate LA competes with the solvent EHA for adsorption on the catalyst. Minute amounts of the deeper hydrogenation products PD, PA and MTHF were observed with $Ru/TiO_2$ (Table 2.6, entry 3), while higher but still low yields of PA were achieved with Ru/H-β with the yields increasing with catalyst amount and reaction time. PD was not observed in the runs with Ru/H-β (Table 2.6, entries 4-6).

### 2.3.4.2 Catalyst Stability in Neat Levulinic Acid

Interestingly, both very limited sintering (Appendix A, Fig. S4) and limited Ru loss (Table 2.3) were observed with $Ru/TiO_2$ in pure LA. $Ru/TiO_2$ showed thus shows good stability not only in dioxane, also but also under more severe conditions such as in EHA or in neat LA. Some sintering was observed with Ru/H-β as in EHA, but less Al was lost to the liquid phase compared to the EHA runs, which can again be attributed to the disappearance of the acid function upon conversion of LA to GVL. No phase change occurred for both supports (Appendix A, Fig. S7). A very small drop in surface area was found for the titania catalyst, consistent with the limited formation of coke as observed by TGA. More coke formed on the acidic catalyst, resulting in a larger drop in surface area and pore volume. More coke was deposited on both catalysts in neat LA than in EHA (Ru/H-β: 10.7 vs 3.4 wt%; $Ru/TiO_2$: 1.8 vs. 0.8 wt%), illustrating that a LA derivative and not EHA is the precursor for coke formation (Table 2.2).

## 2.4 Conclusions

Our study demonstrates that the catalytic performance of the four supported Ru catalysts for the hydrogenation of levulinic acid (LA) is greatly affected by the nature of the support and the solvent choice. The non-acidic catalyst materials selectively gave γ-valerolactone (GVL) as the main and final product, while the zeolite-supported acidic catalyst proved capable of the direct conversion of LA to pentanoic acid (PA) under relatively mild conditions in dioxane as solvent. The strongly acidic sites on the support material accelerate the LA-to-GVL conversion and are essential for the subsequent, most difficult step in the sequence, i.e. the ring-opening step in the conversion of GVL to PA. PA can also be obtained under more severe conditions, using 2-ethylhexanoic acid or neat LA as solvent, but yields dropped as a result of gradual deactivation of the zeolite-supported catalysts. Although many factors may influence the deactivation of the catalyst material, pyridine adsorption and solid-state $^{27}Al$ NMR data clearly show that the deactivation of the catalyst materials can mainly be attributed to loss of acid sites by dealumination. It was found that H-ZSM5 was more resistant to dealumination than H-β. Most coke is formed on the zeolite-supported catalyst materials in neat LA, with XRD indicating preferential coke build-up in the zig-zag channels of H-ZSM5. The results also

show that angelicalactone (AL) is involved as an intermediate in the hydrogenation reaction and that it is a direct precursor for the coke that is deposited mostly on the acidic catalysts. $Ru/TiO_2$ proved to be remarkably stable and selective for GVL formation, also in the reactions in neat LA with very limited coke formation, sintering and leaching of ruthenium being observed. Further studies on the stability of the mainly the acid sites in the zeolite-supported catalysts, under the highly polar and corrosive conditions of LA conversion, should improve the performance of these first promising examples for the direct conversion of LA to PA.

**Acknowledgements**

Cor van de Spek is acknowledged for the TEM measurements. The authors thank the CatchBio User Committee for their valuable suggestions and discussions. Support of NWO for the "Solid State NMR facility for Advanced Materials Science" is gratefully acknowledged. We would like to thank Hans Janssen, Gerrit Janssen and Jan van Os for technical support.

## References


[1] B. Girisuta, L.P.B.M. Janssen, and H.J. Heeres, Chem. Eng. Res. Des. 84 (2006) 339-349.

[2] D.W. Rackemann, and W.O.S. Doherty, Biofuels, Bioprod. Biorefin. 5 (2011) 198-214.

[3] A. Corma, S. Iborra, and A. Velty, Chem. Rev. 107 (2007) 2411-2502.

[4] J.J. Bozell, L. Moens, D.C. Elliott, Y. Wang, G.G. Neuenscwander, S.W. Fitzpatrick, R.J. Bilski, and J.L. Jarnefeld, Resour. Conserv. Recy. 28 (2000) 227-239.

[5] I.T. Horvath, H. Mehdi, V. Fabos, L. Boda, and L.T. Mika, Green Chem. 10 (2008) 238-242.

[6] J.-P. Lange, R. Price, P.M. Ayoub, J. Louis, L. Petrus, L. Clarke, and H. Gosselink, Angew. Chem. Int. Ed. 49 (2010) 4479-4483.

[7] J.C. Serrano-Ruiz, D. Wang, and J.A. Dumesic, Green Chem. 12 (2010) 574-577.

[8] Z.-p. Yan, L. Lin, and S. Liu, Energy Fuels 23 (2009) 3853-3858.

[9] M.G. Al-Shaal, W.R.H. Wright, and R. Palkovits, Green Chem. 14 (2012) 1260-1263.

[10] L.E. Manzer, Appl. Catal. A: Gen. 272 (2004) 249-256.

[11] R.A. Bourne, J.G. Stevens, J. Ke, and M. Poliakoff, Chem. Commun. (2007) 4632-4634.

[12] D.C. Elliott, and J.G. Frye, US Patent 5883266 (1999) Battelle Memorial Institute

[13] J.-P. Lange, U.S. Patent No. 0112326 (2011).

[14] P.J. Van den Brink, K.L. Von Hebel, J.-P. Lange, and L. Petrus, WO2006067171 (2006).

[15] J.Q. Bond, D.M. Alonso, D. Wang, R.M. West, and J.A. Dumesic, Science 327 (2010) 1110-1114.

[16] J.Q. Bond, D.M. Alonso, R.M. West, and J.A. Dumesic, Langmuir 26 (2010) 16291-16298.

[17] E. Lippmaa, A. Samoson, and M. Magi, J. Am. Chem. Soc. 108 (1986) 1730-1735.

[18] G.L. Woolery, G.H. Kuehl, H.C. Timken, A.W. Chester, and J.C. Vartuli, Zeolites 19 (1997) 288-296.

[19] A. Primo, P. Concepcion, and A. Corma, Chem. Commun. 47 (2011) 3613-3615.

[20] P.M. Ayoub, and J.-P. Lange, WO2008142127 (2008).

[21] D. Di Mondo, D. Ashok, F. Waldie, N. Schrier, M. Morrison, and M. Schlaf, ACS Catal. 1 (2011) 355-364.

[22] J. Kornatowski, W.H. Baur, G. Pieper, M. Rozwadowski, W. Schmitz, and A. Cichowlas, J. Chem. Soc., Faraday Trans. 88 (1992) 1339-1343.

[23] C.S. Triantafillidis, A.G. Vlessidis, L. Nalbandian, and N.P. Evmiridis, Micropor. Mesopor. Mater. 47 (2001) 369-388.

[24] T. Barzetti, E. Selli, D. Moscotti, and L. Forni, J. Chem. Soc., Faraday Trans. 92 (1996) 1401-1407.

[25] E.P. Parry, J. Catal. 2 (1963) 371-379.

[26] T. Yashima, and N. Hara, J. Catal. 27 (1972) 329-333.

[27] A. Martin, U. Wolf, S. Nowak, and B. Lücke, Zeolites 11 (1991) 85-87.

[28] J.P. Marques, I. Gener, P. Ayrault, J.C. Bordado, J.M. Lopes, F. Ramôa Ribeiro, and M. Guisnet, Micropor. Mesopor. Mater. 60 (2003) 251-262.

[29] D. Freude, H. Ernst, and I. Wolf, Solid State Nucl. Magn. Reson. 3 (1994) 271-286.

[30] E. Brunner, H. Ernst, D. Freude, T. Fröhlich, M. Hunger, and H. Pfeifer, J. Catal. 127 (1991) 34-41.

[31] J. Kanellopoulos, A. Unger, W. Schwieger, and D. Freude, J. Catal. 237 (2006) 416-425.

[32] Z. Yu, A. Zheng, Q. Wang, L. Chen, J. Xu, J.-P. Amoureux, and F. Deng, Angew. Chem. Int. Ed. 49 (2010) 8657-8661.

[33] E.R.H. van Eck, J.A.Z. Pieterse, and A.P.M. Kentgens, Solid State Nucl. Magn. Reson. 39 (2011) 99-105.

[34] J.-P. Gilson, G.C. Edwards, A.W. Peters, K. Rajagopalan, R.F. Wormsbecher, T.G. Roberie, and M.P. Shatlock, J. Chem. Soc., Chem. Commun. (1987) 91-92.

[35] J. Chen, T. Chen, N. Guan, and J. Wang, Catal. Today 93–95 (2004) 627-630.

[36] M. Muller, G. Harvey, and R. Prins, Micropor. Mesopor. Mater. 34 (2000) 135-147.

[37] L.E. Manzer, U.S. Patent No. 100449 (2006).

# Chapter 3

# Changes in Aluminum Speciation in Zeolite-Supported Ruthenium Catalysts after Levulinic Acid Hydrogenation as Studied by $^{27}$Al 3QMAS NMR and FT-IR

**Abstract**

The influence of a highly-oxygenated, polar protic reaction medium, i.e., levulinic acid in 2-ethylhexanoic acid, on the dealumination of two zeolite-supported ruthenium catalysts (Ru/H-β and Ru/H-ZSM5) has been investigated by $^{27}$Al triple-quantum magic angle spinning (3QMAS) nuclear magnetic resonance (NMR). Upon use of the catalysts in the hydrogenation of levulinic acid, an increase in the heterogeneity in aluminum speciation is found for both Ru/H-ZSM5 and Ru/H-β. For Ru/H-ZSM5, the symmetric, tetrahedral framework aluminum species (FAL) are found to be mainly converted into distorted tetrahedral FAL species, with limited loss of aluminum to the solution by leaching. A severe loss of both FAL and extraframework aluminum (EFAL) species to the liquid phase was observed for Ru/H-β instead. The large decrease in tetrahedral FAL species, in particular, results in a significant decrease in the number of strong acid sites, as corroborated by Fourier transform infrared spectroscopy (FT-IR) and temperature-programmed desorption of ammonia (TPD-$NH_3$) measurements. This decrease in acidity, which shows the inferior stability of the strongly acidic sites in Ru/H-β relative to Ru/H-ZSM5, is considered the main reason for differences seen in catalytic performance between the two catalysts in the hydrogenation of levulinic acid to pentanoic acid.

Based on: Luo W., van Eck E.R.H., Bruijnincx P.C.A., Weckhuysen B.M., *manuscript in preparation.*

## 3.1 Introduction

Zeolites are crystalline materials composed of $SiO_4$ and $[AlO_4]^-$ tetrahedra. The acidity of zeolites is known to be strongly dependent on the type of zeolite structure, on the degree of substitution of aluminum for silicon in the framework and on the distribution of aluminum within the zeolite framework.[1, 2] Hydrolytic removal of aluminum atoms from their framework sites, i.e., zeolite dealumination, results in modification of the number, nature (Brønsted acidic (BAS) vs. Lewis acidic sites (LAS)), strength and location (framework vs. extra-framework) of the acid sites, ultimately altering the overall catalytic properties of zeolites in various ways.[3, 4] Subjecting zeolite materials to a medium of low pH and/or high polarity can, for instance, result in the hydrolytic removal of aluminum atoms from their framework sites. The extent to which this takes place, is known to depend on zeolite structure, applied temperature and composition of the liquid phase. Lavalley et al. have reported, for example, on the dealumination of H-β by mild HCl acid leaching treatment at 373 K.[5] Detka et al. furthermore showed different extents of dealumination of H-β by using aqueous HCl solutions of different concentration (0.1-1.5 M) at various temperatures (303- 373 K) and for various times (5 min to 6 h).[6] Importantly, not only mineral acids, but also the presence of organic acids can lead to framework dealumination. The aluminum content of H-β could, for instance, be reduced by 90% upon treatment at 344 K for 3 h with oxalic acid, which acts as both an acid and a chelating agent to remove framework aluminum and transport it out of the zeolite as water-soluble species.[7] Severe dealumination of H-β with oxalic acid was shown by Prins et al. to occur even at room temperature after 1 h, while a more limited degree of dealumination was observed for H-ZSM5.

While the examples listed above are concerned with the on-purpose dealumination of various zeolites in order to improve their catalytic performance, such changes in zeolite aluminum content and, as a result, acidity can also occur unintentionally if the zeolites are used as catalysts under high temperature, high pressure, liquid-phase conditions. Indeed, those conditions that are typically used for the conversion of renewable substrates to fuels and chemicals.[8] Some examples of such liquid phase, zeolite-catalyzed conversions include the work by Kaldstrom et al., who applied H-β for the conversion of levoglucosan in hot water at 423 K to achieve almost complete conversion

to give degradation products such as glucose, glycolaldehyde, formaldehyde, acetaldehyde and acetic acid,[9] and the work of Lercher and co-workers, who employed a Ni/ZSM-5 catalyst for aqueous-phase upgrading of the major aromatic fraction of pyrolysis oil at 523 K and 50 bar $H_2$,[10] as well as reported on the use of Ni/H-β for the conversion of stearic acid/microalgae oil to liquid alkanes in dodecane at 532 K and 40 bar $H_2$.[11] Fukuoka et al. successfully converted cellulose to a mixture of sugar alcohols by Pt and Ru on modified USY in water at 463 K at a hydrogen pressure of 50 bar, with stable sugar alcohol yields being observed for over 72 h. These few examples illustrate the use of zeolites, in some cases even bifunctional catalysts, with the zeolite serving as support for a hydrogenation metal with renewable substrates; they also highlight the lack of studies on catalyst stability under these conditions, however, as no report is made of changes to the acidity of the zeolite after catalysis.

Some of the hydrothermal conversion processes of renewable substrates even involve the use of renewable organic acids, either as substrate, as intermediate or as end product and as such seem to provide a particularly harsh environment for the zeolites.[12] In this sense, the catalytic valorization of the platform molecule levulinic acid provides a particularly good example of both the great potential of zeolites for such catalytic biomass conversions as well the possible challenges involved. Levulinic acid (LA), which can be produced easily and economically from lignocellulosic biomass, [13-15] is a versatile platform molecule and can be converted into γ-valerolactone (GVL),[16, 17] methyltetrahydrofuran (MTHF),[18] levulinate esters[19, 20] and pentanoic acid (PA) and its esters by sequential hydrodeoxygenation steps.[21] These products can in turn be used as additives,[22, 23] fuel components[24] and as chemical building blocks (see Chapter 1).[15] Zeolites have been studied for the various acid-catalyzed steps involved in the sequence, again on occasion as part of bifunctional catalysts in combination with a metal hydrogenation function. The Shell laboratory reported, for example, on a H-β-based catalyst at 523 K and 80 bar $H_2$ for ethyl levulinate conversion to ethyl pentanoate,[25] and a Pt/H-ZSM5-catalyzed process operating at 523 K and 10 bar for the conversion of GVL to PA.[21, 26] Limited information is again available, however, on the stability of the zeolites and changes in acidity used under the liquid phase conditions listed above. Further insight into such deactivation processes is therefore clearly needed.

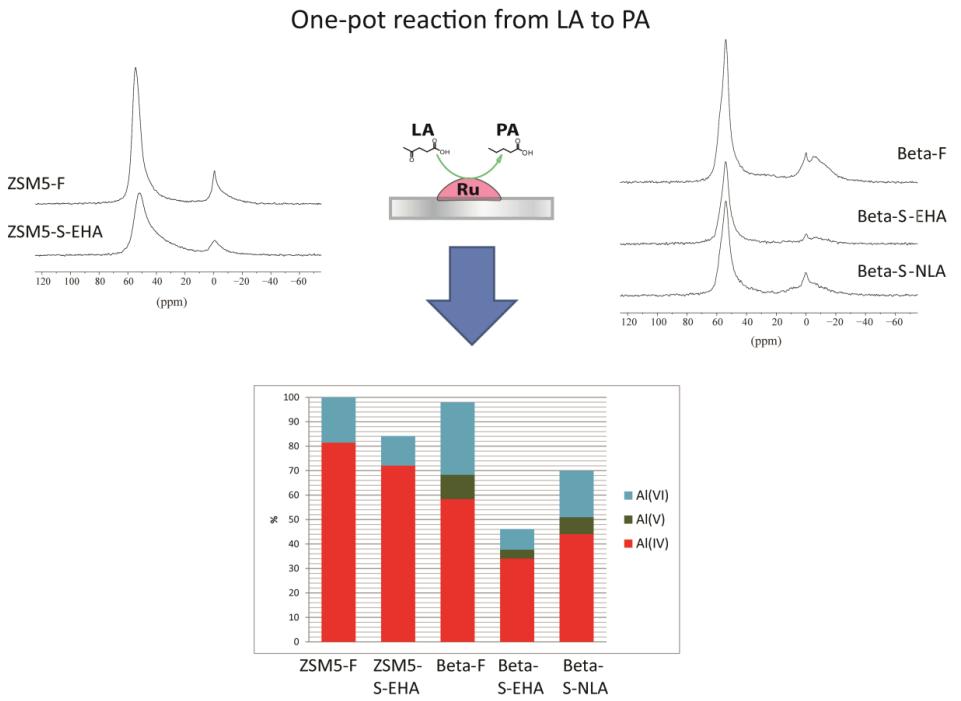


Scheme 3.1. Summary of the results obtained in Chapter 2 on the quantification of changes different aluminum species in zeolite-supported catalysts used in the hydrodeoxygenation of levulinic acid (LA) to pentanoic acid (PA) in 2-ethylhexanoic acid (EHA) or neat LA (NLA). The graph shows the relative amounts of tetrahedral, penta- and octahedral coordinated aluminum normalized to the aluminum content in the fresh Ru/H-ZSM5 catalyst as determined by $^{27}$Al MAS NMR (accuracy ±2%)

We previously reported on Ru catalysts supported on H-β-and H-ZSM5, which are capable of the direct hydrodeoxyenation (HDO) of LA to PA or its esters in dioxane at 473 K and 40 bar $H_2$ (see Chapter 2). In this case, the zeolite support material provided the strong acid sites that are essential for the ring-opening of GVL, which is considered to be rate-limiting in the process. Particular emphasis was put on catalyst stability and deactivation under increasingly severe conditions, with changes in the support as well as to the metal phase being studied. Changes in aluminum content and speciation were studied by FT-IR after pyridine adsorption to distinguish changes in LAS and BAS, AAS to study Al leaching and $^{27}$Al NMR to monitor changes in Al speciation. The stability

studies showed that the highest loss of framework aluminum occurred for Ru/H-β after a 10 h reaction at 473 K in a solution of 2-ethylhexanoic acid (EHA), which was used as a mimic of levulinic acid to provide a harsh environment of constant acid concentration to the catalyst. The first, preliminary studies on changes in Al speciation by quantitative analysis of the one dimensional (1D) solid state $^{27}$Al nuclear magnetic resonance (NMR) spectra showed (1) that more aluminum was lost from the H-β zeolite to solution than from H-ZSM5 and (2) that the extent of leaching was different for the four-, five- and six-coordinated Al species that could be discerned, with larger decreases seen in particular for the latter. The exact changes in Al content and (fractional) speciation are summarized in Scheme 3.1.[27]

To further assess the influence of the reaction environment on the degree of zeolite dealumination and, as a result, on the acidic properties of the catalysts, a more detailed comparison of the aluminum speciation of fresh and spent catalysts is required.[28] While 1D $^{27}$Al magic angle spinning (MAS) NMR has been extensively and successfully applied to investigate the coordination state of Al (e.g. four (Al(IV)) or six-coordinated Al (Al(VI)) in zeolites,[3, 29-32] such measurements also have their limitations. Indeed, each of the different coordination states may consist of different types of Al. These types may often be difficult or even impossible to distinguish as a result of the strongly overlapping signals that these produce in the low-resolution 1D spectra. Their lines are usually broadened by the second-order quadrupolar effect, giving typical quadrupolar line shapes. In addition, structural disorder will further broaden and smear out the quadrupolar line shapes due to a distribution in both quadrupolar interaction as well as isotropic chemical shifts. Two-dimensional $^{27}$Al triple-quantum (3Q) MAS NMR can provide the enhanced resolution needed to study these zeolite materials in more detail. This techniques allows one to obtain a 2D spectrum where the anisotropic part of the quadrupolar interaction is separated from isotropic shift contributions (i.e, the quadrupol-induced shift and the isotropic chemical shift).[38-41] A projection on the F1 dimension will give the isotropic spectrum while a projection on F2 dimension will provide the standard 1D MAS NMR spectrum. 3Q MAS NMR is especially helpful for the analysis of one-dimensional spectra of disordered materials.[34, 36-44] The disorder can be reflected in the line shapes of the 3Q MAS NMR spectra, and translated into interaction parameter distributions. In particular, $^{27}$Al 3Q MAS NMR has been

successfully applied in structural studies of zeolites, allowing the differentiation and even quantification of the different Al species.[4, 36, 45, 46] There has been an increasing interest in the quantification of this disorder recently,[47-49] and a promising model was developed by Czjzek et al.,[50] able to describe the quadrupolar interaction parameter distribution resulting from the structural disorder.

In this work, different Al species are differentiated and the interaction parameter distributions are determined for two fresh and spent zeolite-supported Ru catalysts, namely H-β and H-ZSM5, with $^{27}Al$ 3QMAS NMR. The obtained data have been fitted with the Czjzek model, which quantitatively establishes changes in the state of the various aluminum species. Furthermore, a combination of NMR, temperature-programmed desorption of ammonia (TPD-$NH_3$) and Fourier transform infrared (FT-IR) data provides insights into the changes in acid properties (i.e., amount, nature, and location) and related deactivation behavior of these Ru/zeolite catalysts for the selective hydrogenation of LA to PA.

## 3.2 Experimental Section

### 3.2.1 Catalyst Preparation and Catalytic Testing

1 wt% Ru/H-ZSM5 (Si/Al= 11.5, CBV2314, Zeolyst) and 1 wt% Ru/H-β (Si/Al= 12.5, CP814E, Zeolyst) were prepared with $RuNO(NO_3)_3$ (Alfa Aesar) as ruthenium precursor via a wet impregnation method followed by both calcination and reduction, as detailed in Chapter 2.[27] Fresh zeolite-supported Ru catalysts are labeled ZSM5-F and Beta-F. The catalysts were tested in the conversion of a 10 wt% solution of LA (Aldrich, 98%) in EHA (Aldrich, 99%) at a reaction temperature of 473 K and under 40 bar $H_2$ for 10 h. See Chapter 2 for details. After the catalytic reactions, the spent catalysts were recovered, washed with three times with acetone (Aldrich, >97%) and finally dried under vacuum overnight. The spent catalyst samples are labeled as ZSM5-S-EHA and Beta-S-EHA, respectively. An additional spent Ru/H-β catalyst, labeled Beta-S-LA, was obtained from a similar test reaction at 473 K and 40 bar $H_2$ for 10 h but now run in neat LA rather than in EHA.

### 3.2.2 Temperature-Programmed Desorption of Ammonia

The acidity of different samples was investigated by temperature-programmed desorption (TPD) of $NH_3$ under He flow (25 mL/min) using a Micromeritics AutoChem II equipped with a TCD detector. 0.15 to 0.2 g of catalyst was loaded and dried at 873 K for 1 h, after which the sample was cooled down to 373 K. Subsequently, pulses of ammonia were introduced up to saturation of the sample. The temperature-programmed desorption was performed up to 873 K, with a heating ramp of 5 K/min. The total number of acid sites (mmol $NH_3$/gram zeolite) was determined from the total amount of desorbed ammonia.

### 3.2.3 Infrared Spectroscopy

Fourier transform infrared (FT-IR) spectra were recorded on a Perkin-Elmer 2000 instrument at various temperatures. Self-supported catalyst wafers (12-19 mg/16 mm) were pressed at 3 kbar pressure for 10 s. The wafer was placed inside a synchrotron cell with a $CaF_2$ window. The cell was evacuated to $10^{-6}$ bar followed by drying of the sample at 573 K (3 K/min) for 1 h. The cell was cooled down to 323 K, and the FT-IR spectra of each zeolite sample were recorded at both 573 K and 323 K for hydroxyl group analysis.

Pyridine adsorption measurements were performed for all the samples by introducing the wafer to pyridine (Aldrich, ≥ 99.9%) vapors (3.1 mbar) for 10 s, after which the wafer were kept under these conditions for 30 min to reach equilibrium. Vacuum was subsequently applied for 30 min in order to remove physisorbed and loosely bound pyridine. FT-IR spectra were recorded under vacuum at different temperatures (3 K/min) from 323 to 723 K. For each spectrum, 25 scans were recorded with a resolution of 4 $cm^{-1}$.

### 3.2.4 Nuclear Magnetic Resonance

Solid-state $^{27}Al$ nuclear magnetic resonance (NMR) measurements were performed on a 600 MHz Varian NMR spectrometer using a 1.6 mm T3 design probe. The probe was tuned to 599.99 MHz for protons and 156.341 MHz for $^{27}Al$. Magic angle spinning at 25

kHz was employed. All samples were weighed to enable quantitative measurements. $T_1$ saturation recovery experiments showed that a repetition time of 0.4 s was more than sufficient for all magnetization to relax back to Boltzmann equilibrium. To ensure that intensities are quantitative regardless of the quadrupole coupling constant,[29] the single pulse measurements were done using an radio frequency (rf)-field strength of 10 kHz and a pulse length of 2 μs (equaling a tip angle of 7 degrees). Proton decoupling did not improve spectral quality in the 1D experiments. Care was taken to subtract the small background signal from the MAS rotor, prior to integration of the spectra. Intensities were also corrected for the presence of a small amount of satellite side band intensity that overlaps with the central transition signal by substracting the average intensity of the ± 1 sidebands from the centerband; however, this did not change relative intensities significantly.

$^{27}$Al 3QMAS NMR spectra were recorded using the z-filter sequence [51] with excitation and conversion pulse lengths of 1.8 μs and 0.65 μs respectively at an rf-field strength of 225 kHz and a z-filter pulse of 4 μs at an rf-field strength of 24 kHz was applied to detect the single quantum coherence. During both $t_1$ evolution and acquisition, proton decoupling was employed with a 151 kHz rf-field strength using a spinal sequence, (3.75 μs pulse length, 6$^o$ phase). The 3QMAS NMR spectra were acquired using the States method for phase-sensitive detection in the indirect dimension. After two dimensional (2D) Fourier transformation the data were sheared with a factor of 19/12 and the F1 axis scaling was adjusted to display isotropic spectra in the F1 dimension. The 2D spectra showed lineshapes typical for a distribution in quadrupole parameters. In order to analyze the relative intensities of the different aluminum species $^{27}$Al 3QMAS spectra were analyzed using the EASYGOING deconvolution program.[52, 53] Using an evolutionary algorithm, this program can fit $^{27}$Al 3QMAS spectra, taking into account the distribution of quadrupole parameters according to the Czjek model[46, 47] and a distribution in chemical shifts at the same time for multiple sites. With the distribution parameters thus obtained the 1D $^{27}$Al MAS NMR spectra were analyzed with a Matlab routine that calculates the theoretical distribution spectrum for each site and calculates their relative contribution to the experimental data with singular value decomposition.

### 3.2.5 Atomic Absorption Spectrophotometry

The liquid phase was tested after reaction by flame atomic absorption spectrophotometry (AAS) for the presence of Al. All elements (Al) were analyzed on a ContrAA 700 apparatus using the 396.1 nm line of Al ($N_2O$/acetylene flame).

## 3.3 Results and Discussion

### 3.3.1 Ammonia-TPD and FT-IR Spectroscopy

The acidity, i.e. the quantity and strength of the acid sites, of the fresh catalysts was probed by $NH_3$-TPD. Table 3.1 lists the total amount of acidic sites of ZSM5-F and Beta-F, illustrating the higher acidity of ZSM5-F.

Table 3.1. Acid concentrations calculated from $NH_3$-TPD.

| Catalyst | Total acidity ($mmol/g_{cat}$) | Low T region ($mmol/g_{cat}$) | Low T/Total | High T region ($mmol/g_{cat}$) | High T/Total |
|---|---|---|---|---|---|
| ZSM5-F | 1.35 | 0.93 | 0.69 | 0.42 | 0.31 |
| Beta-F | 1.07 | 0.71 | 0.66 | 0.36 | 0.34 |

FT-IR spectra of the OH stretching region for the fresh and spent catalysts are given in Fig. 3.1a and b. For ZSM5, three main features can be seen, corresponding to -OH groups assigned as Brønsted acid sites (BAS) at 3602 $cm^{-1}$, as Lewis acid sites (LAS) at 3662 $cm^{-1}$ and as terminal silanols at 3735 $cm^{-1}$.[54-56] Only the BAS at 3602 $cm^{-1}$ were found to decrease in intensity for ZSM5-S-EHA, indicating some loss of these species during the catalytic reaction in EHA. For the Beta samples, five features can be seen in the hydroxyl region, associated with different –OH groups at 3604 $cm^{-1}$ (FAL, BAS), 3664 $cm^{-1}$ (LAS), 3735 $cm^{-1}$ (terminal silanols located at the internal surface), 3743 $cm^{-1}$ (terminal silanols located at the external surface), and at 3779 $cm^{-1}$ (LAS, -OH on small, extra-framework aluminum clusters, formed upon dealumination during calcination).[5, 57-59]

The gradual disappearance of the vibrations at 3604, 3664 and 3779 $cm^{-1}$ for both Beta-S-LA and Beta-S-EHA shows that both BAS and LAS sites had disappeared after reaction. A similar reduction in intensity of these particular features has also been reported as a result of acid leaching in previous studies.[57, 58, 60, 61] For Beta-S-LA and Beta-S-EHA a decrease in 3743 and 3735 $cm^{-1}$, with the latter showing a stronger reduction, was also observed, indicating that the terminal silanols located at the internal H-β surface are affected more than the external ones during reaction. Such a reduction in silanol concentration was also observed upon dealumination of H-β in oxalic acid at longer treatment time with condensation of adjacent silanol groups or silicon migration being proposed as possible reasons for this reduction in silanol groups.[7] Yet another cause for this reduction could be an interaction between leached Al species that are released upon dealumination with these silanols that are found in the pores.

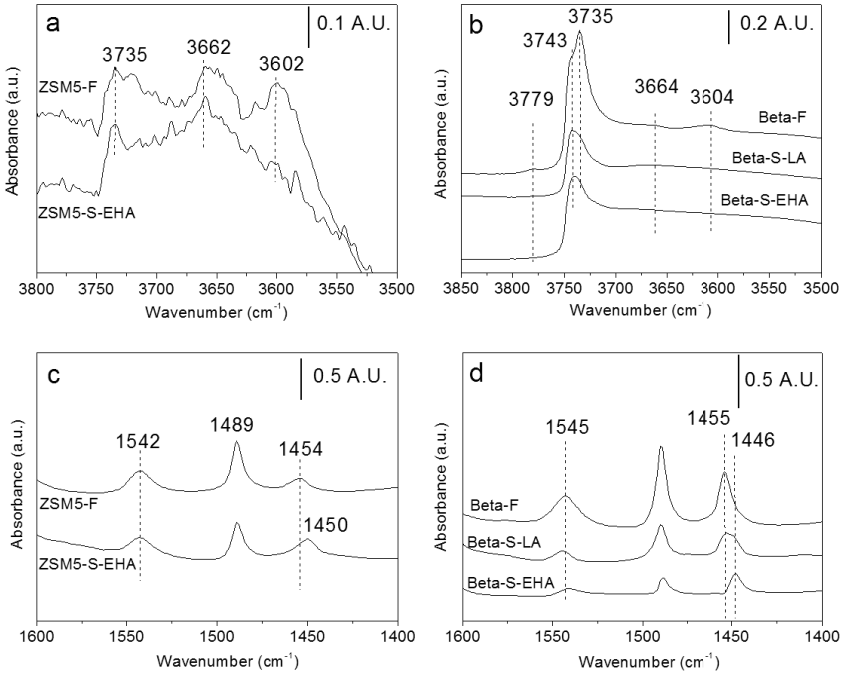


Figure 3.1. FT-IR spectra of the -OH stretching vibration region of ZSM5 (a) and Beta (b); vibrations assigned to BAS and LAS after pyridine adsorption of the fresh and spent ZSM5 (c) and Beta (d) catalysts.

Fig. 3.1c and d show the FT-IR spectra of the fresh and spent zeolite-supported catalysts after pyridine adsorption. The three main features observed are the result of the interaction between pyridine and the acid sites of the zeolites. The band at around 1455 $cm^{-1}$ is attributed to the interaction of pyridine with LAS, the band at 1490 $cm^{-1}$ is typically ascribed to unspecifically adsorbed pyridine on BAS and LAS. The vibration at 1545 $cm^{-1}$ is characteristic for pyridine adsorbed on BAS.[5, 62-64] For the ZSM5 sample, it can be seen that ZSM5-S-EHA shows a limited decrease in Brønsted acid sites compared to the fresh sample ZSM5-F. This small drop in BAS is associated with a small increase in LAS, with the increase in intensity being accompanied by a red-shift of 1454 to 1450 $cm^{-1}$ after the 10 h reaction in EHA. This red shift is thought to be the result of the dealumination process;[65] in particular, it might be the result of some of the EFAL species being coordinated to FAL sites that are located in close proximity.[56, 66] In contrast, the spent H-β samples showed a sharp decrease in intensity of the vibrations at 1455 $cm^{-1}$, 1490 $cm^{-1}$ and 1545 $cm^{-1}$. This drop in pyridine-probed acid sites was even more pronounced for Beta-S-EHA than for Beta-S-LA, suggesting a larger loss of both BAS and LAS for Beta-S-EHA. The EHA conditions are indeed considered more severe, as the catalysts are subjected to a constant acid concentration in this solvent. In the runs in neat LA, the acid is actually reacting away to form GVL, thus gradually lessening the severity of the environment that the catalyst is exposed to.[27] Interestingly, the appearance of a new LAS feature at 1446 $cm^{-1}$ was also observed, which became more distinct for the severely dealuminated samples Beta-S-EHA. Gener et al. has proposed these new LAS vibrations to originate from pyridine molecules that are both coordinated to a LAS as well as interact through an H-bond with a BAS,[65] again implying that some EFAL and BAS are actually in close proximity in the spent catalysts. The mutual attraction of the highly charged EFAL and the negative charge on the FAL of the zeolite prevents the EFAl from being washed out of the pores of the zeolite. Taken together with the observed reduction in silanols and increase of this new LAS for dealuminated Beta samples, the structure of these new LAS could be assigned to EFAL species coordinated to BAS of FAL in close proximity, similar to those discussed above for ZSM5-S-EHA. Indeed, Deng et al. previously proposed two possible structures for such sites to be present in dealuminated HY in their study of the Brønsted/Lewis acid synergy that has been observed for hydrocarbon reactions with these zeolites.[66]

### 3.3.2 Nuclear Magnetic Resonance

#### 3.3.2.1 ZSM5

In the $^{27}$Al 3QMAS NMR spectra of the fresh and spent ZSM5 samples, four peaks can be discerned, two tetrahedral and two octahedral Al resonances, which are discussed in more detail below (Figure 3.4). These resonances show lineshapes typical for species with a distribution in quadrupole parameters. In order to quantify the relative contribution of each type of aluminum in each sample, the line parameters and distribution parameters need to be determined from the 3QMAS NMR spectra.

In crystalline materials the quadrupole interaction gives rise to typical lineshapes, characterised by the quadrupole coupling constant Cq and the asymmetry parameter η. To determine the effect of structural disorder on the NMR spectrum of a quadrupolar nucleus one has to realise that the quadrupole parameters are actually a representation of the electric field gradient (*efg*) tensor which describes the orientational dependence of the strength of the electric field gradients surrounding an atomic nucleus. These *efg*'s arise from the charge distribution around the nucleus. The quadrupolar coupling constant $C_q$ is given by:

$$C_q = \frac{eQV_{ZZ}}{h}$$

Where $V_{ZZ}$ is the largest principal component of the *efg* tensor. While the asymmetry parameter η is given by:

$$\eta = \frac{V_{XX} - V_{YY}}{V_{ZZ}}$$

With $V_{XX}$ and $V_{YY}$ being the other principal components of the *efg* tensor, with the convention that $|V_{ZZ}| \geq |V_{YY}| \geq |V_{XX}|$. Finally, because one is discussing electric field gradients (i.e., a second order derivative of the electric potential), Laplace's equation holds ($\nabla^2 V = 0$) which means that the efg tensor is traceless, i.e. the principal components add up to 0. Hence it would be somewhat naive to assume that structural disorder would lead to a Gaussian distribution in the quadrupole parameters $C_q$ and η

(for instance, η can only range from 0 to 1). However, the efg tensor values do tend to a normal distribution. Czjzek et al.[50] investigated the *efg* distribution in the case of structural disorder by computer simulations. Tensor components of the *efg* at the center of randomly repositioned charges, become normally distributed in the limit of infinite samplings. The resulting probability distribution, as a function of *efg* tensor components, is therefore a multivariate Gaussian. This distribution can be rewritten as a probability density function of quadrupole interaction parameters Cq and has the form:

$$f(C_q,\eta) = \frac{C_q^{d-1}\eta}{\sqrt{2\pi}\sigma^d}\left(1-\frac{\eta^2}{9}\right)exp\left\{\frac{-C_q^2}{2\sigma^2}\left(1+\frac{\eta^2}{3}\right)\right\}$$

Here $\sigma$ is the standard deviation of the multivariate Gaussian probability distribution of the *efg* tensor components and *d* corresponds to the number of independent tensor components. Fig. 3.2 shows an example of such a distribution. Now the isotropic shifts and the distribution parameters can be obtained from the 3QMAS spectra by fitting the peaks to spectra generated by the Czjzek distribution.[53, 67, 68]

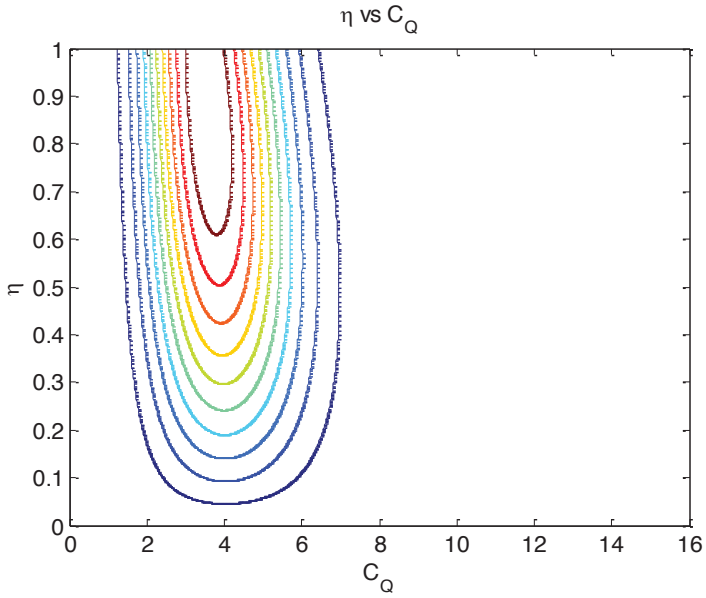


Figure 3.2. Distribution of $C_Q$ vs η for the Czjzek distribution with σ = 2MHz, in this case d = 5. The average $C_Q$ value is 2σ (4 MHz) and the width of the distribution is 1.552 s in this case, while the average value of η is always 0.606.

The 3QMAS NMR spectra were fitted using the EASYGOING deconvolution program.[52, 53] This program can fit 3QMAS NMR spectra based on an evolutionary algorithm, taking into account the distribution of quadrupole parameters according to the Czjek model and a distribution in chemical shifts at the same time for multiple sites. As an example, Fig. 3.3 shows the results of fitting the 3QMAS data of the ZSM5-F sample with EASYGOING.

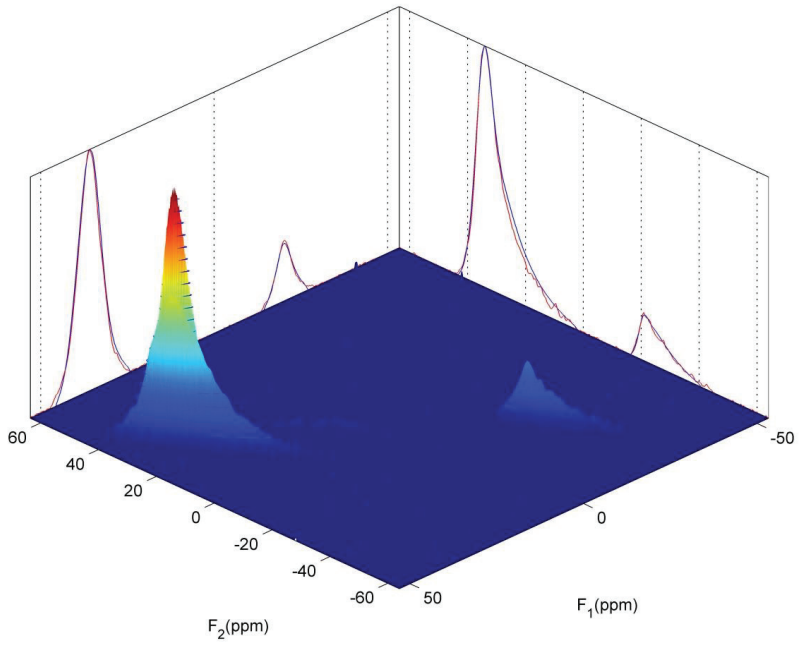


Figure 3.3. Experimental 3QMAS spectrum (colored) and fitted 2D $^{27}$Al NMR spectrum (blue contour lines) of ZSM5-F. The spectrum shows the projections of both the experimental data (red) as well as the fitted data (blue). Note that the chemical shift reference is not set in this Figure.

The program thus already provides us with relative contributions, but it should be noted that small $C_Q$ resonances are usually underrepresented in 3QMAS spectra. Therefore, it was chosen to fit the 1D $^{27}$Al MAS NMR spectra instead, using the parameters obtained from the $^{27}$Al 3QMAS NMR data, except for the intensities. For this purpose a Matlab routine was developed that calculates the theoretical spectra and fits

them to the experimental data with singular value decomposition. The routine produces a good match with the data, as illustrated in Fig. 3.4.

Table 3.2. Fitted peak parameters and intensities for the Ru/H-ZSM5 samples.

| Sample | Al type | $<C_Q>$ (MHz) | $\sigma_Q$ (MHz) | $\delta$iso (ppm) | $\Delta\delta$ (ppm) | Fraction of spectral Intensity | Intensity normalized to ZSM5-F[a] |
|---|---|---|---|---|---|---|---|
| ZSM5-F | Al(IV)-L[b] | 5.96 | 2.98 | 58.0 | 5.5 | 0.51 | 51 |
| | Al(IV)-M | 1.36 | 0.68 | 54.9 | 4.3 | 0.32 | 32 |
| | Al(VI)-L | 5.56 | 2.78 | 0.9 | 4.1 | 0.14 | 14 |
| | Al(VI)-M | 1.60 | 0.80 | 0.0 | 2.4 | 0.04 | 4 |
| ZSM5-S-EHA | Al(IV)-L | 7.68 | 3.84 | 57.4 | 7.2 | 0.70 | 59 |
| | Al(IV)-M | 2.34 | 1.17 | 53.9 | 5.2 | 0.19 | 16 |
| | Al(VI)-L | 5.58 | 2.79 | 1.9 | 5.5 | 0.06 | 5 |
| | Al(VI)-M | 2.28 | 1.14 | 0.5 | 5.0 | 0.05 | 4 |

[a] Based on 1D $^{27}$Al MAS NMR fitting. The total Al signal of ZSM5-F has been normalized by weight and set to 100/g of zeolite; the numbers give the individual contributions of these Al species to the total signal intensity; for ZSM5-S-EHA the total signal intensity was normalized by weight, taking into account the coke content, and compared to the original signal intensity of the fresh sample. The other parameters are based on the $^{27}$Al 3QMAS NMR spectra.

[b] L: large $C_Q$; M: medium $C_Q$.

Table 3.2 shows isotropic chemical shifts ($\delta_{iso}$) and the average quadrupolar coupling constant values ($C_Q$) as determined by the EASYGOING 2D fitting and the relative intensities of the various Al species for ZSM5-F and ZSM5-S-EHA as obtained from the 1D spectra. The intensities relative to the ZSM5 samples have been corrected for weight, and coke content (see Chapter 2 for details on coke deposition). The ratio's of six- to four–coordinated Al species agree well with those that were obtained in Chapter 2 by simple integration of the 1D spectra.[27] The data obtained from the fitting also compares well to the TPD-$NH_3$ results, with the calculated fractions of Al(IV)-M sites, i.e. the ones responsible for ammonia desorption in the high T region, being in good agreement (0.31 for TPD compared to 0.32 for NMR). All other species contribute to desorption in the low T region.

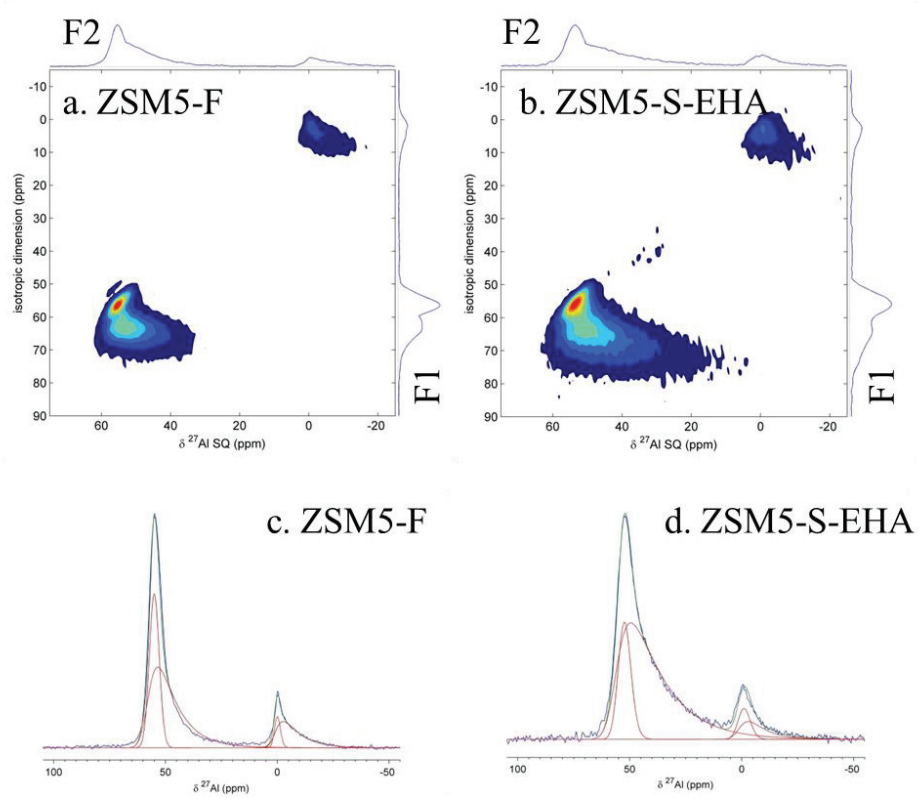


Figure 3.4. $^{27}$Al 3QMAS NMR spectra of (a) ZSM5-F and (b) ZSM5-S-EHA. The 2D spectra are sheared so that the projection on the F1 axis gives an isotropic spectrum; normalized $^{27}$Al MAS NMR spectra of (c) ZSM5-F and (d) ZSM5-S-EHA . blue: experimental, green: fitted, red: simulated peaks.

Fig. 3.4 shows the 2D 3QMAS and 1D $^{27}$Al MAS NMR spectra of ZSM5-F and ZSM5-S-EHA. Both ZSM5-F and spent ZSM5-S-EHA show two types of four-coordinated and two types of six–coordinated aluminum species and their relative intensities change during the catalytic reaction. The Al(IV)-M peak, which has an isotropic shift of around 54 ppm and a small $\langle C_Q \rangle$ of 1.36 MHz, represents tetrahedral framework aluminum (FAL);[69] The Al(IV)-L resonance, with an isotropic shift of around 57 ppm and a $\langle C_Q \rangle$ of 5.96 MHz, shows increased horizontal broadening (evidenced from the F1 and F2 projection) after the catalytic reaction, which is typically attributed to the influence of nearby cationic species. These cationic species could either originate from the hydrogenation metal (Ru) or from EFAL, with the latter being more likely.[41, 70] These perturbed FAL can

therefore best be considered as distorted tetrahedral Al, which most likely originate from tetrahedrally coordinated FAL that are compensated in their negative charge by either EFAL or Ru ions that could have been formed in the calcination or reduction processes.[31, 34, 71] The latter is unlikely, however, as aluminum species interacting strongly with Ru ions would be difficult to observe. The paramagnetic nature of these will enhance both $T_1$ and $T_2$ relaxation and make them become invisible, as also reported previously for Fe-containing zeolites.[32] Moreover, Ru is unlikely to provide this charge compensation in the channels given its low loading (1 wt%) and particle size (mean particle size = 5 nm). In this respect, it seems more likely that the Al(IV)-L signal is the result of EFAL species that are present in the MFI pores, which coordinate to the FAL and cause the distortion.[31, 38, 56, 72-75] The Al(VI)-M species shows the standard parameters for six-coordinated extra-framework aluminum atoms (EFAl, $\delta_{iso}$ around 0 ppm and a small $<C_Q>$ = 1.6 MHz) and can be assigned to octahedral EFAL $Al(OH)_3$-$3H_2O$; the other octahedral Al(VI)-L species with the larger $<C_Q>$ of 5.56 MHz, has been proposed to be three-coordinated FAL species with three additionally adsorbed water molecules.[72] It should be noted that 69% of total acid amount is in the low T region from the TPD-$NH_3$ data, which already suggests that substantial dealumination has occurred already during the catalyst preparation.

Assuming that each peak reflects the same aluminum species in fresh and spent catalysts (which is very likely), then for all species the $<C_Q>$'s become larger for the spent sample. The relative and absolute intensities furthermore change upon catalysis, with the amount of Al(IV)-L increasing slightly and the amount of Al(IV)-M having been more than halved. This suggests the transition of FAL species to distorted FAL species, again thought to be the result of the coordination of dealuminated EFAL to FAL.[37, 56] In contrast, the increase in all $\sigma_Q$ and $C_Q$ parameters points at the increased heterogeneity of the sample; the origin of this broadening is twofold, as the EFAL in the pores are the cause of a short-range polarization effect, while an additional long-range geometrical effect is seen in ZSM5 that gives rise to an increase in all the parameters.[45] The main change in Al speciation after catalysis is therefore the transition of four-coordinated, symmetric FAL (Al(IV)-M) to FAL distorted by coordinated EFAL (Al(IV)-L). Taken together with the slight decrease in BAS as seen in IR, this shows an increase in

the disorder in strong acid sites in ZSM5-S-EHA, as well as a small reduction in their number, upon catalysis.

#### 3.3.2.2 Beta

Figure 3.5 shows the $^{27}$Al 3QMAS and $^{27}$Al MAS NMR spectra for Beta-F, Beta-S-LA and Beta-S-EHA. In Table 3.2, the peak parameters as determined by the EASYGOING 2D fitting and the relative intensities of the various Al peaks obtained from fitting the 1D spectra are listed. In contrast to the H-ZSM5 NMR data, it proved to be very difficult to fit the H-β spectra in the Al(V)/(VI) region; considering that the reaction is BAS-catalyzed, we therefore focus here on the BAS region only for the Beta samples. Indeed, while three types of tetrahedral aluminum (BAS) can be discerned in this case, the octahedral Al signal cannot be successfully fitted with the two resonances used previously (three signals should be used to fit the peak, but the resulting signal-to-noise ratio is too poor and lineshapes are not well described). Furthermore, the five-coordinated Al species that are observed at around 30 ppm have too low an intensity to be fitted satisfactorily. The amounts of Al(V) and Al(VI) listed in the table were therefore obtained from the residual intensity left after the tetrahedral Al fit. The ratio of four- to five-/six-coordinated Al again corresponds well to the one given in Chapter 2.[27] For Beta-F, the two sharp peaks of Al(IV)-S ($\delta_{iso}$ = 53.9 ppm, $\langle C_Q \rangle$ = 1.02 MHz) and Al(IV)-M (δiso = 56.0 ppm, $\langle C_Q \rangle$ = 2.08 MHz, slightly perturbed) represent symmetric tetrahedral FAL species; The Al(IV)-L resonance ($\delta_{iso}$ =59.0 ppm, $\langle C_Q \rangle$ = 5.8 MHz) is a highly perturbed FAL species, probably tetrahedrally-coordinated FAL compensated in their negative charge by EFAL cations, or with EFAL coordinated to a neighboring oxygen atom.[66] It would then be these EFAL that are responsible for the red shift in the LAS signal at 1446 $cm^{-1}$ in the FT-IR spectra after pyridine adsorption. Finally, Al(V) and Al(VI) are assigned to EFAL.[4, 5] The NMR and TPD data are again in a good agreement, with the calculated fraction of Al(IV)-S and Al(IV)-M species, responsible for desorption in the high T region, being 0.32 by NMR, which is close to the 0.34 found by TPD.

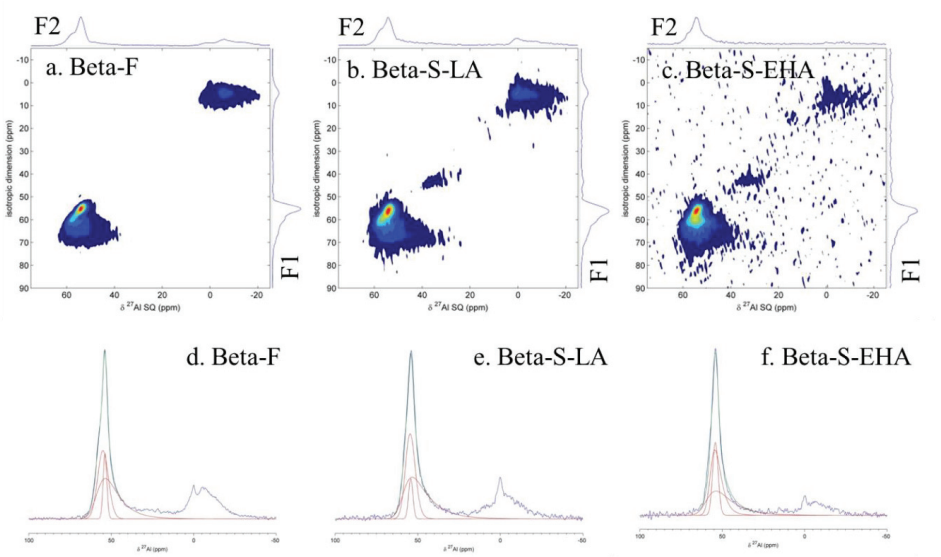


Figure 3.5. $^{27}$Al 3QMAS NMR spectra of (a) Beta-F, (b) Beta-S-LA and (c) Beta-S-EHA. The 2D spectra are sheared so that the projection on the F1 axis gives an isotropic spectrum; normalized $^{27}$Al MAS NMR spectra of (d) Beta-F, (e) Beta-S-LA and (f) Beta-S-EHA. blue: experimental, green: fitted, red: simulated peaks.

After catalysis, the intensity of all the Al species was found to have decreased for the Beta samples. A larger decrease in Al(IV) (FAL, BAS), species was observed for the Beta samples than for the ZSM5 ones, indicating that the former experience more extensive dealumination. An overall loss of ~40% of all the Al(IV) species (BAS) was observed for Ru/H-β after the reaction in EHA. Of the different tetrahedral species, a strong reduction was seen in intensity for Al(IV)-L and Al(IV)-M, but a similar amount of Al(IV)-S was detected. Interestingly, for Beta-S-NLA the Al(IV)-S signal was reduced in intensity by half, even though these conditions in an NLA are considered to be a lot milder than in the EHA run; this suggests that Al(IV)-S can be approached by LA (minimum dimension of 3.3 Å), but not by EHA (minimum dimension of 5.3 Å).

Table 3.3. Fitted peak parameters and intensities for the Ru/H-β samples.

| Sample | Al type | $<C_Q>$ (MHz) | $\sigma_Q$ (MHz) | $\delta_{iso}$ (ppm) | $\Delta\delta$ (ppm) | Fraction of spectral Intensity | Intensity normalised to Beta-F[a] |
|---|---|---|---|---|---|---|---|
| Beta-F | Al(IV)-L[b] | 5.80 | 2.90 | 59.0 | 7.5 | 0.32 | 32 |
| | Al(IV)-M | 2.08 | 1.04 | 56.0 | 6.2 | 0.24 | 24 |
| | Al(IV)-S | 1.02 | 0.51 | 53.9 | 2.2 | 0.08 | 8 |
| | Al(V)/(VI) | | | | | 0.36 | 36 |
| Beta-S-LA | Al(IV)--L | 6.36 | 3.18 | 59.2 | 7.2 | 0.36 | 28 |
| | Al(IV)--M | 2.52 | 1.26 | 55.8 | 5.2 | 0.28 | 21 |
| | Al(IV)--S | 0.44 | 0.22 | 53.9 | 2.6 | 0.06 | 4 |
| | Al5/Al6 | | | | | 0.30 | 23 |
| Beta-S-EHA | Al(IV)-L | 6.44 | 3.22 | 60.0 | 7.8 | 0.29 | 14 |
| | Al(IV)-M | 3.72 | 1.86 | 56.7 | 4.6 | 0.33 | 17 |
| | Al(IV)-S | 1.50 | 0.75 | 54.4 | 3.2 | 0.17 | 8 |
| | Al(V)/(VI) | | | | | 0.21 | 10 |

[a] Based on 1D $^{27}$Al MAS NMR fitting. The total Al signal of Beta-F has been normalized by weight and set to 100/g of zeolite; the numbers give the individual contributions of these Al species to the total signal intensity; for Beta-S-LA and Beta-S-EHA the total signal intensity was normalized by weight, taking into account the coke content, and compared to the original signal intensity of the fresh sample. The other parameters are based on the $^{27}$Al 3QMAS NMR spectra.

[b] S: small $C_Q$; L: large $C_Q$; M: medium $C_Q$.

Five-coordinated aluminum (Al(V)) can be clearly observed from the 1D fits of Beta-F, together with quite some Al(VI) species. Those species are assigned to EFAL (LAS), which are generated via dealumination during the thermo treatment of the zeolites.[37, 76] The total, combined amount Al(V)/(VI) decreased strongly in the Beta-S-LA sample and even more in Beta-S-EHA. All this, together with severe loss of both BAS and LAS seen in IR and the leached Al detected in the liquid phase by AAS, indicate the rapid dissolution of a significant part of the FAL and EFAL into the reaction medium.

### 3.3.3 Catalytic Activity in BAS-Catalyzed Conversion of LA-to-PA

The characterization data presented above now provides additional insight into the differences seen in catalytic performance of the two zeolite-supported Ru catalysts. The materials were tested in the hydrogenation reaction of levulinic acid at 473 K and 40

bar $H_2$, as reported in Chapter 2.[27] While the conversion of LA to GVL can be easily done by a monofunctional Ru catalyst on an inert support, the deeper hydrodeoxygenation to PA requires a bifunctional catalyst containing strong BAS able to catalyze GVL ring-opening, which is considered to be the rate-determining step.[27] The time profiles depicted in Fig. 3.6 for 10 h reactions in EHA show that a two-fold higher PA yield was achieved with Ru/H-ZSM5 (15.5%) compared to Ru/H-β (6.3%), although no PA was produced with Ru/H-ZSM5 at the early stages of reaction. The extent and rate with which BAS sites are lost during catalysis are considered to be responsible for the difference in activity. For Ru/H-ZSM5, the main changes in Al speciation involved the transition of symmetric BAS into BAS distorted by an interaction with formed EFAL, resulting in a decrease in BAS sites upon catalysis in EHA of around 10%, as indicated by both IR and NMR (Fig. 3.1 and Table 3.2); In contrast, in the case of Ru/H-β, a much more severe loss of BAS as well as LAS was observed, resulting in nearly a 40% loss of BAS sites in the catalyst, (Fig. 3.7) ultimately leading to a lower PA yield. It should finally be noted that the amount of Al lost to solution for Ru/H-β was three times the amount of Ru/H-ZSM5, as determined by AAS. This corresponds well to the Al loss as determined by fitting of the NMR data. The lower degree of dealumination that is observed for ZSM5 can be attributed to the smaller channel dimensions (ZSM5: 5.5 × 5.4 Å VS H-β 7.4 × 6.5 Å), less flexible structure (10-ring VS 12-ring) and the smaller amount of crystal defects (less stacking faults).[4, 7, 77]

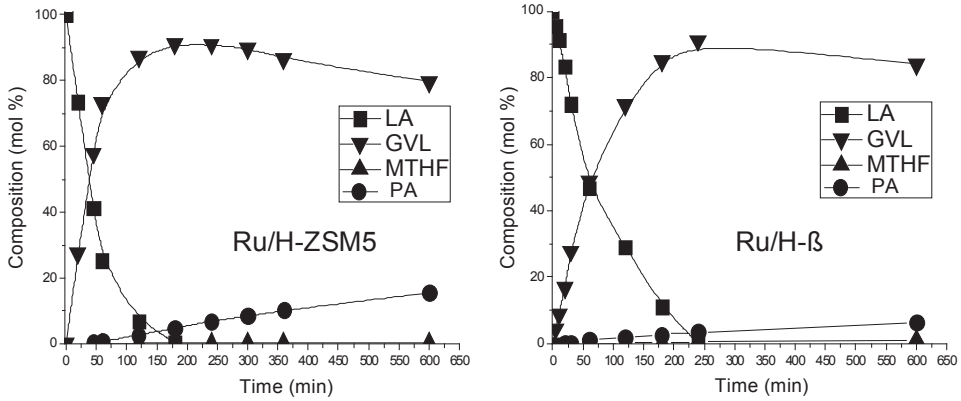


Figure 3.6 Time profiles of the catalytic hydrogenation of 10 wt% levulinic acid in 2-ethylhexanoic acid. Conditions: 473 K, 40 bar, 10 h reaction time, 1wt% Ru loading with different zeolite supports, stirrer speed of 1600 rpm LA: levulinic acid; GVL: γ-valerolactone; MTHF: methyltetrahydrofuran; PA: pentanoic acid.

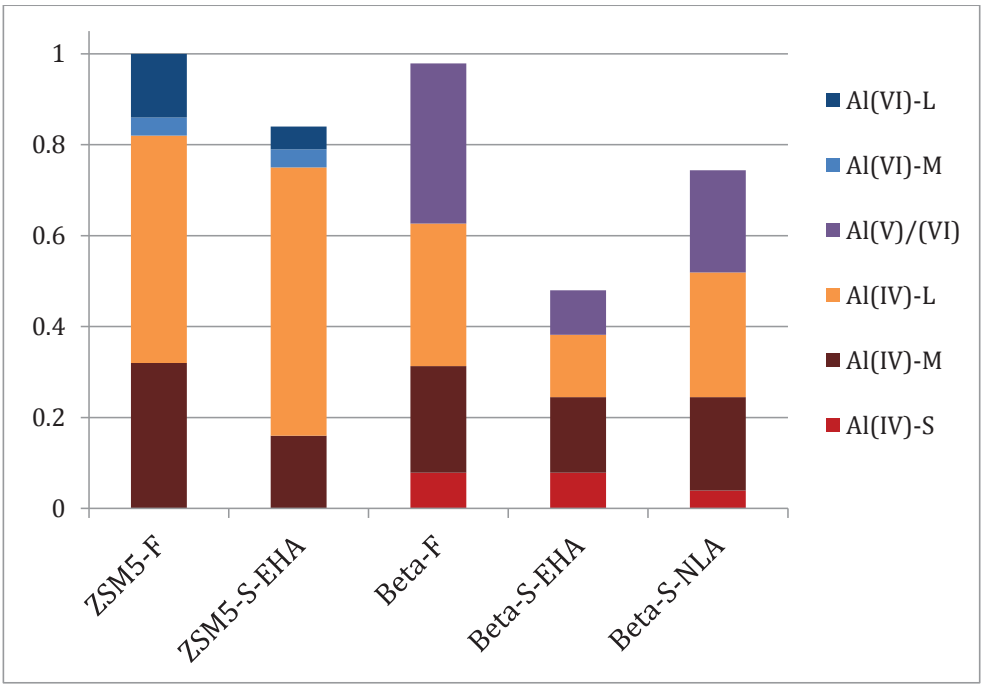


Figure 3.7 Relative amounts of four, five, and six-coordinated aluminum normalized to the aluminum content in ZSM5-F catalyst as determined by $^{27}$Al MAS NMR (accuracy ±2%).

### 3.4 Conclusions

Analysis of the solid-state $^{27}$Al 3QMAS NMR spectra of Ru-based zeolite catalysts, active in the hydrogenation of levulinic acid (LA) into pentanoic acid (PA), allows for quantitative changes in aluminum speciation to be determined. The obtained $^{27}$Al 3QMAS NMR spectra revealed two four-/six-coordinated aluminum species for Ru/H-ZSM5 and three four-coordinated aluminum species for Ru/H-β together with five and six-coordinated aluminum species. After LA hydrogenation in EHA, a slight increase in disorder is found for Ru/H-ZSM5, which is mainly due to the transition of Brønsted-acidic, symmetric FAL into intermediate distorted FAL. In contrast, three four-coordinated aluminum species could be distinguished by $^{27}$Al 3QMAS NMR for Ru/H-β. A much more severe loss of both FAL (BAS) and EFAL (LAS) species was observed for the Ru/H-β catalyst after LA hydrogenation in EHA. Interestingly, there was no loss of

Al(IV)-S for the Ru/H-β catalyst after LA hydrogenation in NLA, which indicates that this aluminum species is most probably located in the small channels of H-β. H–ZSM5 thus shows higher stability towards dealumination than H-β. The loss of catalytic activity (as expressed by the PA yield) for Ru/H-β is related to the significant decrease in BAS (~ 40% loss), which is correlated with the decrease in the number of tetrahedral FAL (Al(IV)-L and Al(IV)-S) species.

**Acknowledgements**

Support of NWO for the 'Solid-state NMR facility for Advanced Materials Science' is gratefully acknowledged.

**References**

[1] A. Corma, Chem. Rev. 95 (1995) 559-614.

[2] Y.V. Kissin, Catal. Rev. 43 (2001) 85-146.

[3] E. Bourgeat-Lami, P. Massiani, F. Di Renzo, P. Espiau, F. Fajula, and T. Des Courières, Appl. Catal. 72 (1991) 139-152.

[4] M. Müller, G. Harvey, and R. Prins, Micropor. Mesopor. Mater. 34 (2000) 135-147.

[5] M. Maache, A. Janin, J.C. Lavalley, J.F. Joly, and E. Benazzi, Zeolites 13 (1993) 419-426.

[6] M. Guisnet, P. Ayrault, C. Coutanceau, M. Fernanda Alvarez, and J. Datka, J. Chem. Soc., Faraday Tran. 93 (1997) 1661-1665.

[7] M.R. Apelian, A.S. Fung, G.J. Kennedy, and T.F. Degnan, J. Phys. Chem. 100 (1996) 16577-16583.

[8] D. Kubička, I. Kubičková, and J. Čejka, Catal. Rev. 55 (2013) 1-78.

[9] M. Kaldstrom, N. Kumar, T. Salmi, and D.Y. Murzin, Cell Chem. Technol. 44 (2010) 203-209.

[10] C. Zhao, and J.A. Lercher, Angew. Chem. Int. Ed. 51 (2012) 5935-5940.

[11] B. Peng, Y. Yao, C. Zhao, and J.A. Lercher, Angew. Chem. Int. Ed. 51 (2012) 2072-2075.

[12] A. Fukuoka, and P.L. Dhepe, Angew. Chem. Int. Ed. 45 (2006) 5161-5163.

[13] D.W. Rackemann, and W.O.S. Doherty, Biofuels, Bioprod. Biorefin. 5 (2011) 198-214.

[14] J.J. Bozell, L. Moens, D.C. Elliott, Y. Wang, G.G. Neuenscwander, S.W. Fitzpatrick, R.J. Bilski, and J.L. Jarnefeld, Resour. Conserv. Recy. 28 (2000) 227-239.

[15] A. Corma, S. Iborra, and A. Velty, Chem. Rev. 107 (2007) 2411-2502.

[16] W.R.H. Wright, and R. Palkovits, ChemSusChem 5 (2012) 1657-1667.

[17] D.M. Alonso, S.G. Wettstein, and J.A. Dumesic, Green Chem. 15 (2013) 584-595.

[18] D.C. Elliott, and J.G. Frye, US Patent 5883266 (1999).

[19] J. Zhang, S. Wu, B. Li, and H. Zhang, ChemCatChem 4 (2012) 1230-1237.

[20] H.J. Bart, J. Reidetschlager, K. Schatka, and A. Lehmann, Ind. Eng. Chem. Res. 33 (1994) 21-25.

[21] J.-P. Lange, R. Price, P.M. Ayoub, J. Louis, L. Petrus, L. Clarke, and H. Gosselink, Angew. Chem. Int. Ed. 49 (2010) 4479-4483.

[22] L. S.V., L. D.A., M. M.E., and T. J.J., SAE Technical Paper 932675 (1993).

[23] I.T. Horvath, H. Mehdi, V. Fabos, L. Boda, and L.T. Mika, Green Chem. 10 (2008) 238-242.

[24] J.C. Serrano-Ruiz, R.M. West, and J.A. Dumesic, Annual. Rev. Chem. Biomol. Eng. 1 (2010) 79-100.

[25] P.J. Van den Brink, K.L. Von Hebel, J.-P. Lange, and L. Petrus, WO2006067171 (2006).

[26] J.-P. Lange, U.S. Patent No. 0112326 (2011).

[27] W. Luo, U. Deka, A.M. Beale, E.R.H. van Eck, P.C.A. Bruijnincx, and B.M. Weckhuysen, J. Catal. 301 (2013) 175-186.

[28] E.G. Derouane, J.C. Védrine, R.R. Pinto, P.M. Borges, L. Costa, M.A.N.D.A. Lemos, F. Lemos, and F.R. Ribeiro, Catal. Rev. 55 (2013) 454-515.

[29] E. Lippmaa, A. Samoson, and M. Magi, J. Am. Chem. Soc. 108 (1986) 1730-1735.

[30] L. Sierra de Saldarriaga, C. Saldarriaga, and M.E. Davis, J. Am. Chem. Soc. 109 (1987) 2686-2691.

[31] D. Freude, H. Ernst, and I. Wolf, Solid State Nucl. Magn. Reson. 3 (1994) 271-286.

[32] E.J.M. Hensen, Q. Zhu, R.A.J. Janssen, P.C.M.M. Magusin, P.J. Kooyman, and R.A. van Santen, J. Catal. 233 (2005) 123-135.

[33] D. Müller, W. Gessner, H.J. Behrens, and G. Scheler, Chem. Phys. Lett. 79 (1981) 59-62.

[34] E.R.H. van Eck, J.A.Z. Pieterse, and A.P.M. Kentgens, Solid State Nucl. Magn. Reson. 39 (2011) 99-105.

[35] O. Kröcher, M. Devadas, M. Elsener, A. Wokaun, N. Söger, M. Pfeifer, Y. Demel, and L. Mussmann, Appl. Catal. B: Environ 66 (2006) 208-216.

[36] A. Omegna, M. Vasic, J. Anton van Bokhoven, G. Pirngruber, and R. Prins, Phys. Chem. Chem. Phys. 6 (2004) 447-452.

[37] J. Kanellopoulos, A. Unger, W. Schwieger, and D. Freude, J. Catal. 237 (2006) 416-425.

[38] A. Samoson, E. Lippmaa, G. Engelhardt, U. Lohse, and H.G. Jerschkewitz, Chem. Phys. Lett. 134 (1987) 589-592.

[39] T.-H. Chen, B.H. Wouters, and P.J. Grobet, J. Phys. Chem. B 103 (1999) 6179-6184.

[40] C.A. Fyfe, J.L. Bretherton, and L.Y. Lam, J. Am. Chem. Soc. 123 (2001) 5285-5291.

[41] S.M.T. Almutairi, B. Mezari, G.A. Filonenko, P.C.M.M. Magusin, M.S. Rigutto, E.A. Pidko, and E.J.M. Hensen, ChemCatChem 5 (2013) 452-466.

[42] D.L.A.G. Grimminck, B. van Meerten, M.H.W. Verkuijlen, E.R.H. van Eck, W. Leo Meerts, and A.P.M. Kentgens, J. Magn. Reson. 228 (2013) 116-124.

[43] J.H. Baltisberger, Z. Xu, J.F. Stebbins, S.H. Wang, and A. Pines, J. Am. Chem. Soc. 118 (1996) 7209-7214.

[44] A. Medek, J.S. Harwood, and L. Frydman, J. Am. Chem. Soc. 117 (1995) 12779-12787.

[45] J.A. van Bokhoven, A.L. Roest, D.C. Koningsberger, J.T. Miller, G.H. Nachtegaal, and A.P.M. Kentgens, J. Phys. Chem. B 104 (2000) 6743-6754.

[46] A. Abraham, S.-H. Lee, C.-H. Shin, S. Bong Hong, R. Prins, and J.A. van Bokhoven, Phys. Chem. Chem. Phys. 6 (2004) 3031-3036.

[47] J.-B. d'Espinose de Lacaillerie, C. Fretigny, and D. Massiot, J. Magn. Reson. 192 (2008) 244-251.

[48] G.L. Caër, and R.A. Brand, J. Phys.: Condens. Matter 10 (1998) 10715.

[49] C. Gérard Le, B. Bruno, and M. Dominique, J. Phys.: Condens. Matter 22 (2010) 065402.

[50] G. Czjzek, J. Fink, F. Götz, H. Schmidt, J.M.D. Coey, J.P. Rebouillat, and A. Liénard, Phys. Rev. B 23 (1981) 2513-2530.

[51] J.-P. Amoureux, C. Fernandez, and S. Steuernagel, J. Magn. Reson., Ser. A 123 (1996) 116-118.

[52] D. Grimminck, B.J.W. Polman, A.P.M. Kentgens, and W.L. Meerts, J. Magn. Reson. 211 (2011) 114-120.

[53] D. Grimminck, B. van Meerten, M.H.W. Verkuijlen, E.R.H. van Eck, W.L. Meerts, and A.P.M. Kentgens, J. Magn. Reson. 228 (2013) 116-124.

[54] V. Bosáček, V. Patzelová, Z. Tvarůžková, D. Freude, U. Lohse, W. Schirmer, H. Stach, and H. Thamm, J. Catal. 61 (1980) 435-442.

[55] B. Wichterlová, Z. Tvarůžková, Z. Sobalík, and P. Sarv, Micropor. Mesopor. Mater. 24 (1998) 223-233.

[56] S. Schallmoser, T. Ikuno, M.F. Wagenhofer, R. Kolvenbach, G.L. Haller, M. Sanchez-Sanchez, and J.A. Lercher, J. Catal. 316 (2014) 93-102.

[57] M. Trombetta, G. Busca, L. Storaro, M. Lenarda, M. Casagrande, and A. Zambon, Phys. Chem. Chem. Phys. 2 (2000) 3529-3537.

[58] A. Janin, M. Maache, J.C. Lavalley, J.F. Joly, F. Raatz, and N. Szydlowski, Zeolites 11 (1991) 391-396.

[59] S.M.C. Menezes, V.L. Camorim, Y.L. Lam, R.A.S. San Gil, A. Bailly, and J.P. Amoureux, Appl. Catal. A: Gen. 207 (2001) 367-377.

[60] S. Dzwigaj, and M. Che, J. Phys. Chem. B 110 (2006) 12490-12493.

[61] E.B. Lami, F. Fajula, D. Anglerot, and T. Des Courieres, Micropor. Mater. 1 (1993) 237-245.

[62] T. Barzetti, E. Selli, D. Moscotti, and L. Forni, J. Chem. Soc., Faraday Trans. 92 (1996) 1401-1407.

[63] E.P. Parry, J. Catal. 2 (1963) 371-379.

[64] T. Yashima, and N. Hara, J. Catal. 27 (1972) 329-333.

[65] J.P. Marques, I. Gener, P. Ayrault, J.C. Bordado, J.M. Lopes, F. Ramôa Ribeiro, and M. Guisnet, Micropor. Mesopor. Mater. 60 (2003) 251-262.

[66] S. Li, A. Zheng, Y. Su, H. Zhang, L. Chen, J. Yang, C. Ye, and F. Deng, J. Am. Chem. Soc. 129 (2007) 11161-11171.

[67] G. Le Caer, and R.A. Brand, J. Phys.: Condens. Matter 10 (1998) 10715-10774.

[68] J.B.D. de Lacaillerie, C. Fretigny, and D. Massiot, J. Magn. Reson. 192 (2008) 244-251.

[69] L.H. Ong, M. Dömök, R. Olindo, A.C. van Veen, and J.A. Lercher, Micropor. Mesopor. Mater. 164 (2012) 9-20.

[70] E.A. Pidko, S.M.T. Almutairi, B. Mezari, P.C.M.M. Magusin, and E.J.M. Hensen, ACS Catal. 3 (2013) 1504-1517.

[71] D.L. Bhering, A. Ramírez-Solís, and C.J.A. Mota, J. Phys. Chem. B 107 (2003) 4342-4347.

[72] Z. Yu, A. Zheng, Q. Wang, L. Chen, J. Xu, J.-P. Amoureux, and F. Deng, Angew. Chem. Int. Ed. 49 (2010) 8657-8661.

[73] S. Li, A. Zheng, Y. Su, H. Fang, W. Shen, Z. Yu, L. Chen, and F. Deng, Phys. Chem. Chem. Phys. 12 (2010) 3895-3903.

[74] E. Brunner, H. Ernst, D. Freude, T. Fröhlich, M. Hunger, and H. Pfeifer, J. Catal. 127 (1991) 34-41.

[75] P.P. Man, and J. Klinowski, J. Chem. Soc., Chem. Commun. (1988) 1291-1294.

[76] S.M. Campbell, D.M. Bibby, J.M. Coddington, R.F. Howe, and R.H. Meinhold, J. Catal. 161 (1996) 338-349.

[77] J.M. Newsam, M.M.J. Treacy, W.T. Koetsier, and C.B.D. Gruyter, Proc. R. Soc. London, Ser. A 420 (1988) 375-405.

# Chapter 4

# Selective, One-pot Catalytic Conversion of Levulinic Acid to Pentanoic Acid over Ru/H-ZSM5

**Abstract**

The direct conversion of levulinic acid (LA) into pentanoic acid (PA) has been studied with six distinct 1 wt% Ru/H-ZSM5 catalysts at 40 bar $H_2$ and 473 K in dioxane. The influence of the cation form of ZSM5, ruthenium precursor and Si/Al ratio of ZSM5 on metal dispersion and acidity has been assessed. A highly active bifunctional 1 wt% Ru/H-ZSM5 catalyst was developed to give an improved PA yield of 91.3% after 10 h reaction time and a PA productivity of 1.157 $mol_{PA}\ g_{Ru}^{-1}\ h^{-1}$, which is the highest reported to date. Both fresh and spent catalysts were characterized by transmission electron microscopy (TEM), $N_2$ physisorption and temperature-programmed desorption of ammonia (TPD-$NH_3$). The simple preparation method allows for a significant fraction of the ruthenium to be located inside the zeolite pores, providing the desired proximity between the hydrogenation function and the strong acid sites, which is key to the conversion of LA into PA. Coke buildup during reaction causes some deactivation of the Ru/H-ZSM5 catalysts, but activity can almost fully be restored after catalyst regeneration by a simple burn-off step.

Based on: Luo W., Bruijnincx P.C.A., Weckhuysen B.M., J. Catal. 320 (2014) 33-41.

## 4.1 Introduction

Levulinic acid (LA) has emerged as one of the most promising renewable platform molecules. Indeed, it provides many opportunities for biobased fuel and bulk chemicals production[1, 2] and can be produced easily and economically from the carbohydrate fraction of lignocellulosic biomass through a simple and high yielding acid hydrolysis process.[3] Several derivatives of LA have been studied as cellulosic fuels or fuel additives; these include γ-valerolactone (GVL),[4] 2-methyltetrahydrofuran (MTHF),[5] pentanoic acid (PA) and its esters (PE),[6] all of which can be obtained by sequential LA hydrodeoxygenation steps (Scheme 4.1). While GVL has received most attention, two recent examples have demonstrated that pentenoic/pentanoic acid-based value chains are also very promising for the production of cellulosic biofuels.[7]

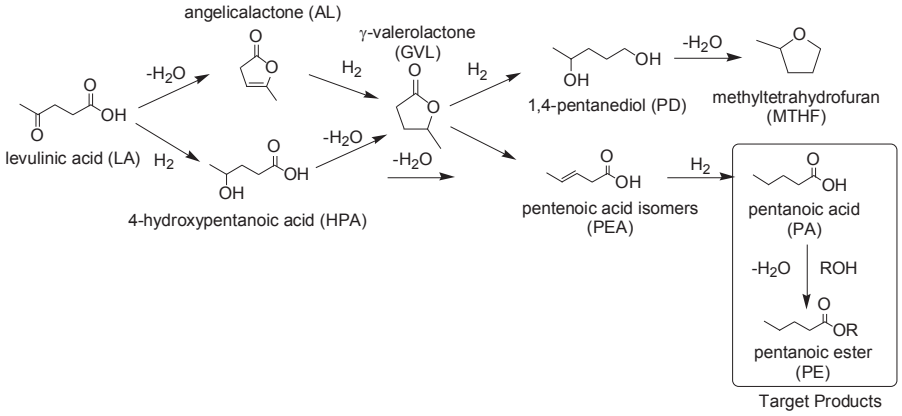


Scheme 4.1. Levulinic acid hydrodeoxygenation platform.

Lange et al. showed, for instance, that so-called valeric biofuels, i.e. pentanoic acid esters, are a superior class of cellulosic biofuels.[6] A multistep catalytic conversion of LA into valeric esters was reported, involving the hydrogenation of LA to GVL over $Pt/TiO_2$, the conversion of GVL to PA by acid-catalyzed ring-opening and the hydrogenation over a bifunctional Pt/H-ZSM5 catalyst and, finally, esterification to the desired pentanoic acid esters (PE) over an acidic ion-exchange resin. In addition to PE synthesis, a comprehensive study of their fuel properties was conducted, which demonstrated their

compatibility for both gasoline and diesel applications and revealed a superior performance.[6]

The Dumesic group also reported on the production of PA, in this case from GVL over a bifunctional $Pd/Nb_2O_5$ catalyst.[8] PA could subsequently be converted into 5-nonanone, i.e., by ketonization and ultimately to hydrocarbon fuels suitable for gasoline and diesel applications.[8] Both approaches thus consist of a two-step conversion of LA into PA and require a catalyst system combining an acid functionality and a hydrogenation function for the second, most difficult step, i.e. the ring-opening/hydrogenation of GVL to PA.

Building on these results, we previously reported on the direct, one-pot conversion of LA to PA and PE, without isolating the GVL intermediate, using bifunctional catalysts consisting of ruthenium supported on H-ZSM5 or H-β. A yield of 45.8 mol% of PA was obtained with 1 wt% Ru/H-ZSM5 in dioxane at 473 K and after 4 h of reaction time.[9] An extensive catalyst deactivation study showed that acid site loss as the result of dealumination is the cause of deactivation under the applied conditions, which involved elevated temperatures and a highly polar and corrosive environment. Relatedly, Fu et al. recently reported the direct conversion of LA to valeric acid and its ester, performing the reaction in ethanol over various bifunctional ruthenium catalyst with 5 wt% $Ru/SBA\text{-}SO_3H$ performing best with a combined PA/PE yield of 94% at 523 K after 6 h of reaction, after a comprehensive optimization of the reaction conditions.[10] Also for this catalyst system, acid site loss was found to be an issue. These first, few examples nonetheless show that the direct conversion is feasible and the promising results warrant further exploration.

The efficient conversion of LA to PA requires a careful balance to be struck between the number, strength and location of the acid and hydrogenation sites, key parameters that in principle can be controlled by careful catalyst synthesis. Herein, we further explore 1wt% Ru/H-ZSM5 as a catalyst for the direct conversion of LA to PA and study the influence of catalyst preparation on activity and selectivity. H-ZSM5 was selected as the acidic support, given its higher instrinsic acid strength than H-Y[11] and the fact that acid leaching (dealumination) was previously found to be more limited with H-ZSM5

than with H-β under the demanding conditions required for the LA-to-PA conversion.[9] In the sequential hydrodeoxygenation of LA to PA (Scheme 2.1), LA can be first converted to GVL, either via ring closure and subsequent hydrogenation involving angelicalactone (AL) as intermediate or via hydrogenation first to 4-hydroxypentanoic acid (HPA) followed by ring closure; GVL can subsequently be ring-opened to PEA and finally hydrogenated to PA; an alternative route differs in the fate of the first intermediate 4-hydroxypentanoic acid (HPA), which can in principle also be directly dehydrated to PEA, followed finally by hydrogenation to PA.[12, 13] The strong acidity of the zeolite would be important for both routes. Putting the strong acid sites and hydrogenation metal in close proximity might furthermore favor the second LA-HPA-PEA-PA route and thus avoid the most difficult step of both sequences, i.e., GVL ring-opening.

To achieve this, controlled deposition/ exchange of ruthenium, especially into the zeolite pores is required. Here, we report on the influence of preparation method and zeolite composition on the catalytic performance and stability of 1wt% Ru/H-ZSM5 catalysts for the LA to PA conversion. The influence of the type of extraframework cations in ZSM5 before wet impregnation, ruthenium precursor, and variation of Si/Al ratio was examined on (1) metal dispersion and distribution, (2) H-ZSM5 acidity, and (3) catalytic performance of the Ru/H-ZSM5 catalysts in the direct, one-pot conversion of LA to PA in dioxane at 473 K. A much improved bifunctional catalyst was developed by a new, simple synthesis method to yield 91.3% PA within a reaction time of 10 h. A comparison of catalysts of varying acidity showed acid strength to be key to the efficient conversion of LA to PA. Finally, insight into the activity, stability and deactivation of the new 1 wt% Ru/H-ZSM5 catalysts is provided.

## 4.2 Experimental Section

### 4.2.1 Catalyst Preparation

Six distinct 1 wt% Ru/H-ZSM5 catalysts were prepared via a wet impregnation method. The requisite amount of precursor solution (22 mL) was prepared with deionized water in a 50 mL round bottom flask equipped with a magnetic stirring bar. The round bottom

flask was submerged in a temperature controlled oil bath and the mixture was then agitated at 303 K using a hot plate stirrer (1000 rpm). After 10 min of stirring, the ZSM5 support was slowly added to the impregnation solution, with an agitation speed of 1000 rpm at 303 K for about 1 h. After mixing of the support with the impregnation solution, the temperature was raised to 358 K and kept at that temperature for 12 h, allowing evaporation of the solvent at a desirable rate. A fine catalyst powder was obtained of homogeneous color, which was then reduced directly at 723 K with a heating ramp 2 K/min under a flow of 10 vol.% $H_2/N_2$ for 6 h. The catalyst sample was subsequently cooled rapidly to room temperature and used without any further modification.

The six 1 wt% Ru/H-ZSM5 catalysts are labeled according to their preparation method. The first indicator denotes the ruthenium precursor used with 'Cl'/'$NH_3$' indicating $RuCl_3$ (99.9%, Acros Chemicals)/$Ru(NH_3)_6Cl_3$ (99%, ABCR), respectively; the second indicator, 'A'/'H', indicates if the cation of the ZSM5 support was either $NH_4^+$ or $H^+$ prior to impregnation; the last indicator depicts the Si/Al ratio of ZSM5. Four ZSM5 materials were used in this study with Si/Al ratios of 11.5 (CBV2314, $S_{BET}$ = 425 $m^2/g$), 25 (CBV5524G, $S_{BET}$ = 425 $m^2/g$), 40 (CBV8014, $S_{BET}$ = 425 $m^2/g$), and 140 (CBV28014, $S_{BET}$ = 400 $m^2/g$; all from Zeolyst).

Two 1 wt% Ru/H-ZSM5 catalysts, Ru/H-ZSM5(Cl, H, 11.5) and Ru/H-ZSM5(Cl, A, 11.5) were prepared with $RuCl_3$ as the ruthenium precursor and CBV2314 as the support; for Ru/H-ZSM5(Cl, H, 11.5) the ammonium-form of ZSM5 was converted to H-ZSM5 before impregnation by heating $NH_4$-ZSM5 at 1 K/min to 393 K for 1 h and at 2 K/min to 823 K for 4 h; the other four 1 wt% Ru/H-ZSM5 catalysts were prepared with $Ru(NH_3)_6Cl_3$ as precursor and used the ammonium form of the four ZSM5 zeolites of different Si/Al ratio: Ru/H-ZSM5($NH_3$, A, 11.5), Ru/H-ZSM5($NH_3$, A, 25), Ru/H-ZSM5($NH_3$, A, 40) and Ru/H-ZSM5($NH_3$, A, 140).

For comparison, a parent ZSM5(11.5) sample (CBV2314) without having been impregnated was similarly treated at 723 K with a heating ramp of 2 K/min under a flow of 10 vol.% $H_2/N_2$ for 6 h. Catalyst regeneration of Ru/H-ZSM5($NH_3$, A, 11.5) was performed by heating the spent catalyst to 723 K with a heating ramp of 2 K/min under a flow of 10 vol.% $H_2/N_2$ for 4 h.

### 4.2.2 Catalyst Characterization

#### 4.2.2.1 Transmission Electron Microscopy

The bright field and high angle annular dark field (HAADF) of transmission electron microscopy (TEM) images were obtained using a Tecnai 20FEG microscope operating at 200 kV. The ruthenium particle diameters counted from more than 200 particles for each sample were measured using iTEM software (soft Imaging System GmbH). For non-symmetrical particle shapes, both the largest and shortest diameter was measured to obtain an average value.

#### 4.2.2.2 $N_2$ Physisorption

$N_2$ physisorption isotherms were recorded to determine surface areas and pore volumes using a Micromeritics Tristar 3000 set-up operating at 77 K. All samples were outgassed for 12 h at 473 K in a nitrogen flow prior to the physisorption measurements. BET surface areas were determined using 10 points between 0.06 and 0.25. Micropore volumes ($cm^3/g$) were determined by *t*-plot analysis for *t* between 3.5 and 5.0 Å to ensure inclusion of the minimum required pressure points.

#### 4.2.2.3 Temperature-Programmed Desorption of Ammonia

Catalyst acidity was investigated by temperature-programmed desorption of ammonia (TPD-$NH_3$) under He flow (25 mL/min) using a Micromeritics AutoChem II equipped with a TCD detector. 0.15 - 0.2 g of catalyst was loaded and dried at 873 K for 1 h, after which the sample was cooled down to 373 K. Subsequently, pulses of ammonia were introduced up to saturation of the sample. The temperature-programmed desorption was performed up to 873 K, with a heating ramp of 5 K/min. The total number of acid sites (mmol $NH_3$/gram zeolite) was determined from the total amount of desorbed ammonia.

#### 4.2.2.4 Thermal Gravimetric Analysis

TGA-MS measurements of the spent catalysts were performed with a Perkin–Elmer Pyris 1 apparatus. The sample was initially heated to 423 K for 1 h with a temperature ramp of 10 K/min in a 20 mL/min flow of argon to exclude physisorbed water and acetone, followed by a ramp of 5 K/min to 973 K in a 10 mL/min flow of oxygen to burn off the coke. Analysis was performed with a quadrupole Pfeiffer Omnistar mass spectrometer, which was connected to the outlet of the TGA apparatus. Ion currents were recorded for $m/z$ values of 18 and 44.

### 4.2.3 Catalyst Activity and Stability Testing

LA hydrodeoxygenation reactions were conducted in a 100 mL Parr batch autoclave reactor equipped with a thermocouple, a pressure transducer and gauge and overhead stirring. In a typical run, the batch reactor was loaded with a 10 wt% levulinic acid solution (6.0 g, 51.7 mmol) in dioxane (54 g) and the 1 wt% Ru catalyst (0.6 g). The reactor was sealed, purged three times with argon, heated to 473 K and subsequently charged with $H_2$ to 40 bar. This was taken as the starting point of the reaction. Reactions were run for 10 h with a stirring speed of 1600 rpm; this stirring speed was previously shown to be sufficient for avoiding external mass transfer limitations, guarantying the reactions to be operated in the kinetic regime (see Chapter 2).[9] After the reaction, the autoclave was cooled to room temperature, $H_2$ was released and 2 wt% anisole was added as internal standard. The catalyst was separated by centrifugation, filtration and finally washed with acetone.

The experiments aimed at higher PA yields as well as the stability tests were run at a higher catalyst loading. These reactions were conducted in a 50 mL Parr batch autoclave reactor at 473 K for 10 h using a hydrogen pressure of 40 bar and a stirring speed of 1600 rpm. These runs were performed with 10 wt% levulinic acid (2.5 g, 21.5 mmol) in dioxane (22.5 g) over 1 wt% Ru/ZSM5(11.5) catalysts (0.5 g).

The reaction products were analyzed using a Varian gas chromatograph equipped with a VF-5 ms capillary column and flame ionization detector (FID). Products were

identified with a Shimadzu GC–MS with a VF-5 ms capillary column. The gas phase reaction products were analyzed by an online dual channel Varian CP4900 micro-GC equipped with a $CO_X$ column and thermal conductivity detector (TCD), for analysis of $H_2$, $CO_2$, CO and $CH_4$.

### 4.3 Results and Discussion

A series of six distinct 1 wt% Ru/H-ZSM5 catalysts were prepared, by varying the cation form and Si/Al ratio of the zeolite as well as the ruthenium precursor salt, and tested in the hydrodeoxygenation of LA. The influence of the extraframework cation ($NH_4^+$ vs. $H^+$) of the ZSM5 support with a Si/Al ratio of 11.5 and impregnation salt ($RuCl_3$ vs. $Ru(NH_3)_6Cl_3$) on the catalysts' physicochemical properties and performance were assessed by comparison of Ru/H-ZSM5(Cl, H, 11.5), Ru/H-ZSM5(Cl, A, 11.5) and Ru/H-ZSM5($NH_3$, A, 11.5). Four different Si/Al ratios varying from 11.5 to 40 were examined with Ru/H-ZSM5($NH_3$, A, 11.5), Ru/H-ZSM5($NH_3$, A, 25), Ru/H-ZSM5($NH_3$, A, 40) and Ru/H-ZSM5($NH_3$, A, 140), all prepared with the $Ru(NH_3)_6Cl_3$ precursor and the zeolites in the ammonium form. As ruthenium is known to form the volatile oxides $RuO_2$ and $RuO_4$, and to severely sinter when contacted with oxygen above 373 K,[14] the traditional calcination step was omitted and wet impregnation step was followed directly by a prolonged reduction step of 6 h, in order to fully decompose the ruthenium precursor and prepare catalysts with a better dispersion of ruthenium.

#### 4.3.1 Physicochemical Characterization of the Catalysts

The measured physicochemical properties of the six catalysts are given in Table 4.1. Ruthenium particle sizes, falling in the range of 1.7 - 4.9 nm, and dispersions were determined by TEM (Appendix B, Fig. S1). The number and strength of acid sites of the parent zeolite ZSM5(11.5) and the six zeolite-supported catalysts were determined by temperature-programmed desorption of ammonia (TPD-$NH_3$, Fig. 4.1, Table 4.2). The TPD-$NH_3$ traces could be divided into two clearly distinguishable parts, with desorption being observed at a low-temperature range (LT) from 430 to 580 K and a high-temperature range (HT) from 590 to 740 K. These LT and HT ranges correspond to weak and strong acid sites, respectively.[15, 16]

The metal dispersion as well as the acidity of the catalyst was found to depend strongly on the cation in the zeolite used for the impregnation step. Ru/H-ZSM5(Cl, H, 11.5), for instance, showed a ruthenium dispersion of 0.39 (average particle size of 3.3 nm), which was slightly better than that of Ru/H-ZSM5(Cl, A, 11.5) of 0.26 (particle size of 4.9 nm). In both cases, ruthenium particles can be mainly found at the external surface of the zeolite. While giving a better Ru dispersion, a significant decrease in strong acid sites (HT) with concomitant large increase in weak acid sites (LT) was seen when $H^+$-type ZSM5 was used for the impregnation (Fig. 4.1). This is undesirable as strong acid sites are essential to efficient PA production. Ru/H-ZSM5(Cl, H, 11.5) actually contained the largest amount of LT (0.23 mmol/$g_{cat}$) and lowest amount of HT (0.34 mmol/$g_{cat}$) of the three catalysts made with the Si/Al = 11.5 ZSM5 support (Table 4.2, entry 2-4). If one takes into account that bare $NH_4^+$-ZSM5 zeolite subjected to the same reduction conditions as the other ruthenium-loaded zeolites contains 0.57 HT and 0.04 mmol/$g_{cat}$ LT (Table 4.2, entry 1), then it is clear from the results above that, conversion of the zeolite from $NH_4^+$ to $H^+$ form prior to impregnation is not beneficial, giving the resulting large drop in acid strength. This transition of strong acid sites to weak ones during the pretreatment process at 823 K was attributed to the extraction of framework aluminium species (Fig. 4.1).[17] The use of $NH_4^+$-ZSM5 is therefore preferred for the synthesis of the bifunctional catalyst.

The Ru dispersion could be further improved by using $Ru(NH_3)_6Cl_3$ as precursor on $NH_4^+$-ZSM5 to give Ru/H-ZSM5($NH_3$, A, 11.5). This preparation method gave the smallest average particle size of 1.7 nm of all the Ru/H-ZSM5 catalyst, resulting in a significant increase in Ru dispersion to 0.76 (Table 4.1, entry 4). Previous studies also showed that large ruthenium particles were obtained by impregnation of X, L and ZSM-5 zeolites with ruthenium chloride after calcination and $H_2$-reduction,[18] while small ruthenium clusters could be obtained by ion exchange of $Na^+$-Y zeolites with aqueous solutions of $Ru(NH_3)_6Cl_3$.[14, 19 20, 21] The higher dispersion obtained with $Ru(NH_3)_6Cl_3$ was thought to be the result of strong interactions between negatively charged porous framework of ZSM5 and the ruthenium cations formed upon dissolution

Table 4.1. Physicochemical properties of fresh (F) Ru/H-ZSM5 and spent (S) catalysts after reaction at 473 K, 40 bar $H_2$ after 10 h in dioxane.

| | Catalyst | BET ($m^2/g$) | | Micropore surface area ($m^2/g$) | | Micropore volume ($cm^3/g$) [a] | | Pore volume ($cm^3/g$) [b] | | Average Ru particle size (nm)[c] | | Ru dispersion ZSM5 [d] | | Coke content (wt%)[e] |
|---|---|---|---|---|---|---|---|---|---|---|---|---|---|---|
| 1 | ZSM5 (11.5) | 379 | | 295 | | 0.14 | | 0.22 | | - | | - | | - |
| | **Ru/H-ZSM5** | **F** | **S** | **F** | **S** | **F** | **S** | **F** | **S** | **F** | **S** | **F** | **S** | |
| 2 | (Cl, H, 11.5) | 333 | 126 | 247 | 112 | 0.12 | 0.06 | 0.20 | 0.09 | 3.3±1.4 | 6.6±2.6 | 0.39 | 0.20 | 8.0 |
| 3 | (Cl, A, 11.5) | 371 | 53 | 266 | 51 | 0.13 | 0.03 | 0.23 | 0.05 | 4.9±1.4 | 6.7±2.2 | 0.26 | 0.19 | 9.2 |
| 4 | ($NH_3$, A, 11.5) | 324 | 137 | 251 | 107 | 0.12 | 0.05 | 0.19 | 0.06 | 1.7±0.4 | 3.8±0.9 | 0.76 | 0.34 | 7.6 |
| 5 | ($NH_3$, A, 25) | 377 | 208 | 242 | 137 | 0.12 | 0.07 | 0.26 | 0.18 | 4.3±1.5 | 5.0±1.9 | 0.30 | 0.26 | 5.8 |
| 6 | ($NH_3$, A, 40) | 390 | 267 | 237 | 161 | 0.12 | 0.08 | 0.27 | 0.21 | 4.8±1.6 | 6.1±2.0 | 0.27 | 0.21 | 4.0 |
| 7 | ($NH_3$, A, 140) | 363 | 337 | 221 | 168 | 0.11 | 0.08 | 0.21 | 0.20 | 6.2±3.2 | 7.4±1.9 | 0.21 | 0.17 | 1.6 |

[a] data obtained by the t-plot method

[b] data obtained by single point adsorption

[c] data obtained by TEM

[d] data estimated by TEM: $D=6*(\nu_m/a_m)/d$. Where $\nu_m$ is bulk metal atomic density of Ru ($13.65\times 10^{-3}$ $nm^3$), $a_m$ is the surface area occupied by an atom on a polycrystalline surface of Ru ($6.35\times 10^{-2}$ $nm^2$), d is the cluster size of Ru metal.

[e] data determined by TGA

of $Ru(NH_3)_6Cl_3$ in water; conversely, the lower dispersions and larger particle sizes observed outside of ZSM5 with $RuCl_3$ are the result of weaker interactions between metal salt and support.[18] An additional, important benefit of using $Ru(NH_3)_6Cl_3$ is that with this precursor, the largest amount of strong acid sites is preserved (0.48 mmol/g). Indeed, the temperature of maximum ammonia desorption in the HT region is at 686 K, which is the closest to the maximum of 719 K observed for the original, non-impregnated zeolite (Table 4.2, entry 4). The use of $Ru(NH_3)_6Cl_3$ thus improved metal dispersion as well as efficiently preserved the amount and strength of strong acid sites on ZSM5.

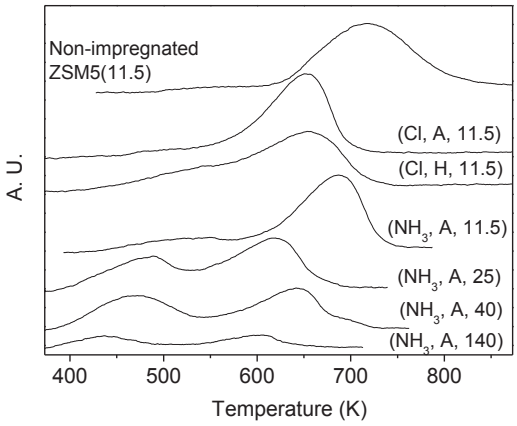


Figure 4.1. TPD-$NH_3$ profiles of the parent ZSM5 and the six 1 wt% ZSM5-supported catalysts.

Variation of the zeolite's Si/Al ratio was also found to affect ruthenium dispersion. Expectedly, the total number of acid sites and fraction of strong acid sites of the 1wt% Ru/H-ZSM5 catalysts decreased with increasing the Si/Al ratio from 11.5 to 140 (Table 4.2, entry 4-7). The average ruthenium particle size in turn was found to gradually increase from 1.7 to 6.2 nm with increasing Si/Al ratio (Table 4.1, entry 4-7). A similar increase in average particle size from 1.4 to 6.1 nm upon increasing the Si/Al ratio from 11.5 to 500 was also seen by Park et al.[22] for platinum supported on ZSM5. The difference in the distribution of strong and weak acid sites might responsible for the observed differences in the Ru dispersion, with those zeolites richer in HT sites stabilizing smaller Ru clusters. For Pt/H-ZSM5 it is known, for instance, that highly acidic zeolites lead to higher Pt dispersion, with computational studies pointing at the stabilizing interaction between Pt and a Brønsted acidic proton.[23]

Table 4.2. Amount and type of acid sites as determined by $NH_3$-TPD.

| | Catalyst | LT region maximum desorption (K) | Amount of weak sites (mmol/$g_{cat}$) | HT region maximum desorption (K) | Amount of strong acid sites (mmol/$g_{cat}$) | Total acidity (mmol/$g_{cat}$) |
|---|---|---|---|---|---|---|
| 1 | Non-impregnated ZSM5 (11.5) | 559 | 0.04 | 719 | 0.57 | 0.61 |
| | **Fresh Ru/H-ZSM5** | | | | | |
| 2 | (Cl, H, 11.5) | 544 | 0.23 | 657 | 0.34 | 0.57 |
| 3 | (Cl, A, 11.5) | 575 | 0.10 | 655 | 0.44 | 0.54 |
| 4 | ($NH_3$, A, 11.5) | 517 | 0.12 | 686 | 0.48 | 0.60 |
| 5 | ($NH_3$, A, 25) | 476 | 0.20 | 615 | 0.31 | 0.51 |
| 6 | ($NH_3$, A, 40) | 467 | 0.25 | 636 | 0.24 | 0.49 |
| 7 | ($NH_3$, A, 140) | 434 | 0.07 | 597 | 0.07 | 0.14 |

Additional insights into the distribution of ruthenium might be obtained from the observed decreases in pore volume and the number of acid sites, as these changes give an indication of the fraction of small ruthenium clusters deposited/exchanged into the ZSM5 pores, i.e. those that are difficult to be visualized in TEM. Lercher et al., for instance, previously reported on a decrease in pore volume and acid density of ZSM5 when a significant fraction of Ni was located inside the ZSM5 pores.[24] A similar decrease, reported by Park et al. after introduction of platinum[22] on ZSM5, was again attributed to the fraction of Pt deposited inside the ZSM5 pores. The surface areas and pore volumes of the Ru catalysts as determined by $N_2$ physisorption are listed in Table 4.1. Compared to the non-impregnated zeolite ZSM5(11.5), wet impregnation of ZSM5(11.5) with Ru with the different precursors resulted in a drop in pore volume and acid density in most cases (Tables 4.1 and 4.2), indicating the formation of small Ru particles inside the zeolite pores. The pore volume of ZSM5(11.5) dropped from 0.22 to 0.20 $cm^3/g$ and 0.19 $cm^3/g$ for Ru/H-ZSM5(Cl, H, 11.5) Ru/H-ZSM5($NH_3$, A, 11.5), respectively (Table 4.1, entry 1, 2, 4), whereas no loss in pore volume was observed for Ru/H-ZSM5(Cl, A, 11.5).

The 0.02 $cm^3/g$ decrease in pore volume observed for Ru/H-ZSM5(Cl, H, 11.5) might also have an additional origin. A significant increase in the fraction of weak acid sites is

seen for this catalyst, which points at a partial pore blockage by migration of Al to extraframework sites upon transition of the $NH_4^+$-ZSM5 to the $H^+$-ZSM5 prior to impregnation.[17, 25] The drop in pore volume and much better ruthenium dispersion for Ru/H-ZSM5($NH_3$, A, 11.5) indicate that this catalyst has the largest fraction of Ru particles deposited inside the zeolite channel system.

### 4.3.2 Catalytic Performance

Catalytic activity of the six 1wt% Ru/H-ZSM5 catalysts was initially compared at 473 K and 40 bar $H_2$ with a 10 wt% solution of LA in dioxane and a stirrer speed of 1600 rpm, conditions that are identical to those of our previous study. As reported, dioxane decomposition takes place to a limited extent in the presence of strongly acidic catalysts, yielding ethanol, 2-ethoxyethanol, and butanol as decomposition products, amongst others. The secondary PE products that are formed with these solvent-derived alcohols (up to 25 mol% max.) should be considered as PA and are included in the total PA yields reported below. The activity of the catalysts is reported in Table 4.3 in terms of initial PA productivity, expressed as $mol_{PA}\, g_{Ru}^{-1}\, h^{-1}$. The time on-line concentration profiles of substrate and products are depicted in Fig. 4.3. Trace amounts of MTHF were found, but no PD was observed in any of the reactions, indicating that the LA-GVL-MTHF route is insignificant over the 1 wt% Ru/H-ZSM5 catalysts under the applied conditions. As can be seen from the time profiles, GVL is initially formed as the primary product, with selectivity to PA increasing over time as a result of the consecutive reactions.

The variation in metal location, dispersion and acidity as a result of the different preparation methods are clearly reflected in the catalytic activity and PA productivity (Fig. 4.2a-c). For example, Ru/H-ZSM5(Cl, A, 11.5) gave a higher PA yield of 23.3 mol% PA and productivity of 0.451 $mol_{PA}\, g^{-1}{}_{Ru}\, h^{-1}$ than Ru/H-ZSM5(Cl, H, 11.5) did (7.2 mol% and 0.250 $mol_{PA}\, g^{-1}{}_{Ru}\, h^{-1}$) after 10 h of reaction (Fig. 4.2a, b and Table 4.3, entry 1, 2). It should be noted that Ru/H-ZSM5(Cl, A, 11.5) has more strong acid sites but a lower metal dispersion than Ru/H-ZSM5(Cl, H, 11.5). This implies that acidity plays a more important role than ruthenium dispersion in PA production, which is in an agreement

with our previous study in which the acid-catalyzed GVL ring-opening was shown to be rate-limiting.[9]

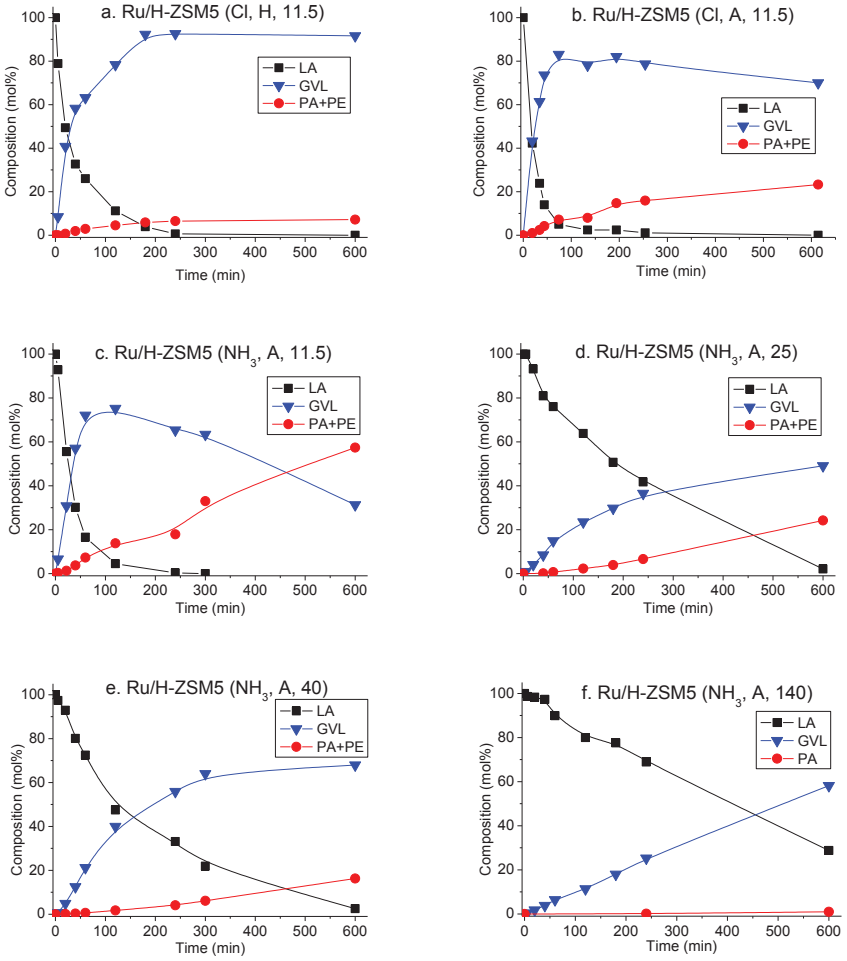


Figure 4.2. Time profiles of the catalytic hydrodeoxygenation of 10 wt% LA in dioxane at 473 K and 40 bar $H_2$ pressure, 1 wt% Ru/H-ZSM5, stirrer speed of 1600 rpm. LA: levulinic acid; GVL: γ-valerolactone; PA+PE: pentanoic acid and its esters.

Ru/H-ZSM5($NH_3$, A, 11.5) gave a PA yield of 57.4 mol%, showing that the change of ruthenium precursor in the preparation method resulted in a rather substantial increase in PA production. More importantly, the rate of PA formation does not seem to slow down, even after 10 h of reaction time; this in contrast to Ru/H-ZSM5(Cl, H, 11.5)

which already shows some signs of deactivation after 3 h of reaction (Fig. 4.2a,c). The use of $Ru(NH_3)_6Cl_3$ as the precursor thus clearly improves catalyst performance in terms of PA yield. Based on the characterization data discussed above, this can be attributed to the good preservation of strong acid sites and the improved deposition of ruthenium particles also inside the zeolite pores leading to close proximity of the active sites in the bifunctional catalyst.

Clear differences in selectivity and activity are also observed upon variation of the Si/Al ratio of ZSM5 (Fig. 4.2d-f and Table 4.3 entry 3-6). Full LA conversion was achieved with Ru/H-ZSM5 ($NH_3$, A, 11.5) after 5 h (Fig. 4.2c), while 2.1, 2.5, and 27.8 mol% of LA were still left after 10 h reaction with the catalysts with Si/Al ratios of 25, 40 and 140, respectively. PA productivity of the Ru/H-ZSM5 catalysts decreased accordingly, with Ru/H-ZSM5($NH_3$, A, 140) having produced hardly any PA after 10 h. These results are in line with Pan et al. who also included a 5 wt% Ru/H-ZSM5 catalyst with a high Si/Al ratio of 50 in their screening studies and observed a low PA productivity of 0.033 $mol_{PA}$ $g^{-1}_{Ru}$ $h^{-1}$ at the higher reaction temperature of 513 K (Table 4.3, entry 13).[10]

The PA yield can be further improved with a slight increase in catalyst loading under otherwise standard conditions of 473 K and 40 bar $H_2$. A PA yield of 91.3 mol% could thus be achieved with 1wt% Ru/ZSM5($NH_3$, A, 11.5) after a 10 h reaction with an excellent mass balance of 99.0% (Table 4.3, entry 7), corresponding to a productivity of 1.042 $mol_{PA}$ $g_{Ru}^{-1}$ $h^{-1}$. This productivity is at least six fold higher than the highest PA productivity of 0.16 $mol_{PA}$ $g_{Ru}^{-1}$ $h^{-1}$ recently reported by Fu et al. for the production of PA+PE from LA over 5 wt% Ru/SBA-$SO_3H$, a reaction which was run at the higher temperature of 513 K (Table 4.3, entry 12).[10] A 4 h run with 1wt% Ru/H-ZSM5($NH_3$, A, 11.5) allowed for a direct comparison with our previously reported Ru/H-ZSM5 catalyst (Table 4.3, entry 10 and 11), which was prepared with $RuNO(NO_3)_3$ as precursor via a wet impregnation method followed by both calcination and reduction.[9] The new results show that an improved yield and productivity can be obtained with the new catalyst (64.5 mol% PA/1.157 $mol_{PA}$ $g^{-1}_{Ru}$ $h^{-1}$ vs. 45.8 mol% PA/ 0.822 $mol_{PA}$ $g_{Ru}^{-1}$ $h^{-1}$).

Table 4.3. One-pot hydrodeoxygenation of levulinic acid (LA) to pentanoic acid (PA).

| | Catalyst | C-balance (%) | LA conv. (%) | GVL yield (%) | PA yield (%)[a] | productivity ($mol_{PA}\ g^{-1}_{Ru}\ h^{-1}$) |
|---|---|---|---|---|---|---|
| **Catalyst screening[b]** | | | | | | |
| 1 | (Cl, A, 11.5) | 93.3 | 100 | 70.0 | 23.3 (4.7) | 0.451 |
| 2 | (Cl, H, 11.5) | 98.8 | 100 | 91.6 | 7.2 (0.9) | 0.169 |
| 3 | ($NH_3$, A, 11.5) | 88.7 | 100 | 31.3 | 57.4 (17.7) | 0.629 |
| 4 | ($NH_3$, A, 25) | 76.4 | 97.9 | 50.1 | 24.2 (8.0) | 0.135 |
| 5 | ($NH_3$, A, 40) | 86.8 | 97.5 | 68.0 | 16.3 (4.5) | 0.131 |
| 6 | ($NH_3$, A, 140) | 88.0 | 72.2 | 58.2 | 1.0 (0.0) | 0.009 |
| **PA yield optimization for ($NH_3$, A, 11.5) and catalyst reuse[c]** | | | | | | |
| 7 | 1st run[d] | 99.0 | 100 | 7.7 | 91.3 (25.0) | 1.042 |
| 8 | 2nd run | 94.3 | 100 | 21.3 | 66.4 (17.7) | 0.547 |
| 9 | 3rd run after coke burn-off | 91.1 | 100 | 9.9 | 81.2 (25.2) | 0.685 |
| **Comparison with literature results** | | | | | | |
| 10[e] | ($NH_3$, A, 11.5) | 93.4 | 100 | 28.9 | 64.5 (18.9) | 1.157 |
| 11[e] | 1wt% Ru/H-ZSM5 | 96.0 | 100 | 50.2 | 45.8 (16.3) | 0.822 |
| 12[f] | 5 wt% Ru/SBA-$SO_3H$ | 100 | 100 | 4.0 | 90.0 | 0.060[g]<br>0.160[h] |
| 13[g] | 5 wt% Ru/H-ZSM5 | 93.0 | 99.0 | 43.0 | 49.0 | 0.033 |

a. The total PA yield is given; this value includes the PE yield which is given in parentheses.

b. Conditions: 1wt% Ru/H-ZSM5, 51.7 mmol of LA, 0.6 g of catalyst, 54 g dioxane, 10 h, 473 K and 40 bar $H_2$.

c. Conditions: 1wt% Ru/H-ZSM5 , 21.5 mmol of LA, 0.5 g of catalyst, 22.5 g dioxane, 10 h, 473 K and 40 bar $H_2$.

d. See Fig. S2 for dependence of productivity on catalyst/substrate ratio.

e. Conditions: 21.5 mmol of LA, 0.3 g of catalyst, 22.5 g dioxane, 4 h, 473 K and 40 bar $H_2$. See ref. 9 for details.

f. Conditions: 4 mmol of LA, 0.2 g of catalyst, 10 mL of ethanol, 6 h, 523 K and 40 bar $H_2$. See ref. 10 for details.

g. PA productivity obtained after 6 h reaction time at 523 K.

h. Highest PA productivity obtained at 513 K. See ref. 10 for details.

The excellent activity of the 1wt% Ru/H-ZSM5($NH_3$, A, 11.5) catalyst in the direct, one-pot conversion of LA to PA can be mainly attributed to the improved dispersion of small ruthenium particles and the number and accessibility of the strong acid sites that are

required for this reaction. The time-on-line profiles with Ru/H-ZSM5($NH_3$, A, 11.5) show (Fig. 4.2c and 4.3a) that only GVL is detected as intermediate in the reaction, which indicates that PA is dominantly formed via the LA-GVL-PEA-PA route. PA is, however, already detected at low LA conversions, which might indicate that the LA-HPA-PEA-PA route, which avoids the most difficult GVL-PEA step, also occurs, possibly facilitated by the close proximity of the ruthenium and strong acid sites in the H-ZSM5 pores. Although HPA is hard to detect due to its instability under the applied conditions, it has been reported that reactive intermediates can be stabilized in zeolites pores via the confinement and nest effects.[26-29] The HPA intermediate might be stabilized by a strong acid site in the ZSM5 pores and subsequently directly dehydrated to PEA, rather than it being ring-closed to GVL. Dumesic et al. previously proposed the HPA to PEA route to be thermodynamically relevant at 523 K.[13] Recently, Xin et al. achieved a 95% selectivity of PA by the electrochemical reduction of LA to PA at pH 0 on a Pb electrode in an electrocatalytic (flow) cell reactor, also suggesting the same LA-HPA-PEA-PA pathway.[12]

### 4.3.3 Catalyst Stability and Reuse

The spent catalysts were characterized to detect any changes in either the metal phase or the zeolite support. TEM pictures of the spent catalysts are given in Appendix B, Fig. S1 and the average ruthenium particle sizes are given in Table 4.1. For all catalysts, different extents of sintering occurred as evidenced by the slight increase in ruthenium particle size after 10 h of reaction. We already previously observed that leaching of ruthenium is very limited under the employed reaction conditions.[9]

The $N_2$ physisorption data (Table 4.1) shows a significant drop in surface area of 62% and 86% for the spent Ru/H-ZSM5(Cl, H, 11.5) and (Cl, A, 11.5) catalysts, as a result of 8.0 wt% and 9.2 wt% coke build-up on the catalyst surface during reaction, determined by TGA(-MS). Ru/H-ZSM5($NH_3$, A, 11.5), the catalyst giving the best PA yield, suffered a little less from coke formation (7.6 wt%). Upon increase of the Si/Al ratio, the amount of coke deposition was found to decrease, consistent with the drop in support acidity.

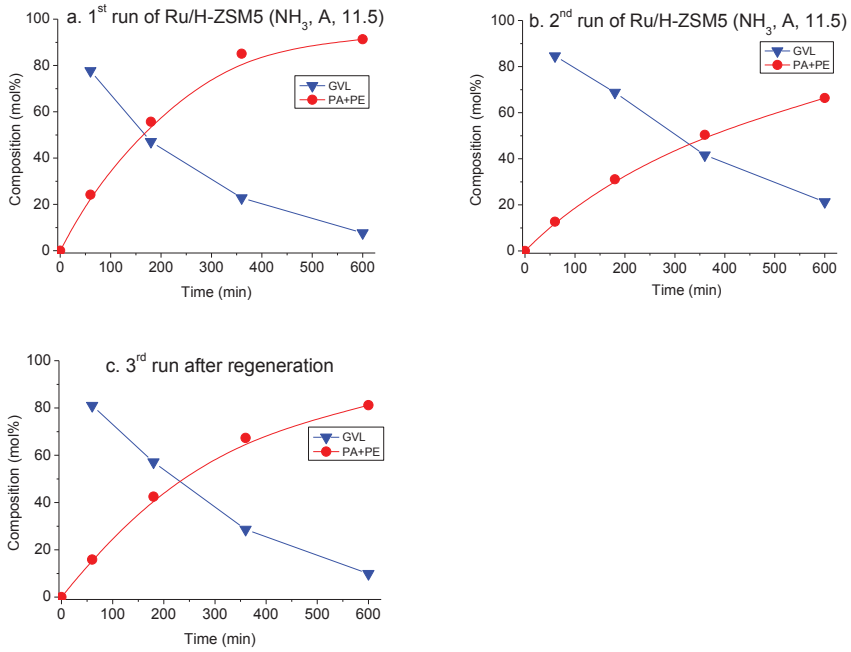


Figure 4.3. Time profiles of the catalytic hydrodeoxygenation of 10 wt% LA in dioxane at 473 K, 40 bar $H_2$, 10 h reaction time, with wt% Ru/H-ZSM5($NH_3$, A, 11.5), stirrer speed of 1600 rpm. GVL: γ-valerolactone; PA: pentanoic acid and its esters; LA conversion achieved 100% for all three runs within 1 h and is therefore not depicted.

The time on-line concentration profiles upon reuse of 1 wt% Ru/H-ZSM5($NH_3$, A, 11.5) are shown in Fig. 4.3. The 1 wt% Ru/H-ZSM5($NH_3$, A, 11.5) catalyst was assessed in two consecutive runs, then followed by a third run after a regeneration step involving coke burn-off at 723 K under a dilute hydrogen flow. While complete LA conversion was observed within 1 h reaction time for all three runs, the yield of PA decreased from 91.3 to 66.4 mol% upon two consecutive 10 h runs, with a concomitant drop in PA productivity from 1.042 to 0.547 $mol_{PA}\,g^{-1}_{Ru}\,h^{-1}$ (Table 4.3). From the time-profile (Fig 4.3b), it can be seen that not the conversion to GVL, but rather the GVL-PA step was slowed down, again pointing to the GVL ring-opening step to be most difficult. Upon regeneration, the spent catalyst recovered after two runs gave an increase in PA yield to 81.2 mol% in the third run, indicating that PA production activity of the catalyst could be almost completely restored by the coke burn-off process.

After regeneration, a bimodal particle size distribution was observed for Ru/H-ZSM5($NH_3$, A, 11.5) with high angle annular dark field scanning TEM imaging (HAADF) showing small particles (< 2 nm) as well as larger particles (ranging from 5 to 14 nm) located on the external surface of ZSM5 (Appendix B, Fig S2). This bimodal distribution points at a significant fraction of ruthenium being originally located inside the zeolite pores.

Table 4.4. Physicochemical properties of fresh Ru/H-ZSM5($NH_3$, A, 11.5) and spent catalyst after reaction at 473 K, 40 bar after 10 h in dioxane.

| | Catalyst of 1wt% Ru/H-ZSM5 | BET ($m^2$/g) | Micro-pore surface area ($m^2$/g) | Micro-pore volume ($cm^3$/g)[a] | Mesopore volume ($cm^3$/g)[a] | Average Ru particle size (nm)[b] | Ru dispersion ZSM5[c] | Coke content (wt%)[d] | LT Maxi-mum (K) | Amount of weak acid sites (mmol/$g_{cat}$) | HT Maxi-mum (K) | Amount of strong acid sites (mmol/$g_{cat}$) | Total acid amount (mmol/$g_{cat}$) |
|---|---|---|---|---|---|---|---|---|---|---|---|---|---|
| 1 | Fresh ($NH_3$, A, 11.5) | 324 | 251 | 0.12 | 0.07 | 1.7±0.4 | 0.76 | | 517 | 0.12 | 686 | 0.48 | 0.60 |
| 2 | Spent after 1st run | 137 | 107 | 0.05 | 0.03 | 3.8±0.9 | 0.34 | 7.6 | 555 | 0.16 | 670 | 0.43 | 0.59 |
| 3 | Spent after 2nd run | 91 | 77 | 0.04 | 0.03 | 6.9±2.1 | 0.19 | 9.9 | 536 | 0.24 | 667 | 0.35 | 0.59 |
| 4 | Regeneration after 2nd run | 333 | 246 | 0.12 | 0.08 | 5.8±2.5 | 0.22 | 1.1 | | | | | |
| 5 | Spent after 3rd run | | | | | | | | 576 | 0.17 | 651 | 0.42 | 0.59 |

[a] data obtained by the t-plot method

[b] data obtained by TEM

[c] data estimated by TEM: $D=6*(\nu_m/a_m)/d$. Where $\nu_m$ is bulk metal atomic density of Ru ($13.65\times 10^{-3}$ $nm^3$), $a_m$ is the surface area occupied by an atom on a polycrystalline surface of Ru ($6.35\times 10^{-2}$ $nm^2$), d is the cluster size of Ru metal.

[d] data determined by TGA

While some sintering does take place, the fact that PA yields can be almost completely restored shows that, the strong acidity of the ZSM5 must be mostly recovered upon regeneration. The TPD measurements show that the spent catalysts in three consecutive runs maintain the total acidity of the fresh one (Table 4.4), suggesting that Al leaching is

very limited under the applied reaction conditions and that the coke that is deposited does not block the accessibility of the acid sites for ammonia. The overall strength of the acid sites is reduced upon the first and second run, however, as some of the strong acid sites are converted to weak acid sites and the remaining strong sites are on average less strong (Table 4.4, entry 1-3 and Appendix B, Fig. S3). The spent catalyst after the 3rd run shows a number of strong acid sites that is larger than that of the spent catalyst after the 2nd run, and almost the same as the spent catalyst after the 1st run (Table 4.4, entry 2, 3, 5). Compared to the spent catalyst after 1st run, the shift of the HT peak maximum of the spent regenerated catalyst from 670 K to 651 K (Table 4.4, entry 2, 5) suggests, however, that a small amount of aluminium is irreversibly converted to extraframework species during reaction and regeneration. Additionally, most of the coke (89%) could be removed in the regeneration step, fully recovering the porosity of the fresh Ru/H-ZSM5($NH_3$, A, 11.5) (Table 4.4, entry 1, 4). These results show that coke formation is the main reason for deactivation, as it weakens the acid strength and blocks the accessibility of ZSM5.

## 4.4 Conclusions

A highly active and selective bifunctional 1wt% Ru/H-ZSM5 catalyst was developed for the direct, one-pot conversion of levulinic acid to pentanoic acid. Exploration of various synthesis parameters, including ruthenium precursor salt and cation form of the zeolite, resulted in a simple preparation method for catalysts with an improved dispersion of ruthenium, localized also in the pores of the zeolite, as well as an improved amount and strength of strong acid sites. The 1wt% Ru/H-ZSM5 catalyst gives an excellent yield of 91.3% PA under relatively mild conditions and shows the highest productivity of 1.157 $mol_{PA}\, g_{Ru}^{-1}\, h^{-1}$ reported to date. Better control over the density of in particular strongly acidic sites was key to achieve this high productivity, as these sites are needed for the most difficult step in the tandem conversion of LA to PA. The new preparation method furthermore improves the proximity between the hydrogenation and ring-opening/dehydration functions of the catalysts, as a result of the deposition of small Ru clusters into the pores of ZSM5, which is beneficial for PA production. Deactivation of 1 wt% Ru/H-ZSM5($NH_3$, A, 11.5) is primarily caused by carbon residue deposition on the strong acid sites, which weakens the strong acid sites owing to coke coverage.

**Acknowledgements**

Cor van der Spek (TEM), Nazila Masoud ($N_2$ physisorption), Rafael de Lima Oliveira ($N_2$ physisorption) and Marjan Versluijs-Helder (TGA), all from Utrecht University, are acknowledged for the measurements.

**References**

[1] J.J. Bozell, and G.R. Petersen, Green Chem. 12 (2010) 539-554.

[2] J.J. Bozell, L. Moens, D.C. Elliott, Y. Wang, G.G. Neuenschwander, S.W. Fitzpatrick, R.J. Bilski, and J.L. Jarnefeld, Resour. Conserv. Recy. 28 (2000) 227-239.

[3] D.W. Rackemann, and W.O.S. Doherty, Biofuel. Bioprod. Bior. 5 (2011) 198-214.

[4] I.T. Horvath, H. Mehdi, V. Fabos, L. Boda, and L.T. Mika, Green Chem. 10 (2008) 238-242.

[5] V. Pace, P. Hoyos, L. Castoldi, P. Domínguez de María, and A.R. Alcántara, ChemSusChem 5 (2012) 1369-1379.

[6] J.-P. Lange, R. Price, P.M. Ayoub, J. Louis, L. Petrus, L. Clarke, and H. Gosselink, Angew. Chem. Int. Ed. 49 (2010) 4479-4483.

[7] R. Palkovits, Angew. Chem. Int. Ed. 49 (2010) 4336-4338.

[8] J.C. Serrano-Ruiz, D. Wang, and J.A. Dumesic, Green Chem. 12 (2010) 574-577.

[9] W. Luo, U. Deka, A.M. Beale, E.R.H. van Eck, P.C.A. Bruijnincx, and B.M. Weckhuysen, J. Catal. 301 (2013) 175-186.

[10] T. Pan, J. Deng, Q. Xu, Y. Xu, Q.-X. Guo, and Y. Fu, Green Chem. 15 (2013) 2967-2974.

[11] F. Lónyi, A. Kovács, and J. Valyon, J. Phys. Chem. B 110 (2006) 1711-1721.

[12] L. Xin, Z. Zhang, J. Qi, D.J. Chadderdon, Y. Qiu, K.M. Warsko, and W. Li, ChemSusChem 6 (2013) 674-686.

[13] J.C. Serrano-Ruiz, R.M. West, and J.A. Dumesic, Annu. Rev. Chem. Biomol. Eng. 1 (2010) 79-100.

[14] J.J. Verdonck, P.A. Jacobs, M. Genet, and G. Poncelet, J. Chem. Soc., Faraday Trans. 76 (1980) 403-416.

[15] C.V. Hidalgo, H. Itoh, T. Hattori, M. Niwa, and Y. Murakami, J. Catal. 85 (1984) 362-369.

[16] F. Lónyi, and J. Valyon, Micropor. Mesopor. Mater. 47 (2001) 293-301.

[17] S.M. Campbell, D.M. Bibby, J.M. Coddington, R.F. Howe, and R.H. Meinhold, J. Catal. 161 (1996) 338-349.

[18] V.I. Pârvulescu, S. Coman, P. Palade, D. Macovei, C.M. Teodorescu, G. Filoti, R. Molina, G. Poncelet, and F.E. Wagner, Appl. Surf. Sci. 141 (1999) 164-176.

[19] R.M. Dalla Betta, and M. Boudart in: Proceedings of the 5th International Congress on Catalysis (J. Hightower ed.), Amsterdam, North-Holland. 1973, 1329.

[20] D.J. Elliott, and J.H. Lunsford, J. Catal. 57 (1979) 11-26.

[21] L.A. Pedersen, and J.H. Lunsford, J. Catal. 61 (1980) 39-47.

[22] S. You, I. Baek, Y. Kim, K.-E. Jeong, H.-J. Chae, T.-W. Kim, C.-U. Kim, S.-Y. Jeong, T. Kim, Y.-M. Chung, S.-H. Oh, and E. Park, Korean J. Chem. Eng. 28 (2011) 744-750.

[23] P. Treesukol, K. Srisuk, J. Limtrakul, and T.N. Truong, J. Phys. Chem. B 109 (2005) 11940-11945.

[24] C. Zhao, and J.A. Lercher, Angew. Chem. Int. Ed. 51 (2012) 5935-5940.

[25] G.L. Woolery, G.H. Kuehl, H.C. Timken, A.W. Chester, and J.C. Vartuli, Zeolites 19 (1997) 288-296.

[26] E.G. Derouane, J. Catal. 100 (1986) 541-544.

[27] E. Kikuchi, H. Nakano, K. Shimomura, and Y. Morita, J. Jpn. Pet. Inst. 28 (1985) 210-213.

[28] M. Brändle, and J. Sauer, J. Am. Chem. Soc. 120 (1998) 1556-1570.

[29] A. Vjunov, M.Y. Hu, J. Feng, D.M. Camaioni, D. Mei, J.Z. Hu, C. Zhao, and J.A. Lercher, Angew. Chem. Int. Ed. 53 (2014) 479-482.

# Chapter 5

# Supported Bimetallic Nano-Alloys as Highly Active, Selective and Stable Catalysts for the Hydrogenation of Levulinic Acid to γ-Valerolactone

**Abstract**

The hydrogenation of levulinic acid (LA) to γ-valerolactone (GVL) is a key reaction in many of the biorefinery schemes that aim at converting lignocellulose into renewable fuels and chemicals. We report on the development of highly active, selective and stable supported metal catalysts for LA-to-GVL and on the beneficial effects of alloying. Bimetallic random alloys of Au-Pd and Ru-Pd were prepared by a modified impregnation ($M_{Im}$) method and characterized by a combination of advanced microscopic and spectroscopic techniques. The Au-Pd/$TiO_2$ ($M_{Im}$) material showed a dramatic ~27-fold increase in activity (i.e., TOF = 0.102 $s^{-1}$) compared to its monometallic counterparts, which was attributed to to an electronic modification of Pd. The 1% Ru-Pd/$TiO_2$ ($M_{Im}$) catalyst was not only exceptionally active (TOF = 0.638 $s^{-1}$), but also showed excellent, sustained selectivity to GVL (99%). The dilution and isolation of Ru active sites by Pd is thought to be responsible for this superior catalytic performance. Alloying furthermore greatly improved the stability of both bimetallic catalysts.

Based on: Luo W.*, Sankar M.*, Beale A.M., He. Q, Kiely C.J., Bruijnincx P.C.A., Weckhuysen B.M., *Submitted for publication;* Sankar, M, Luo, W., Bruijnincx, P. C. A., Weckhuysen, B. M., Patent Application PCT/NL2014/050569

* Both authors contributed equally to this work.

## 5.1 Introduction

The increasing energy appetite of an ever growing global population, the accumulation of $CO_2$ in the atmosphere and the difficulties associated with the exploitation of finite fossil fuel reserves, have all stimulated the search for alternative feedstocks for our chemicals and fuels production. It is also driving the essential transition to a more sustainable, renewables-based society.[1-4] Various renewable feedstocks and many catalytic conversion routes, involving a multitude of intermediates and a plethora of end products, are currently being explored for the production of base chemicals and transportation fuel components from biomass in biorefinery-type operations. A small number of compounds have emerged, however, which have the potential to play a pivotal role as primary biorefinery building blocks, *i.e.* the so-called renewable platform molecules.[5]

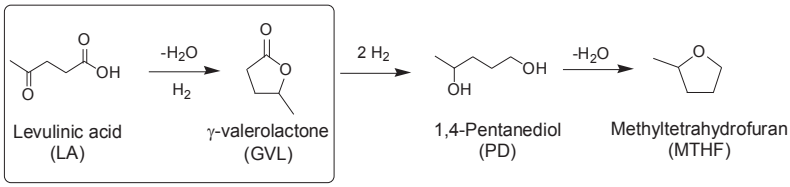


Scheme 5.1. GVL, PD and MTHF can be obtained by consecutive LA hydrogenation and dehydration steps.

Levulinic acid (LA) is one of these promising platform molecules, as it is produced easily and economically from the carbohydrate fraction of lignocellulosic biomass through a simple and high yield acid hydrolysis process.[6-8] Many value-added products for transportation fuel and/or base chemical production can in turn be obtained from LA, including polymer monomers (*e.g.* succinic and adipic acid), solvents (*e.g.* γ-valerolactone, methyltetrahydrofuran (MTHF)),[9] plasticizers (*e.g.* 1,4-pentanediol (PD)),[9] as well as bulk chemical and fuel components and precursors (*e.g.* butenes,[10] valeric acid esters,[11] nonanone[12]). Many of these routes actually involve γ-valerolactone (GVL), a versatile platform molecule in its own right,[13] as an intermediate, making the hydrogenation of LA (or its esters) to GVL a reaction of

immense importance in fostering economically sustainable bio-refinery developments (Scheme 5.1).[10, 11, 14]

A large number of catalyst materials have been reported for LA hydrogenation, including both homogeneous and heterogeneous metal-based catalysts. The use of heterogeneous catalysts for this reaction, which should be in principle more suitable for the large-scale manufacturing of GVL, has been recently reviewed by Palkovits et al.[14] Supported monometallic catalysts comprising noble metals are the most studied class of catalysts, and are typically used in the temperature range of 298 to 523 K with hydrogen pressures ranging from 1 to 150 bar in the liquid phase. A perusal of productivities for the various heterogeneous catalysts listed by Palkovits et al. shows that ruthenium-based catalysts typically give the highest GVL productivities, with Ru/C, for instance, being highly active and selective for hydrogenation of LA. Indeed, selectivities in excess of 95% at full conversion have been reported in dioxane,[15] water,[12] alcohol and neat LA[16] under different reaction conditions. While carbon supports are known to be stable in the highly polar and acidic liquid phase of a LA hydrogenation process, a downside of using carbon supports is that they do not survive the multiple regeneration cycles typically required for reactivation by burning-off coke at high temperatures.[11] In this latter respect, other supports such as metal oxides may be more suitable. $TiO_2$ is a particularly promising, alternative on account of the high activity of $TiO_2$-supported metal catalysts, their good stability under reaction conditions and potential for post-reaction catalyst regeneration.[11, 17, 18]

Supported bimetallic catalysts have been widely used as heterogeneous catalysts for many organic transformations including selective oxidation,[19] hydrogenation,[20, 21] hydrogenolysis,[22, 23] reforming reactions[24, 25] and many more.[26] The combination of two metals in appropriate proportions and nanostructures can often lead to superior catalytic performance be it in terms of activity, selectivity or stability compared to their monometallic analogues.[27] The possible advantages of supported bimetallic catalysts have not yet been fully exploited for biomass conversion reactions, especially for the conversion of LA to GVL.[14, 28] The limited examples available in the literature on the utilization of bimetallic catalysts for this transformation have actually met with limited success. For instance, Dumesic et al. alloyed Ru with Re to address the

rapid deactivation of monometallic Ru/C with time-on-stream when sulfuric acid was present in an aqueous solution of LA and formic acid.[29] While the Ru-Re alloy formation improved catalyst stability and activity in the presence of sulfuric acid, the bimetallic catalyst was considerably less active than the monometallic Ru in absence of sulfuric acid. Dumesic et al. reported that alloying Sn with Ru/C led to highly stable and GVL-selective catalysts in the hydrogenation of LA in a 2-sec-butylphenol solvent, but again at the expense of activity.[30] Lange et al. on the other hand, concluded that alloying of supported Pt catalysts with other metals, such as Re or Ru, did not actually improve performance, but instead led to reduced initial activity and enhanced deactivation when operated in liquid LA.[11]

As with monometallic catalysts, the catalytic performance of supported bimetallic catalysts is highly dependent on the compositional and structural characteristics of the bimetallic nanoparticles, features that are ultimately determined by the method of preparation.[31] Although many synthesis strategies have been reported, precise control over both particle size and the extent of alloy mixing, in a reproducible and straightforward manner, is still a challenge. Recently, one of us reported a stabilizer-free, convenient, "excess-anion" modified impregnation methodology (denoted here as $M_{Im}$) for the synthesis of supported bimetallic gold-palladium catalysts.[32] This $M_{Im}$ method provides access to catalysts with a very narrow particle size distribution and quite uniform composition of the two metals in a homogeneous random alloy structure. The Au-Pd catalysts were reported to be very active in the direct synthesis of hydrogen peroxide as well as for the solvent-free aerobic oxidation of alcohols.[33]

Here, we demonstrate that the controlled synthesis of supported bimetallic nanoparticles via the $M_{Im}$ methodology has a dramatic, positive effect on activity, selectivity and stability in the hydrogenation of LA to GVL. We report two different bimetallic catalysts, namely 1% Au-Pd/$TiO_2$ and 1% Ru-Pd/$TiO_2$ (both with equimolar metal ratio), and compare their performance with the corresponding monometallic counterparts in the LA-to-GVL reaction. Finally, further insights into the reasons for the superior catalytic activity and selectivity displayed by these two $M_{Im}$-derived bimetallic systems were provided by a combination of scanning transmission electron microscopy (STEM), X-ray absorption spectroscopy (XAS), X-ray photoelectron spectroscopy (XPS)

and Fourier transform infrared (FT-IR) spectroscopy studies using CO as a probe molecule.

## 5.2 Experimental Section

### 5.2.1 Catalyst Preparation

All the supported monometallic and bimetallic catalysts were prepared from their corresponding metal chloride precursors via a modified wet-impregnation method that involves using an excess of chloride anions ($M_{Im}$).[32] All catalysts prepared by this modified impregnation method are represented as $M_{Im}$ catalysts.

Modified impregnation ($M_{Im}$) method:
Precursor solutions: $HAuCl_4.xH_2O$ (>99.9%, Sigma Aldrich) was dissolved in deionized water to form a solution with a gold concentration of 9.34 mg/mL. $RuCl_3$ (99.9%, Acros Chemicals) was dissolved in deionized water to form an aqueous solution with a ruthenium concentration of 5.28 mg/mL. The $PdCl_2$ salt (<99 %, Sigma Aldrich) was dissolved in 0.5 M HCl under vigorous stirring and gentle warming to obtain a solution with a resultant palladium concentration of 3.02 mg/mL. This solution was slowly cooled and used as the palladium precursor.

In a typical catalyst synthesis, the requisite amount of precursor solution(s) was charged into a clean 50 mL round bottomed flask fitted with a magnetic stirrer, after which the requisite amount of concentrated HCl (37.5%) was added and the volume of the precursor/HCl solution finally adjusted to 25 mL to obtain a final HCl concentration of 0.5 M in deionized water. The round bottom flask was submerged in a temperature-controlled oil bath and the mixture was then agitated vigorously at 298 K using a hot plate stirrer. To the stirred precursor solution, the requisite amount of the support (P-25 $TiO_2$, Evonik-Degussa) was added very slowly with constant stirring at 298 K over nearly 30 min. After complete support addition, the slurry was stirred vigorously and then the temperature was raised to 358 K. The slurry was stirred at this temperature overnight until all water had evaporated. The solid powder obtained, denoted as the "dried sample", was ground thoroughly and then reduced in a furnace at 723 K (*ca.* 2

K/min ramp rate) under a flow of 5 % $H_2$/He for 4 h. All the monometallic and bimetallic catalysts were prepared with a 1 wt% (total) metal content on a 1 g scale and in the case of the bimetallic $M_{Im}$ catalysts, the two metals were added in an equimolar metal ratio.

A 1% Ru/$TiO_2$ ($M_{Im}$, 0 M HCl) catalyst, without the addition of HCl, was also prepared with the similar methodology. The requisite amount of the precursor $RuCl_3$ solution was charged into a clean 50 mL round bottomed flask fitted with a magnetic stirrer and then the solution was made up to 25 mL with deionized water, and no HCl was added. The following processes are the same as mentioned in the previous $M_{Im}$ method.

### 5.2.2 Catalyst Testing

All the catalytic hydrogenation reactions of LA to GVL were performed in dioxane using a high-pressure autoclave reactor fitted with an overhead stirrer. The reactions were run in a 100 mL Parr batch autoclave at a temperature of 473 K for 10 h using a hydrogen pressure of 40 bar and a stirring speed of 1600 rpm. Reactions were performed with 10 wt% levulinic acid (6.0 g, 51.7 mmol) in dioxane (54 g) with 1 wt% of catalyst (0.6 g). 1 mL of solution was sampled at various intervals during the reaction. Before the reaction, the batch autoclave reactor was loaded with catalyst, substrate and solvent, purged three times with argon after which the reaction mixture was heated to reaction temperature and charged with $H_2$ to 40 bar. This was taken as the starting point of the reaction. After the reaction was cooled to room temperature, the $H_2$ pressure was released and 2 wt% anisole was added as internal standard. The catalyst was separated by centrifugation, filtration and finally washed with acetone.

The reaction products were analyzed using a Shimadzu GC-2010A gas chromatograph equipped with a CP-WAX 57-CB column (25 m × 0.2 mm × 0.2 μm) and flame ionization detector (FID). Products were identified with a GC–MS from Shimadzu with a CP-WAX 57CB column (30 m × 0.2 mm × 0.2 μm). The gas phase reaction products were analyzed by an on-line dual channel Varian CP4900 micro-GC equipped with a $CO_X$ column and thermal conductivity detector (TCD), for analysis of $H_2$, $CO_2$, CO and $CH_4$.

### 5.2.3 Catalyst characterization

#### 5.2.3.1 Scanning Transmission Electron Microscopy and Scanning Electron Microscopy

Samples for examination by scanning transmission electron microscopy (STEM) were prepared by dispersing the dry catalyst powder onto a holey carbon film supported by a 300 mesh copper TEM grid. STEM high angle annular dark field (HAADF) images of the metallic particles were obtained using an aberration corrected JEM ARM-200F STEM operating at 200 kV. Energy dispersive of X-ray (EDX) spectra were acquired from individual nanoparticles larger than 1 nm in size by rastering the beam over the entire particle, while using a JEOL Centurio 0.9sr silicon drift detector. The sample powders were also dispersed onto an Al-stub and examined in SE and backscatter mode in a Hitachi 4300LV scanning electron microscope (SEM) equipped with an energy dispersive X-ray spectrometer to determine if there were any μm-scale metal particles present.

#### 5.2.3.2 Transmission Electron Microscopy

TEM measurements were conducted in bright field imaging mode using a Tecnai 20FEG transmission electron microscope operating at 200 kV. The mean Ru particle diameters were calculated by determining the size of more than 200 particles per sample using iTEM software (Soft Imaging System GmbH). For non-symmetrical particle shapes, both the largest and shortest diameter was measured to obtain an average value.

#### 5.2.3.3 X-Ray Absorption Fine Structure

X-ray absorption spectroscopy (XAS) measurements were performed on station BM26A and BM23 at the ESRF.[34] The measurements were carried out in air on self-supporting wafers in transmission mode using a Si(111) monochromator at the Au $L_3$ edge, Pd K-edge and Ru K-edge with the respective monometallic foils used as reference materials. All data were subjected to background correction using Athena (*i.e.* IFFEFFIT

software package) followed by either single or dual shell extended X-ray absorption fine structure (EXAFS) fitting analyses performed using the DL-EXCURV program.[35, 36]

#### 5.2.3.4 X-ray Photoelectron Spectroscopy

The X-ray photoelectron spectroscopy (XPS) measurements were carried out on a Thermo Scientific K-Alpha, equipped with a monochromatic small-spot X-ray source and a 180° double focusing hemispherical analyzer with a 128-channel detector. Spectra were obtained using an aluminium anode (Al $K_\alpha$ = 1486.6 eV) operating at 72 W and a spot size of 400 μm. Survey scans were measured at a constant pass energy of 200 eV and more detailed region scans at a pass energy of 50 eV. The background pressure of the system was 2 x $10^{-9}$ mbar, and during measurement it was 3 x $10^{-7}$ mbar (of argon) because of the charge compensation dual beam source.

#### 5.2.3.5 $N_2$ Physisorption

$N_2$ physisorption isotherms were recorded to determine surface areas and pore volumes using a Micromeritics Tristar 3000 set-up operating at 77 K. Bimetallic catalysts were outgassed for 12 h at 473 K in a nitrogen flow prior to the physisorption measurements. BET surface areas were determined using 10 points between 0.06 and 0.25. Micropore volumes ($cm^3/g$) were determined by *t*-plot analysis for *t* between 3.5 and 5.0 Å to ensure inclusion of the minimum required pressure points.

#### 5.2.3.6 FT-IR Spectroscopy after CO Adsorption:

Fourier transform infrared (FT-IR) spectra were recorded on a Perkin-Elmer 2000 instrument with each spectrum consisting of 25 scans recorded at a resolution of 4 $cm^{-1}$. Self-supported catalyst wafers (37 ± 10 mg/16 mm) were pressed at 3 kbar pressure for 10 s. The wafer was placed inside a synchrotron cell with a $CaF_2$ window. The cell was evacuated to $10^{-6}$ mbar and the sample was subsequently dried at 573 K (3 K/min) for 1 h. The cell was cooled down to 87 K with liquid nitrogen and connected to a gas chamber that permitted adjustment of the pressure of CO injected into the cell. CO adsorption was studied at 87 K at stepwise increasing pressures with fresh catalysts

previously reduced in $H_2$ at 723 K. CO desorption was also studied at 87 K during the evacuation process, and followed by temperature programmed desorption (3 K/min) from 87 to 573 K for 30 min under high vacuum conditions (~$10^{-6}$ mbar).

## 5.3 Results and Discussion

### 5.3.1 Hydrogenation of Levulinic Acid

Initially, we tested 1% Au-Pd/$TiO_2$ ($M_{Im}$) for the hydrogenation of LA to GVL under batch conditions with a 10 wt% solution of LA in dioxane at 473 K and 40 bar $H_2$. This bimetallic catalyst has been widely studied for various reactions,[19, 37, 38] but has never been tried for this key hydrogenation reaction. We also synthesized the corresponding monometallic 1% Au/$TiO_2$ ($M_{Im}$) and 1% Pd/$TiO_2$ ($M_{Im}$) catalysts and tested them under identical reaction conditions for comparison. The time-on-line yield of GVL (in mol%) is presented for all the three catalysts in Fig. 5.1a. The complete, individual time-on-line profiles detailing LA consumption and product formation for these three catalytic reactions are presented in Fig. 5.2a. The monometallic Au and Pd catalysts were found to be almost inactive under our standard reaction conditions with LA molar conversions of only 3.6% and 2.5% after 4 h, respectively.

Consequently, the GVL productivities for these two catalysts are very low at 0.073 $mol_{GVL}\ g_{metal}^{-1}\ h^{-1}$ (TOF = 0.004 $s^{-1}$) and 0.054 $mol_{GVL}\ g_{metal}^{-1}\ h^{-1}$ (TOF = 0.005 $s^{-1}$), respectively (Fig. 5.1b). In strong contrast, the bimetallic 1% Au-Pd/$TiO_2$ ($M_{Im}$) catalyst displayed a substantially higher catalytic activity under identical conditions, with 90% of LA having been converted after 4 h with 97.5% selectivity towards GVL (quantitative conversion of LA after 5 h, with 97.3 % selectivity to GVL). This corresponds to a GVL productivity of 1.97 $mol_{GVL}\ g_{metal}^{-1}\ h^{-1}$ (TOF = 0.102 $s^{-1}$), *i.e.* ~ a 27-fold increase in productivity and ~ 20-fold increase in TOF as compared to the supported monometallic Au and Pd catalysts (Fig. 5.1b). Small amounts of PD (0.4%) and MTHF (0.3%) are also formed as by-products, at the expense of GVL, by consecutive hydrodeoxygenation reactions (Scheme 5.1).

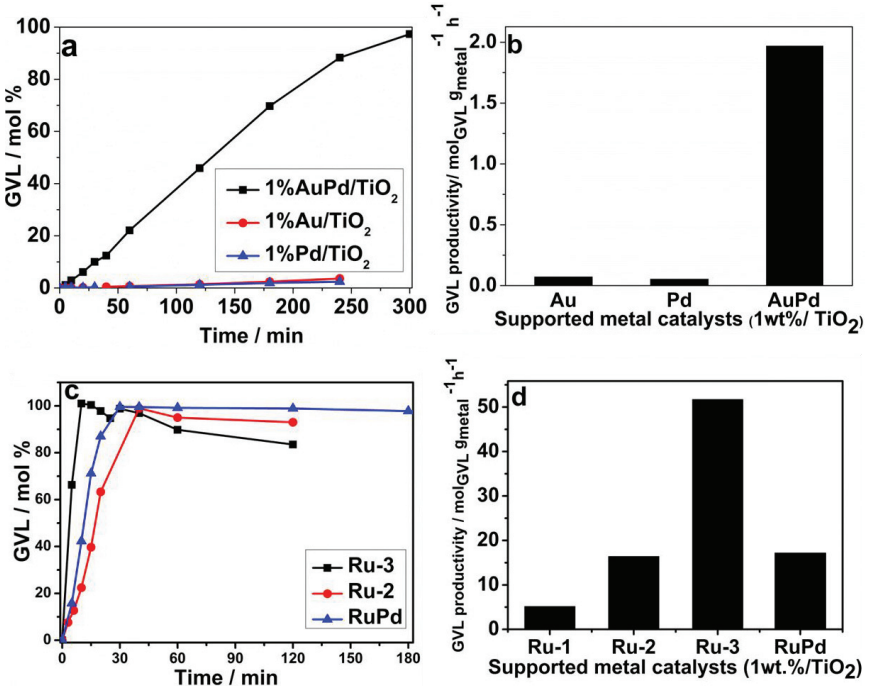


Figure 5.1. (a) Production of GVL as a function of time during the hydrogenation of LA using monometallic 1% Au/$TiO_2$ ($M_{Im}$) (●) and 1% Pd/$TiO_2$ ($M_{Im}$) (▲) and bimetallic 1% Au-Pd/$TiO_2$ ($M_{Im}$) (■) catalysts; (b) Comparison of GVL productivities of $TiO_2$ supported Au, Pd and Au-Pd catalysts after 4 h of reaction time. (c) Production of GVL as a function of time during the hydrogenation of LA using monometallic 1% Ru/$TiO_2$ ($M_{Im}$) (●, Ru-2), 1% Ru/$TiO_2$ ($M_{Im}$, 0 M HCl) (■, Ru-3) and bimetallic 1% Ru-Pd/$TiO_2$ ($M_{Im}$) (▲, RuPd) catalysts: (d) Comparison of GVL productivities of supported 1% Ru/$TiO_2$ ($W_{Im}$) (Ru-1), 1% Ru/$TiO_2$ ($M_{Im}$) (Ru-2), 1% Ru/$TiO_2$ ($M_{Im}$, 0 M HCl) (Ru-3) and 1% Ru-Pd/$TiO_2$ ($M_{Im}$) (RuPd). Reaction conditions: T: 473 K; P: 40 bar $H_2$; 10 wt% LA in dioxane; LA to Ru weight ratio = 1000.

Encouraged by this promising result and taking into account that the most active LA hydrogenation catalysts are typically ruthenium-based, we extended our modified impregnation methodology and synthesized a bimetallic 1% Ru-Pd/$TiO_2$ ($M_{Im}$) catalyst. This material was tested for the hydrogenation of LA to GVL under our standard reaction conditions and the results are presented in Fig. 5.1c. After 30 min of reaction time (Fig. 5.2b), quantitative conversion of LA (> 99%) was observed with a very high

selectivity of 99.6 % to GVL, corresponding to a productivity of 17.2 $mol_{GVL}\,g^{-1}{}_{metal}\,h^{-1}$ (TOF = 0.638 $s^{-1}$). Again, for comparison, we prepared and tested the corresponding monometallic 1% $Ru/TiO_2$ ($M_{Im}$) catalyst. After 40 min of reaction time, LA got quantitatively converted with a 99.0% selectivity to GVL (productivity of 16.4 $mol_{GVL}\,g^{-1}{}_{metal}\,h^{-1}$, TOF = 0.536 $s^{-1}$) (Fig. 5.2c).

Table 5.1. $N_2$ physisorption data of fresh (F) and spent (S) bimetallic $M_{Im}$ catalysts and metal leaching into the liquid phase after reaction in dioxane as determined by AAS.

| Catalyst | Status | Time | BET ($m^2/g$) | Pore volume ($cm^3/g$) | Coke content (wt%) | Ru(Au) loss (%)/ppm | Pd loss (%)/ppm |
|---|---|---|---|---|---|---|---|
| 1% $Ru\text{-}Pd/TiO_2$ | F | | 52.4 | 0.35 | | | |
| | S | 2 h | 52.3 | 0.34 | | | |
| | S | 2 h * 3 | 48.0 | 0.35 | 2.3 | 1.0/0.5 | 0.4/0.2 |
| 1% $Au\text{-}Pd/TiO_2$ | F | | 51.5 | 0.35 | | | |
| | S | 4 h | 47.0 | 0.35 | | | |
| | S | 4 h * 3 | 50.2 | 0.32 | 2.3 | 0.5/0.3 | 1.1/0.4 |

Nevertheless, a decrease in GVL selectivity (to 93.0%) was actually observed for the monometallic 1% $Ru/TiO_2$ ($M_{Im}$) catalyst after a prolonged reaction time of 2 h. Some PD (1.2%) and MTHF (0.7%) was also detected after 2 h (Scheme 5.1). In contrast, with the bimetallic 1% $Ru\text{-}Pd/TiO_2$ ($M_{Im}$) catalyst the molar selectivity of GVL remained stable at ~ 99% even after a prolonged reaction time of 2 h and complete conversion of LA. Compared to the dramatic improvement in catalyst activity seen upon alloying Au with Pd, the improvement in GVL production upon alloying Pd with Ru is more limited (compared to the monometallic Ru catalyst, Appendix Table S5.1), but alloying did, importantly, help in achieving and maintaining a very good selectivity for GVL as well as improved the stability of the catalyst (vide infra).

The stabilities of both bimetallic catalysts (1% $Au\text{-}Pd/TiO_2$ and 1% $Ru\text{-}Pd/TiO_2$) were examined by performing three consecutive runs under typical reaction conditions (Fig. 5.4). Catalytic activity and selectivity were also compared at different LA conversion levels, and the results show that GVL selectivities and yields are sustained for both

bimetallic catalysts upon the multiple reuse. No drop in activity and selectivity, limited leaching of metal phase and minimal loss of surface area (Table 5.1) were furthermore observed, providing further evidence that no significant deactivation occurred of both bimetallic catalysts during the three consecutive runs.

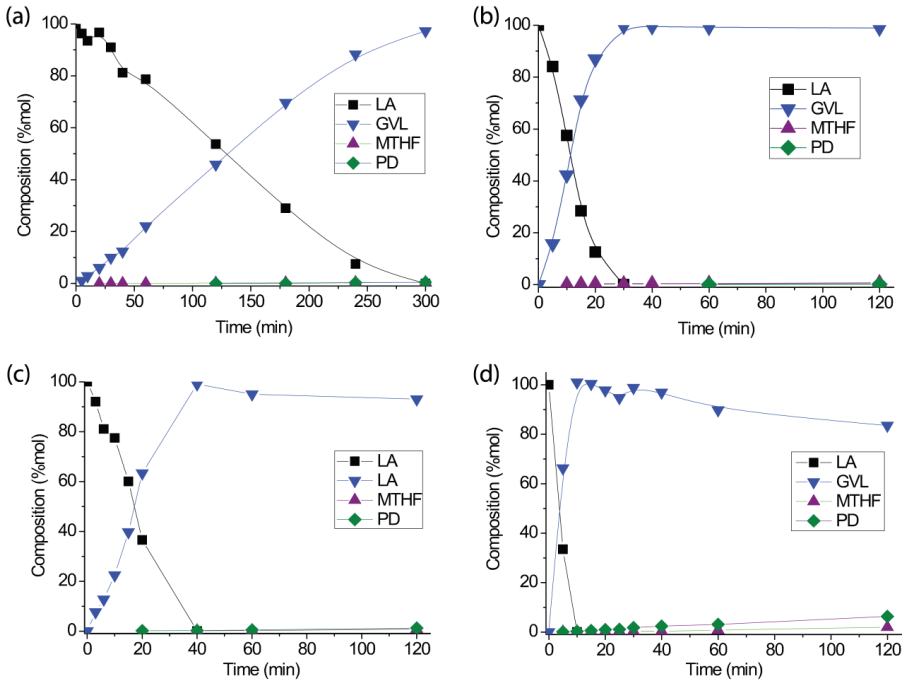


Figure 5.2. Temporal evolution of product(s) including GVL (▼), MTHF (▲) and PD (♦) and the consumption of LA (■) during its hydrogenation using (a) bimetallic 1% Au-Pd/$TiO_2$ ($M_{Im}$) (b) 1% Ru-Pd/$TiO_2$ ($M_{Im}$) (c) monometallic 1% Ru/$TiO_2$ ($M_{Im}$) and (d) 1% Ru/$TiO_2$ ($M_{Im}$, 0 M HCl). Reaction conditions: T: 473 K; P: 40 bar $H_2$; 10 wt% LA in dioxane, and a substrate/metal weight ratio of 1000.

Although the addition of HCl to the precursor mixture is an essential part of the $M_{Im}$ preparation methodology[32] for generating alloys of uniform composition, it is of course not necessarily required for the monometallic catalyst syntheses. In addition to the monometallic catalysts prepared via $M_{Im}$ for initial benchmarking, we also synthesized a 1% Ru/$TiO_2$ ($M_{Im}$, 0 M HCl) catalyst without the use of excess HCl. This catalyst showed exceptionally high activity in the hydrogenation of LA to GVL,

displaying a GVL productivity of 51.7 $mol_{GVL}$ $g^{-1}_{metal}$ $h^{-1}$ (TOF = 1.946 $s^{-1}$) (Fig. 5.2d, Appendix C, Fig. S1). This is much higher than the 16.4 $mol_{GVL}$ $g^{-1}_{metal}$ $h^{-1}$ value obtained for 1% $Ru/TiO_2$ ($M_{Im}$) (TOF = 0.536 $s^{-1}$) prepared with an excess of 0.5 M HCl. 1% $Ru/TiO_2$ ($M_{Im}$, 0 M HCl) thus outperforms all the catalysts tested by us (Fig. 5.1d) and, as far as we are aware, others (Appendix C, Table S1).[14] The GVL productivity of a 1% $Ru/TiO_2$ ($W_{Im}$) catalyst, prepared by conventional wet-impregnation followed by calcination and reduction in our previous studies,[18] was found to be only 5.14 $mol_{GVL}$ $g^{-1}_{metal}$ $h^{-1}$ (TOF = 0.233 $s^{-1}$) under identical reaction conditions. This value is more consistent with those supported Ru catalysts listed in the recent LA hydrogenation review of Palkovits et al.[14] This demonstrates the importance of designing system-specific synthesis strategies to achieve exceptionally high catalytic activity. It should be noted, however, that all monometallic Ru catalytic systems suffer from a decrease in selectivity to GVL as a function of time, with PD and MTHF being formed after prolonged reaction times. In addition an increase in mean Ru particle size was noted even after a reaction time of 2 h (Fig. 5.4).

### 5.3.2 Catalyst Characterization

The composition and nanostructure of both bimetallic catalysts were first characterized by aberration-corrected STEM (AC-STEM). Analysis of high angle annular dark field (HAADF) images of the 1% Au-Pd/$TiO_2$ ($M_{Im}$) sample gave a mean size of the supported metal particles of 1.5 nm (Figs. 5.3a, b). XEDS analysis of individual nm-scale samples confirmed these nanoparticles to be Au-Pd alloys (Figs. 5.3c, d). Small sub-nm clusters were also apparent in this material (Appendix C, Fig. S2a), as were a limited amount of larger Au particles in the 0.1-0.5 μm size range (Appendix C, Fig. S3). A comparable HAADF-STEM study of the 1% Ru-Pd/$TiO_2$ ($M_{Im}$) sample shows that the mean size of the supported metal particles was slightly smaller at 1.2 nm (Figs. 5.3e, f)). Once again, many sub-nm clusters were apparent (Appendix C, Fig. S2b), but SEM analysis did not show any μm scale particles for this sample (Appendix C, Fig. S4). XEDS analysis confirmed that the nm-scale particles were indeed Ru-Pd alloys (Figs. 5.3g-i).

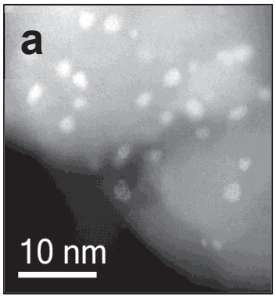
a
10 nm

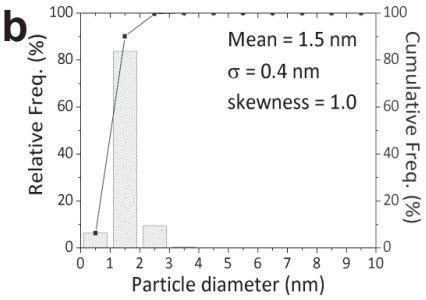
b
Mean = 1.5 nm
σ = 0.4 nm
skewness = 1.0
Relative Freq. (%)
Cumulative Freq. (%)
Particle diameter (nm)

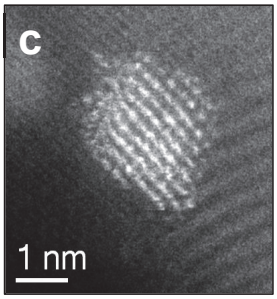
c
1 nm

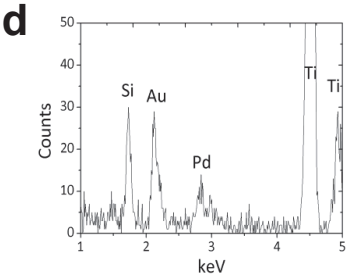
d
Si
Au
Pd
Ti
Ti
Counts
keV

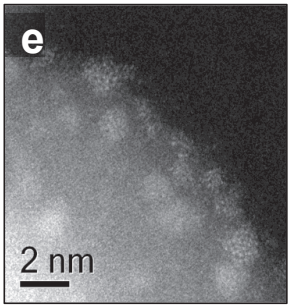
e
2 nm

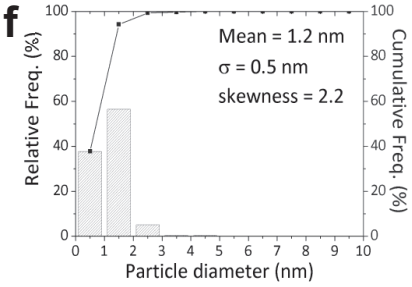
f
Mean = 1.2 nm
σ = 0.5 nm
skewness = 2.2
Relative Freq. (%)
Cumulative Freq. (%)
Particle diameter (nm)

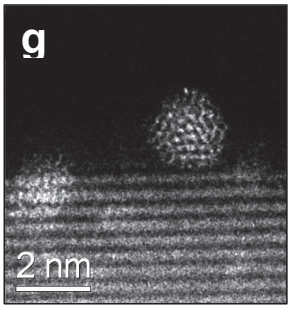
g
2 nm

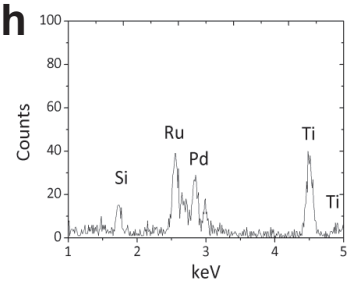
h
Si
Ru
Pd
Ti
Ti
Counts
keV

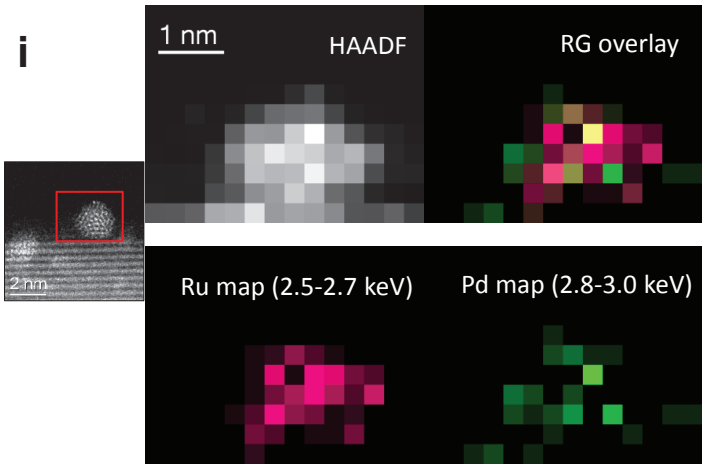


Figure 5.3. STEM analysis of the 1% Au-Pd/$TiO_2$ ($M_{Im}$) and 1% Ru-Pd/$TiO_2$ ($M_{Im}$) catalysts. 1% Au-Pd/$TiO_2$ ($M_{Im}$): (a) HAADF image showing typical particle sizes; (b) corresponding particle size distribution derived from measurements of over 500 particles; (c) HAADF image of an individual metal nanoparticle and (d) its corresponding XEDS spectrum confirming it is a Au-Pd alloy; 1% Ru-Pd/$TiO_2$ ($M_{Im}$): (e) HAADF image showing typical particle sizes; (f) corresponding particle size distribution derived from measurements of over 500 particles; (g) HAADF image of an individual metal nanoparticle; (h) its corresponding EDX spectrum. (i) EDX spectral imaging of 1% Ru-Pd/$TiO_2$ ($M_{Im}$) and corresponding elemental maps: Pd (green), Ru (pink) and Ru/Pd overlay, showing that the supported metal particles are indeed Ru-Pd alloys.

Any changes in the metal particle size of fresh and spent catalysts were examined by TEM, and the mean diameters of the metal particles are given in Fig. 5.4. All spent monometallic catalysts show an increase in the metal particle size and broadening of the distribution after the 1$^{st}$ catalytic run. In contrast, both bimetallic materials showed no or only a marginal increase in particle size, even after three catalytic runs, clearly illustrating the advantageous effect alloying has on stability.

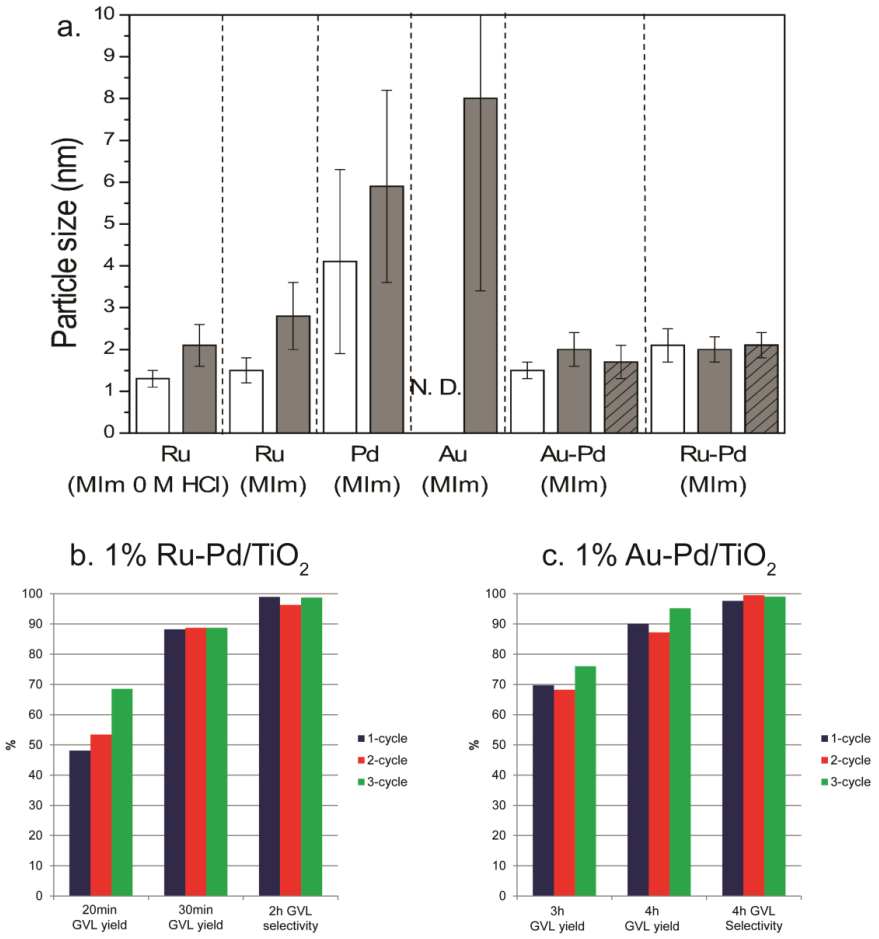


Figure 5.4. (a) Comparison of mean metal particle sizes for the fresh and spent Ru, Pd, Ru-Pd and Au-Pd catalysts prepared by the $M_{Im}$ methodology using TEM. (Blank bar = fresh catalyst; Grey bar = spent catalyst after 1 run; Gray, striped bar = spent catalyst after 3 consecutive runs); Recyclability of (b) bimetallic 1% Ru-Pd/$TiO_2$ ($M_{Im}$) and (c) 1% Au-Pd/$TiO_2$ ($M_{Im}$) catalysts. Recyclability tests were performed at different LA conversion levels and GVL selectivities. No significant catalyst deactivation was detected after three consecutive runs.

To better understand how representative the structures found by STEM are for the entirety of the catalyst sample, the materials were also characterized by extended X-ray absorption fine structure (EXAFS) measurements (Table 5.2, Figs. 5.5-5.6). The

presence of bimetallic species is indeed confirmed by the EXAFS data recorded at the Au $L_3$, Pd K and Ru K edges.

Table 5.2. EXAFS parameters for the bimetallic catalysts determined from an analysis of the Au $L_3$, Pd K and Ru K edges.[a]

| Sample | Au-Au R (Å) | (N) | $2\sigma^2$ (Å$^2$) | Au-Pd (Å) | (N) | $2\sigma^2$ (Å$^2$) | Pd-Pd R (Å) | (N) | $2\sigma^2$ (Å$^2$) | Pd-Au R (Å) | N | $2\sigma^2$ (Å$^2$) |
|---|---|---|---|---|---|---|---|---|---|---|---|---|
| 1% AuPd/$TiO_2$ ($M_{lm}$) [b] | 2.80 | 4.8 | 0.017 | 2.77 | 2.5 | 0.014 | 2.75 | 1 | 0.014 | 2.78 | 2.0 | 0.016 |
| 1% Au/$TiO_2$ ($M_{lm}$) | 2.84 | 10.0 | 0.017 | | | | | | | | | |
| | Ru-O | | | Ru-Ru (Pd) | | | Pd-O | | | Pd-Pd (Ru) | | |
| 1% RuPd/$TiO_2$ ($M_{lm}$) | 2.0 | 3.0 | 0.011 | 2.69 | 2 | 0.023 | 2.0 | 1.7 | 0.009 | 2.72 | 1.8 | 0.019 |
| 1% Pd/$TiO_2$ ($M_{lm}$) | | | | | | | 2.0 | 2.0 | 0.010 | 2.73 | 4.0 | 0.019 |
| 1% Ru/$TiO_2$ ($M_{lm}$ 0 M HCl) | 1.96 | 2 | 0.007 | 2.67 | 6 | 0.013 | | | | | | |

a. $E_f \sim \pm 15$ eV; R values for all data range from 28 – 38%; Afac values, 0.94 (Pd/Ru) and 0.98 Au. Debye-Waller factors were initially determined from the 1% Au-Pd/$TiO_2$ ($M_{lm}$) sample and not refined for remaining Au-Pd samples.

b. a Pd-O contribution at 2.02 Å, N = 1, $2\sigma^2 = 0.0013$ Å$^2$ is also present.

The resultant bimetallic coordination numbers are given in Table 1. For the 1% Au-Pd/$TiO_2$ ($M_{lm}$) sample, confirmation of the presence of bimetallic species can be seen immediately from the Fourier transform (FT) data at both edges. Two intense peaks in the FTs are observed as a consequence of a 'π phase flip' in the backscattering amplitude from 6 Å$^{-1}$ for Au (or indeed for all elements where Z > 78) resulting in a splitting of the major contribution in the FT into a high and low r component.[39, 40] This occurs when two elements are present in equivalent amounts; often the splitting and intensity of the low r contribution becomes more intense with an increasing number of bimetallic bonds. A mismatch in the total coordination number from an analysis of the Au $L_3$-edge (7.3) and Pd (3.0) K-edge data is testament to a large number

of Au-Au contributions due to the presence of large (~μm sized) clusters in this sample in addition to the nm-sized bimetallic species. From a Pd K-edge perspective, the smaller overall coordination number suggests that much of the Pd is associated with Au although the higher Au contribution (consistent with STEM-XEDS) suggests these larger species to be Au-rich.

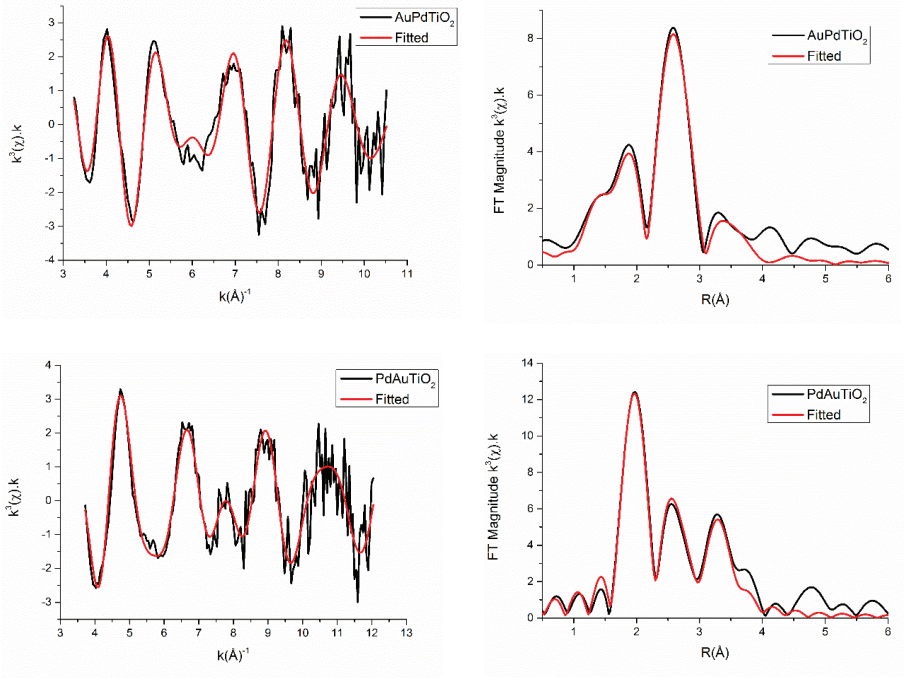


Figure 5.5. Isolated Au $L_3$ and Pd K-edge EXAFS and associated Fourier-Transform data for the 2-shell fits for 1% Au-Pd/$TiO_2$ ($M_{Im}$). Black line: data, red line: fit. EXAFS spectra were fitted in k-space.

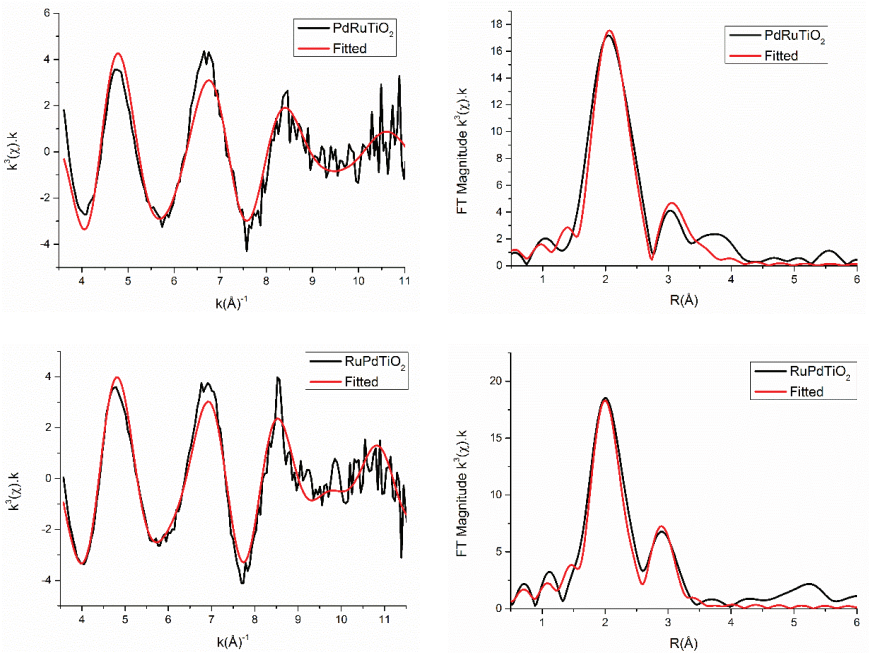


Figure 5.6. Isolated Pd and Ru K-edge EXAFS and associated Fourier-Transform data for the 2-shell fits for 1% Pd-Ru/$TiO_2$ ($M_{Im}$). Black line: data, red line: fit. EXAFS spectra were fitted in k-space.

For the 1% Ru-Pd/$TiO_2$ ($M_{Im}$) sample, the similarity in X-ray scattering efficiency precludes distinguishing between the bimetal components. However, instead, a first shell analysis assuming one metal-metal (M-M) scatterer type can be performed on the basis that STEM-XEDS confirms the bimetallic nature of the species in the 1% Ru-Pd/$TiO_2$ ($M_{Im}$) catalyst. The closeness in the coordination numbers of both species from an analysis of both edges supports the notion that the Pd and Ru exist in a similar environment (*i.e.* within intimately mixed bimetallic particles). The large number of M-O bond distances determined and the low M-M coordination numbers seen for both edges are also consistent with the STEM analysis in that the particles are very small; smaller than that seen for the 1% Au-Pd/$TiO_2$ ($M_{Im}$) sample. In addition, the shorter distances of the Ru-O and Ru-Ru bonds with 1% Ru/$TiO_2$ ($M_{Im,}$ 0 HCl) as compared to 1% Ru-Pd/$TiO_2$ ($M_{Im}$) indicate that even smaller particles are present in the 1% Ru/$TiO_2$ ($M_{Im,}$ 0 M HCl) catalyst, as noted previously by TEM.

All fresh monometallic and bimetallic catalysts were also characterized by XPS (Fig. 5.7, Table 5.3). Due to overlap of the Au $4f_{5/2}$ and Pd 4s peaks, only the Au $4f_{7/2}$ signal could be used to assess the electronic properties of Au; the Pd $3d_{3/2}$ signals were used to study the electronic properties of Pd, as the Pd $3d_{5/2}$ and Au $4d_{5/2}$ peaks overlapped. The C 1s signal (an artefact from the sample holder) was used as an internal reference.

For the monometallic 1% Au/$TiO_2$ ($M_{Im}$) catalyst the Au $4f_{7/2}$ signal is observed at 84.2 eV (Fig. 5.7a), which is close to the B.E. reported for Au/$TiO_2$[41-43] and Au/$Fe_2O_3$.[44] For the 1% Au-Pd/$TiO_2$ ($M_{Im}$) material a small negative shift of -0.2 eV, from 84.2 to 84.0 eV, was observed for the Au $4f_{7/2}$ peak. Similar small negative shifts of -0.25 eV to -0.56 eV in Au$4f_{7/2}$ B.E.s have previously been observed for Au-Pd surfaces and nanoparticles,[45-48] and have been attributed to a build-up of negative charge on the Au atoms upon Au-Pd alloy formation. The positive shift of +0.3 eV from 340.6 to 340.9 eV seen for the Pd $3d_{3/2}$ peak (Fig. 5.7b) in turn suggests deposition of some positive charge onto the Pd atoms. Such electron donation from Pd to Au in the Au-Pd nanoalloy has been previously reported for "crown-jewel" structured Pd-Au nanoclusters and was attributed to the higher electronegativity of Au (2.4) as compared to Pd (2.2).[47] Alternatively, the positive shift could also be the result of partial oxidation of Pd. It should be kept in mind that the EXAFS data shows that Pd is predominantly found in the Au-Pd particles, but some is also present as metallic Pd and Pd-O species. The latter species were also seen for Au-Pd/$SiO_2$ catalysts.[49] Indeed, both the 1% Au-Pd/$TiO_2$ ($M_{Im}$) and 1% Pd/$TiO_2$ ($M_{Im}$) samples showed weak peaks at around 342.6[46] and 337.2 eV,[50] which confirm the presence of Pd oxide on the surface of both samples. The Ti 2p and O 1s peaks were observed at the same B.E. for the three 1% Au/$TiO_2$ ($M_{Im}$), 1% Au-Pd/$TiO_2$ ($M_{Im}$) and 1% Pd/$TiO_2$ ($M_{Im}$) catalysts, suggesting that there is a similar level of interaction between metal and support in all these materials (Fig. 5.7e-f).

For the Ru-Pd series of materials, owing to the overlap of the Ru $3d_{3/2}$ and $Ru^{n+}$ $3d_{5/2}$ signals with the C 1s signal (an artefact from the sample holder, Fig. 5.7c), only the metallic state of Ru can be studied via the Ru $3d_{5/2}$ signal. The Ru $3d_{5/2}$ peak of supported $Ru^0$ on $TiO_2$ was reported at 280.1 eV by Elmasides *et al*.[51] For 1% Ru/$TiO_2$ ($M_{Im}$, 0 M HCl), a positive shift of +0.8 eV of the Ru $3d_{5/2}$ signal to 280.9 eV was observed, together with negative shifts of both the Ti 2p and O 1s peaks; in addition, shoulder

peaks appeared on the Ti 2p and O 1s signals, which point at a metal-support interaction, which results from electron transfer from Ru to $TiO_2$ with the concomitant reduction of some $Ti^{4+}$ into $Ti^{3+}$, that is much stronger than for the corresponding 1% Pd/$TiO_2$ ($M_{Im}$) sample (Fig. 5.7e-f). For the 1% Ru-Pd/$TiO_2$ ($M_{Im}$) catalyst, the Ru $3d_{5/2}$ peak is instead observed at 280.6 eV. This, together with the smaller changes observed in the Ti 2p and O 1s signals (Fig. 5.7e-f), indicate that the interaction between Ru and $TiO_2$ in 1% Ru-Pd/$TiO_2$ ($M_{Im}$) is weaker than in the 1% Ru/$TiO_2$ ($M_{Im}$, 0 M HCl) material. The Pd $3d_{5/2}$ (+0.9 eV) and Pd $3d_{3/2}$ (+1.0 eV) peaks furthermore show a positive shift and larger Pd oxide contribution compared to monometallic 1% Pd/$TiO_2$ ($M_{Im}$), which is indicative of the presence of highly dispersed and positively charged Pd species on the surface of the 1% Ru-Pd/$TiO_2$ ($M_{Im}$) catalyst. EXAFS data (Table 5.3) also suggests a more pronounced Pd-O character in 1% Ru-Pd/$TiO_2$ ($M_{Im}$) and the presence of Pd oxide is further confirmed by IR after CO adsorption (vide infra). All this thus suggests that at the metal surface Ru is less positively charged as a result of a weaker interaction of Ru with the support, while Pd is highly positively charged with some Pd-O character at the surface. It should finally be noted that no residual Cl could be detected by XPS in any of the monometallic and bimetallic $M_{Im}$ catalysts, except for a trace amount of Cl in the 1% Au/$TiO_2$ ($M_{Im}$) catalyst.

For the Ru-Pd series of materials, owing to the overlap of the Ru $3d_{3/2}$ and $Ru^{n+}$ $3d_{5/2}$ signals with the C 1s signal (an artefact from the sample holder, Fig. 5.7c), only the metallic state of Ru can be studied via the Ru $3d_{5/2}$ signal. The Ru $3d_{5/2}$ peak of supported $Ru^0$ on $TiO_2$ was reported at 280.1 eV by Elmasides *et al.*[51] For 1% Ru/$TiO_2$ ($M_{Im}$, 0 M HCl), a positive shift of +0.8 eV of the Ru $3d_{5/2}$ signal to 280.9 eV was observed, together with negative shifts of both the Ti 2p and O 1s peaks; in addition, shoulder peaks appeared on the Ti 2p and O 1s signals, which point at a metal-support interaction, which results from electron transfer from Ru to $TiO_2$ with the concomitant reduction of some $Ti^{4+}$ into $Ti^{3+}$, that is much stronger than for the corresponding 1% Pd/$TiO_2$ ($M_{Im}$) sample (Fig. 5.7e-f).

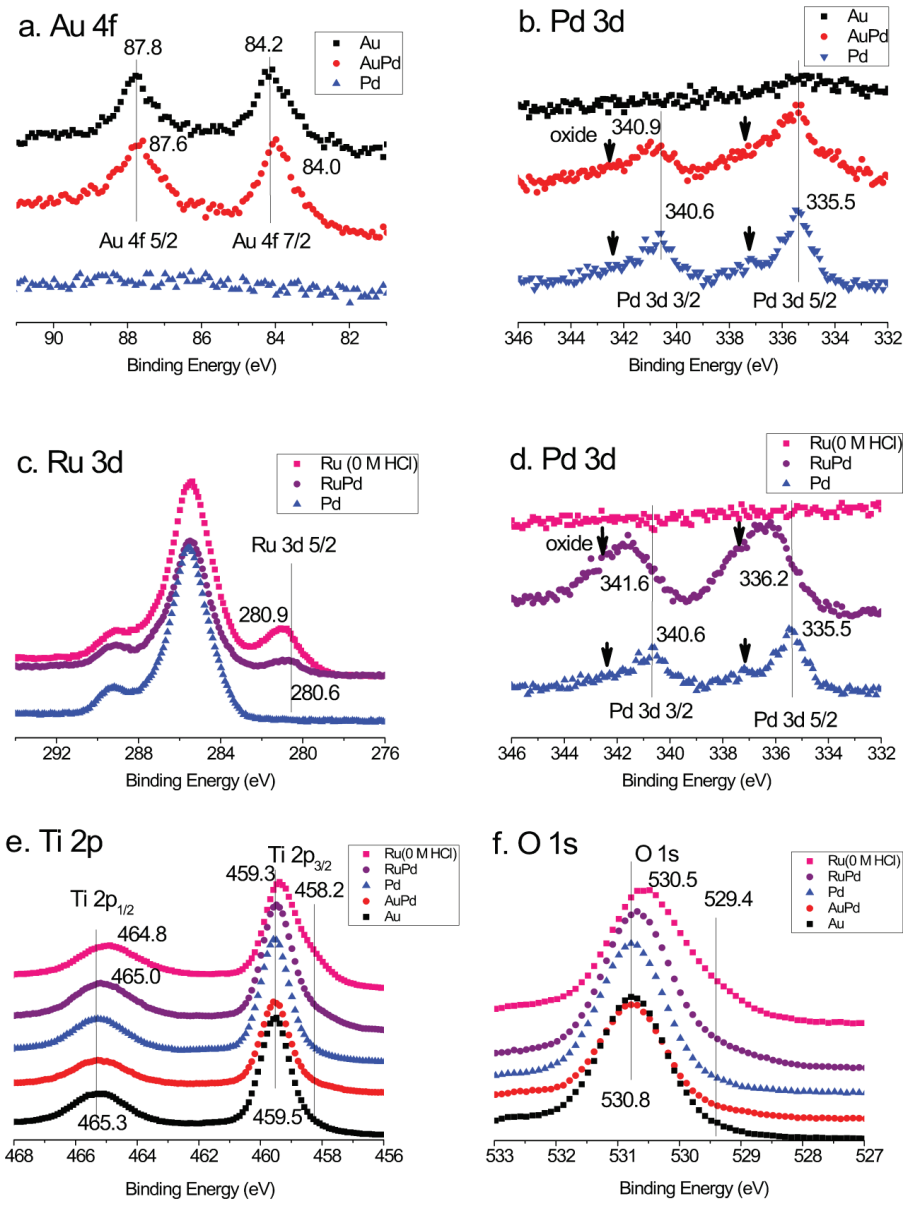


Figure 5.7. XPS spectra of selected $M_{Im}$ catalysts (red squares – 1% $Ru/TiO_2$ ($M_{Im}$, 0 M HCl); purple diamonds 1% $Ru\text{-}Pd/TiO_2$ ($M_{Im}$); blue triangles – 1%$Pd/TiO_2$ ($M_{Im}$); Black squares – 1% $Au/TiO_2$ ($M_{Im}$); red-diamonds – 1% $AuPd/TiO_2$ ($M_{Im}$)). The spectral regions shown are (a) Au 4f, (b) Pd 3d, (c) Ru 3d, (d) Pd 3d, (e) Ti 2p and (f) O 1s.

Table 5.3. Measured XPS binding energies (BE) for different $M_{Im}$ catalysts.

| Catalyst ($M_{Im}$) | B.E. Ti $2p_{1/2}$ | B.E Ti $2p_{3/2}$ | B.E. Ti $2p_{3/2}$ | B.E. O 1s | B.E. O 1s | B.E. Au $4f_{7/2}$ | B.E. Pd $3d_{3/2}$ | B.E. Ru $3d_{5/2}$ |
|---|---|---|---|---|---|---|---|---|
| 1% $Ru/TiO_2$ (0 M HCl) | 464.8 | 459.3 | 458.2 | 530.5 | 529.4 | | | 280.9 |
| 1% $Ru\text{-}Pd/TiO_2$ | 465.0 | 459.5 | 458.2 | 530.7 | 529.4 | | 341.6 | 280.6 |
| 1% $Pd/TiO_2$ | 465.3 | 459.5 | | 530.8 | | | 340.6 | |
| 1% $Au\text{-}Pd/TiO_2$ | 465.3 | 459.5 | | 530.8 | | 84.0 | 340.9 | |
| 1% $Au/TiO_2$ | 465.3 | 459.5 | | 530.8 | | 84.2 | | |

For the 1% $Ru\text{-}Pd/TiO_2$ ($M_{Im}$) catalyst, the Ru $3d_{5/2}$ peak is instead observed at 280.6 eV. This, together with the smaller changes observed in the Ti 2p and O 1s signals (Fig. 5.7e-f), indicate that the interaction between Ru and $TiO_2$ in 1% $Ru\text{-}Pd/TiO_2$ ($M_{Im}$) is weaker than in the 1% $Ru/TiO_2$ ($M_{Im}$, 0 M HCl) material. The Pd $3d_{5/2}$ (+0.9 eV) and Pd $3d_{3/2}$ (+1.0 eV) peaks furthermore show a positive shift and larger Pd oxide contribution compared to monometallic 1% $Pd/TiO_2$ ($M_{Im}$), which is indicative of the presence of highly dispersed and positively charged Pd species on the surface of the 1% $Ru\text{-}Pd/TiO_2$ ($M_{Im}$) catalyst. EXAFS data (Table 5.3) also suggests a more pronounced Pd-O character in 1% $Ru\text{-}Pd/TiO_2$ ($M_{Im}$) and the presence of Pd oxide is further confirmed by IR after CO adsorption (vide infra). All this thus suggests that at the metal surface Ru is less positively charged as a result of a weaker interaction of Ru with the support, while Pd is highly positively charged with some Pd-O character at the surface. It should finally be noted that no residual Cl could be detected by XPS in any of the monometallic and bimetallic $M_{Im}$ catalysts, except for a trace amount of Cl in the 1% $Au/TiO_2$ ($M_{Im}$) catalyst.

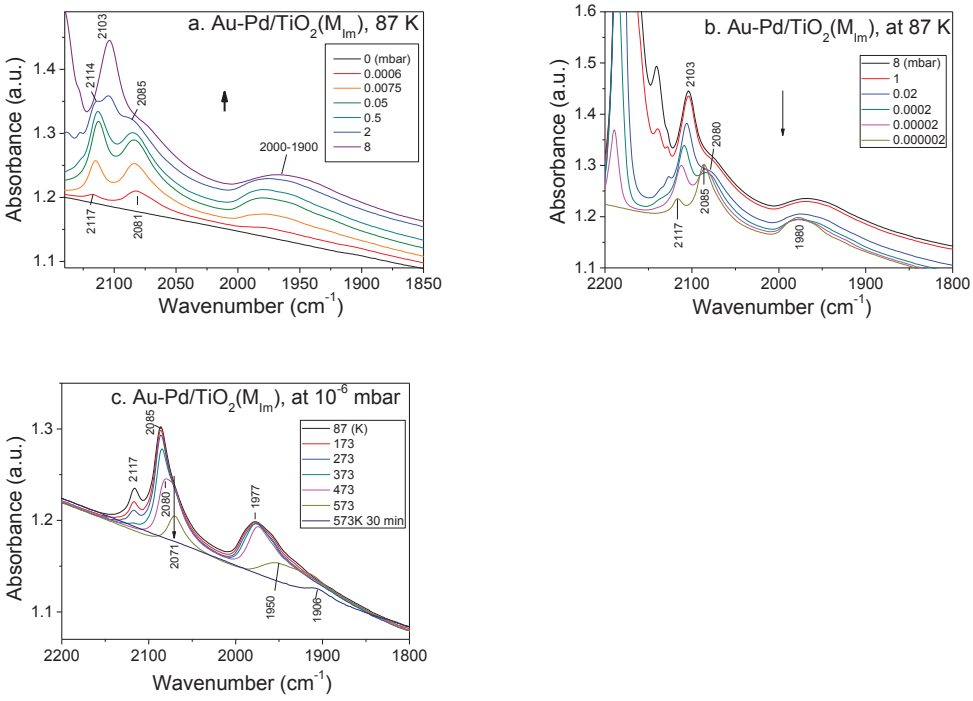


Figure 5.8. FT-IR spectra of CO adsorbed on 1% Au-Pd/$TiO_2$ ($M_{Im}$). (a) Stepwise adsorption, (b) desorption from 8 to $10^{-6}$ mbar at 87 K, and (c) temperature-programmed desorption (TPD) of CO IR at $10^{-6}$ mbar.

The FT-IR spectra of all mono- and bimetallic catalysts after CO adsorption are shown in Fig. 5.8-5.11. The spectra can be divided into a high (2150-2000 $cm^{-1}$) and low (2000-1900 $cm^{-1}$) frequency region, corresponding to carbonyl species adsorbed in a linear or bridged fashion, respectively.[52] The spectra of the monometallic 1% Au/$TiO_2$ ($M_{Im}$) and 1% Pd/$TiO_2$ ($M_{Im}$) catalysts showed little CO adsorption at variable pressure (Appendix C, Figs. S5-6). Fig. 5.8a shows the changes in the FT-IR spectra of adsorbed CO over 1% Au-Pd/$TiO_2$ ($M_{Im}$) at 87 K upon stepwise increase in CO pressure. The three spectral features at 2117, 2081 and 2000-1900 $cm^{-1}$, which are already detected at low CO coverage ($p_{CO}$ = 6 × $10^{-4}$ mbar), can be assigned to linear Au-CO(L), linear Pd-CO(L) and bridging Pd-CO(B) species, respectively.[53-58] Notably, a feature similar to the one at 2081 $cm^{-1}$ has been ascribed by Goodman *et al.,* [58] to CO linearly adsorbed on

isolated Pd atoms in Au-Pd alloy films. An increase in CO pressure to 2 mbar caused the Au-CO(L) feature at 2117 $cm^{-1}$ to red-shift to 2114 $cm^{-1}$, which is similar to the red-shift from 2116 to 2108 $cm^{-1}$ noted by Goodman and co-workers for Au-CO in their Au-Pd model catalyst system;[57-60] simultaneously, the Pd-CO(L) signal blue-shifted from 2081 to 2085 $cm^{-1}$ with increasing CO coverage. These shifts indicate a strong electronic interference between the adsorbed Au-CO(L) and Pd-CO(L) species at elevated CO pressure, and again point at the direct adjacency of Au and Pd atoms. Upon applying high vacuum and heating (Figs. 5.8b-c), the Au-CO(L) feature vanishes at 473 K, while the Pd-CO(L) feature remains up to 573 K, indicating enhanced CO adsorption on Pd. The new, weakly absorbed CO species that is observed at 2103 $cm^{-1}$ and first appeared at 0.5 mbar of CO can be assigned to CO adsorption on monometallic Pd species, according to literature precedence.[53, 58, 61] Finally, the absence of any signal between 2200 and 2125 $cm^{-1}$ for 1% Au-Pd/$TiO_2$ ($M_{Im}$) at low CO pressures, suggests that Au does not bear a positive charge (Fig. 5.8).

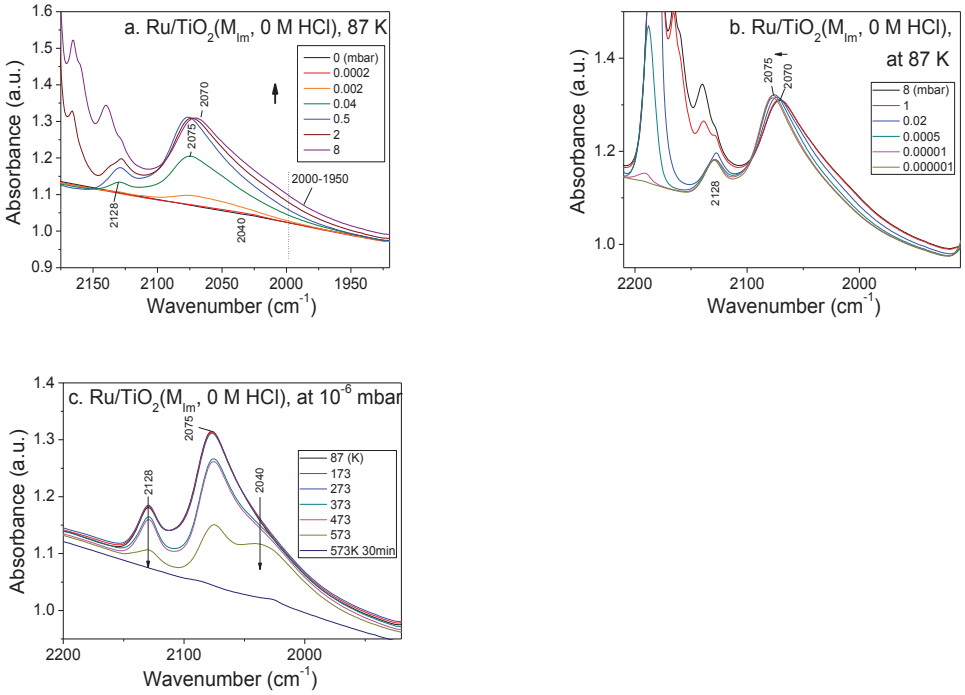


Figure 5.9. FTIR spectra of CO adsorbed on 1wt% Ru/$TiO_2$ ($M_{Im}$, 0 M HCl): (a) Stepwise adsorption from $10^{-6}$ to 8 mbar at 87 K, (b) Stepwise desorption from 8 to $10^{-6}$ mbar at 87 K, and (c) TPD of CO IR at $10^{-6}$ mbar.

Taken together, the partial negative charge on Au as seen in XPS, the confirmation of a Au-Pd nanoalloy structure by STEM and EXAFS, the evidence obtained by IR for isolated Pd species and the close proximity of Au and Pd in FT-IR, all suggest electron transfer from Pd to Au in the 1% Au-Pd/$TiO_2$ ($M_{Im}$) catalyst. Such electron transfer from Pd to Au has also been suggested recently for "crown-jewel"-structured Pd-Au nanoclusters.[47] Finally, it should be noted that CO adsorption on Pd is much stronger upon Au-Pd alloy formation (Fig. 5c, d), something which was also observed with a model Au-Pd catalyst,[58] indicating a strong modification of the Pd electronic structure upon mixing with Au at the nanoscale. This electronic modification of Pd in the Au-Pd alloy is thought to be the origin of the observed significant increase in catalytic activity in the conversion of LA to GVL (*i.e.* a ~ 27 fold increase in productivity).[27, 62]

For 1% Ru/$TiO_2$ ($M_{Im}$, 0 M HCl), at a low CO pressure of 0.002 mbar (Fig. 5.9a), a feature at 2075 $cm^{-1}$ with a shoulder at 2040 $cm^{-1}$ developed, which could be assigned to $Ru^{\delta+}$-CO (L), and $Ru^0$-CO (L) species, respectively.[63-66] In addition, a broad peak was seen centered around 1880 $cm^{-1}$ for all the Ru-containing samples due to the presence of $Ru^{4+}$=O overtones.[66, 67] With further increase of the CO pressure to 0.04 mbar, a band at 2128 $cm^{-1}$ and a low-frequency 'tail' at *ca.* 2000-1950 $cm^{-1}$ appeared simultaneously, attributed to two different CO adsorbed on oxidized Ru species; multi-coordinated $Ru^{n+}$-$(CO)_x$ (x>2) (L) and $Ru^{n+}$-(CO) (L) respectively [64, 68, 69]. In particular, the $Ru^{\delta+}$- CO(L) band at 2075 $cm^{-1}$ has a higher intensity than the $Ru^0$-CO(L) band at 2040 $cm^{-1}$ at 87 K, combined with the evidence for a shorter distance of Ru-O species of 1.96 A in XAFS, and an electron transfer from Ru to $TiO_2$ in XPS (Fig. 5.7e-f, 5.9 and Table 5.4), suggests a stronger metal support interaction. Notably, a strong and abundant adsorption of CO on Ru (Fig. 5.9b-c), especially $Ru^{\delta+}$-CO(L) at 2075 $cm^{-1}$, was indicated in the temperature-programmed desorption profile, and the absolute IR intensities in Ru/$TiO_2$ ($M_{Im}$, 0 M HCl) spectra is the highest amongst all the $M_{Im}$ catalysts compared.

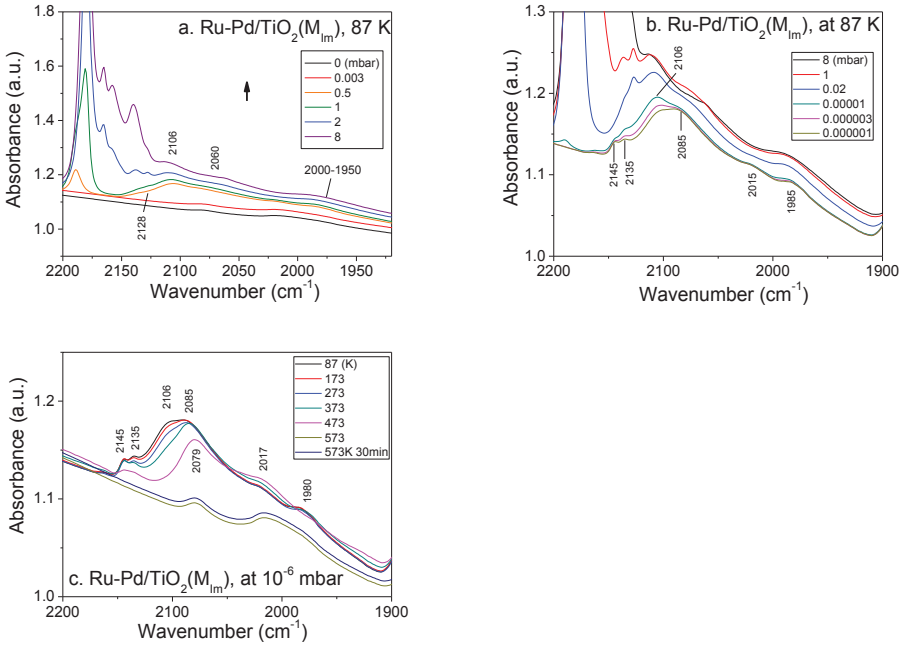


Figure 5.10. FTIR spectra of CO adsorbed on Ru-Pd/$TiO_2$ ($M_{Im}$): (a) Stepwise adsorption, (b) desorption from 8 to $10^{-6}$ mbar at 87 K, and (c) TPD of CO IR at $10^{-6}$ mbar.

For the 1% Ru-Pd/$TiO_2$ ($M_{Im}$) catalyst (Fig. 5.10), overlap between the bands corresponding to CO adsorbed on Ru and Pd makes differentiation of the adsorbed species more difficult. Furthermore, little electron transfer between Ru and Pd is expected based on the similar electronegativity value of the two metals (*i.e.* 2.2). In line with the XPS and EXAFS data, the FT-IR spectra of CO adsorption and desorption do, however, the bands at 2150-2085 $cm^{-1}$ can be attributed to $Pd^{2+}$-CO (L) species,[70, 71] indicating the presence of oxidized Pd species. This still suggest that Ru and oxidized Pd are present in the Ru-Pd alloy, as does the temperature programmed reduction data (Appendix C, Fig. S8).

It should be noted that while the FT-IR spectra of 1% Ru-Pd/$TiO_2$ ($M_{Im}$) and 1% Ru/$TiO_2$ ($M_{Im}$, 0 M HCl) are very similar at 473 K under high vacuum (Figs. 5.9, 5.10 and 5.11), less CO is found to be adsorbed under these conditions on 1% Ru-Pd/$TiO_2$ ($M_{Im}$). The attenuated intensity of $Ru^{\delta+}$-CO (L)[22-24] at 2075 $cm^{-1}$ is indicative of a weakening

of the interaction between Ru and $TiO_2$, as is also evidenced by the longer Ru-O bond lengths found by EXAFS and the more limited partial Ti reduction seen by XPS for 1% Ru-Pd/$TiO_2$ ($M_{Im}$) (Fig. 5.7 and Table 5.3). These observations provide some insight into the observed improved performance that is found for the 1% Ru-Pd/$TiO_2$ ($M_{Im}$) catalyst. The lack of sintering of Ru is suggested to be the result of a stabilization effect[27, 57] in which the presence of Pd species on the surface dilutes and isolates the active Ru sites; at the same time, the catalyst can maintain its excellent selectivity, as the weakened interaction between support and metal effectively 'switches-off' any consecutive hydrogenation reactions.

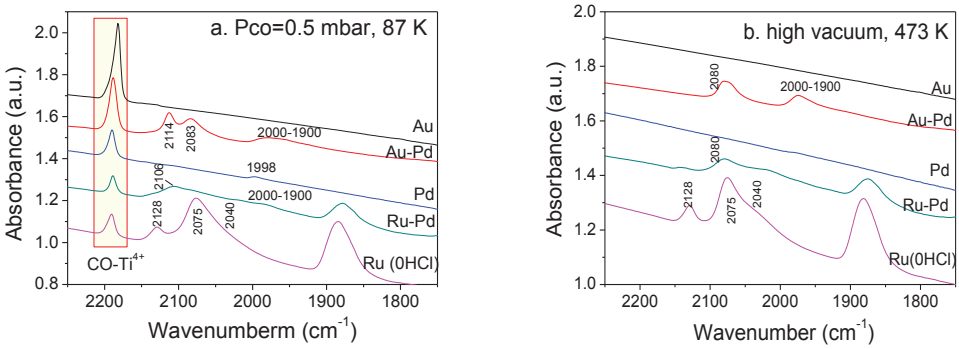


Figure 5.11. FT-IR spectra of CO adsorption on $M_{Im}$ catalysts at indicated temperature and pressure: (a) at 87 K and $p_{co}$ = 0.5 mbar and (b) at 473 K and $p_{co} \approx 10^{-6}$ mbar.

Finally, the CO adsorption data could be fitted with a Temkin-Pyzhev isotherm (Appendix C, Fig. S7), which allowed for a semi-quantitative correlation between CO adsorption and catalytic activity. Assuming similar extinction coefficients for the linearly adsorbed CO species detected in the 2100-2000 $cm^{-1}$ region on the various materials, the amount of linearly adsorbed CO obtained from the IR experimental data was found to be correlated with the activity of the catalysts at low temperature (Fig. 5.11b).

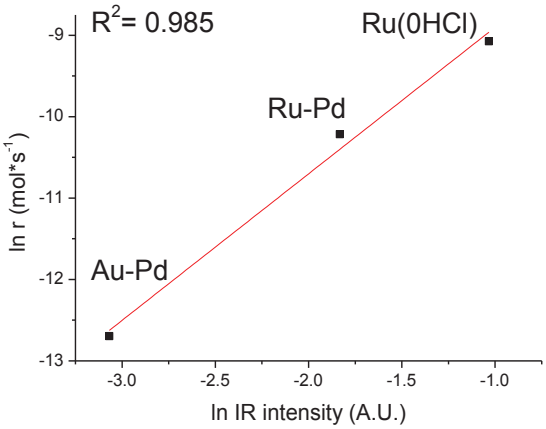


Figure 5.12. Plot of the natural logarithm of reaction rate versus intensity of adsorbed linear CO peak for different catalysts at 473 K, the reaction temperature for the LA to GVL conversion.

Furthermore, the initial rate of LA to GVL transformation seems to correlate with the amount of CO that is linearly adsorbed at the reaction temperature (Fig. 5.11b-5.12). Interestingly, Cao et al. recently reported that a small amount of CO (ca. 1000 ppm) already had a significant, negative effect on LA hydrogenation over supported platinum-group metals suggesting that the active sites for both CO adsorption and LA to GVL hydrogenation are indeed related.[72] Consequently, CO adsorption can be used to semi-quantitatively predict a catalyst's activity for the hydrogenation of LA to GVL.

### 5.4 Conclusions

$TiO_2$-supported bimetallic Au-Pd and Ru-Pd catalysts, synthesized by a modified impregnation ($M_{Im}$) method, were shown to be highly active in the hydrogenation of levulinic acid to γ–valerolactone. Extensive characterization by STEM, XAFS, XPS and FT-IR after CO adsorption showed these catalysts to consist of well-dispersed Au-Pd or Ru-Pd nano-alloys on $TiO_2$. Alloying was found to have two distinct effects. First, an electronic effect is seen for 1% Au-Pd/$TiO_2$, with catalytic activity resulting from the modification of the electronic properties of Pd upon alloying, as evidenced by XPS and FT-IR after CO adsorption. Alloying two relatively inactive metals thus leads to a

remarkable increase in the catalytic activity for LA to GVL. Second, a stabilization effect is seen for 1% Ru-Pd/$TiO_2$, with Pd (oxide) species diluting and isolating the active Ru sites, resulting in excellent selectivity to GVL by switching-off consecutive hydrogenation reactions. Both the Ru-Pd and Au-Pd nano-alloy catalysts actually show very good stability with limited sintering, and little leaching of active metals or surface area drop even after three consecutive catalytic runs. In addition, a variation in the synthesis method of the benchmark monometallic 1% Ru/$TiO_2$ catalyst actually led to the discovery of a catalyst with an exceptionally high activity (51.7 $mol_{GVL}\, g^{-1}{}_{metal}\, h^{-1}$ and TOF = 1.946 $s^{-1}$). These findings open up new possibilities for the application of bimetallic catalysts, synthesized using carefully designed strategies, in bio-based fuel and chemicals production.

**Acknowledgements**

Cor van de Spek (Utrecht University), Dr. Jinbao Gao (Utrecht University) and M. W. G. M. (Tiny) Verhoeven (Eindhoven University of Technology) are acknowledged for the TEM, $N_2$ physisorption, and XPS measurements, respectively.

## References


[1] C.O. Tuck, E. Pérez, I.T. Horváth, R.A. Sheldon, and M. Poliakoff, Science 337 (2012) 695-699.

[2] M. Poliakoff, and P. Licence, Nature 450 (2007) 810-812.

[3] G.W. Huber, S. Iborra, and A. Corma, Chem. Rev. 106 (2006) 4044-4098.

[4] P.C.A. Bruijnincx, and B.M. Weckhuysen, Angew. Chem. Int. Ed. 52 (2013) 11980-11987.

[5] J.J. Bozell, and G.R. Petersen, Green Chem. 12 (2010) 539-554.

[6] J.J. Bozell, L. Moens, D.C. Elliott, Y. Wang, G.G. Neuenscwander, S.W. Fitzpatrick, R.J. Bilski, and J.L. Jarnefeld, Resour. Conserv. Recycl. 28 (2000) 227-239.

[7] D.W. Rackemann, and W.O.S. Doherty, Biofuels, Bioprod. Biorefin. 5 (2011) 198-214.

[8] B. Girisuta, L.P.B.M. Janssen, and H.J. Heeres, Ind. Eng. Chem. Res. 46 (2007) 1696-1708.

[9] V. Pace, P. Hoyos, L. Castoldi, P. Domínguez de María, and A.R. Alcántara, ChemSusChem 5 (2012) 1369-1379.

[10] J.Q. Bond, D.M. Alonso, D. Wang, R.M. West, and J.A. Dumesic, Science 327 (2010) 1110-1114.

[11] J.-P. Lange, R. Price, P.M. Ayoub, J. Louis, L. Petrus, L. Clarke, and H. Gosselink, Angew. Chem. Int. Ed. 49 (2010) 4479-4483.

[12] J.C. Serrano-Ruiz, D. Wang, and J.A. Dumesic, Green Chem. 12 (2010) 574-577.

[13] D.M. Alonso, S.G. Wettstein, and J.A. Dumesic, Green Chem. 15 (2013) 584-595.

[14] W.R.H. Wright, and R. Palkovits, ChemSusChem 5 (2012) 1657-1667.

[15] L.E. Manzer, App. Catal. A: Gen. 272 (2004) 249-256.

[16] M.G. Al-Shaal, W.R.H. Wright, and R. Palkovits, Green Chem. 14 (2012) 1260-1263.

[17] A. Primo, P. Concepcion, and A. Corma, Chem. Commun. 47 (2011) 3613-3615.

[18] W. Luo, U. Deka, A.M. Beale, E.R.H. van Eck, P.C.A. Bruijnincx, and B.M. Weckhuysen, J. Catal. 301 (2013) 175-186.

[19] D.I. Enache, J.K. Edwards, P. Landon, B. Solsona-Espriu, A.F. Carley, A.A. Herzing, M. Watanabe, C.J. Kiely, D.W. Knight, and G.J. Hutchings, Science 311 (2006) 362-365.

[20] X. Peng, Q. Pan, and G.L. Rempel, Chem. Soc. Rev. 37 (2008) 1619-1628.

[21] S. Hermans, R. Raja, J.M. Thomas, B.F.G. Johnson, G. Sankar, and D. Gleeson, Angew. Chem. Int. Ed. 40 (2001) 1211-1215.

[22] M. Ichikawa, L. Rao, T. Ito, and A. Fukuoka, Faraday Discuss. Chem. Soc. 87 (1989) 321-336.

[23] A.M. Ruppert, K. Weinberg, and R. Palkovits, Angew. Chem. Int. Ed. 51 (2012) 2564-2601.

[24] J.M. Parera, and J.N. Beltramini, J. Catal. 112 (1988) 357-365.

[25] Z. Wei, J. Sun, Y. Li, A.K. Datye, and Y. Wang, Chem. Soc. Rev. 41 (2012) 7994-8008.

[26] J. Araña, P. Ramirez de la Piscina, J. Llorca, J. Sales, N. Homs, and J.L.G. Fierro, Chem. Mater. 10 (1998) 1333-1342.

[27] D.M. Alonso, S.G. Wettstein, and J.A. Dumesic, Chem. Soc. Rev. 41 (2012) 8075-8098.

[28] M. Sankar, N. Dimitratos, P.J. Miedziak, P.P. Wells, C.J. Kiely, and G.J. Hutchings, Chem. Soc. Rev. 41 (2012) 8099-8139.

[29] D.J. Braden, C.A. Henao, J. Heltzel, C.C. Maravelias, and J.A. Dumesic, Green Chem. 13 (2011) 1755-1765.

[30] S.G. Wettstein, J.Q. Bond, D.M. Alonso, H.N. Pham, A.K. Datye, and J.A. Dumesic, Appl. Catal. B: Environ. 117–118 (2012) 321-329.

[31] P. Paalanen, B.M. Weckhuysen, and M. Sankar, Catal. Sci. Tech. 3 (2013) 2869-2880.

[32] M. Sankar, Q. He, M. Morad, J. Pritchard, S.J. Freakley, J.K. Edwards, S.H. Taylor, D.J. Morgan, A.F. Carley, D.W. Knight, C.J. Kiely, and G.J. Hutchings, ACS Nano 6 (2012) 6600-6613.

[33] M. Morad, M. Sankar, E. Cao, E. Nowicka, T.E. Davies, P.J. Miedziak, D.J. Morgan, D.W. Knight, D. Bethell, A. Gavriilidis, and G.J. Hutchings, Catal. Sci. Tech. 4 (2014) 3120-3128.

[34] S. Nikitenko, A.M. Beale, A.M.J. van der Eerden, S.D.M. Jacques, O. Leynaud, M.G. O'Brien, D. Detollenaere, R. Kaptein, B.M. Weckhuysen, and W. Bras, J. Synchrotron Rad. 15 (2008) 632-640.

[35] M. Newville, J. Synchrotron Rad. 8 (2001) 322-324.

[36] B. Ravel, and M. Newville, J. Synchrotron Rad. 12 (2005) 537-541.

[37] F. Gao, and D.W. Goodman, Chem. Soc. Rev. 41 (2012) 8009-8020.

[38] R.N. Dhital, C. Kamonsatikul, E. Somsook, K. Bobuatong, M. Ehara, S. Karanjit, and H. Sakurai, J. Am. Chem. Soc. 134 (2012) 20250-20253.

[39] A.G. McKale, B.W. Veal, A.P. Paulikas, S.K. Chan, and G.S. Knapp, Phys. Rev. B 38 (1988) 10919-10921.

[40] A.M. Beale, and B.M. Weckhuysen, Phys. Chem. Chem. Phys. 12 (2010) 5562-5574.

[41] Y.-S. Su, M.-Y. Lee, and S. Lin, Catal. Lett. 57 (1999) 49-53.

[42] A. Zwijnenburg, A. Goossens, W.G. Sloof, M.W.J. Crajé, A.M. van der Kraan, L. Jos de Jongh, M. Makkee, and J.A. Moulijn, J. Phys. Chem. B 106 (2002) 9853-9862.

[43] B. Schumacher, V. Plzak, M. Kinne, and R.J. Behm, Catal. Lett. 89 (2003) 109-114.

[44] D. Horváth, L. Toth, and L. Guczi, Catal. Lett. 67 (2000) 117-128.

[45] C.W. Yi, K. Luo, T. Wei, and D.W. Goodman, J. Phys. Chem. B 109 (2005) 18535-18540.

[46] F. Liu, D. Wechsler, and P. Zhang, Chem. Phys. Lett. 461 (2008) 254-259.

[47] H. Zhang, T. Watanabe, M. Okumura, M. Haruta, and N. Toshima, J. Catal. 305 (2013) 7-18.

[48] L. Delannoy, S. Giorgio, J.G. Mattei, C.R. Henry, N. El Kolli, C. Méthivier, and C. Louis, ChemCatChem 5 (2013) 2707-2716.

[49] K. Qian, and W. Huang, Catal. Today 164 (2011) 320-324.

[50] W.-J. Shen, M. Okumura, Y. Matsumura, and M. Haruta, Appl. Catal. A: Gen. 213 (2001) 225-232.

[51] C. Elmasides, D.I. Kondarides, W. Grünert, and X.E. Verykios, J. Phys. Chem. B 103 (1999) 5227-5239.

[52] K.I. Hadjiivanov, and G.N. Vayssilov, Adv. Catal., Academic Press. 307-511.

[53] W.K. Kuhn, J. Szanyi, and D.W. Goodman, Surf. Sci. 274 (1992) L611-L618.

[54] F. Boccuzzi, A. Chiorino, S. Tsubota, and M. Haruta, J. Phys. Chem. 100 (1996) 3625-3631.

[55] F. Gao, Y. Wang, and D.W. Goodman, J. Am. Chem. Soc. 131 (2009) 5734-5735.

[56] N.E. Kolli, L. Delannoy, and C. Louis, J. Catal. 297 (2013) 79-92.

[57] M. Chen, D. Kumar, C.-W. Yi, and D.W. Goodman, Science 310 (2005) 291-293.

[58] T. Wei, J. Wang, and D.W. Goodman, J. Phys. Chem. C 111 (2007) 8781-8788.

[59] D.C. Meier, V. Bukhtiyarov, and D.W. Goodman, J. Phys. Chem. B 107 (2003) 12668-12671.

[60] Chen, Y. Cai, Z. Yan, and D.W. Goodman, J. Am. Chem. Soc. 128 (2006) 6341-6346.
[61] P. Gelin, A.R. Siedle, and J.T. Yates, J. Phys. Chem. 88 (1984) 2978-2985.
[62] F. Tao, Chem. Soc. Rev. 41 (2012) 7977-7979.
[63] J.L. Robbins, J. Catal. 115 (1989) 120-131.
[64] G.H. Yokomizo, C. Louis, and A.T. Bell, J. Catal. 120 (1989) 1-14.
[65] E. Guglielminotti, and G.C. Bond, J. Chem. Soc. Faraday Trans. 86 (1990) 979-987.
[66] K. Hadjiivanov, J.C. Lavalley, J. Lamotte, F. Maugé, J. Saint-Just, and M. Che, J. Catal. 176 (1998) 415-425.
[67] T. Lopez, P. Bosch, M. Asomoza, and R. Gomez, J. Catal. 133 (1992) 247-259.
[68] N.M. Gupta, V.S. Kamble, R.M. Iyer, K.R. Thampi, and M. Gratzel, J. Catal. 137 (1992) 473-486.
[69] C. Elmasides, D.I. Kondarides, S.G. Neophytides, and X.E. Verykios, in: F.V.M.S. Mendioroz, A. Corma, and G.F. José Luis, (Eds.), Stud. Surf. Sci. Catal., Elsevier. 3083-3088.
[70] D. Tessier, A. Rakai, and F. Bozon-Verduraz, J. Chem. Soc. Faraday Trans. 88 (1992) 741-749.
[71] Y. Li, B. Xu, Y. Fan, N. Feng, A. Qiu, J.M.J. He, H. Yang, and Y. Chen, J. Mol. Catal. A: Chem. 216 (2004) 107-114.
[72] X.-L. Du, L. He, S. Zhao, Y.-M. Liu, Y. Cao, H.-Y. He, and K.-N. Fan, Angew. Chem. Int. Ed. 50 (2011) 7815-7819.

# Chapter 6

# Summary, Concluding Remarks and Future Perspectives

## 6.1 Summary

The current production of both fuels and chemicals relies heavily on nonrenewable fossil resources. The finite nature of these resources, combined with the adverse effects on global climate that their use causes, makes this reliance unsustainable. A shift towards a more sustainable society that makes use of renewable resources, such as biomass, is therefore necessary. This realization has provoked many research efforts into this field. In particular, the valorization of lignocellulosic biomass is receiving major attention, given its general abundance and nonedible nature. It is important to note in this respect that the current petrochemical refineries produce not only fuels, but also the platform chemicals from which the large array of chemical end products is eventually produced. To be able to compete economically, so should biorefineries.

Levulinic acid (LA), which can be produced from the sugar fractions of lignocellulosic biomass, has been identified as one such sustainable platform molecule that could play a major role in future biorefineries. A myriad of value-added products can be produced from LA, for instance by a sequence of selective catalytic hydrogenation/deoxygenation reactions (Scheme 6.1). Products that can be obtained by this approach include γ-valerolactone (GVL), methyltetrahydrofuran (MTHF), 1,4-pentanediol (PD), and pentanoic acid (PA). These LA-derived products can be used in numerous fields, including their application as building blocks for polymers, additives, resins, herbicides, and pharmaceuticals or directly as antifreeze agents, solvents, plasticizers, oxygenated fuel additives and liquid biofuels.

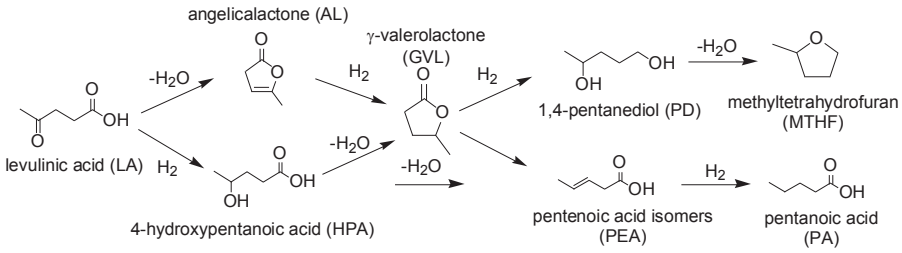


Scheme 6.1. Hydrodeoxygenation of levulinic acid.

The fact that these value-added products are all obtained by similar, consecutive hydrogenation and dehydration reactions, poses a challenge to their production, and puts strict requirements on the selectivity of the catalytic production processes. Furthermore, the stability of the catalyst materials used in these types of reactions is of prime concern, given the acidity of the substrate and the often highly polar, hydrothermal and corrosive conditions under which these conversions typically take place.

The work described in this PhD thesis is aimed at (1) the development of new and improved heterogeneous catalysts for the selective hydrodeoxygenation (HDO) of LA and (2) a better fundamental understanding of the relation between structure of these catalysts and their performance in terms of activity/selectivity in LA HDO reactions. To this extent, the influence of the support and the metal phase of heterogeneous HDO catalysts on activity, selectivity and stability was studied. Catalyst synthesis methodologies were furthermore optimized to improve performance and stability. These efforts were complemented by extensive characterization of the catalyst materials with various techniques, including temperature-programmed desorption of ammonia (TPD-$NH_3$), $N_2$ physisorption, atomic absorption spectrophotometry (AAS), thermal gravimetric analysis (TGA), (scanning) transmission electron microscopy ((S)TEM), X-ray diffraction (XRD), X-ray absorption (XAS) and photoelectron spectroscopy (XPS), Fourier transform-infrared spectroscopy (FT-IR, after pyridine/CO adsorption) and solid state $^{27}Al$ nuclear magnetic resonance ($^{27}Al$ NMR), to be able to relate structure with performance.

The large influence of the nature of the support, in particular its acidity, of four Ru catalysts on the catalytic performance in the hydrogenation of LA is described in **Chapter 2**. The supported 1wt% Ru catalysts ($Ru/TiO_2$, $Ru/Nb_2O_5$, Ru/H-ZSM5, Ru/H-β) were prepared by wet impregnation and tested in a batch reactor under conditions of varying severity. The non-acidic catalysts (i.e., $Ru/TiO_2$ and $Ru/Nb_2O_5$) selectively gave GVL as the main and final product, while the zeolite-supported acidic catalysts (i.e., Ru/H-ZSM5 and Ru/H-β) proved capable of the direct conversion of LA into PA under relatively mild conditions in dioxane. The strongly acidic sites on the support accelerate the LA-to-GVL conversion and are essential for the subsequent, most difficult step in the

reaction sequence, i.e. the ring-opening of GVL to PEA. PA could also be obtained under more severe conditions, using 2-ethylhexanoic acid (2-EHA) or neat LA as the solvent, but yields dropped as a result of gradual deactivation of the zeolite-supported catalysts. The neat reactions and the reactions in 2-EHA, a non-reactive mimic of LA of similar acidity, were performed to assess catalyst stability under these very demanding conditions. Although many factors influence the deactivation of the acid-supported catalysts, pyridine adsorption and solid state $^{27}$Al NMR data show that deactivation could be mainly attributed to loss of acid sites by dealumination, with H-ZSM5 being more resistant to dealumination than H-β (Fig. 6.1). Coke formation is limited, but occurred most on the zeolite-supported catalysts in neat LA. Subtle changes in the XRD patterns actually indicated preferential coke build-up in the zig-zag channels of H-ZSM5 (Fig. 6.1). TGA-MS data furthermore showed that AL is involved as an intermediate in the reaction and that it is a direct precursor for the coke that is deposited, mostly on the acidic catalysts. Further studies on the nature, location and stability of the acid sites in the zeolite-supported catalysts, under the highly polar and corrosive conditions of LA conversion, should allow for improvements to be made in the stability and performance of these first, promising examples of catalysts for the direct conversion of LA to PA. Finally, Ru/$TiO_2$ was shown to be remarkably stable and selective for GVL, even for reactions in neat LA, as very limited coke formation, sintering or leaching of ruthenium was observed.

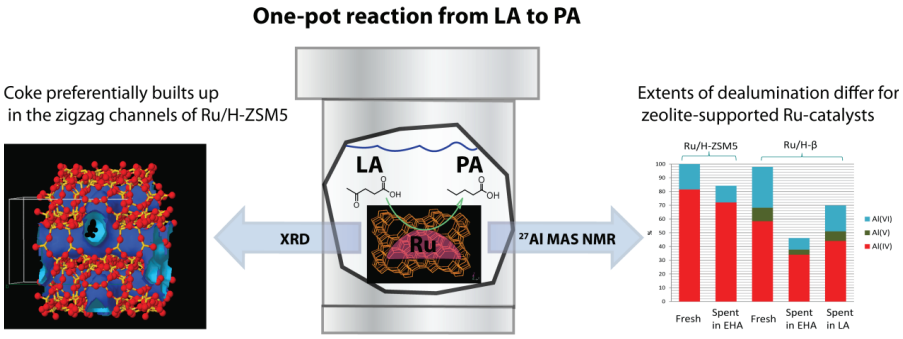


Figure 6.1. Zeolite-supported Ru catalysts provide the first example of the direct conversion of LA to PA. Extensive characterization studies revealed acid-site loss by dealumination to be the cause of gradual deactivation.

**Chapter 3** is concerned with a follow-up study of this process of gradual deactivation by dealumination that was observed for the zeolite-supported Ru catalysts used in the hydrogenation of LA in Chapter 2. A detailed description of the influence of the highly oxygenated reaction medium (2-ethylhexanoic acid (EHA) and neat LA) on dealumination of the zeolite-supported ruthenium catalysts (Ru/H-β and Ru/H-ZSM5), is given, based on both FT-IR and $^{27}$Al MAS NMR studies. Making use of 2D $^{27}$Al triple-quantum magic angle spinning (3QMAS) NMR results, the combined data allowed differentiation between various Al species present in the fresh and spent catalysts, providing more insights into the changes in acid properties (i.e., amount, nature, and location) of the Ru/zeolite catalysts that occur under the applied reaction conditions (Fig. 6.2).

Fitting of the solid-state $^{27}$Al 3QMAS NMR spectra allowed for quantitative changes in aluminum speciation to be determined. Two types of four-coordinated and two types of six-coordinated aluminum species could be discerned for Ru/H-ZSM5, while three four-coordinated aluminum species were observed for Ru/H-β, together with five- and six-coordinated aluminum species. After LA hydrogenation in EHA, a slight increase in disorder is found for Ru/H-ZSM5, which is mainly due to the transition of Brønsted acidic (BAS), symmetric framework aluminum (FAL) into intermediate distorted FAL. A much more severe loss of both FAL (BAS) and Lewis-acidic, extra-framework aluminum species (EFAL, LAS) was observed for the Ru/H-β catalyst after LA hydrogenation in EHA. Interestingly, there was no loss of one particular, four-coordinated aluminum species, labeled as Al(IV)-S, for the Ru/H-β catalyst after LA hydrogenation in NLA, which indicates that this aluminum species is most probably located in the small channels of H-β. H–ZSM5 thus shows higher stability towards dealumination than H-β. The loss of catalytic activity (as seen in the drop of PA yield) for Ru/H-β is attributed to the significant decrease in BAS (~ 40% loss). The sites that are lost were identified as symmetric tetrahedral FAL (Al(IV)-L and Al(IV)-S) species.

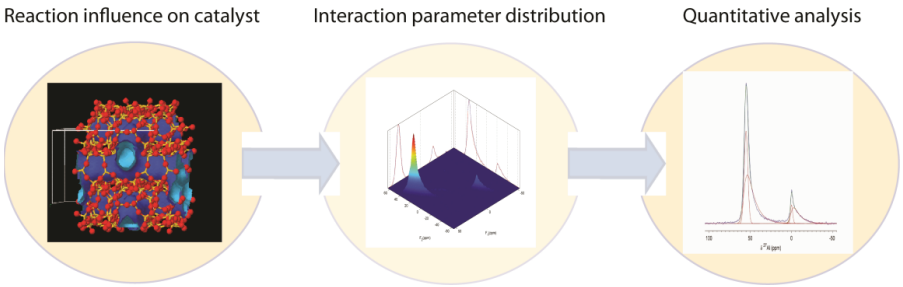


Figure 6.2. Quantitative analysis of changes in aluminum speciation in zeolite-supported ruthenium catalysts after the hydrogenation of levulinic acid.

As shown in Chapter 2, it is possible to directly convert levulinic acid (LA) to pentanoic acid (PA) over 1 wt% Ru/zeolite catalysts at 40 bar $H_2$ and 473 K in dioxane, with the highest yield of 45.8 mol% of PA being obtained with 1 wt% Ru/H-ZSM5. With the aim of developing a more selective LA-to-PA process, **Chapter 4** describes how catalyst performance in the direct, one-pot conversion of LA to PA can be much improved by optimization of the synthesis method of the Ru/H-ZSM5 catalyst. The tested variations in Ru/H-ZSM5 preparation methodology aimed to achieve improved metal dispersion and close proximity of metal and acid sites, in particular.

The influence of the cation form of ZSM5, the ruthenium precursor and the Si/Al ratio of ZSM5 on metal dispersion and acidity were assessed. A bifunctional 1wt% Ru/H-ZSM5 catalyst was developed that showed an improved yield of PA (and its esters) of 91.3% after 10 h of reaction time with an initial PA productivity of 1.157 mol $g_{Ru}^{-1}$ $h^{-1}$, which is the highest number reported thus far for this one-pot conversion directly from LA. The simple preparation method, which makes use of $Ru(NH_3)_6Cl_3$ as ruthenium precursor for the impregnation of $NH_4^+$-ZSM5 (Si/Al= 11.5) and involves direct reduction after drying, improved the dispersion of ruthenium in the Ru/H-ZSM5 catalyst. Indeed, Ru was also found to be located inside the pores of the zeolite, and this preparation method better retained the number and strength of the strong acid sites of the zeolite. The strong acid site density was actually found to be key to the efficient conversion of LA to PA. The resulting close proximity of the hydrogenation metal and the strong acid sites, is also thought to benefit PA production significantly. Deactivation of the Ru/H-ZSM5 catalyst is observed upon reuse of the catalyst; in this case primarily as a result of coke

coverage of the strong acid sites, but PA yields can be recovered by a simple coke burn-off step (Fig. 6.3).

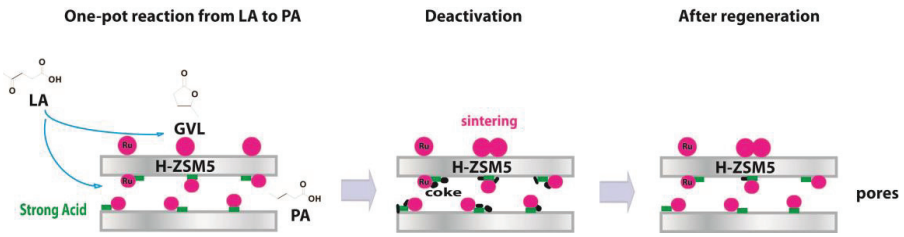


Figure 6.3. Improvements in catalyst synthesis yielded an excellent Ru/H-ZSM5 catalyst for the direct, one-pot reaction from LA to PA. Catalyst deactivation is mainly caused by coke-buildup and activity can be restored by a simple catalyst regeneration step.

**Chapter 5** is concerned with the development of mono- and bimetallic $TiO_2$-supported catalysts for the selective hydrogenation of LA to GVL. Highly active, selective, and stable supported metal catalysts were synthesized by a modified impregnation method ($M_{Im}$). The $M_{Im}$ method involves the use of an excess of chloride anions in the impregnation step, which is essential for efficient alloying of Ru and Pd and Au and Pd, followed by direct reduction in a dilute hydrogen atmosphere. This methodology was shown to be highly beneficial for this catalytic transformation.

The random nano-alloy structure of well-dispersed Au-Pd or Ru-Pd nanoparticles on $TiO_2$ was confirmed by STEM, FT-IR after CO adsorption and XAS analysis (Fig. 6.4). The Au-Pd/$TiO_2$ material showed a remarkably 20-fold increase in catalytic activity (1.97 $mol_{GVL}\ g_{metal}^{-1}\ h^{-1}$) in the hydrogenation of LA compared to similarly prepared monometallic Au and Pd catalysts, which were both almost completely inactive. This marked increase in activity is attributed to a synergistic effect resulting from the electronic modulation of Pd by electron transfer from Pd to Au. While the Ru-Pd/$TiO_2$ (17.2 $mol_{GVL}\ g_{metal}^{-1}\ h^{-1}$) material proved to be only slightly more active than an identically prepared Ru/$TiO_2$ catalyst (16.4 $mol_{GVL}\ g_{metal}^{-1}\ h^{-1}$), in this case alloying was found to greatly improve both the stability and selectivity of the catalyst. The excellent, sustained selectivity to GVL is thought to be the result of the dilution of Ru in Pd in the nano-alloy, thus switching off the consecutive hydrogenation reactions that are observed with the monometallic Ru catalyst. Not only the Ru-Pd catalyst, but also the

Au-Pd nano-alloy showed good stability upon reuse in three consecutive catalytic runs, with similar activities, limited sintering and leaching of the metals or loss in surface area being observed.

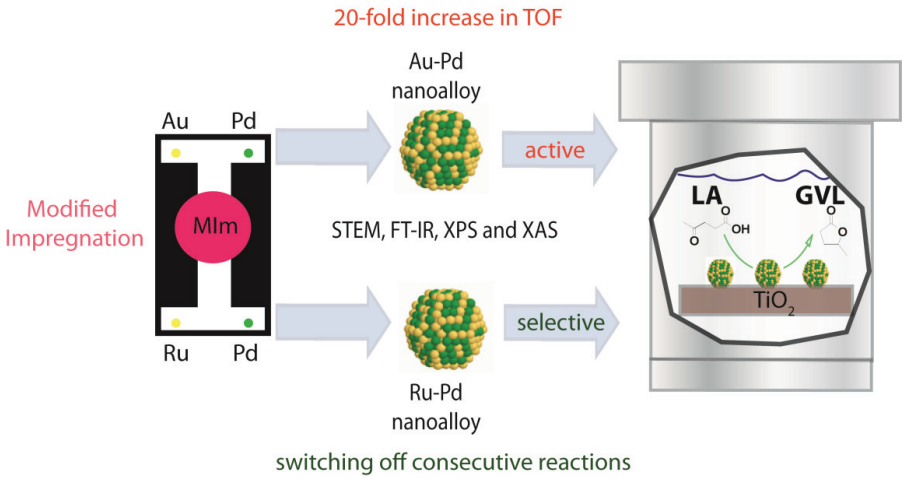


Figure 6.4. Different effects of alloying are observed for Au-Pd and Ru-Pd bimetallic catalysts in the hydrogenation of LA to GVL.

A variation on the modified impregnation synthesis method, i.e. direct reduction, but omission of the excess anions in the impregnation step, actually led to the discovery of an exceptionally active $Ru/TiO_2$ catalyst showing a catalytic productivity of 51.7 $mol_{GVL}\, g_{metal}^{-1}\, h^{-1}$. The greatly improved activity could be attributed to a strong metal-support interaction, caused by electron transfer from Ru to $TiO_2$. Finally, a linear relationship was observed for the three most active catalysts in a plot of natural logarithm of rate against the amount of linearly adsorbed CO measured by FT-IR, which indicates that CO adsorption could be used to quantitatively reflect and predict activity for this LA to GVL reaction.

## 6.2 Concluding Remarks

The results described in this PhD thesis contribute to a better understanding of the various factors influencing catalyst performance in LA hydrodeoxygenation reactions. The support- and solvent-dependent product selectivity, extent and mode of catalyst deactivation, influence of preparation methodology for bifunctional and bimetallic

catalysts on performance, all provide further insight into the relation between structure and activity of these materials.

With regards to the conversion of LA to GVL, it is clear that while the choice of hydrogenation metal is most important, the choice of support also strongly impacts stability and selectivity of the catalysts. Of the tested catalysts, $Ru/TiO_2$ proved to best, combining excellent selectivity with remarkable stability, with very limited coke formation, sintering and leaching of ruthenium being observed. Acidic supports do accelerate the dehydration step involved in lactone formation, but also give rise to coke formation and, as a result, gradual catalyst deactivation. The activity and selectivity of the $Ru/TiO_2$ catalyst could be greatly modified by either a variation in the synthesis method or by careful alloying the metal with a second one. For the monometallic ruthenium catalysts, control over the strength of the metal-support interaction, as well as over particle size proved crucial for activity. Improvements in activity can come at the expense of selectivity. Indeed, as the whole LA hydrodeoxygenation platform consists of similar catalytic steps, a catalyst that is too active, can easily lead to losses in GVL yield as a result of consecutive reactions. Random alloying of ruthenium with palladium, as a result of a modified synthesis method that involves excess anions in the impregnation step and direct reduction afterwards, allowed for better control over activity vs. selectivity, as the presence of the Pd species dilutes and isolates the active Ru sites, thus resulting in a more optimal metal-support interaction, amongst others. Alloying Au and Pd also produced a dramatic effect, with a large increase in activity being observed upon combining these metals, which are themselves almost inactive under the applied conditions. The results show the potential of bimetallic catalysts, be it nano-alloys or not, in the HDO of LA. This topic, which is still largely unexplored for this reaction, warrants further exploration and should not be limited to improvements in GVL productivity, but should also be extended to alloying to improve the stability and resistance against typical biorefinery impurities.

If deeper hydrogenation reactions are targeted, specifically the HDO of LA to PA, the hydrogenation metal needs to be complemented by strong acid sites. As shown in this thesis, bifunctional catalysts in which the support provides the strong acid sites are preferred. It should be noted in this respect that loss of selectivity in the LA-to-GVL

reaction is typically the result of PD or MTHF formation rather than PA production, highlighting the specific requirements of the latter. Indeed, the experiments show that strongly acidic sites are required for the GVL ring-opening step, which is rate limiting under the applied conditions.

Although many factors may influence the deactivation of the acid-supported catalyst materials, dealumination of the support and resulting loss of acid sites was found to be most important. The limited number of zeolite supports tested showed that H-ZSM5 was more resistant to dealumination and coke deposition than H-β, providing clues for further catalyst improvement. The sintering of ruthenium that is observed for this Ru/H-ZSM5 catalyst needs to be addressed, though, to ensure proper reusability or stability with time on stream for this class of catalysts. Here, it was already shown that improved synthesis methods, aimed at optimization of the dispersion of ruthenium, its proximity to the acid sites and, importantly, the retention of strongly acidic sites in the bifunctional catalyst, resulted in greatly improved performance in the LA-to-PA conversion. The combined results thus highlight the specific catalyst requirements for two of the major routes of LA hydrodeoxygenation platform. The issue of severe sintering of ruthenium that was observed in the initial studies is also addressed, at least to a great extent, with the improved synthesis methodology.

### 6.3 Future Perspectives

It is clear from the above that the severe conditions to which catalysts are subjected in LA conversion processes, i.e. the typically highly polar, hydrothermal and corrosive conditions, pose significant challenges to the development of stable and economical catalysts. The many studies reported on the hydrodeoxygenation LA (mainly to GVL) are almost unanimous in the observation that supported noble-metal catalysts, in particular Ru and Pt, typically perform best. Given the high costs associated with the use of such metals, long-term operational catalyst stability is, of course, essential and more extensive studies are required with a focus on the stability of both support and metal phase. The results presented in this PhD thesis on the stability of $Ru/TiO_2$ catalysts for the conversion of LA to GVL show promise and warrant further investigation. The use of other promising supports, such as $ZrO_2$ and $CeO_2$, for which stability has already been

demonstrated under similar conditions, and improved synthesis methods for well-defined and optimally anchored metal nanoparticles can lead to further improvements in catalyst stability. Indeed, further examination is required to rationalize the influence of metal-support interactions on catalyst performance. It should also be noted that while most studies agree on favorable metal-support combinations, most of the tested catalysts are actually commercial ones. As a result, there is still a lot of room for studies aimed at understanding how chosen synthesis parameters affect eventual catalyst performance in LA HDO reactions.

Alternatively, less expensive, alternate metals can be explored for LA HDO reactions to reduced catalyst costs. Replacing the noble-metal based catalysts with non-noble ones, first row transition metals capable of doing the HDO reactions, for instance, comes with great challenges not only with regards to maintaining a sufficient level of catalyst productivity, but in particular with regards to stability. Indeed, stability against leaching and contamination of the product stream as a result of this, is of concern here.

The results reported also show that the performance of the monometallic noble metal catalysts can be much improved by alloying. The very limited number of studies on bi- or multimetallic catalysts for LA HDO shows that there is still much room for exploration in this direction and different combinations of various metals need to be tested. The use of alloys comes with an additional challenge in terms of the catalyst characterization effort that is required and preferably should be complemented in the future with information on (changes in) the composition of the alloy under reaction conditions, as obtained with in-situ characterization techniques. Such operando spectroscopy studies would also provide more insight into the various modes of deactivation. Support deactivation, be it by coke deposition, acid site loss, or loss of structural integrity, is also a major concern for the bifunctional catalysts that are required for one-pot, direct deeper HDO of LA. The improvements in catalyst preparation presented here have already allowed us to, at least partially, overcome these drawbacks. Still, novel acidic materials that show improved stability under the severe conditions are required, in addition to the already previously noted need for systematic comparison of preparation methodologies. In addition, the development of

bi-/multi-metallic system combined with an acid function can also be very interesting for the future studies.

Research efforts focused at the points made above will provide insight into what is required of a catalyst in terms of the nature and stability of the metal and support phases for the different LA HDO reactions. It should be kept in mind, however, that the LA to be converted will eventually originate from a real process, involving lignocellulosic pretreatment, component separation and hydrolysis steps and, as a result, will contain various impurities that can also greatly influence catalyst performance. Formic acid, formed in stoichiometric amounts if C6-sugars are converted to LA, and traces of the mineral acids used for the dehydration process, e.g. sulfuric acid, can lead to catalyst deactivation, for instance. It has already been shown that sulfuric acid had a detrimental effect on the Ru/C-catalyzed conversion of LA to GVL, as strong catalyst deactivation was observed. Interestingly, this could be partially averted by the addition with Re (albeit at the expense of activity compared to the original Ru/C catalyst), again pointing at the potential that multimetallic catalysts have. Various approaches can be followed to deal with these impurities. One can, for instance, focus on efficient separation, for instance by converting LA to more hydrophobic esters, facilitating their removal from the aqueous, acidic reaction mixture and further limiting the spill over of mineral acid to the organic phase. Catalyst studies would have to focus on the conversion of these esters rather than the free acid. Alternatively, catalyst formulation can be adapted in such a way that resistance against these impurities is introduced. The latter strategy has so far only been limitedly studied, but any solutions found to this issue could have a large impact, as many related catalytic biomass conversion processes face the same challenge.

Further studies are therefore required to design and develop better catalysts for the conversion of platform molecules, such as LA, to value-added chemicals and fuel components, as economically viable routes are essential for the successful implementation of biorefineries and ultimately the transition to a more sustainable society.

# Nederlandse Samenvatting

Fossiele brandstoffen zijn momenteel de belangrijkste bron voor de productie van zowel brandstoffen als chemicaliën. Het feit dat deze bronnen eindig zijn, gecombineerd met de negatieve effecten die het verbruik van deze materialen hebben op het klimaat, maken het gebruik ervan onhoudbaar voor de toekomst. Daarom is het belangrijk dat er wordt overgeschakeld op duurzamere energiebronnen, zoals biomassa. Er wordt daarom volop onderzoek gedaan naar de efficiënte omzetting van biomassa naar waardevolle eindproducten. Een belangrijk voorbeeld hiervan is de valorisatie van lignocellulosische biomassa, omdat dit soort biomassa alom aanwezig is en niet als voedselbron gebruikt wordt. Het is belangrijk om hierbij op te merken dat de huidige petrochemische installaties naast brandstoffen ook bulkchemicaliën produceren die vervolgens als bouwstenen dienen voor het brede scala aan chemicaliën en materialen dat uiteindelijk wordt geproduceerd. Om commercieel aantrekkelijk te zijn zullen de bioraffinaderijen van de toekomst dit ook moeten doen.

Levulinezuur (LA) kan worden geproduceerd uit de suikerfracties van lignocellulose en het is de verwachting dat deze duurzame chemische bouwsteen een belangrijke rol kan gaan spelen in deze toekomstige bioraffinaderijen. Verschillende producten met toegevoegde waarde kunnen geproduceerd worden van LA na een reeks van selectieve, katalytische hydrogenatie- en deoxygenatiestappen (Schema 1). Op deze manier kunnen verschillende producten zoals γ-valerolacton (GVL), methyltetrahydrofuraan (MTHF), 1,4-pentaandiol (PD) en pentaanzuur (PA) worden verkregen. Deze LA-derivaten kunnen gebruikt worden voor verschillende doeleinden; ze kunnen dienen als chemische bouwsteen voor polymeren, additieven, harsen, onkruidverdelgers en medicijnen, of direct gebruikt worden als antivries, oplosmiddelen, weekmakers, brandstofadditieven of vloeibare biobrandstoffen.

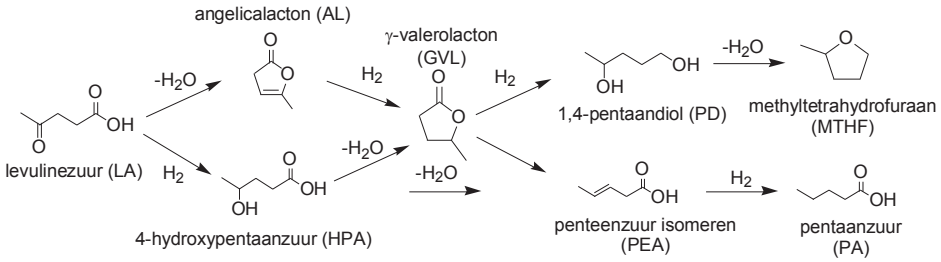


Schema 1. Hydrodeoxygenatie van levulinezuur.

Omdat al deze producten worden verkregen door opvolgende hydrogenatie- en dehydratiestappen die plaats vinden bij ongeveer dezelfde condities, is het een grote uitdaging deze verschillende producten te verkrijgen met een hoge selectiviteit. Verder is de stabiliteit van de katalysatoren die gebruikt worden voor dit type reacties een punt van zorg, gezien de zuurgraad van het substraat en de vaak zeer polaire, hydrothermale en corrosieve condities waarbij deze reacties plaatsvinden.

Het onderzoek beschreven in deze PhD thesis is gericht op (1) de ontwikkeling van nieuwe en verbeterde heterogene katalysatoren voor de selectieve hydrodeoxygenatie (HDO) van LA en (2) het verkrijgen van een beter begrip van de relatie tussen de structuur en de katalytische activiteit en selectiviteit van deze materialen. Hiertoe is de invloed bestudeerd van het dragermateriaal en het metaal van de gedragen metaalkatalysatoren die gebruikt zijn voor de HDO reacties op katalysatoractiviteit, -selectiviteit en -stabiliteit. Ook is de bereidingswijze van de katalysatoren geoptimaliseerd om de stabiliteit en de prestaties van het katalysatormateriaal te verhogen. Dit werk werd gecomplementeerd door een uitgebreide karakterisatie van de materialen met verschillende technieken, zoals temperatuur-geprogrammeerde ammoniak desorptie ($NH_3$-TPD), stikstoffysisorptie, atomaire absorptiespectrometrie (AAS), thermogravimetrische analyse (TGA), (raster) transmissie-elektronenmicroscopie ((S)TEM), Röntgendiffractie (XRD), Röntgenstraling absorptie (XAS) en foto-elektron spectroscopie (XPS), Fourier transform infraroodspectroscopie (FT-IR, na pyridine en CO adsorptie) en vaste-stof $^{27}$Al nucleaire magnetische resonantie ($^{27}$Al NMR), met het doel om de structuur van de katalysatormaterialen te kunnen relateren aan de katalytische eigenschappen.

De grote invloed van de eigenschappen van het dragermateriaal, in het bijzonder de zuurheid van de drager, van vier verschillende Ru katalysatoren op de katalytische eigenschappen tijdens de hydrogenatie van LA is beschreven in **Hoofdstuk 2**. De 1 gewichtsprocent (wt%) Ru katalysatoren ($Ru/TiO_2$, $Ru/Nb_2O_5$, Ru/H-ZSM5, Ru/H-β) werden bereid door middel van een natte impregnatiemethode en werden getest in een batchreactor onder verschillende condities. De katalysatoren met de niet-zure dragers ($Ru/TiO_2$ en $Ru/Nb_2O_5$) produceerden selectief GVL als eindproduct, terwijl de zure katalysatoren (Ru/H-ZSM5 en Ru/H-β) de directe omzetting van LA tot PA mogelijk maakten onder relatief milde condities. Sterke zure sites op de drager versnellen niet alleen de omzetting van LA tot GVL, maar zijn ook essentieel voor de moeilijkste stap in de reactie: het openen van de lactonring in GVL tot PEA. PA kan ook verkregen worden onder meer extreme reactiecondities, door 2-ethylhexaanzuur (2-EHA) of zuiver LA als oplosmiddel te gebruiken. De opbrengst nam echter af over de tijd in deze oplosmiddelen omdat de katalysator langzaam deactiveerde onder deze condities. Reacties in zuiver LA en 2-EHA, een niet-reactief molecuul dat qua zuurgraad sterk lijkt op LA, werden gedaan om de stabiliteit van de katalysator te bestuderen onder de zware condities van de reactie. Hoewel veel factoren bijdragen aan de deactivatie van de zure dragers, hebben pyridine adsorptie en vaste stof $^{27}Al$ NMR laten zien dat het verlies van de zure sites in het katalysatormateriaal de belangrijkste oorzaak is. De zeoliet H-ZSM5 vertoonde minder dealuminatie dan H-β (Figuur 1). Verder was de vorming van koolstofrijke afzettingen op de katalysatoren over het algemeen beperkt. Dit gebeurde het meest tijdens de reacties met de zeoliet-gedragen Ru katalysatoren in zuiver LA. Subtiele veranderingen in het Röntgendiffractiepatroon van de gebruikte katalysator lieten zien dat deze afzettingen bij voorkeur vormden in de zig-zagkanalen van H-ZSM5 (Figuur 1). Uit TGA metingen bleek verder dat AL niet alleen als intermediair betrokken is in de reactie, maar dat dit molecuul ook direct betrokken is bij de vorming van de koolstofrijke afzettingen op de katalysator. Verdere studies naar de aard, locatie en stabiliteit van de zure sites in de zeolietdragers onder de zeer polaire en corrosieve condities van LA-conversie, kunnen leiden tot verbeteringen in de stabiliteit en prestaties van deze eerste, veelbelovende voorbeelden van katalysatoren voor de directe conversie van LA tot PA. Tenslotte bleek $Ru/TiO_2$ opmerkelijk stabiel en selectief te zijn voor GVL, zelfs tijdens reacties in zuiver LA; de waargenomen stabiliteit is te

danken aan een zeer beperkte afzetting van koolstof op het materiaal en het feit dat het metaal niet sinterde of oploste in het reactiemengsel.

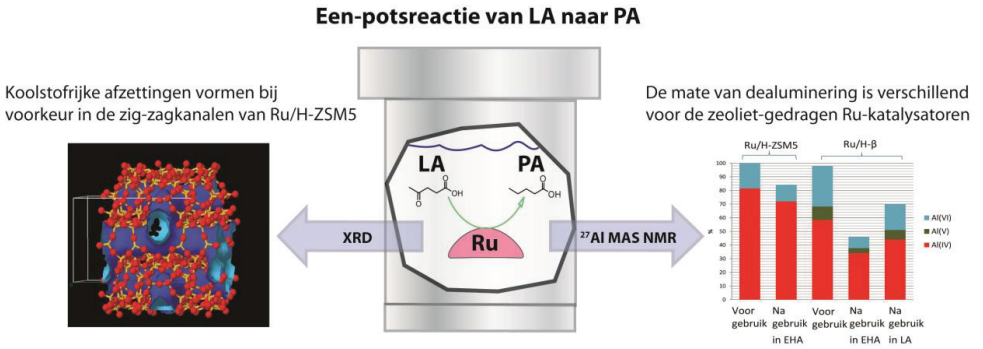


Figuur 1. Zeoliet-gedragen Ru katalysatoren leveren het eerste voorbeeld van de directe conversie van LA naar PA. Uitgebreide karakterisatiestudies toonden aan dat het verlies van zure sites door dealuminatie de oorzaak is van de geleidelijke deactivatie van de katalysatormaterialen.

In **Hoofdstuk 3** wordt de deactivatie van Ru katalysatoren door dealuminatie van de zeolietdragers, zoals beschreven in Hoofdstuk 2, verder onderzocht. Veranderingen in de aard en hoeveelheid van verschillende aluminiumdeeltjes tussen de verse en gedeactiveerde katalysator zijn bestudeerd met FT-IR na pyridine adsorptie en $^{27}$Al MAS NMR (Figuur 2). Met behulp van 2D $^{27}$Al triple-quantum magic angle spinning (3QMAS) NMR, konden de verschillende Al species aanwezig in de verse en gedeactiveerde katalysator worden geïdentificeerd en verschillen gekwantificeerd. Deze informatie verschaft inzicht in veranderingen in de zuurheid van het dragermateriaal (zoals de hoeveelheid, chemische samenstelling en locatie van de zure sites) van de Ru/zeoliet katalysatoren onder reactiecondities.

Op basis van de vaste-stof $^{27}$Al 3QMAS NMR spectra konden de veranderingen in aluminium samenstelling kwantitatief worden geanalyseerd. Zo konden twee verschillende viervoudig- en twee zesvoudig-gecoördineerd aluminium worden onderscheiden voor Ru/H-ZSM5, terwijl Ru/H-β uit drie soorten viervoudig gecoördineerd aluminium bestond, naast vijf- en zesvoudig gecoördineerde Al deeltjes. Na hydrogenering in LA, bleek een beperkt aantal van de Brønsted-zure, symmetrische aluminium deeltjes in het kristalrooster te zijn omgezet in deeltjes met een lagere

symmetrie. Ru/H-β vertoonde veel sterkere veranderingen in de aard en het aantal van de verschillende aluminiumdeeltjes. Een relatief groot aantal van de Brønsted-zure aluminiumdeeltjes die zich oorspronkelijk in het kristalrooster bevonden, werden onttrokken aan het rooster en daarbij omgezet in Lewiszure Al deeltjes tijdens de hydrogeneringsreactie in EHA. Het is daarbij opmerkelijk dat een specifiek type vier-gecoördineerd Al, aangegeven als Al(IV)-S, niet veranderde tijdens de reactie, iets wat erop wijst dat dit type Al zich in de kleine poriën van H-β bevindt. Een belangrijke conclusie van dit werk is dus dat H-ZSM5 een grotere stabiliteit vertoont met betrekking tot aluminiumverlies dan H-β. De lagere katalytische activiteit van Ru/H-β wordt toegewezen aan het significante verlies (~40%) van de Brønsted-zure sites.

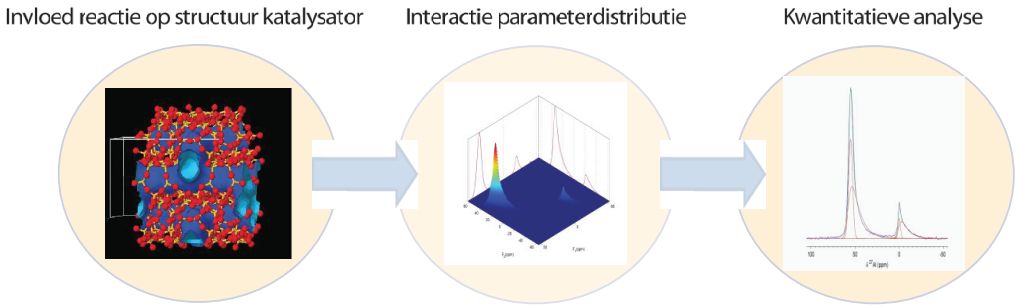


Figuur 2. Kwantitatieve analyse van de verscheidenheid en veranderingen in Al deeltjes in de zeoliet-gedragen Ru katalysatoren voor de hydrogenatie LA.

Zoals beschreven in Hoofdstuk 2 is het mogelijk om levulinezuur direct om te zetten naar pentaanzuur met behulp van een 1 wt% Ru/zeoliet katalysator bij 40 bar $H_2$ en 473 K in dioxaan. De hoogste opbrengst onder deze condities van 45.8 mol% PA werd behaald met de 1wt% Ru/H-ZSM5 katalysator. Met als doel een meer selectief LA-naar-PA proces te ontwikkelen, beschrijft **Hoofdstuk 4** hoe de katalysatorproductiviteit voor deze reactie verbeterd kan worden door de synthesemethode van de Ru/H-ZSM5 katalysator te optimaliseren. De geteste variaties in de synthese van Ru/H-ZSM5 hadden als specifiek doel de metaaldispersie en de nabijheid van metaal- en zure sites te optimaliseren (Figuur 3).

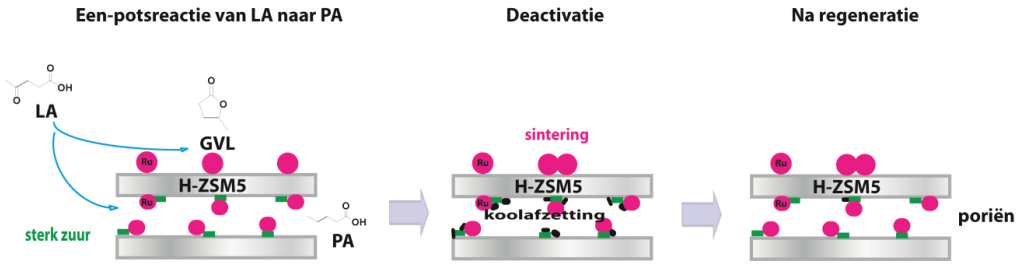


Figuur 3. Verbeteringen in de katalysatorsynthese hebben geleid tot een uitstekende Ru/H-ZSM5 katalysator voor de directe één-potsreactie van LA naar PA. Katalysatordeactivatie wordt voornamelijk veroorzaakt door afzetting van koolstofrijke verbindingen en de activiteit van de katalysator kan hersteld worden door een eenvoudige regeneratiestap.

De invloed van het type kation in ZSM5, de rutheniumprecursor, alsook de Si/Al ratio van ZSM5 op de metaaldispersie en de zuurheid van het materiaal werden onderzocht. Optimalisering van de synthese van de 1wt% Ru/H-ZSM5 katalysator resulteerde in een sterk verbeterde opbrengst van PA (en de bijbehorende esters) van 91.3% na 10 uur reactietijd met een initiële PA productiviteit van 1.157 mol $g_{Ru}^{-1}$ $h^{-1}$; dit is op moment van schrijven de hoogst gerapporteerde productiviteit voor deze één-pots conversie vanuit LA. De eenvoudige bereidingsmethode, die gebruik maakt van de rutheniumprecursor $Ru(NH_3)_6Cl_3$ voor de impregnatie van $NH_4^+$-ZSM5 (Si/Al = 11.5) en die verder bestaat uit een directe reductiestap na drogen van het materiaal na de impregnatie, verbeterde de dispersie van ruthenium in de Ru/H-ZSM5 katalysator. Ruthenium werd inderdaad aangetroffen in de poriën van de zeoliet en deze bereidingswijze slaagde er beter in de sterkte en het aantal van de zure sites in de zeoliet te behouden. Het aantal sterk zure sites bleek cruciaal voor de efficiënte conversie van LA naar PA. De resulterende dichte nabijheid van het hydrogenerende metaaldeeltje en sterk zure sites komt de productie van PA waarschijnlijk ook ten goede. Hergebruik van de Ru/H-ZSM5 katalysator liet zien dat de katalysator gedeeltelijk zijn activiteit had verloren, in dit geval voornamelijk als gevolg van de afzetting van koolstofrijke verbindingen op de sterke zure sites. De PA opbrengst kon echter eenvoudig worden hersteld door de organische afzettingen af te branden.

**Hoofdstuk 5** beschrijft de ontwikkeling van mono- en bi-metallische $TiO_2$-gedragen katalysatoren voor de selectieve hydrogenatie van LA naar GVL. Zeer actieve, selectieve, en stabiele metaalkatalysatoren werden gesynthetiseerd door middel van een gemodificeerde impregnatiemethode ($M_{Im}$). De $M_{Im}$ methode gebruikt een overmaat aan chloride-ionen in de impregnatiestap, wat essentieel is voor de efficiënte legering van Ru en Pd en Au en Pd. De impregnatie wordt, na drogen van het materiaal, weer direct gevolgd door een reductiestap in een verdunde waterstofatmosfeer. Deze $M_{Im}$ methodologie bleek een zeer gunstige uitwerking te hebben op de prestaties van de katalysatoren in de omzetting van LA naar GVL.

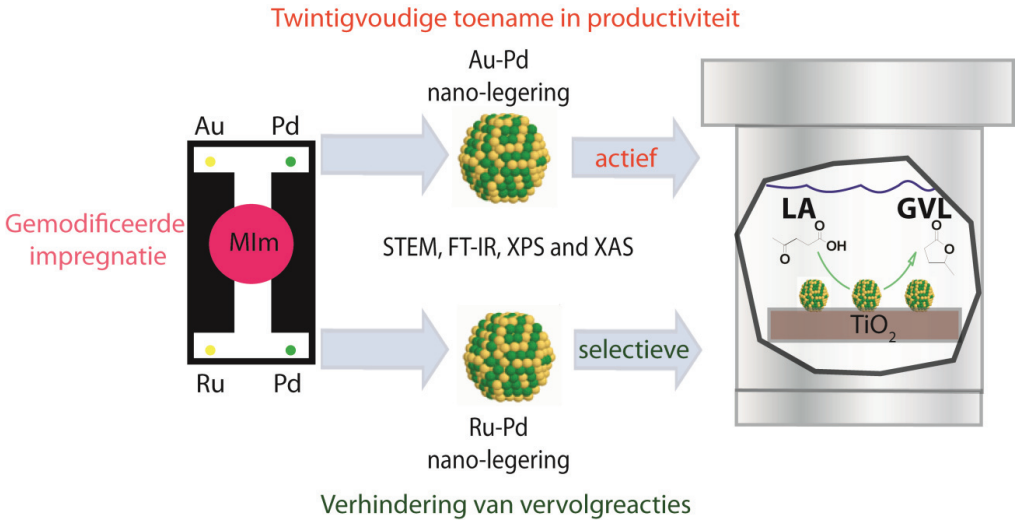


Figuur 4. Bi-metallische katalysatoren vertonen twee verschillende, positieve effecten van legeren in de reactie van LA naar GVL.

STEM, FT-IR na CO adsorptie en XAS analyses lieten zien dat de structuur van de goed-gedispergeerde Au-Pd of Ru-Pd nanodeeltjes op $TiO_2$ bestaat uit volledig gemengde, nano-legeringen (Figuur 4). Het Au-Pd/$TiO_2$ materiaal gaf een opmerkelijke 20-voudige verbetering in katalytische productiviteit (1.97 $mol_{GVL}\ g_{metaal}^{-1}\ h^{-1}$) in vergelijking met de mono-metallische Au en Pd katalysatoren, die beiden vrijwel inactief waren. Deze sterke toename in katalytische activiteit wordt toegedicht aan een synergistisch effect dat het gevolg is van een elektronische beïnvloeding van Pd door elektronenverschuiving van Pd naar Au. Hoewel het Ru-Pd/$TiO_2$ materiaal (17.2 $mol_{GVL}\ g_{metal}^{-1}\ h^{-1}$) slechts iets beter bleek te zijn dan Ru/$TiO_2$ dat op een identieke wijze bereid was (16.4 $mol_{GVL}\ g_{metal}^{-1}\ h^{-1}$),

bleek de legering in dit geval de stabiliteit en selectiviteit van de katalysator sterk te verbeteren. De uitstekende, constante selectiviteit naar GVL is vermoedelijk het gevolg van de verdunning van Ru door Pd in de nano-legering, waardoor de verdere hydrogenatiereacties die wel plaatsvinden bij de mono-metallische katalysator nu verhinderd worden. Zowel de Ru-Pd als de Au-Pd nano-legeringen bleken stabiel te zijn in drie opeenvolgende katalytische proeven. Hergebruik van de katalysatoren liet een vergelijkbare activiteit zien, een zeer beperkt sinteren of oplossen van de metaaldeeltjes en een minimaal verlies aan actief katalysatoroppervlak. Een variatie op de gemodificeerde impregnatie synthesemethode, waarbij wel de directe reductiestap, maar niet de overmaat aan anionen in de impregnatiestap werd gebruikt, leidde tot de ontdekking van een zeer actieve $Ru/TiO_2$ katalysator, met een productiviteit van 51.7 $mol_{GVL}\ g_{metal}^{-1}\ h^{-1}$. Deze sterk verbeterde activiteit is het gevolg van een sterke metaal-drager interactie, veroorzaakt door elektronenverschuiving van Ru naar $TiO_2$. Tot slot werd een lineair verband gevonden voor de drie meest actieve katalysatoren tussen de natuurlijke logaritme van de reactiesnelheid en de hoeveelheid lineair-geadsorbeerd CO, zoals gemeten met FT-IR. Deze correlatie laat zien dat CO adsorptie gebruikt kan worden als kwantitatieve maat voor de activiteit van dit soort gedragen metaalkatalysatoren in de omzetting van LA naar GVL.

# Appendices

# Appendix A

**1. Temperature-Programmed Desorption of Ammonia (TPD-$NH_3$)**

**2. Transmission Electron Microscopy (TEM)**

**3. X-Ray Diffraction (XRD)**

**4. Atomic Absorption Spectrophtometry (AAS)**

**5. Thermal Gravimetric Analysis-Mass Spectrometry (TGA-MS)**

**6. Two Dimensional $^{27}$Al Triple-Quantum Magic Angle Spinning Nuclear Magnetic Resonance (2D $^{27}$Al 3Q MAS NMR)**

**1. TPD- $NH_3$**

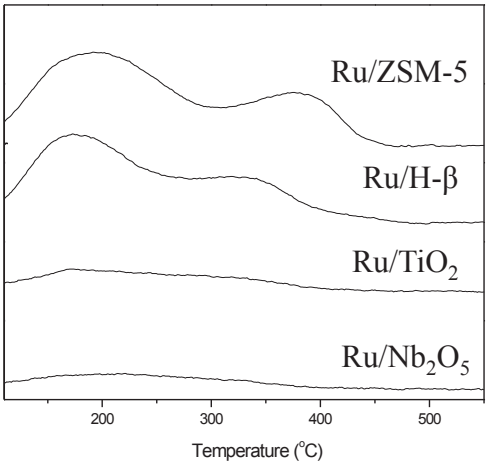


Figure S1. $NH_3$-TPD profiles of the four supported Ru catalysts.

**2. TEM images**

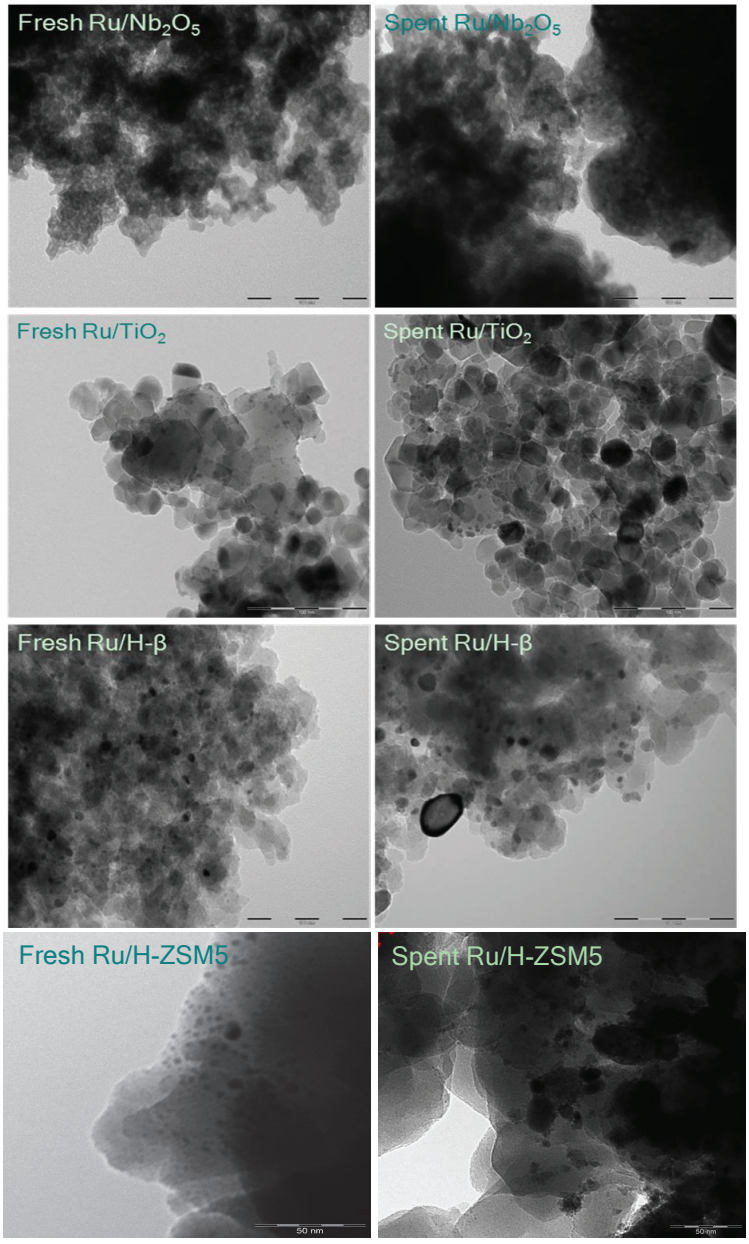


Figure S2. Bright field TEM images of the Ru catalysts before (fresh) and after (spent) reaction in dioxane.

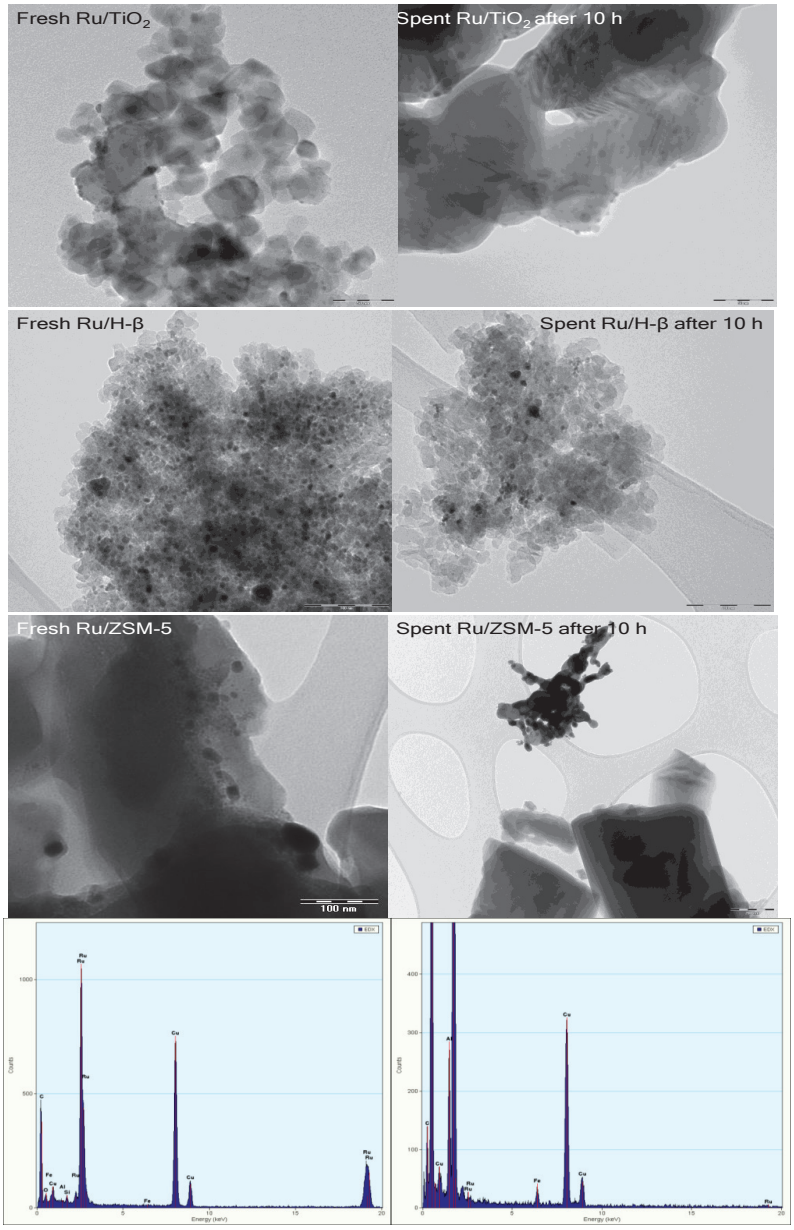


Figure S3. Bright field TEM images of the Ru catalysts before (fresh) and after (spent) reaction in 2-ethylhexanoic acid; bottom left: EDX of Ru-rich area of spent Ru/H-ZSM5; bottom right: EDX of Ru-poor area of spent Ru/H-ZSM5.

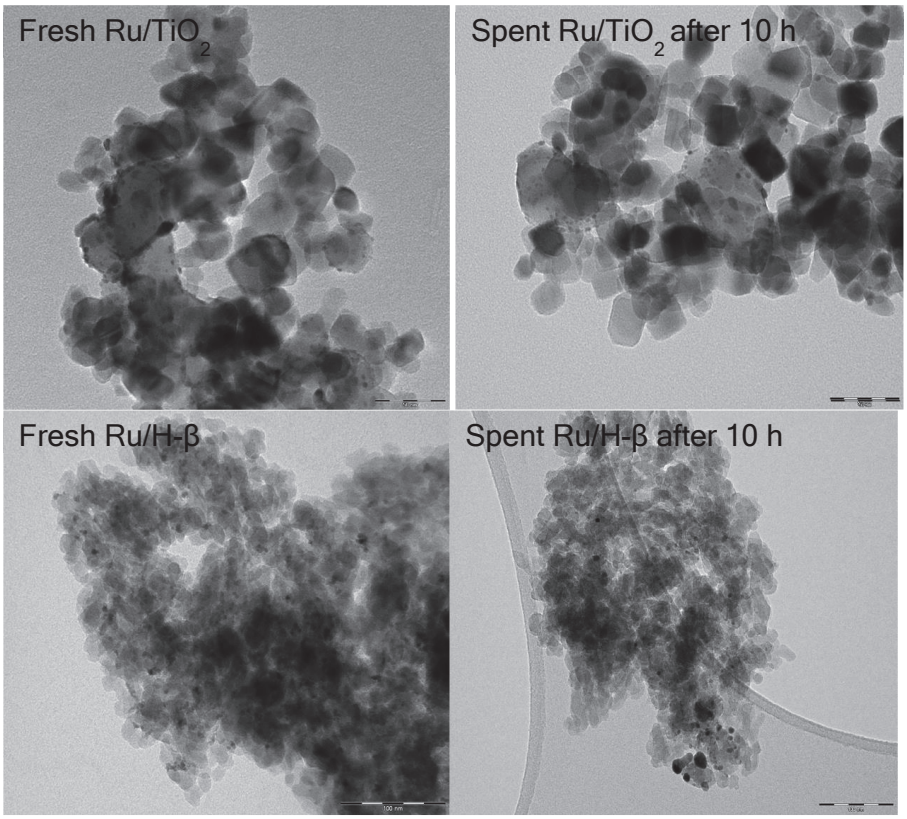


Figure S4. Bright field TEM images of the Ru catalysts before (fresh) and after (spent) reaction in neat levulinic acid.

**3. XRD**

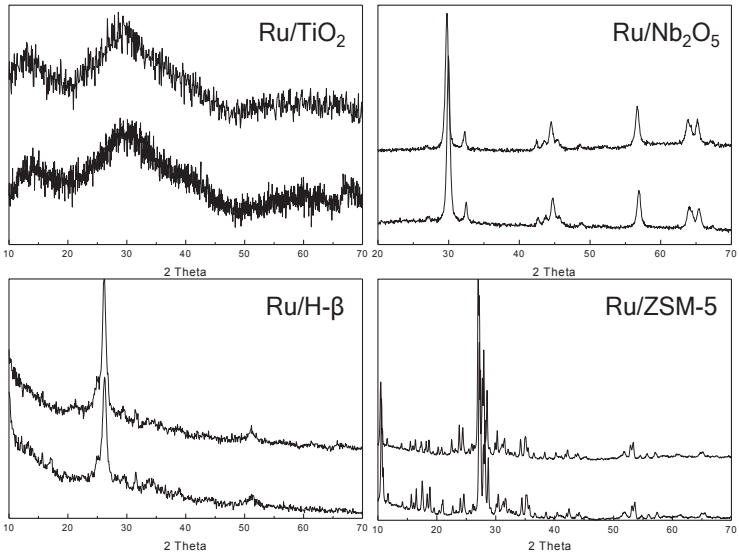


Figure S5. XRD patterns of fresh (bottom) and spent (top) Ru catalysts after reaction in dioxane.

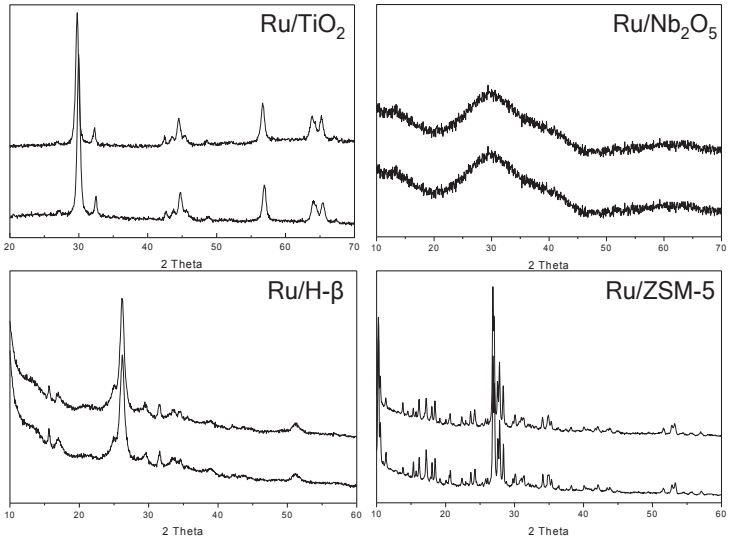


Figure S6. XRD patterns of fresh (bottom) and spent (top) Ru catalysts after reaction in EHA.

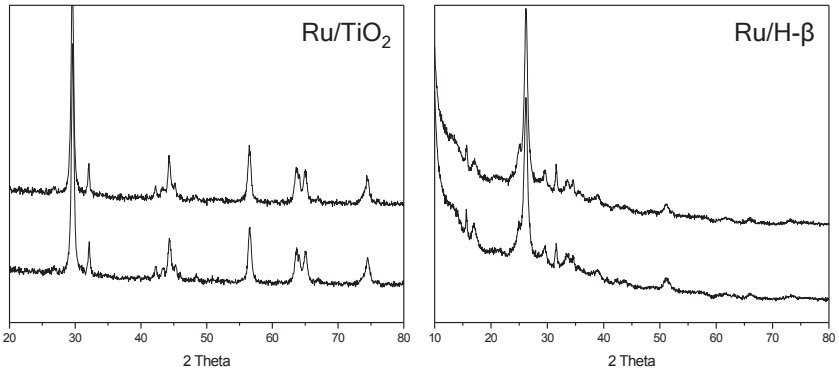


Figure S7. XRD patterns of fresh (top) and spent (bottom) catalysts after reaction in NLA.

**4. AAS**

Table S1. AAS of leached iron after reaction with H-β in EHA

| Entry | Fe (μg/mL) | Total Fe (μg) |
|---|---|---|
| 11 | 0.4 | 10 |
| 13 | 0.8 | 20 |
| 16 | 1.0 | 25 |
| 17 | 0.2 | 5 |

(Entry numbers match with the entry numbers in Table 2.4)

**5. TGA-MS**

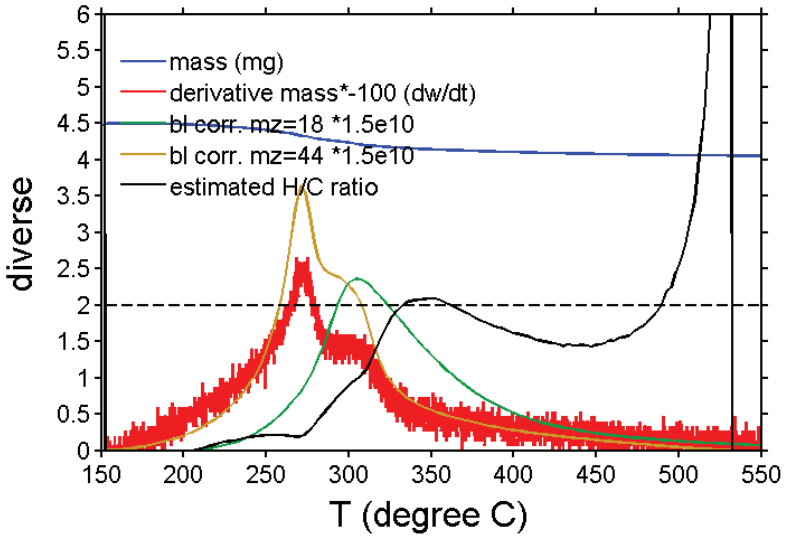


Figure S8. H/C ratio curve from TGA-MS of the spent Ru/H-β catalyst after a 10 h of reaction in EHA.

Figure S8 shows the mass loss (blue line), the derivative of the mass loss (red), the $CO_2$ (brown) and $H_2O$ (green) signals detected by mass spectroscopy, and the H/C ratio (black). For the calculation of the H/C ratio, the temperature range of 420 to 823 K was divided by 500 equally-spaced points and the integral between two points was determined and correlated with the amount of $CO_2$ and $H_2O$, according to equation:

H/C =(2*1/7.2*area $H_2O$ /18)/(1/1.29*area $CO_2$/44) [1]. The H/C ratio shows a plateau at 1.4 in the temperature range from 698 to 733 K.

## 6. 2D $^{27}$Al 3QMAS NMR

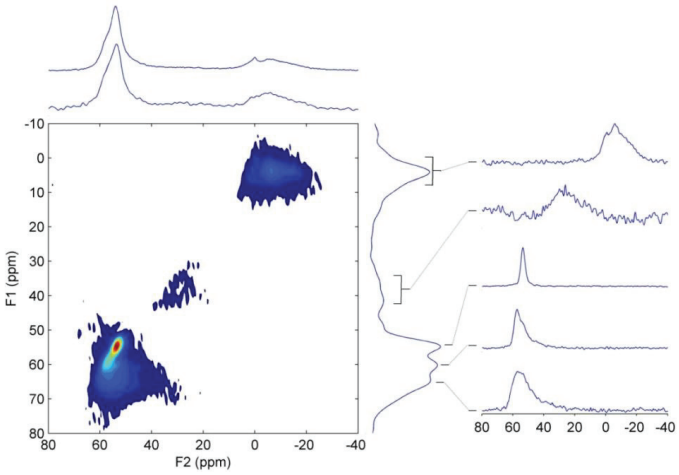


Figure S9. 2D $^{27}$Al z-filtered 3QMAS NMR spectrum of fresh Ru/H-β. The projection on the F2 axis is given directly above the 2D spectrum. For comparison the 1D single pulse spectrum is shown on top of that. To the right is the isotropic projection on the F1 axis, clearly showing the presence of octahedral aluminum, penta-coordinated aluminum and 3 types of 4-coordinated aluminum. A slice through each isotropic peak in F1 is given to the right of the F1-projection. For the 5 and 6-coordinated the sum over the relevant F1-region is depicted.

The 2D $^{27}$Al 3QMAS NMR spectra (Figure S9 shows the spectrum of fresh Ru/H-β as an example) were used to determine the limits of integration for the relative amounts of tetrahedral, penta-coordinated and octahedral aluminum species. The 3QMAS NMR data are discussed in detail in Chapter 3.

**Reference**

[1] M. Maciejewski, and A. Baiker, Thermochim. Acta 295 (1997) 95-105.

# Appendix B

**1. Bright Field Transmission Electron Microscopy**

**2. High Angle Annular Dark Field Microscopy(HAADF)**

**3. Temperature-Programmed Desorption of Ammonia (TPD-$NH_3$)**

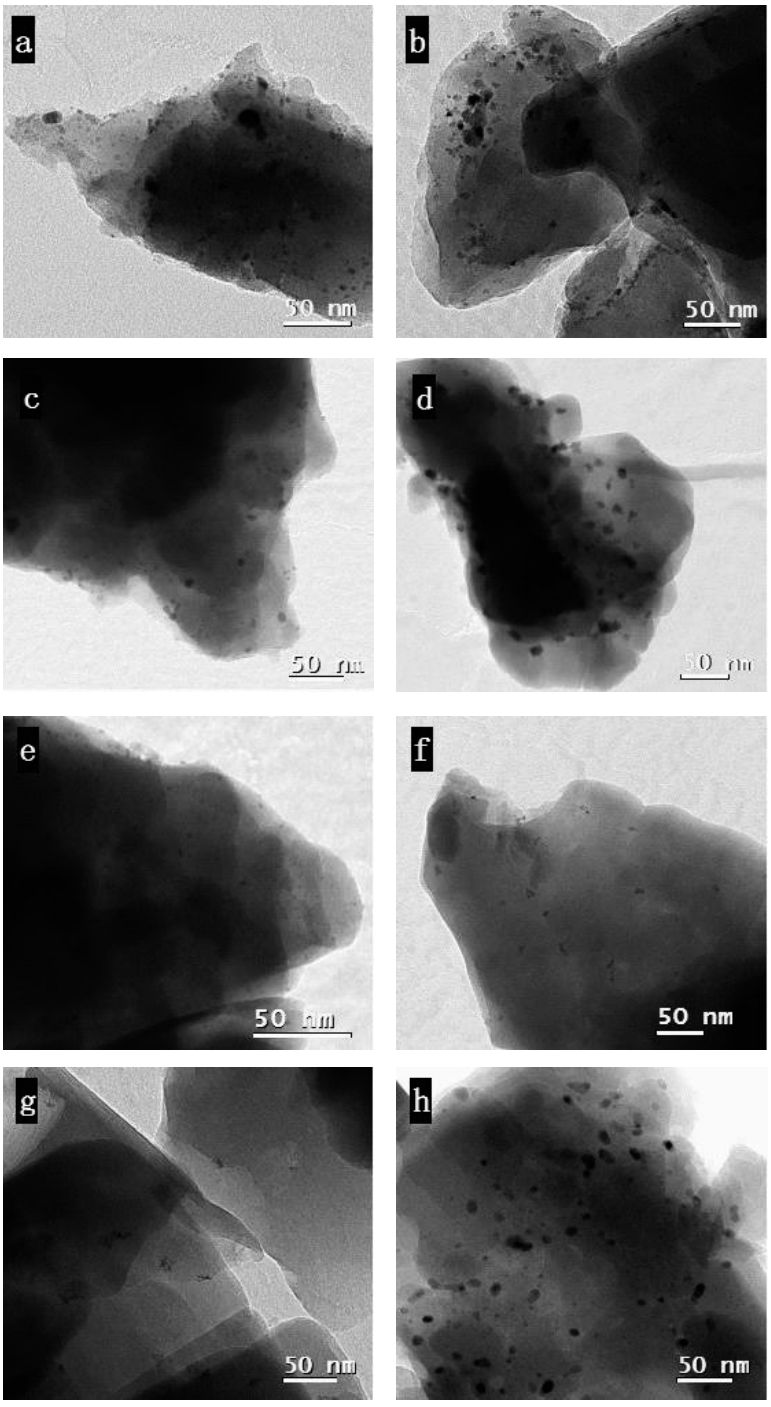
a
50 nm
b
50 nm
c
50 nm
d
50 nm
e
50 nm
f
50 nm
g
50 nm
h
50 nm

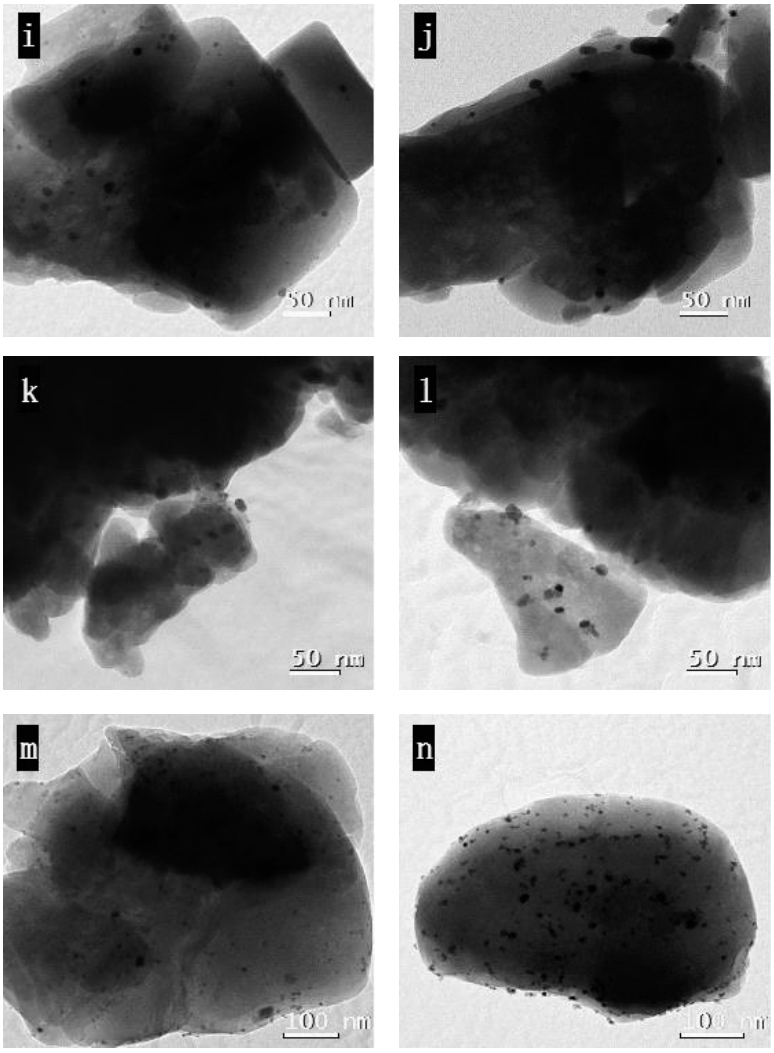


Figure S1. Bright Field TEM images of fresh and spent catalysts:
(a, b) fresh and spent Ru/H-ZSM5(Cl, H, 11.5); (c, d) fresh and spent Ru/H-ZSM5(Cl, A, 11.5); (e, f, g, h) fresh Ru/H-ZSM5($NH_3$, A, 11.5), spent catalyst, spent after direct reuse and regeneration after decoking (i, j) fresh and spent Ru/H-ZSM5($NH_3$, A, 25); (k, l) fresh and spent Ru/H-ZSM5($NH_3$, A, 40); (m, n) fresh and spent Ru/H-ZSM5($NH_3$, A, 140).

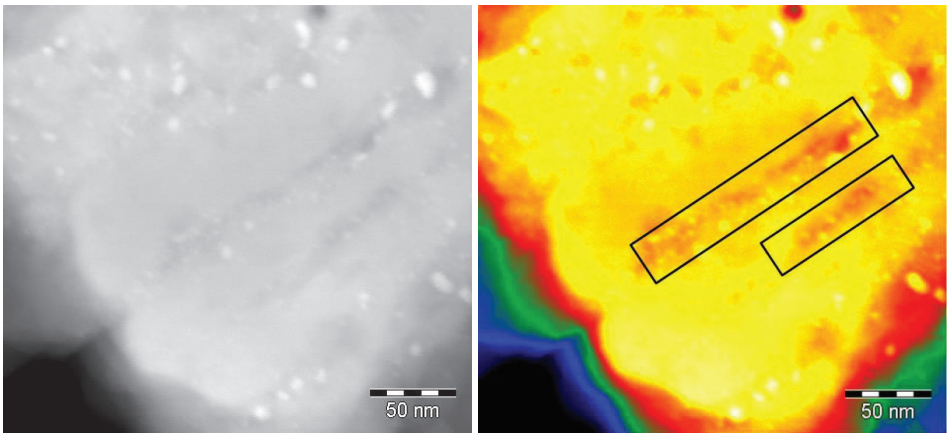


Figure S2. HAADF images of a regenerated Ru/H-ZSM5($NH_3$, A, 11.5) sample after coke burn-off; (left) in grey; (right) in color.

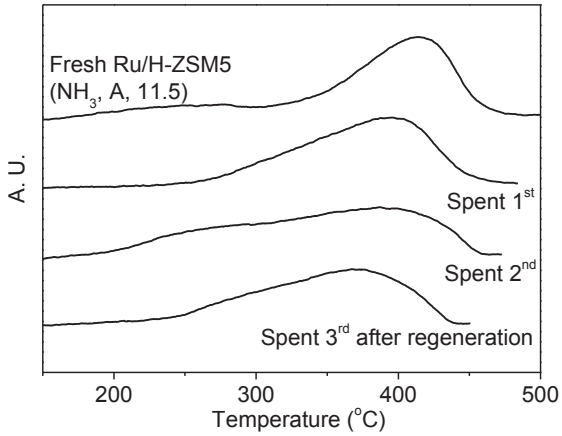


Figure S3. TPD-$NH_3$ profiles of the fresh Ru/H-ZSM5($NH_3$, A, 11.5) catalyst and after several recycle steps and regeneration.

# Appendix C

**1. Catalyst Testing**

**2. Electron Microscopy**

**3. X-ray Aborption Fine Structure (XAFS)**

**4. Fourier Transform Infrared (FT-IR) after CO Adsorption**

**5. Temperature-Programmed Reduction (TPR)**

**6. Comparison of Reported GVL Productivities**

## 1. Catalyst Testing

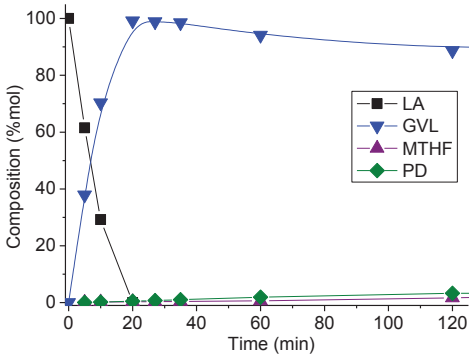


Figure S1. Temporal evolution of product(s) including GVL (▼), MTHF (▲) and PD (♦) and the consumption of LA (■) during its hydrogenation using monometallic 1% $Ru/TiO_2$ ($M_{Im}$, 0 M HCl) with the same the same Ru loading as in the run with the bimetallic 1% $Ru\text{-}Pd/TiO_2$ ($M_{Im}$) catalyst. Reaction conditions: T: 473 K; *p*: 40 bar $H_2$; 10 wt% LA in dioxane, and a substrate/metal weight ratio of 2000.

## 2. Electron Microscopy

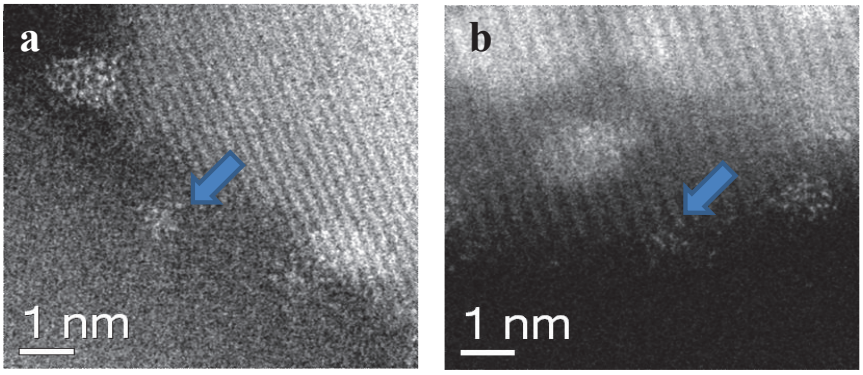


Figure S2. Representative high angle annular dark field (HAADF) images of the (a) 1% $Au\text{-}Pd/TiO_2$ ($M_{Im}$) and (b) 1% $Ru\text{-}Pd/TiO_2$ ($M_{Im}$) samples showing the existence of sub-nm metal clusters.

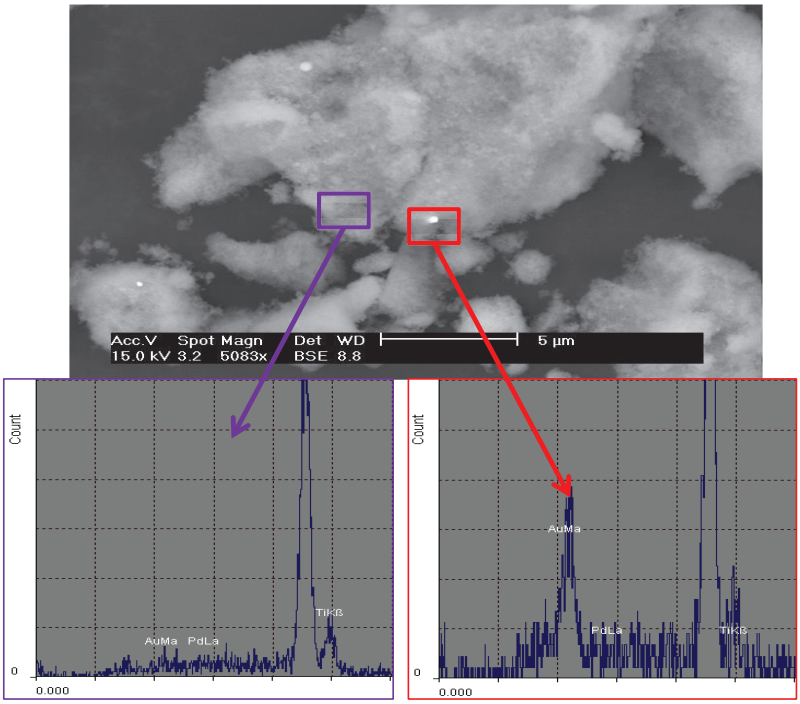


Figure S3. A representative SEM backscattered electron image of the 1% Au-Pd/$TiO_2$ ($M_{Im}$) sample, showing evidence for metal particles in the 0.1-0.5 µm size range. EDX analysis of such particles confirmed them to be Au.

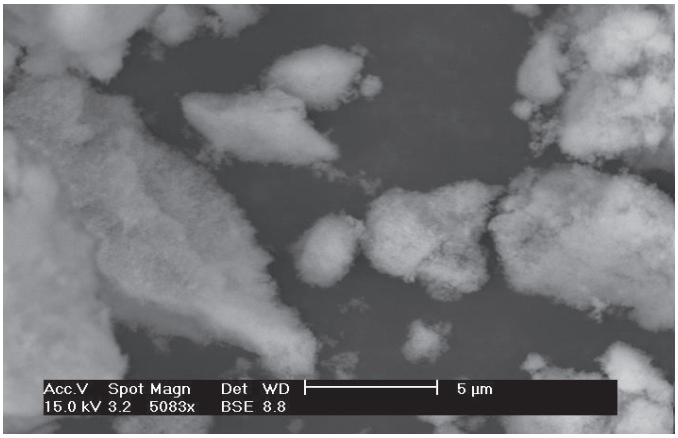


Figure S4. A representative SEM backscattered electron image of the 1% Ru-Pd/$TiO_2$ (MIm) sample, confirming that no micron-scale metal particles were present.

## 3. XAFS

XAFS spectroscopy measurements were performed on station BM26A and BM23 at the ESRF operating at 6 GeV in 2/3 fill mode with a current of 200 mA. The station was equipped with a Si (111) double crystal monochromator, and ion chambers for measuring incident and transmitted beam intensities for recording X-ray absorption spectra. The measurements were carried out in air on self-supporting wafers (approximately 100 mg) in transmission mode using a Si(111) monochromator at the Au L3 edge, Pd K-edge and Ru K-edge with the respective monometallic foils (10 um) used as calibrants for the monochromator. Measurements were performed at room temperature in normal step scanning mode; the time taken for each scan was ca. 40 min (a step size of 0.5 eV and counting time of 1 s/point was used for collection of data around the edge). To improve the signal-to-noise ratio, multiple scans were taken. All data were subjected to background correction using Athena (*i.e.* IFFEFFIT software package for pre and post edge background subtraction and data normalisation). XAFS spectra were normalized from 30 to 150 eV above the edge energy, while the EXAFS spectra were normalized from 150 eV to the last data point using the Autobk algorithm. Normalisation was performed between $\mu(E)$ and $\mu_0(E)$ via a line regression through the data in the region below the edge and subtracted from the data. A quadratic polynomial is then regressed to the data above the edge and extrapolated back to $E_0$. The extrapolated value of the post edge polynomial at $E_0$ is used as the normalisation constant. This threshold energy ($E_0$) is normally determined using either the maximum in the 1$^{st}$ derivative, approximately 50 % of the rising absorption egde, or immediately after any pre-edge or shoulder features. The isolated EXAFS spectra were analysed using the DL-EXCURV programme. Data were analysed using a least squares single or dual shell EXAFS fitting analyses performed on data that had been phase corrected using muffin-tin potentials. Amplitude reduction factors ($S_o^2$) of 0.83 and 0.94 obtained from fitting an Au and Pd metal foil, was also used in the analysis.

## 4. FT-IR after CO Adsorption

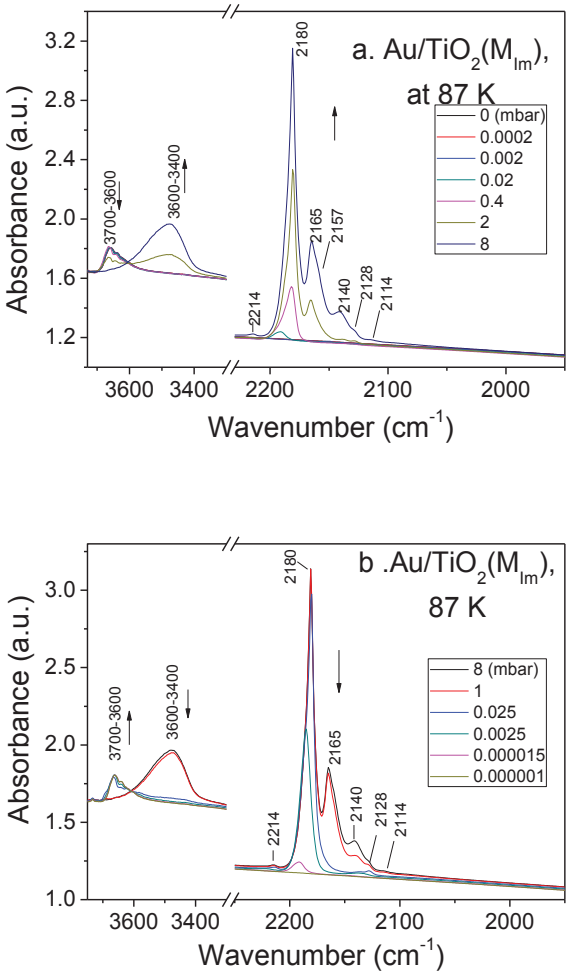


Figure S5. FT-IR of adsorbed CO on 1% $Au/TiO_2$ ($M_{Im}$) during (a) stepwise adsorption and (b) stepwise desorption under reduced pressure at 87K.

Mainly weak CO interactions with the support surface were observed on 1% $Au/TiO_2$ ($M_{Im}$), and only a marginal amount of Au-CO(L) at 2114 $cm^{-1}$ is observed at 8 mbar CO pressure.

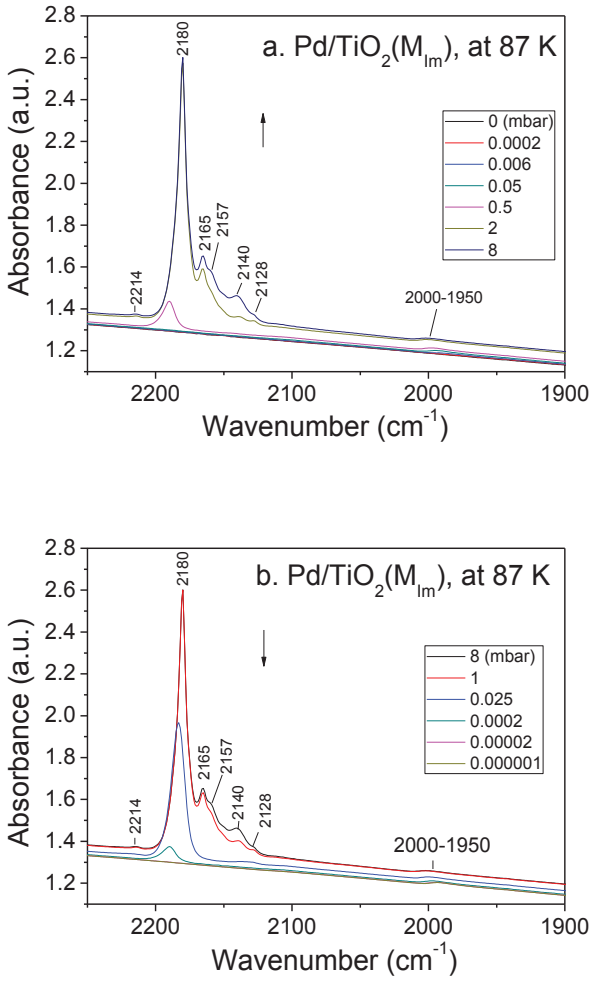


Figure S6. FT-IR of adsorbed CO during (a) stepwise adsorption and (b) stepwise desorption under reduced pressure over 1% $Pd/TiO_2$ ($M_{Im}$) catalyst at 87 K.

Most features for 1% $Pd/TiO_2$ ($M_{Im}$) arise from weakly adsorbed CO on the support. The weak broad feature at 2000-1950 $cm^{-1}$ that remains after evacuation is assigned to trace amounts of bridging carbonyl species on $Pd/TiO_2$ ($M_{Im}$). [1-3]

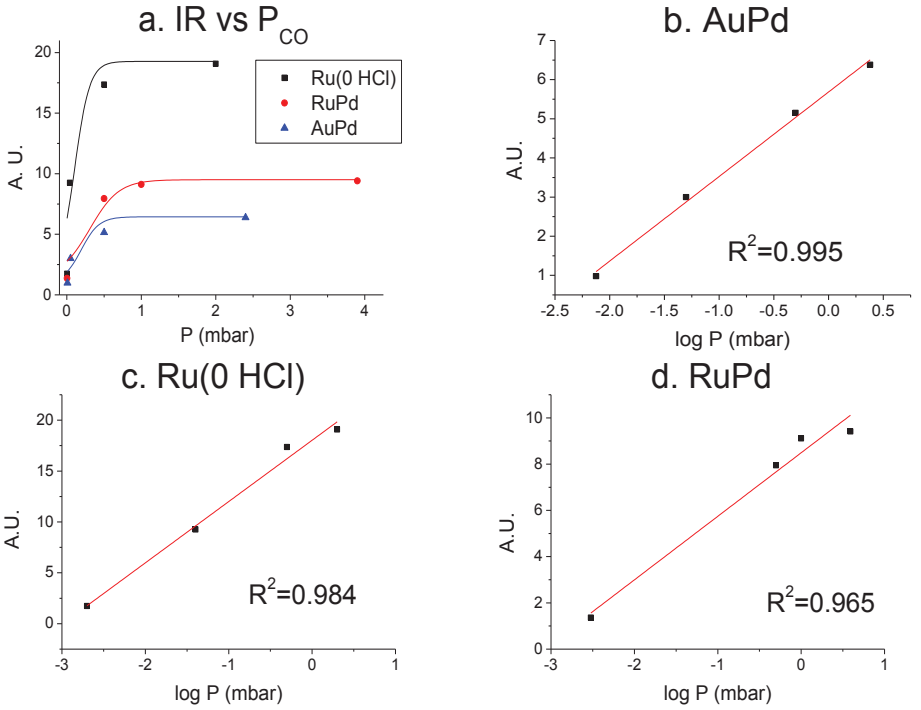


Figure S7. (a) Plot of the adsorbed linear CO peak intensity as a function of different $P_{CO}$ values; Absorbed linear CO peak intensity for the metallic region versus logarithm of $P_{CO}$ with (b) 1% Au-Pd/$TiO_2$ ($M_{Im}$) (c) 1%Ru/$TiO_2$ ($M_{Im}$, 0 M HCl) and (d) 1% Ru-Pd/$TiO_2$ ($M_{Im}$) catalysts.

A good linearity is observed by plotting the logarithm of $p_{CO}$ against M-CO peak area (coverage). The logarithmic relation can be represented by a Temkin-Pyzhev adsorption isotherm:

$$\Theta = a \ln (b^* P_{CO}).$$

where Θ is the coverage of CO, and a and b are constants. The amount of linearly adsorbed CO obtained from the IR experimental data was found to be linearly correlated with the activity of the catalysts, expressed as initial rate, in a logarithmic plot.

## 5. TPR

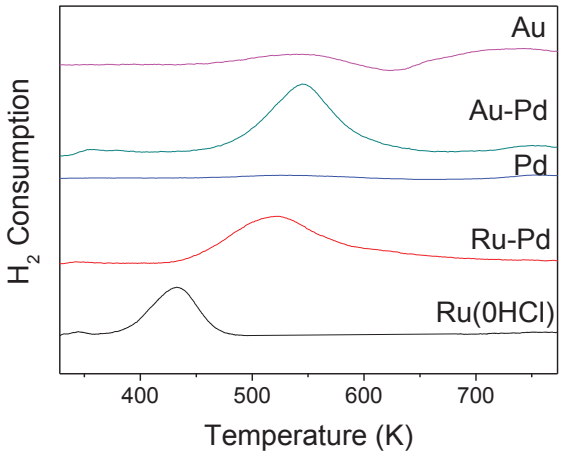


Figure S8. Temperature-programmed reduction (TPR) profile of all the monometallic and bimetallic catalysts after oxidation of the fresh catalysts at 353 K for 4 h.

The shift of the reduction peak observed Ru-Pd alloy to a higher temperature, indicates the formation of oxide phases formed in Ru-Pd, which are more difficult to reduce than either monometallic Ru or Pd.

## 6. Comparison of Reported GVL Productivities

Table S1. Productivity of different catalysts in the hydrogenation of LA to GVL, adapted from reference [4].

| Catalyst | Productivity ($mol_{GVL}$ $g^{-1}_{metal}$ $h^{-1}$) | Reaction Conditions | Reference |
|---|---|---|---|
| 1% $Ru/TiO_2$ ($M_{Im}$ 0HCl) | 51.7 | 473 K, 40 bar, in dioxane | Current work |
| 1% $Ru/TiO_2$ ($M_{Im}$) | 16.4 | 473 K, 40 bar, in dioxane | Current work |
| 1% $Au/TiO_2$ ($M_{Im}$) | 0.073 | 473 K, 40 bar, in dioxane | Current work |
| 1% $Pd/TiO_2$ ($M_{Im}$) | 0.054 | 473 K, 40 bar, in dioxane | Current work |
| 1% $AuPd/TiO_2$ ($M_{Im}$) | 1.97 | 473 K, 40 bar, in dioxane | Current work |
| 1% $RuPd/TiO_2$ ($M_{Im}$) | 17.2 | 473 K, 40 bar, in dioxane | Current work |
| 1% $Ru/TiO_2$ ($W_{Im}$)[a] | 5.14 | 473 K, 40 bar, in dioxane | [5] |
| 5% Ru/C | 5.33 | 463 K, 12 bar, neat LA | [6] |
| 5% Ru/C | 1.12 | 403 K, 12 bar, ethanol/ water | [6] |
| 5% $Ru/TiO_2$(P25) | 0.90 | 403 K, 12 bar, ethanol/ water | [6] |
| 5% $Ru/TiO_2$ | 0.45 | 423 K, 35 bar, in water | [7] |
| 0.6% $Ru/TiO_2$ | 0.46 | 423 K, 35 bar, in water | [7] |
| 5% Pd/C | 0.08 | 538 K, 1 bar, in dioxane | [8] |
| 5% Ru/C + Amberlyst-70 | 5.63 | 343 K, 30 bar, in water | [9] |
| RuSn(3.6: 1)/C | 0.36 | 493 K, LA and FA in alkyl-phenol solvent | [10] |
| 15% RuRe(3:4)/C | 0.014 | 423 K, 5 bar $N_2$, equimolar (2.2 mol/L) LA and FA and $H_2SO_4$ (0.5 mol/L) | [11] |
| 1 mol% $Au/ZrO_2$ | 1.68 | 423 K, 5 bar $N_2$, equimolar LA and FA | [12] |

a. A 1% $Ru/TiO_2$ ($W_{Im}$) catalyst was also prepared by a conventional wet impregnation method from its nitrate precursor.[5]

## References


[1] W.K. Kuhn, J. Szanyi, and D.W. Goodman, Surf. Sci. 274 (1992) L611-L618.

[2] Y. Li, B. Xu, Y. Fan, N. Feng, A. Qiu, J.M.J. He, H. Yang, and Y. Chen, J. Mol. Catal. A: Chem. 216 (2004) 107-114.

[3] E. Ozensoy, and D.W. Goodman, Phys. Chem. Chem. Phys. 6 (2004) 3765-3778.

[4] W.R.H. Wright, and R. Palkovits, ChemSusChem 5 (2012) 1657-1667.

[5] W. Luo, U. Deka, A.M. Beale, E.R.H. van Eck, P.C.A. Bruijnincx, and B.M. Weckhuysen, J. Catal. 301 (2013) 175-186.

[6] M.G. Al-Shaal, W.R.H. Wright, and R. Palkovits, Green Chem. 14 (2012) 1260-1263.

[7] A. Primo, P. Concepcion, and A. Corma, Chem. Commun. 47 (2011) 3613-3615.

[8] P.P. Upare, J.-M. Lee, D.W. Hwang, S.B. Halligudi, Y.K. Hwang, and J.-S. Chang, J. Ind. Eng. Chem. 17 (2011) 287-292.

[9] A.M.R. Galletti, C. Antonetti, V. De Luise, and M. Martinelli, Green Chem. 14 (2012) 688-694.

[10] D.M. Alonso, S.G. Wettstein, J.Q. Bond, T.W. Root, and J.A. Dumesic, ChemSusChem 4 (2011) 1078-1081.

[11] D.J. Braden, C.A. Henao, J. Heltzel, C.C. Maravelias, and J.A. Dumesic, Green Chem. 13 (2011) 1755-1765.

[12] X.-L. Du, L. He, S. Zhao, Y.-M. Liu, Y. Cao, H.-Y. He, and K.-N. Fan, Angew. Chem. Int. Ed. 123 (2011) 7961-7965.

# List of Publications and Presentations

**A. Publications**

Luo W., Deka U., Beale A.M., van Eck E.R.H., Bruijnincx P.C.A., Weckhuysen B.M., "Ruthenium-catalyzed Hydrogenation of Levulinic Acid: Influence of the Support and Solvent on Catalyst Selectivity and Stability", J. Catal. 301 (2013) 175-186.

Luo W., van Eck E.R.H., Bruijnincx P.C.A., Weckhuysen B.M., "Changes in Aluminum Speciation in Zeolite-Supported Ruthenium Catalysts after Levulinic Acid Hydrogenation as Studied by $^{27}$Al 3QMAS NMR and FT-IR", to be submitted.

Luo W., Bruijnincx P.C.A., Weckhuysen B.M., "Selective, One-pot Catalytic Conversion of Levulinic Acid to Pentanoic Acid over Ru/H-ZSM5", J. Catal. 320 (2014) 33-41.

Luo W.*, Sankar M.*, Beale A.M., He. Q, Kiely C.J., Bruijnincx P.C.A., Weckhuysen B.M., "Highly Active, Selective and Stable Supported Nano-Alloys for the Hydrogenation of Levulinic Acid to γ-Valerolactone", submitted for publication.
* Both authors contributed equally to this work.

Sankar, M, Luo, W., Bruijnincx, P. C. A., Weckhuysen, B. M., "Supported Monometallic and Bimetallic Catalysts for the Hydrogenation of Levulinic Acid", Patent Application PCT/NL2014/050569

**B. Oral Presentation**

Luo W., Deka U., Beale A.M., van Eck E.R.H., Bruijnincx P.C.A., Weckhuysen B.M., "Ruthenium-catalyzed Hydrogenation of Levulinic Acid: Influence of the Support and Solvent on Catalyst Selectivity and Stability", 23rd North American Catalysis Meeting (NAM23), June 2013, Louisville, Kentucky, United States of America.

**C. Poster Presentations**

Luo W., Bruijnincx P.C.A., Weckhuysen B.M., "Ruthenium-catalyzed Hydrogenation of Levulinic Acid: Influence of the Support and Solvent on Catalyst Selectivity and Stability", 12th Netherlands Catalysis and Chemistry Conference, March 2011, Noordwijkerhout, The Netherlands.

Luo W., Deka U., Beale A.M., van Eck E.R.H., Bruijnincx P.C.A., Weckhuysen B.M., "Ruthenium-catalyzed Hydrogenation of Levulinic Acid: Influence of the Support and Solvent on Catalyst Selectivity and Stability", 13th Netherlands Catalysis and Chemistry Conference, March 2012, Noordwijkerhout, The Netherlands.

Luo W., Deka U., Beale A.M., van Eck E.R.H., Bruijnincx P.C.A., Weckhuysen B.M., "Ruthenium-catalyzed Hydrogenation of Levulinic Acid: Influence of the Support and Solvent on Catalyst Selectivity and Stability", 11th European Congress on Catalysis, September, 2013, Lyon, France.

# Acknowledgements

Life for me is a journey full of treasures and adventures. The most precious things are not always related with material fortune, but with the true experiences and fond memories, which are not going to fade away with time. For me, four years and ten months in the Inorganic Chemistry and Catalysis Group has been definitely a special and exiting period. In what follows, I would like to express my sincere gratitude to all the people who have contributed to make this Utrecht period unforgettable.

The first and biggest 'Dank u' is to Bert, my 'godfather' in science. In my toddler stage of my PhD period, your sharp criticism always brought me back to the right track. Although experiencing growing pains, I am so grateful for your most-needed suggestions, directly and timely. Without your guidance, patience, support and criticism, my work would not have turned from a 'caterpillar' into a 'butterfly'. So many good moments flow in front of my eyes, from our interview calls, our group and day-out meetings, your special new year's wishes, your swift response to emails, Christmas dinners, etc. Your endless enthusiasm and focused attitude, like you have a B.M.W. engine inside, inspire and touch me the most. Thank you very much again for all your inputs and efforts.

Pieter, my dear respectful 'elder brother', I can never thank you enough for your endless help and encouragement. So many times, you have aided me out of a dilemma when I was struggling, and cheered me up when I fell into frustration. My PhD thesis has benefitted greatly from your input, suggestions and helpful ideas. Your logic, patience, preciseness and humbleness make an excellent complement to my jumpy thinking style, irritableness, carelessness and self-conceit. I sincerely appreciate your meticulous aids in correcting my posters, presentations and articles and approachability for me whenever I needed you, and I often felt guilty for bringing you additional work during your spare time. What impressed me a lot as I was working with you is your capacity in time balance and truly understanding the various differences in cultures and characters. I am proud to be one of your early stage PhD students.

Krijn, the kind suggestions from the short discussions, and the knowledge learned by following your course, inspired my deep thinking in heterogeneous catalysis. Your image as a great teacher is engraved in my memory. Frank, your elegance in manners and kindness from the dinner chats reflect a standard of what a gentleman should be. Harry, your amiability and easy-going nature brought the most lovely and positive energy to the whole group. Petra, your passion and sincerity bring a new, wisp of redolent breeze to the professors' team.

Andy, the talented, humorous expert in XAFS and XRD, thank you for your contributions and expertise, as well as for your patience when answering so many of my stupid questions. You broadened my vision on X-rays with your funky and humorous style. Sankar, the modest master in material synthesis, it was a great pleasure to work with

you, starting from the corridor discussions and chats. I wish our collaboration will never end. I am impressed by your mildness and kindness inside your soul. I wish you lots of success in the academic world and all the best for your family. Ernst, a special place should be reserved for you with your NMR contributions. Thanks for your warm reception and all the valuable input. Chris and Qian, I appreciate a lot your STEM input from Leigh University and wish I can once show my gratitude to you in person. Anna, it is a great pleasure to work with you in this collaborated project, and I wish all the success for you in the coming year; Erik, thank you so much for your positive opinions during discussions and backing me up from the Groningen side. Furthermore, Jean-Paul Lange, Hans Gosselink, Ed de Jong, Jan Kees van der Waal, Lei Zhang, and all the industrial committee members within the CatchBio consortium, are greatly acknowledged for the helpful suggestions and fruitful discussions in the past four years.

My research can never be finished without the quiet and under-rewarded practical supports. Dymph and Monique, I sincerely appreciate your help when dealing with my visa affairs and daily trifles. Ad$^{E}$, interactions with you are always full of fun (such as in Don Quijote), and your kind personality and words of wisdom never make a beam-trip boring. You are the real uncle-like 'jonger' and most-like the Dutch 'expendable' in our group. Tom, although you retired for a while, your warm smile and humor will never fade away in my mind. Ad$^{M}$, I would like to give you a big 'thank you' for your lightning-speed technical support, and highlight your silent contributions for the whole group. Marjan, a lot of joy and beauty is gained with your photos, and thanks for your instruction of XRD and TGA-MS. Cor, the time of searching for small particles or clusters leaves me a very good image of you, as a person with a hospitable 'core'. Herrick, thanks for your efforts for some new trial experiments with me, and brightening me up with your Scottish stories. Fouad, my No. 1 Moroccan friend, a cool African rapper, thanks for your nice, special instruction of the IR facilities. I enjoyed various interesting topics we talked about and many interesting moments we shared together, and I appreciate that you appeared as a fantastic and colorful 'magician' in my PhD life.

Thousands of miles away from home, adjusting to a new professional environment is needed to make a PhD project enjoyable. Therefore, I would like to thank the following people for making my life in the Wentgebouw easy and comfortable. Davide (the warm 'receptionist' in Schiphol and my 'introducer' to the group), Dilek and Maria (lovely ladies with a warm smile and hospitality), Philipp**,** Amélie, Hidkazo and Latin (beautiful people with a clear tolerance for my jokes), Peter H (Popai driving me to the Central Station), Jinbao (patient, super-nice classical beauty), Ard (a kind and serious MJ fan helping me in TGA), Eduardo (stylish magnet for awesome parties), Jovana (the 'Madusa-curly' lady), Lukasz (the kind, big neighbor brother), Hirsa (fabulous Salsa dancing queen), Peter N (African fabulous dancer), Matti (deep thinker), Tamara (athletic model from the army), Joe Z (American, gentle, multilingual machine), Javi (warm Spanish sun), Piter (happy and considerable borrel organizer), Annelie (a gladsome spidergirl), Mathijs (Dutch gentleman), Simon and Matt (the UK Dual), Andrei

(Vampire master Dracula), Anne (the 'Dutch' from Danish tale), Gonzalo (Xavi from Alicante), Luis (sunflower hippie), Adri (a 'fruitful' PhD), Eli (Geek of hacker), Marianne (baby face meisje), Upakul (warm dandy Buddhist), Rob ('Mideast' awesome monkey), Jesper (Veenendaal 'red-beard' Tintin), Arjan (the warm tank-man), Inge (pretty cat-walker Sheila), Zoran (Zoarium of Djokovic and Ronaldo), Tomas (warm teddy bear), Bart (hidden rocky dragon), Ilona (feminine true-temper warrior), Evelien (a big well-behaved next-door meisje), Daniel (shy transcendental crane), Hendrik (humorous, cautious monk), Peter M (knight-spirit Peter Pan), Sonia (warm, passionate flammingo), Carlo (tender considerable mafia), Sankara (a 'true' vegetarian), Yuen (modern homey hermit), Charlotte (elegant romantic rose), Young-min (a nice smiling Korean big bro), Peter de P (actor-like handsome), Johan (devout Christian). Thanks for you folks paced upon during my early PhD journey, and you all shined in my Wentgebouw memories.

I would give very special thanks to my former roommates, Emiel (Master Edward Cullen), thanks for setting a very good example of being a PhD student; Clare (warm-hearted pussycat), thanks for being so nice and hospitable for organizing so many fancy events with your elegant ladies; Qingyun (spicy pepper), thanks for having you talking and eating with me so many times together, and your incisive jokes on me, I appreciate your toughness and kindness a lot. Joe S (Mr. DiCaprio), thanks a lot for your warm Chinese greeting and your kind help in language matters. Thomas (knight of Nutcracker), it is great pleasure to have you for wonderful tours in Aachen and USA.

The second stage of my PhD period in David de Wiedgebouw was also full of joy. Many thanks for the enjoyable atmosphere provided by you lovely people. Dimitrije (awesome sunny hulk), Rafael (Brazilian Ninja turtle), Zafer (soft-hearted gentle turkey), Robin (cute Harry Potter), Korneel (quiet beard cat), Arjen (nice alcohol-keeper), Roy (van Persie-like flower), Fernando (likesome communicative questioner), Jan Philipp (kind neighbor bro), Ines D (active happy girl), Ines L (warm material master), Sophie (bosom French sister), Fiona (Irish S-line Jolie), Michael (mild smilling big bro), Gareth (Welsh gentle Pitt), Reshmi and Sisiwati (southeast Asian sun), Nazila (cautious Persian cat), Mustafa (loyal handsome waiting for the love), Frank (cool motorbike player), Mozaffar (Senior Alibaba bro), Sam (smart wakeful werewolf), Jeroen (drinking wolverine), JX (Singorean anthomaniac pancake), Peter B (rocky Garfield), Ramon (Dutch Gangnam-style rocker), Rogier (mild giraffe), Gang (lovely Panda), Ivan (the 'sunny' towser), Joris (flying Dutch-bowlinger), Pasi (funky punk), Egor (the newbie vodka), Jamal (the pirate who took my boat :-)), Marleen (Evelien's lost sister), Suwarno (Indonesia nice bro), Angelo (DDW's deep watcher), Diego (Mexican big straw-hat), Elena (elegant Russian Chihuahua), Monica (solar goddess), Florian (the new X-(ray)man), Sang-ho (Korean basketball bro), Ana and Ara (the song-like 'Spanish sisters'), Selvedin, Christoph, Pengfei, Jelle, Ying, Sandra, Rosa, Tao, Ozgun, Bo, Boyang, Anton, Marianna, Homer, Fang, it was indeed a great pleasure to work with you who bring so great diversity and various expertises, and I wish all the best for your life in Utrecht and the coming future. So many good memories in this period of journey suddenly come across to my mind. The nice group day-outs and lab-uitjes, the annual

Christmas dinners, the nice borrel times, the long island ice tea borrels, the exploration of Athens, cocktails on Miami beach, awesome club nights and various parties, etc. Many thanks for your appearance in my life, tolerance of my rudeness and sharing various fun together.

I will never forget the other extrinsic indirect contributors to my life, Peter S, Steffen, Francesca, Suresh, Seyed, Elli, Youngkook, and Vital, many thanks for your kind interactions. Especially, deep appreciation to a unique couple, my Dutch Papa Paulo, and Mama Maria, thanks for driving me to the family doctor, showing me around the neighborhood, sharing your life experience and helping in daily affairs. You shelter me with full of warmness and love, which resulted in a peaceful and comfortable life in Zeist.

The final appreciation goes to my Chinese folks and family:

时光如白驹过隙，飘雪无痕。离家万里，多亏了你们这帮兄弟朋友才让我的荷兰生活魅影婆娑，色彩斑斓。感谢王洪洪（村长和兄弟）和张芳（细心善良嫂），吴泰宇（导游界的金色兄弟）和吕琼（大嘴女汉子），傅鸥（善良的闸北纯男），李巍（潇洒二师弟），胡立斌（忠厚餐馆哥）和周丽芳（善良快语嫂），周厚江（狂热毅力哥）和戴思思（美丽清新嫂），梁馗旭（倜傥粗口弟），李嘉伦（超纯好萌弟），李璋（悠哉居家弟），杨帆（媚丽甜心妹），王雨婷（美辣重庆妹），吴斌和庞垚（青岛筷子组合），刘堃（刚猛三师弟），高露（爽快幽默妹），史姝（北京俏佳妞），方睿和硕伟（海峡对岸好球友），张兴林和刘小曼夫妇（知心好邻居），黄文涛（进取早起男），张金强（笑面西北男），刘一宏（热情好大厨），魏一璞（文艺小清新），杨俐（乖巧学生妹），李小倩（知性温柔妹），张磊和敖芳夫妇（温和细心兄和贤淑雷厉嫂），陈家琦（缜密严谨逻辑男），李晔（干练俏女郎），胡宏和张经纬（对门温暖好邻居），刘金峰（憨厚大吃货），张浩（灵活温情胖），王子鸣（旋风小厨将），杨浩然（‘精壮’热血男），张帅（闷厚直肠男），韩梦茹（宅萌小萝莉），彭博和赵一鸣（同道博中友），范峰滔（风发学术哥），孙志祥（温情柔和男），阿雷（忘年道中友），高金宝（温存细心姐），钱庆云（泼辣女汉子），王刚（可靠性情男），刘芳（呆萌小学妹），魏莹和张玲夫妇（天然萌若呆和贤良德淑美），杨鹏飞（天外飞仙哥），冯博（日系纯良博），刘铂洋（摄影发烧友），  王青青（知心善良姐），石洋（憨纯实在男）。感谢生命中有你们，祝你们诸事顺利！苟富贵，勿相忘哈。

最后，我要感谢我的家人。阿原，感谢你默默善良温柔无私的付出，还有可爱美丽猩猩相惜的陪伴，感谢阿力克先生的信任和刘辉女士的支持。爸爸老罗，谢谢你的教导和真挚的爱，勤劳勇敢善良的妈妈权玉芬女士，感谢你最无私的爱和最厚重的支持。散落在世界各处的亲戚朋友们，谢谢你们对我的关怀。还有逝去在天堂的长辈们，谢谢你们对我儿时的关怀和启迪，愿祥和和宁谧永存。

여러분 모두를 사랑합니다！ Wenhao Luo (罗文豪)

# Curriculum Vitae

Wenhao Luo was born on March 18th 1984 in Jilin (China). In 2002, he started his undergraduate studies in Materials Chemistry at Nankai University (China) and received his Bachelor of Science degree in 2006. At the same time, he succeeded in obtaining a Bachelor of Business Administration degree from Tianjin University (China). In the same year, he was recommended without entrance exam to the Graduate School of Nankai University where he started his Master's research on the hydrodesulphurization of Mo-based catalysts in the Institute of New Catalytic Material Science, under the supervision of Prof. Dr. K. Tao. He obtained his Master of Science degree from Nankai University in 2009.

In September 2009, Wenhao Luo started his PhD project entitled 'Fundamental Studies on Hydrogenation of Levulinic Acid' in the group of Inorganic Chemistry and Catalysis of Utrecht University (The Netherlands) under the supervision of Prof. Dr. B.M. Weckhuysen and Dr. P.C.A. Bruijnincx. This research project has been part of the Catchbio program, a Dutch consortium focusing on catalytic biomass valorization, which includes 21 partners from most Dutch universities, research institutes and industries operating in the field of catalysis research. The results of this research project are described in this PhD thesis.

Since July 2014 Wenhao Luo is a Postdoctoral Fellow in the group of Prof. Dr. J.A. Lercher at the Technische Universität München (Germany).